SCOFIELD, Gordon Lloyd, 1925-
RADIATIVE HEAT TRANSFER FROM AN ARBITRARY PLANE SOURCE TO A SEMI-INFINITE AEROSOL.

The University of Oklahoma, Ph.D., 1968
Engineering, mechanical

University Microfilms, Inc., Ann Arbor, Michigan

THE UNIVERSITY OF OKLAHOMA

GRADUATE COLLEGE

RADIATIVE HEAT TRANSFER FROM AN ARBITRARY PLANE SOURCE TO A SEMI-INFINITE AEROSOL

A DISSERTATION

SUBMITTED TO THE GRADUATE FACULTY

in partial fulfillment of the requirements for the

degree of

DOCTOR OF PHILOSOPHY

BY

GORDON LLOYD SCOFIELD

Norman, Oklahoma

1968

RADIATIVE HEAT TRANSFER FROM AN ARBITRARY PLANE

SOURCE TO A SEMI-INFINITE AEROSOL

APPROVED BY

D. G. Harden

J. E. Francis

Allen H. Weber

DISSERTATION COMMITTEE

ACKNOWLEDGMENTS

The work which has led to this dissertation has been supported by the National Science Foundation and the University of Missouri at Rolla.

In any undertaking of this scope there is always an individual who is instrumental in providing the counsel and encouragement at times when it is most necessary. Dr. Tom J. Love has been such an individual for me, and I am pleased to convey my gratitude for his confidence and support throughout the entire program of advanced study leading to this work.

Dr. John E. Francis, whose helpful nature has been a source of support during this period, will be remembered with appreciation.

Dr. Edward F. Blick, whose enthusiasm has been infectious, has contributed valuable assistance throughout my program as have Dr. Darrel G. Harden, Dr. C. Phillip Colver, and Dr. Allen H. Weber.

The help of Dr. H. D. Keith, of the University of Missouri at Rolla, in coordinating the computer work done at Rolla, is gratefully acknowledged.

This experience has been a family venture from its inception and I owe a considerable debt of gratitude to my wife, Nancy, and to our children, Cathy and Terry, for their support and encouragement.

ABSTRACT

Radiative heat transfer directly to the droplets of a semi-infinite aerosol located above a finite plane area source is analyzed in this work. A practical orientation is maintained during the analysis by considering the problem of evaporating the water droplets in a natural fog located over an airport runway. The departures of this work from that of previous investigations include multiple anisotropic scattering, and the use of a relatively large finite source at a relatively low temperature to effect heat transfer to the surrounding fog.

The aerosol models used are isotropic monodispersions of water droplets. Volume extinction coefficients representative of natural fog, spanning the range from 2.5 to 80 km^{-1}, are investigated. Two ratios of absorption coefficient to extinction coefficient are analyzed, and a number of scattering functions, including isotropic and strong forward scattering, are investigated.

The analytical model is a probabilistic one and involves the Monte Carlo method of following individual photons, considered as energy bundles, along a series of probable paths and interaction events with the aerosol droplets. Direct radiative heat transfer to the droplets is modeled with monochromatic radiation at a wavelength of 10 microns. A long rectangular source and circular source are investigated because of the number of practical applications for which these shapes might provide a satisfactory model.

The results of the investigation are given as tables of the spatial distribution of absorption interactions in the aerosol, and as curves of the spatial locations having a common constant relative evaporation time called relative isochrons. Practical insight into the effect of various changes in the important radiative parameters is provided by a number of comparative illustrations that portray the significant findings of this research.

The direct energy exchange between the finite area source and the droplets of the surrounding semi-infinite aerosol is shown to be significant. The practical implications of this method of thermal dissipation of natural fog are appealing.

TABLE OF CONTENTS

LIST OF TABLES

LIST OF ILLUSTRATIONS

RADIATIVE HEAT TRANSFER FROM AN ARBITRARY PLANE SOURCE TO A SEMI-INFINITE AEROSOL

CHAPTER I

INTRODUCTION

The work reported here was conceived during discussions between the author and his advisor, Dr. T. J. Love, on the possibility of dispersing natural aerosols, such as fog, by means of radiative heat exchange. Certain aspects of the problem suggested that advantages might accrue to a system utilizing this mode of heat transfer.

As soon as the study of aerosols and their dispersal moves beyond a casual interest in the problem, the multidisciplinary complexion of the field emerges. A partial list of the disciplines that have been found to be of significant help in this study would include the related branches of physics, micrometeorology, mechanical engineering and geophysics. One of the major annoyances that arises, due to the multidisciplinary contributions, is the matter of vocabulary including such factors as dimensional units, definitions and nomenclature. Rather than add further confusion in this matter, this work will endeavor to use, or transform to, the vocabulary of radiative heat transfer as expressed by Love (1) or that of micrometeorology as exemplified by Munn (2).

Actually, the field of aerosols can be studied on the extensive macroscale of the astrophysicist or at the microscopic level of the physicist or chemist. This work will be interested in a physical scale which places the problem in the province of the mechanical engineer interested in radiative heat transfer and that of the micrometeorologist. According to Munn (2), micrometeorology is restricted to areas smaller than a city and depths within the surface boundary layer of the atmosphere, perhaps the lowest one hundred meters.

While the work reported herein is focused on natural fog, it has a much broader implication regarding the entire field of aerosols. The term aerosol is intended throughout to infer a suspension of very small particles in a gas. This is a less restrictive definition than originally intended, see Green and Lane (3); however, it does represent the current connotation of the word. Other names which are synonomous with aerosols are particulate clouds and disperse systems. Some of the common names given to specific examples of aerosols include fog, cloud, smoke, smog, haze, dust, and mist. Such names usually infer something of the nature and origin of the particulate cloud.

Aerosol research has tended to be associated with the physical properties of the particles or the optical properties of the composite disperse system. Two references that provide good background material on both the physical and optical properties are Green and Lane (3) and Middleton (4).

Leonardo da Vinci is credited with realizing the importance of particles in the atmosphere and called it a turbid medium. Schuster (5) considered a "foggy atmosphere" as one in which scattering played a significant role. The scattering aspect of an aerosol, including those composed of absorbing particles, is discussed by Love (6), Deirmendjian (7), Penndorf (8,9), and Van De Hulst (10). Rochelle (11) has an excellent bibliography on scattering.

Wagman (12) gives a candid account of problems in atmospheric aerosol research and points up the continuing difficulties in determining particle size, size distribution, and optical properties. The September 1967 issue of the Journal of the Air Pollution Control Association (13) is devoted to aerosol research current at the time of publication.

When attention is focused on natural fog it becomes apparent that there is considerable wisdom in the words of H. R. Byers as quoted by George (14), "It is unwise to attempt an exact definition of fog." As an example, clouds and fog are considered members of the same aerosol family. A commonly used definition states that fog is a cloud in contact with the ground.

There are many specific names given to fogs in order to differentiate them according to their origin and nature. One of the simplest differentiations is that between cold fog and warm fog. Cold fog refers to fog at or below 32°F. A cold fog, which is made up of water droplets, is in a supercooled and therefore, unstable state. For this reason it can be precipitated by the introduction of particles that cause the formation of ice particles in the fog. Dry ice and silver iodide have been found satisfactory for this function, and the economics of this type of fog dissipation is excellent. Several commercial airports use this system. The work of Belyaev and Pavlova (15) is a representative publication in this interesting field and touches on the meteorological implications of local fog dispersal. Hicks (16) reports on improved visibility near airports due to seeding with liquified propane. Ice fog, a subdivision of cold fog, is not in an unstable state and therefore does not dissipate under similar treatment. These fogs occur at very low temperatures, perhaps forty to fifty degrees below zero Fahrenheit, and the difficulties of dispersing them are related by Downie and Smith (17) and Robertson (18). Cold fog, including ice fog, is not studied directly in this research.

The warm fogs, formed above $32^{\circ}F$, are the ones on which the research reported in this dissertation is concentrated. The decision to analyze this particular type of fog only slightly simplifies the number of different kinds of fog that are encountered. As an example, the terms radiation fog, continental fog and mountain fog are used by various investigators more or less synonymously. These names are used for fogs which contain a rather large number of droplets per unit volume, have a relatively small mean droplet size, and are usually formed where small nuclei, such as those which might be created by industrial pollution, are available. The work of Arnulf and others (19) deals with this type of fog.

A second type of warm fog is often called advection fog, coastal fog or maritime fog. These fogs form near the seacoast and tend to have nuclei of salt crystals. Due to the hygroscopic nature of these nuclei, the droplets that are formed tend to be of relatively large mean size, though not so numerous per unit volume as those of the radiation fog. Houghton and Radford (20) have reported on their extensive work with this type of fog.

The discovery that natural fog will not form in the absence of condensation nuclei is credited to John Aitken, see Humphreys (21). While this discovery is over seventy five years old, knowledge of nuclei and their action in fog making is still rudimentary.

An interesting and informative survey of various methods that might be used for local fog dissipation has been reported by Houghton and Radford (22). Pilié (23) discusses coalescence, due to seeding with hygroscopic nuclei or electrostatic attraction, as a method of improving visibility through precipitation of the droplets and by decreasing the scattering due to fewer but larger drops. The general method being considered in the research reported herein is that of evaporation by heating, sometimes called thermal dissipation.

Downie and Smith (17) give an excellent summary of the various thermal systems that have been installed. In Great Britain, during World War II, a system under the code name of FIDO (Fog Investigation and Dispersal Operation) was used for fog dispersal at some airports. This system used oil burners, located at frequent intervals, in lines parallel to the runways. Although the system was considered successful for wartime operation, it did impose a significant economic consideration in that it used as much as one hundred thousand gallons of fuel oil per hour according to Green and Lane (3). A similar system was installed at Los Angeles International Airport. This system had an initial cost of $1,325,000 but was abandoned when it was unable to cope with a particularly heavy fog. This installation was far more sophisticated, in terms of centralized automatic control, than any used during World War II. FIDO type systems were also reported at Arcata, California and studied for possible installation at the large air base at Thule, Greenland.

A modification of the concept of a line of fuel oil burners is also reported by Downie and Smith (17). This system utilized turbojet aircraft engines, or turbojet aircraft, located appropriately along the runways, as sources of heat. The advantage of this system was considered to be its mobility and its ability to use surplus equipment available at a small initial cost.

A similar system, of slightly different concept, was investigated by Fiock and Dahl (24). It was composed of a series of stainless steel pipe-furnaces with the combustion taking place inside the pipes and producing pipe surface temperatures as high as 2000°F. The furnaces were placed at intervals along the runway and were designed to transfer heat by radiation to the fog. The system employed a reflector on each furnace to focus the heat over the runway. The results of these studies were discouraging, and no system of this type is known to have been installed.

One serious disadvantage common to the thermal systems reported above is their need for periodic maintenance and check out during that time of year when they are not in use. A second disadvantage of these on-site fossil fuel burning devices is that they produce an exhaust effluent which is rich in water vapor, thus contributing to the problem itself as well as its solution.

It is not surprising that other investigators have been aware of the advantages of radiative transfer to the aerosol. Houghton and Radford (22) report on the interest of Dr. Vannevar Bush in this problem. Dr. William P. Elliott (25), during a seminar on fog at the University of Oklahoma in November, 1967, encouraged the work of this investigation in view of the fact that it would include effects of all radiative transfer phenomena. Most of the previous work has been empirical in nature, and when an analytical approach was used, it usually treated the aerosol as a lumped system.

Among the advantages related to the use of the radiative mode of heat transfer is the fact that heat is transferred directly to fog droplets located at some distance from the source. There are certain transparent wavelength intervals, called "windows", for the suspending medium, humid air, which can be used to effect this direct transfer at a distance. This interval is located approximately between 7.5 and 13.5 microns, in wavelength, for water droplets suspended in air. The continuous absorption spectrum of the water droplets is well suited to this selective interval type transfer. The selection of the physical geometry of the source, as well as its disposition with regard to the aerosol to be dissipated, possesses a freedom of design not available for on-site fossil fuel fired systems. For example, the runway itself could be used as the source at an airport. Various source characteristics of radiative flux distribution can be achieved for a wide range of practical applications.

The objectives of the research undertaken by the author represent a significant departure from previously reported dissipation studies. This work will employ analytical tools to approach the problem and will endeavor to achieve significant numerical results by considering the disposition of radiant energy emitted by the source and its eventual sequence of interactions, including multiple scattering, with the surrounding semi-infinite aerosol.

The practical implications of this problem will be kept in mind throughout. The sources of emission selected will be large finite areas. One source will be a long narrow rectangle similar to an airport runway or taxi strip. A second source will be a circular pad similar to that which might be used as a landing pad at a heliport. These sources could be heated by imbedded pipes or other heating elements. These source configurations represent a distinct departure from previous work.

Because of the selection of the source, it will be imperative that the temperatures be kept at levels which will not impair the use of the facility for its intended purpose. Instead of using a small source at a high temperature such as reported by Fiock and Dahl (24), this study will use a large area at a moderate temperature. As will be pointed out later in this work, the temperatures selected will tend to cause a high percentage of the emitted flux to be in the wavelength interval which yields direct transfer to the droplets. In this way the source emissions can be used in an efficient manner.

The analytical model will take into account such matters as diffuse emission from the source, mean free path considerations for photons, multiple scattering, and absorption of the radiant energy by the aerosol. The analytical model will allow changes in the important parameters such as scattering function, absorption coefficient to extinction coefficient ratio, and physical model dimensions. Parameters characterizing the aerosol will also be subject to change within the limits of physical and optical properties established by referenced investigations.

In other words, a very general approach is desired which will allow a maximum of freedom in modeling both the source and the aerosol. The analytical model chosen is a probabilistic one and the solution is achieved through a Monte Carlo approach. This approach involves following individual photons, considered as individual energy bundles, along paths where probability considerations are employed at each point of decision or interaction. A large number of photon histories is required in order to be sure that the results of this method will be an accurate characterization of the radiative transfer.

The use of high speed digital computing facilities is essential to studies of this type. The IBM System 360/40 computer at the Merrick Laboratories of the University of Oklahoma, and the IBM System 360/50 computer at the University of Missouri at Rolla were found to be quite satisfactory for this purpose.

CHAPTER II

PHYSICAL MODEL

As implied by the title of this work, the approach developed can be applied to an arbitrary plane area source; however, as already noted in the introduction, attention will be centered on two geometries having strong practical implications. The first is a rectangular shape, long compared to its width. Such a shape might be a model for an airport runway, an airport taxi strip or a highway. The second shape is circular and might represent a helicopter landing pad or perhaps the crown of a piston in an internal combustion engine with an injected or aspirated aerosol in the combustion space. In either case, the radiant energy streaming from the source will produce interactions, scatterings and absorptions, in the surrounding aerosol. A gray diffuse source will be used so that the emitted energy is a function of neither direction nor wavelength.

It is the history of the interactions that is sought, namely to be able to determine where an interaction took place and what type of interaction it was. The practical nature of the models selected suggests that photons need not be followed after they achieve a relatively large distance of separation from the source. For the purpose of making this distance explicit, an imaginary boundary, called an accounting shell or envelope, is fixed surrounding the source. Interactions inside this shell are documented while the photon is considered to escape for accounting purposes when it moves outside the shell. The base plane, contiguous with the source, is an integral part of the accounting envelope. Since it will be of interest to know the specific locations of the photon interactions with the particles of the aerosol, the interior of the accounting shell is subdivided into a series of smaller volumes, called subspaces, in this work. The size of these subspaces is a compromise between several important factors. They should be large enough to have a sufficient number of interactions within each subspace to have statistical implications. They must be small enough to fit reasonably the criterion that the distribution of interactions within the subspace be nearly uniform. In addition, they should reflect the practical aspects of model geometry, including symmetry. The most realistic way to resolve the problem of subspace size and the requisite number of photon-particle interactions, is to select a physically meaningful disposition of subspaces and then determine the number of original emissions, or photon histories, required to achieve convergence to a stable numerical result.

The basic or reference coordinate system is a fixed system of orthogonal cartesian axes, which form a right handed rectangular system. All photon path tracing is done in spherical coordinates from a given point of emission or interaction to the next point of interaction. The spherical coordinates are related to a set of translated orthogonal cartesian axes whose origin is at the starting point of each photon path. The resulting spherical coordinates of each photon-particle interaction are then converted to rectangular coordinates in the translated coordinate system and then transformed back to rectangular coordinates related to the fixed basic or reference coordinate axes. Knowing the coordinates of the point of interaction, with respect to the reference system, allows the decision to be made as to whether the point is inside or outside the accounting envelope. An illustration of the reference axis system and the translated axis system, as employed in the analytical phase of this work, is given on Figure 4-7.

Long Rectangular Source

The physical model and reference coordinate system selected for this case is shown in Figure 2-1.

The very long diffuse source, radiating to a uniform dispersion of aerosol particles, supports the assumption that there would be a uniform axial distribution of interactions, except near the ends of the accounting envelope. The limits within which this assumption is valid have been investigated, for the radiative parameters used in this research, and the results are given in Appendix A.

The radial distribution of radiative interactions is the variable to be determined and mapped. Because of the symmetry of the source and the accounting shell, this mapping can be done in the Y-Z plane. Further, the mapping will be symmetrical about the Z axis, the left hand quadrant being a mirror image of the right hand quadrant. Since the interactions are not a function of axial position, it would be possible to consider a small representative source. Emissions from this source could be followed in three dimensions until an interaction is achieved. The point of the interaction can then be folded back into a two dimensional plot, indicative of the radial position only, in the Y-Z plane. This plane mapping just described might be thought of a a projection of the points of interaction.

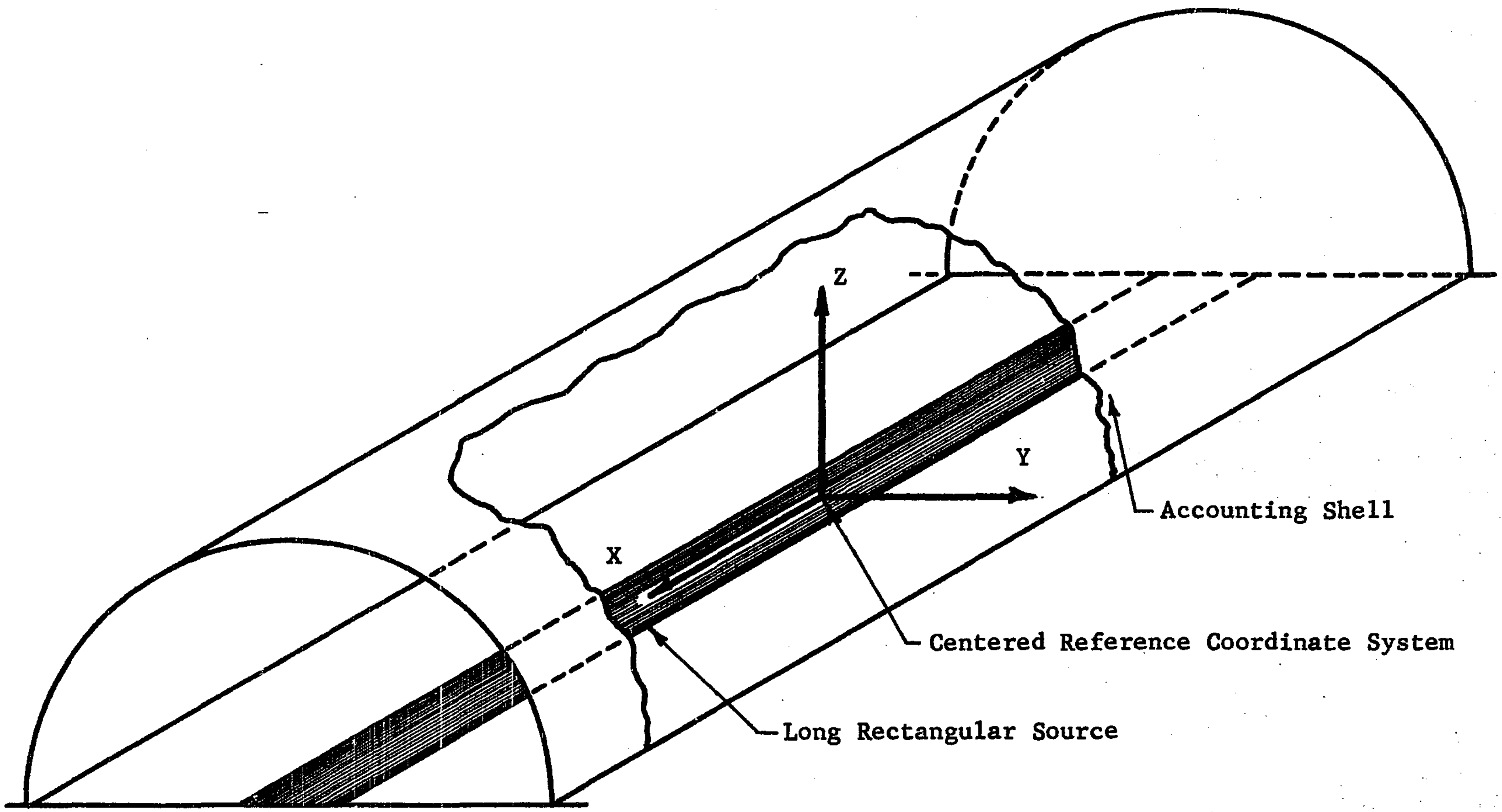

FIGURE 2-1 PHYSICAL MODEL AND REFERENCE COORDINATE SYSTEM FOR LONG RECTANGULAR SOURCE

In order to complement the physical and interaction symmetry, the right hand quadrant of the cross section of the accounting envelope is divided into sixty subspaces as indicated in Figure 2-2. A matrix type notation is used to designate these subspaces. This notation is used throughout the remainder of this research. The columns of the matrix are the rays, numbered one through six, while the rows of the matrix represent radial increments, numbered one through ten. A subspace designated V(4,7) refers to the space located along ray number four and in the radial increment numbered seven. This particular subspace is indicated on Figure 2-2. In a tabular array of subspace data, the numerical value associated with this particular subspace would be in the fourth column and in the seventh row.

Circular Source

The physical model and reference coordinate system selected for this case is shown in Figure 2-3. Again, the basic coordinate system is a right handed orthogonal cartesian system. Photon tracing is done in spherical coordinates as in the rectangular case, and transformed back to the fixed reference coordinate system as required.

Considering the circular source to be diffuse and the dispersion of the aerosol to be uniform, there should be a uniform distribution of interactions, for a fixed radial location described by a constant radius vector and polar angle, for all azimuthal positions. Any vertical cross section of the accounting shell, such as that provided by the Y-Z plane, would show an identical radial distribution of photon interactions. This would allow folding the three dimensional distribution into a two dimensional mapping in the Y-Z plane. Further, the distribution in such a plane would

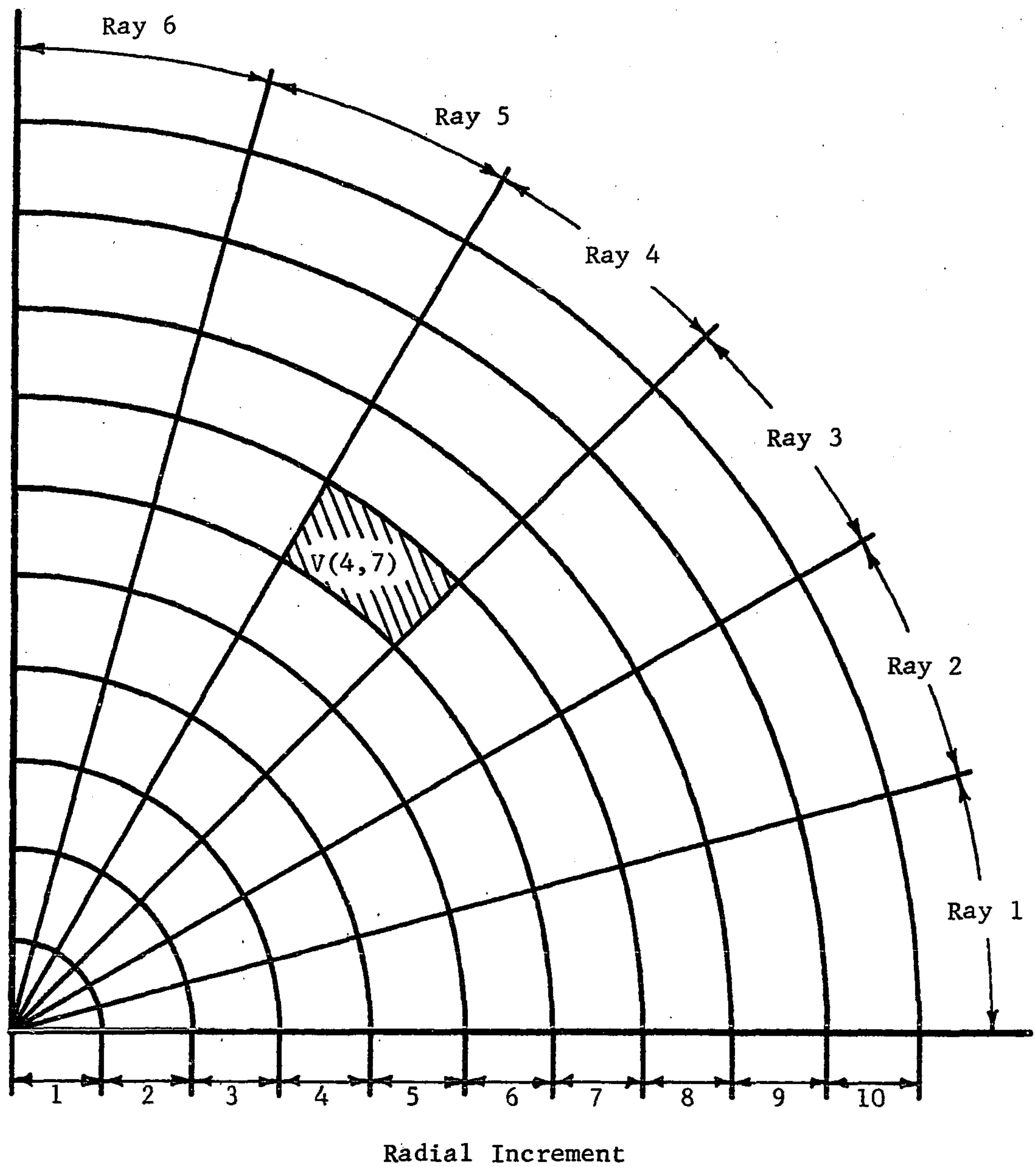

FIGURE 2-2 SUBDIVISION OF ACCOUNTING ENVELOPE CROSS SECTION INTO SIXTY SUBSPACES

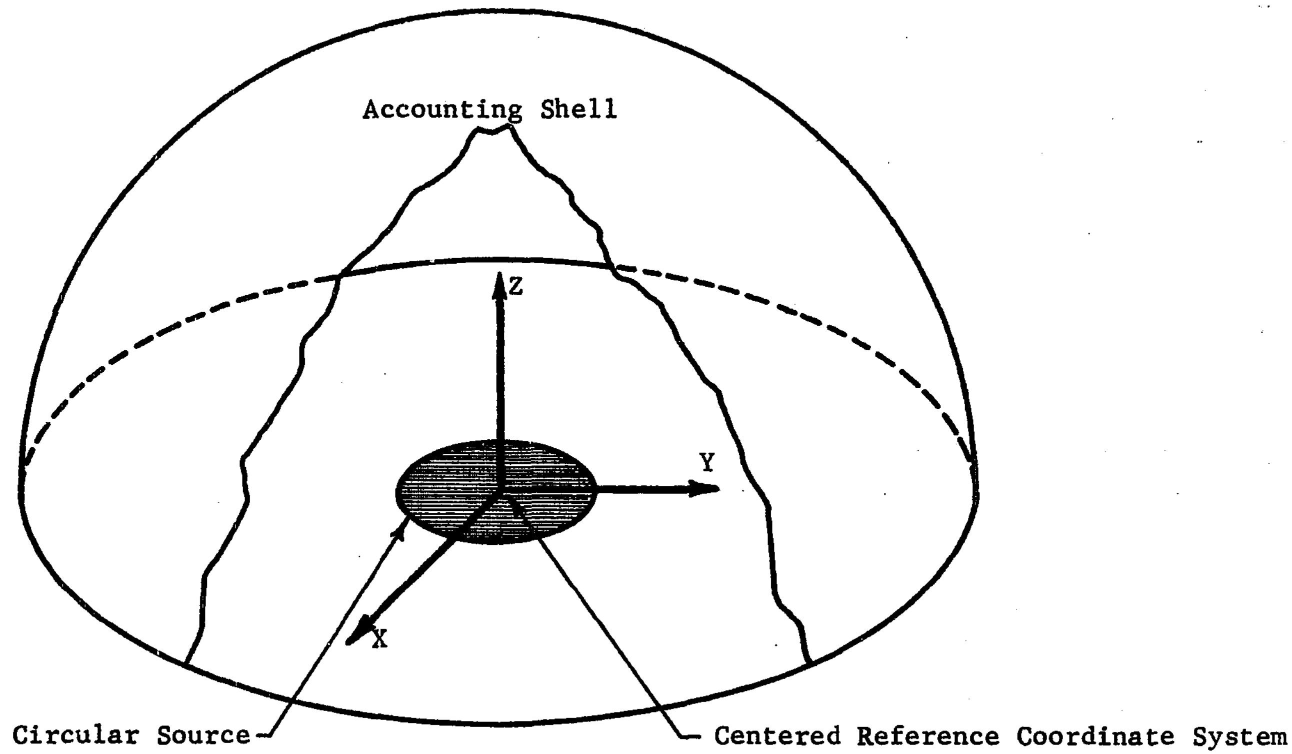

FIGURE 2-3 PHYSICAL MODEL AND REFERENCE COORDINATE SYSTEM FOR CIRCULAR SOURCE

be symmetrical about the Z axis. For this reason, only the right hand quadrant need be mapped in order to define the interaction distribution. The same subdivision of this mapping quadrant, as used for the rectangular source, would be satisfactory. Figure 2-2 will again represent the subspaces of the accounting envelope and the matrix designation for these spaces will remain unchanged.

Closure

The volumes represented by the subspace cross sections for the rectangular source and the circular source are not the same. Numerical evidence of this fact is given in Appendix F, where two explicit subdivisions of the accounting shells for these two source geometries are given.

The subspaces defined for both cases are considered small enough to have nearly uniform distribution of photon interactions. When numerical parameters, proportional to the photon interactions, are calculated for each subspace, these parameters are considered to act at the center of gravity of the subspace cross section.

This particular subdivision of the accounting envelope has been found to give satisfactory convergence to a stable numerical result, for a reasonable number of original emissions, and in a reasonable amount of computer time. This convergence is investigated and the results reported in Appendix B.

CHAPTER III

PROBABILITY AND MONTE CARLO BACKGROUND

The analytical approach to the research reported here is a probabilistic one. Photon histories are generated by following them from their point of origin on the areal source to their eventual escape from the accounting shell or absorption. All events in the history are governed by probability considerations. This approach is called the Monte Carlo method. The objective of this chapter is to set the necessary probability background so that it can be used to establish specific probability functions for the various events in the photon history. Insight into some of the more difficult questions raised by this analytical approach is provided by related studies reported in the appendices or through specific references.

Individuals with knowledge of probability theory can skip this chapter without impairing their understanding of the remainder of this dissertation.

Probability Background

In order that this work be reasonably complete, this section on probability has been included. It is certainly not a rigorous treatment of probability theory; however, every effort has been made to avoid any contradiction with fundamentals. Parzen (26) and Uspensky (27) have served as useful references in probability theory.

A phenomenon that can be characterized by the property that it does not always lead to the same outcome for a given set of conditions but does lead to outcomes which possess statistical regularity is called a random phenomenon. Photon interactions with the particles of an aerosol represent such phenomena. In other words, a number between 0 and 1 represents the fraction of the observations that result in a given outcome. A random event tends to achieve a stable frequency, for a given outcome, as the number of observations is increased toward infinity. The stable limit reached is called the probability of the event.

Some phenomena have only a finite number of possible outcomes, and, therefore, a countable number of event probabilities. This situation is called the discrete case, and the event probabilities are said to have discrete probability distribution. The toss of a coin or a die would be an example of a discrete probability phenomenon.

This type of probability distribution can be related by means of either probability function shown in Figure 3-1. The distributions shown in Figure 3-1 could be those for the toss of an unbiased coin. If outcome A represents heads and outcome B represents tails, the mass distribution function is equal for the two possible outcomes. Mass is analogous to the number of times a given outcome is observed, as a proportion of the total trials, in a large number of trials. On the basis of this definition of mass, the total mass would be equal to unity. If these event frequencies, or masses, are plotted in a cumulative stair step fashion at their related outcomes, the result is a distribution function curve that starts at zero, and in a finite number of discrete steps reaches a final value of unity.

Certain laws of probability are fundamental and must not be contradicted. Some of these fundamentals have already been introduced in the

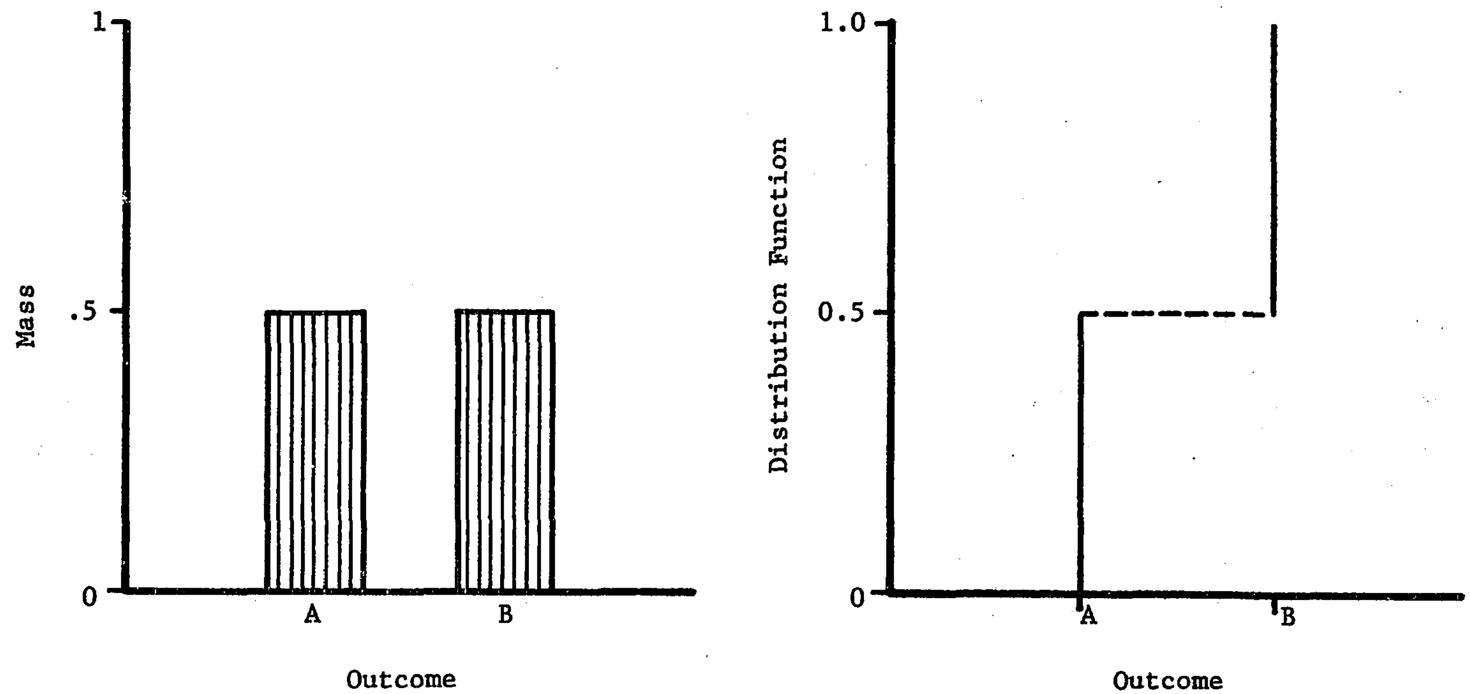

FIGURE 3-1 RELATED DISCRETE PROBABILITY MASS AND DISTRIBUTION FUNCTIONS

discrete probability discussion. First, the probability of any event cannot be negative. Second, any event must be one of the possible events out of the totality of all possibilities. The third fundamental states that the probability of the outcome of an event, being either of two possible outcomes, is the sum of the probabilities of the individual outcomes.

With the discrete distribution function known, visualize the following experiment. Assume that a very large supply of random numbers is available and that these numbers are uniformly distributed between 0 and 1. The experiment consists of selecting one of these random numbers, setting it equal to a value of the distribution function, and finding the outcome favored by this trial. If the experiment is repeated a very large number of times and if the random numbers are uniformly distributed, the frequency of a given outcome can be determined. This frequency is the number of experiments favorable to a given outcome compared to the total number of experiments. This frequency is the probability of occurrence of the specific outcome and is the same as could be derived from the mass function.

When a phenomenon has an infinity of possible outcomes, it is called the continuous case and has a continuous probability distribution. The probability of a specific outcome in this case is 0; however, the probability that the outcome will fall in a finite interval of the probability distribution is greater than 0 but less than 1. For example, consider a quality control problem. The length of an object, accurate to within a suitable tolerance, is measured to determine the fraction of total production that is acceptable. If an exact length were specified, no objects would be expected to meet this criterion.

The probability fundamentals cited for the discrete case are applicable here, with some additions and modifications. The first two fundamentals remain unchanged. The third fundamental for a continuous case would state that the sum of the probabilities of two adjacent intervals must equal the probability of a single interval extending over the same range as the two adjacent intervals. A fourth fundamental declares that an infinitesimal interval produces an infinitesimal probability.

A stochastic variable is a continuous variable quantity with a specified range of values, each of which can, by chance, be attained with a definite probability. Uniform probability distribution is said to exist when the probabilities attached to any two equal intervals within its range are equal.

In most continuous cases, uniform distribution of probability does not exist throughout the range of the stochastic variable. In these cases the following analogy is useful. Assume mass is distributed in the some continuous manner along a line. This distribution satisfies all the probability fundamentals outlined above. The mass contained in an infinitesimal increment of length is infinitesimal and so forth. Using a small increment of length allows the following definition of mean density over the increment.

$$\text{Mean Density} = \frac{\Delta m}{\Delta x}, \qquad 3.1$$

where Δm represents mass and Δx represents the length of the increment. If the length increment between x and $x + \Delta x$ is selected, the density at x can be written as

$$\text{Density at } x = \lim_{\Delta x \to 0} \frac{\Delta m}{\Delta x}. \qquad 3.2$$

This density can be generated for all values of x, and as a result, a continuous density function is generated. The resulting density function is called w(x) in this work.

Considering w(x) to be known, or that it can be approximated with satisfactory accuracy, the mass contained in any interval, (a,b), within the range of the length, can be represented by

$$\text{Mass}(a,b) = \int_a^b w(x)\,dx\,. \tag{3.3}$$

Existence of the intergral in equation 3.3 is assumed.

Now the analogy is carried over to the case of probability. Assuming probability is analogous to mass, it is possible to define a mean probability density comparable to the mass density of equation 3.1.

$$\text{Mean Probability Density} = \frac{P(x,x+\Delta x)}{\Delta x}\,, \tag{3.4}$$

where $P(x,x+\Delta x)$ represents the total probability contained between x and $x+\Delta x$. The variable, x, is now a stochastic variable.

Continuing the analogous line of development leads to

$$\text{Probability Density at } x = \lim_{\Delta x \to 0} \frac{P(x,x+\Delta x)}{\Delta x}\,, \tag{3.5}$$

which is comparable to equation 3.2.

This probability density function can be generated for all values of the stochastic variable within its range of definition. The function is continuous, for the case being studied, and is called f(x).

The probability that the stochastic variable lie in the interval (a,b), an interval within the range of definition, is

$$\frac{P(a,b)}{P(-\infty,+\infty)} = \frac{\int_a^b f(x)\,dx}{\int_{-\infty}^{+\infty} f(x)\,dx} = \int_a^b f(x)\,dx = P(a,b)\quad, \tag{3.6}$$

where P(a,b) is the probability that the stochastic variable lie within the interval indicated by the values in the parentheses.

This last expression is consistant with the fundamental laws of probability so long as

$$f(x) \geq 0 \text{ for all } x \quad ,$$

and

$$\int_{-\infty}^{+\infty} f(x)\,dx = 1 \quad .$$

The range of the stochastic variable may be either finite or infinite. If the lower limit of this range is assumed to be $-\infty$, and the point s is some value within the range of definition of the variable, a ratio of probabilities can be established as

$$\frac{P(-\infty,s)}{P(-\infty,+\infty)} = \frac{\int_{-\infty}^{s} f(x)\,dx}{\int_{-\infty}^{+\infty} f(x)\,dx} = \int_{-\infty}^{s} f(x)\,dx = F(s) \quad , \qquad 3.7$$

where F(s) is the probability that x will not exceed s. This proportion can be defined for all possible values of s, within the range of the stochastic variable x, giving rise to the distribution function F(x). F(x) is a monotonic increasing function since $f(x) \geq 0$ has been imposed as a fundamental restriction. The value of F(x) is 0 from $-\infty$ to the lower limit of the range of the stochastic variable, and is 1 from the upper limit of the range to $+\infty$.

Now f(x) is called the probability density function because it tells the rate at which probability is being added for a given increment of the stochastic variable. F(x) is called the probability distribution function and gives the cumulative probability from the lower limit to the upper limit of the range of the stochastic variable. The probability density function can be defined as equal to 0 everywhere outside the range. This information is illustrated on Figure 3-2, where the range has been selected as the interval (a,b).

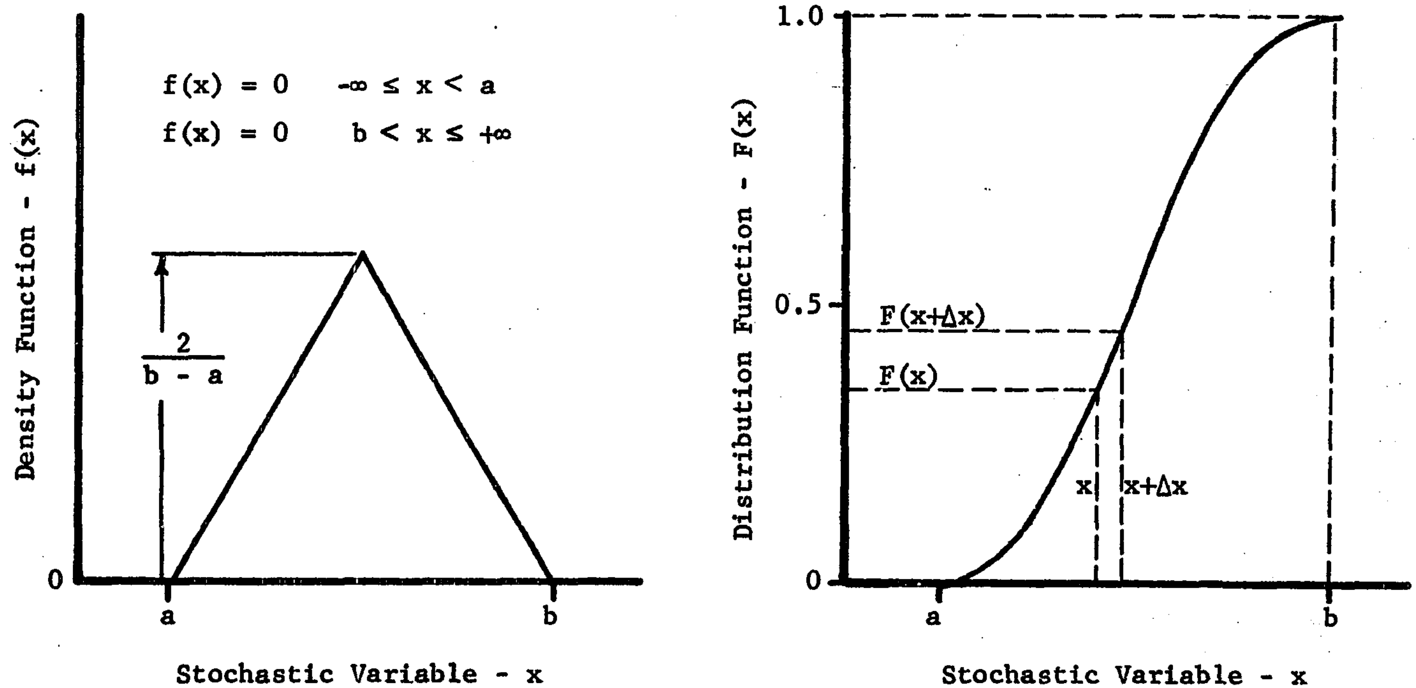

FIGURE 3-2 RELATED CONTINUOUS PROBABILITY DENSITY AND DISTRIBUTION FUNCTIONS

In the event a probability density or distribution function is not known, it is necessary to rely on physical laws and reasonable hypotheses to characterize the function.

As in the case of the discrete probability distribution, the next step is to visualize a series of experiments and their outcomes. Assume that a very large number, N_t, of random numbers, uniformly distributed between 0 and 1, is available. An experiment consists of selecting one of these random numbers and setting it equal to the distribution function. The object of the experiment is to determine the value of the stochastic variable x that is specified by this random selection of a value for the distribution function. The experiment must be repeated a very large number of times.

Appealing to the fundamentals of uniform distribution, the number of experiments that fall in the increment from F(x) to F(x+Δx), compared to the total number of experiments can be established as

$$\frac{N[F(x),F(x+\Delta x)]}{N_t} = F(x+\Delta x) - F(x) \; . \qquad 3.8$$

Since F(x) is a monotonic increasing function, there is a unique value of x for each value of the distribution function, or for each random number used to portray the distribution function in the experiments. For this reason the fraction of the total number of experiments that fall between F(x) and F(x+Δx) is equal to the fraction of the experiments that are favorable to the stochastic variable increment from x to x+Δx. In equation form this is

$$\frac{N(x,x+\Delta x)}{N_t} = F(x+\Delta x) - F(x) = \left[\frac{F(x+\Delta x) - F(x)}{\Delta x}\right]\Delta x \; . \qquad 3.9$$

This last equation tells the frequency, or probability, with which a random number, from a group of uniformly distributed between 0 and 1, generates a value for the stochastic variable within a given increment.

Rearranging equation 3.9, and taking the limit of both sides of the resulting expression, leads to

$$\lim_{\Delta x \to 0} \frac{N(x,x+\Delta x)}{N_t \cdot \Delta x} = \lim_{\Delta x \to 0} \left[\frac{F(x+\Delta x) - F(x)}{x}\right] = \frac{dF(x)}{dx} \quad . \qquad 3.10$$

Differentiating both sides of equation 3.7, which defines the probability distribution function, gives

$$dF(x) = f(x)dx \qquad \text{or} \qquad \frac{dF(x)}{dx} = f(x) \quad . \qquad 3.11$$

Substituting equation 3.11 into equation 3.10 yields

$$\lim_{\Delta x \to 0} \frac{N(x,x+\Delta x)}{N_t \cdot \Delta x} = \lim_{\Delta x \to 0} \frac{P(x,x+\Delta x)}{\Delta x} = f(x) \quad . \qquad 3.12$$

The implication of the above development is that if a large number of uniformly distributed random numbers, between 0 and 1, are used to characterize values of the distribution function, F(x), these experiments will generate the appropriate probability density function for the stochastic variable.

Joint probability plays an important role in the analytical model, and some mention of the fundamentals for this situation should prove helpful. First of all, the discussion is restricted to statistically independent variables, the type to be encountered in later developments.

As an example of this restriction, consider the random selection of the rectangular coordinates of a point on a large rectangular plane. By reason of statistical independence, the determination of a value for x within its range will not restrict in any way the value that y can take on within its range. Let the specific coordinates selected be designated by

X and Y. What is the probability that the coordinates chosen will fall within the small area $a < X < b$ and $c < Y < d$?

A natural extension of the development for the single variable case gives the probability that the two coordinates lie in the selected small area as

$$P(XY) = \int_a^b \int_c^d p(x,y)\,dxdy \quad , \qquad 3.13$$

where $p(x,y)$ is the joint probability density function and is subject to the same fundamental rules as the individual variable density function. These fundamentals are

$$p(x,y) \geq 0 \text{ for all } x \text{ and } y \ ,$$

and

$$\int_{-\infty}^{+\infty} \int_{-\infty}^{+\infty} p(x,y)\,dxdy = 1 \quad .$$

Due to the independent nature of the variables, the density functions are independent. The joint density function can be expressed as the product of the two independent density functions so that

$$p(x,y) = f(x) \cdot g(y) \quad . \qquad 3.14$$

Equation 3.13 can now be rewritten as

$$P(XY) = \int_a^b f(x)\,dx \cdot \int_c^d g(y)\,dy \quad . \qquad 3.15$$

This development allows the joint probability for the continuous case to be written symbolically as

$$P(XY) = P(a,b) \cdot P(c,d) \quad . \qquad 3.16$$

For the discrete case, with events A and B independent, the expression comparable to equation 3.16 is

$$P(AB) = P(A) \cdot P(B) \quad . \qquad 3.17$$

The implication of these last two equations simply is that for joint probabilities of independent variables or events, it is possible to reduce the problem to the solution of individual variable or event probabilities which are amenable to the treatment developed in this discussion on probability background.

Monte Carlo Method and Random Number Generation

The principles of the Monte Carlo method have already been introduced through the imaginary experiments conducted to generate probability mass and density functions from their related distribution functions. The method involves a large number of trials of the same experiment performed with random numbers uniformly distributed between 0 and 1. The random numbers are required to model the random phenomena, as defined at the beginning of the section on probability background. The uniform distribution is required so that the results of a large number of trials will reproduce the probability density function.

Although some problems may arise in defining what is meant by a large number of trials, once this factor has been established, the digital computer is ideally suited to carry out the experiments. From the previous discussion it can be said that a large number of trials has been reached when the frequencies of the related outcomes for the specific random events become stable.

Obtaining the random numbers with the requisite uniform distribution demanded by the Monte Carlo method can be a complex problem. Kovach (28) provides an excellent short description of this problem and its potential solutions. He points out the storage problems associated with the use of tabulated random numbers. The finite number of tabulated values available could be a handicap in a very large problem. He indicates the relatively inefficient computer use of such tabulated information and suggests consideration of other methods.

A second method involves computer generated random numbers, more accurately called pseudo-random numbers. This method has the advantage of being efficient in computer demands and generates practically limitless quantities without repeating. A further advantage is that all calculations can be repeated for program check out and comparison. Froberg (29) provides a short review of various methods used in programming computers to generate pseudo-random numbers.

The generation of pseudo-random numbers, hereafter simply called random numbers, was accomplished for this research by using a subroutine recommended by IBM for use with the IBM System/360 computer. All calculations were performed on this computer system either at the University of Oklahoma or at the University of Missouri at Rolla. This subroutine uses a power residue method, produces uniformly distributed numbers between 0 and 1, and will produce 2^{39} terms before repeating. A copy of this subroutine is attached to this work as part of Appendix H.

It was considered essential that the randomness of the numbers generated and the uniformity of their distribution be checked. The subroutine is initiated by the selection of a starting integer number. The IBM manual simply directs that this first entry may be any odd integer number with nine or fewer digits. In order to check this simple instruction, three different starting numbers were programmed, and the output of the subroutine evaluated as to randomness and distribution. A reasonably large number of generated random numbers was used. The outcome of this study is attached as Appendix C.

The outcome of this evaluation was reassuring, particularly in view of the fact that a rather finite sample size was used. None of the starting numbers was significantly better than the others. This subroutine was adopted as the mechanism for generating uniformly distributed random numbers as required to implement the Monte Carlo method used in this study.

CHAPTER IV

ANALYTICAL MODEL

The background has now been set for the application of the Monte Carlo method to the specific problem of this research. In order to set the overall objective for this chapter, a word description of the basic problem should prove helpful.

The problem is to determine what happens when a large number of photons, or bundles of energy, are released to interact with the particles of a surrounding aerosol. The coordinates of the point of release must be selected according to the temperature distribution and surface configuration of the source. Higher temperatures favor a higher rate of photon release. The direction of release must be selected on the basis of the shape and surface condition of the source. Once the photon has been released, it will continue in the same direction until it suffers an interaction with a particle. The distance traveled is called the free path of the photon, and this distance has a probability distribution. As soon as the end of a free path has been reached, an interaction, either a scattering or an absorption, will take place. In the event of a scattering, which represents a change in direction of the photon, the leaving direction will be governed by a probability distribution. The implication of continuing photon free paths between scattering interactions is clear. If the interaction is an absorption, the photon is captured and the photon history is terminated at the spatial point of absorption. Specific boundary conditions, such as penetration of the accounting shell, can be imposed to terminate photon histories. After termination, a new history is initiated by the release of another photon from the source. The generation of photon histories continues until sufficient histories have been documented to achieve stable event frequencies which are characteristic of the actual physical problem. Conductive and convective heat transfer to the droplet will not be considered in this work. The quasi-monochromatic nature of the radiant energy directly to the droplets of the aerosol allows each photon to characterize an equal amount of energy.

Among the references found most helpful in constructing this analytical model were those of Stockham (31), Howell and Perlmutter (32), Perlmutter and Howell (33), Howell and others (34), Corlett (35), and Campbell (36).

Emission Point

The physical shape of the source for the problems analyzed is either a plane circular area or a plane rectangular area. An isothermal source is chosen on the basis of the practical implications of the problem.

A differential area for the circular source is shown in Figure 4-1. With uniform source temperature, a uniform distribution of photon release is expected. In other words, the number of photons emitted from a differential area, dA, compared to the total emitted from the entire source is equal to the ratio of the differential area to the total area. This is comparable to saying that the probability of a photon being released from the differential area is

$$\frac{N(dA)}{N(A_t)} = \frac{r\ dr d\Phi}{\pi R^2} = p(r,\Phi)\, dr d\Phi \ , \qquad 4.1$$

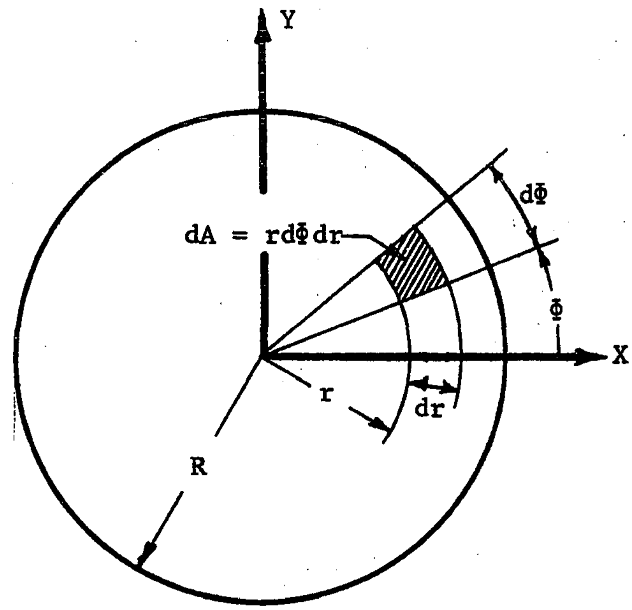

FIGURE 4-1 GEOMETRY OF CIRCULAR SOURCE

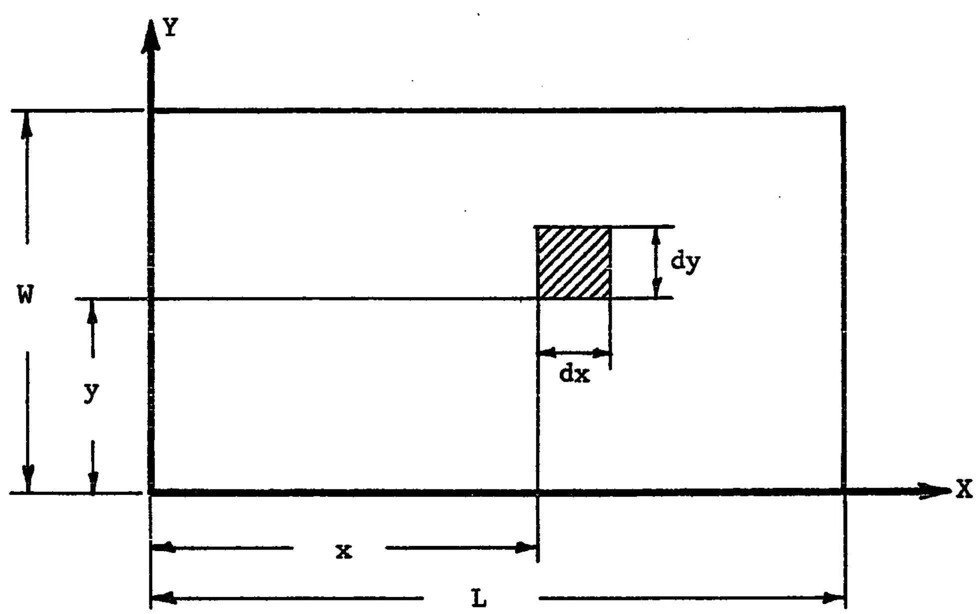

FIGURE 4-2 GEOMETRY OF RECTANGULAR SOURCE

where $N(dA)$ is the number of photons emitted from the differential area, dA, and $N(A_t)$ is the total number of photons emitted from the source. $p(r,\Phi)$ is the joint probability density function, and the other parameters are defined on Figure 4-1.

Now the fundamental laws of probability demand certain properties of a joint probability density function. These are

$$p(r,\Phi) \geq 0 \quad \text{which for this case is} \quad \frac{r}{\pi R^2} \geq 0 \ ,$$

and

$$\int_{-\infty}^{+\infty}\int_{-\infty}^{+\infty} p(r,\Phi)\,dr\,d\Phi = \int_0^{2\pi}\int_0^{R} \frac{r}{\pi R^2}\,dr\,d\Phi = 1 \ .$$

Both of these conditions are satisfied for this density function since r takes on only positive values, and the probability density function can be defined as 0 outside the domain of the problem as expressed in the limits of integration.

The variables r and Φ can be selected in a manner that is consistant with statistical independence so that

$$p(r,\Phi) = f(r) \cdot g(\Phi) \quad \text{or} \quad \frac{r}{\pi R^2} = \frac{2r}{R^2} \cdot \frac{1}{2\pi} \ . \qquad 4.2$$

The multiplication and division by a factor of 2 is required since the individual density functions must also meet fundamental probability laws.

Appealing to the previous development of probability principles,

$$P(0,r) = \int_0^{r} \frac{2r}{R^2}\,dr = F(r) = \frac{r^2}{R^2} \ , \qquad 4.3$$

and

$$P(0,\Phi) = \int_0^{\Phi} \frac{1}{2\pi}\,d\Phi = F(\Phi) = \frac{\Phi}{2\pi} \ , \qquad 4.4$$

where $F(r)$ and $F(\Phi)$ represent distribution functions for the individual variables. Knowledge of these distribution functions sets the stage for the series of experiments in which a large number of uniformly distributed random numbers is set equal to the distribution function. This method generates the appropriate probability density function for the joint distribution of the position variables r and Φ.

The differential area for the rectangular source is shown in Figure 4-2. With a constant temperature source, implying uniform distribution of photon emission, the probability that a photon is released from the differential area is

$$\frac{N(dA)}{N(A_t)} = \frac{dx \cdot dy}{L \cdot W} = p(x,y)\,dxdy \ , \qquad 4.5$$

where the elements of the equation are analogous to those in equation 4.1, or defined on Figure 4.2.

The first probability fundamental states that $p(x,y) \geq 0$ is required, and in this specific case the equivalent statement, $1/L \cdot W \geq 0$, is true for the coordinate system chosen. The second fundamental is also satisfied as shown by

$$\int_{-\infty}^{+\infty} \int_{-\infty}^{+\infty} p(x,y)\,dxdy = \int_0^W \int_0^L \frac{dxdy}{L \cdot W} = 1 \ .$$

Now the joint probability density function can be broken down into the product of the two individual independent density functions.

$$p(x,y) = f(x) \cdot g(y) = \frac{1}{L} \cdot \frac{1}{W} \ . \qquad 4.6$$

The individual probability distribution functions can be written as

$$P(0,x) = \int_0^x \frac{dx}{L} = F(x) = \frac{x}{L} \ , \qquad 4.7$$

and

$$P(0,y) = \int_0^y \frac{dy}{W} = F(y) = \frac{y}{W} \ . \qquad 4.8$$

While the previous developments are correct for the general case of finding the point of emission for an isothermal source of circular or rectangular shape, a simplification might be possible for the rectangular source. Figure 2-1 shows that the reference coordinate system was centered in the source in order to take advantage of symmetry for the source and accounting shell. The plan view of this source and coordinate system in the X-Y plane, the plane of the source, is shown on Figure 4-3.

Because of the uniform distribution of interactions in the axial direction, the length dimension is not a critical factor, except that length must be long enough to maintain small end losses. Appendix A provides an investigation of end losses and concludes that for a long rectangular source, such as an airport runway, the end losses are not significant over the majority of the emitting length. Neglecting end losses is comparable to assuming an infinite length, and this model, coupled with the uniform axial distribution of interactions, sets the stage for the simplification. Since the radial distribution of interactions is symmetrical about the Z axis, only the emissions from one half the width of the source need be considered. Since the interactions are uniform in the axial direction, any small rectangular source, half the width of the long rectangular source, should produce the same radial distribution of interactions as any other similar small area at another axial location. Such a small finite area is shown crosshatched on Figure 4-3. The reasoning that brought about the reduction to a small finite area as the source model could be used to further diminish the dimension in the axial direction, and in the limit of this reduction the source model becomes a line. The length of this line is one half the width of the long rectangular source, and it can be considered as a portion of the Y axis in the centered reference coordinate system.

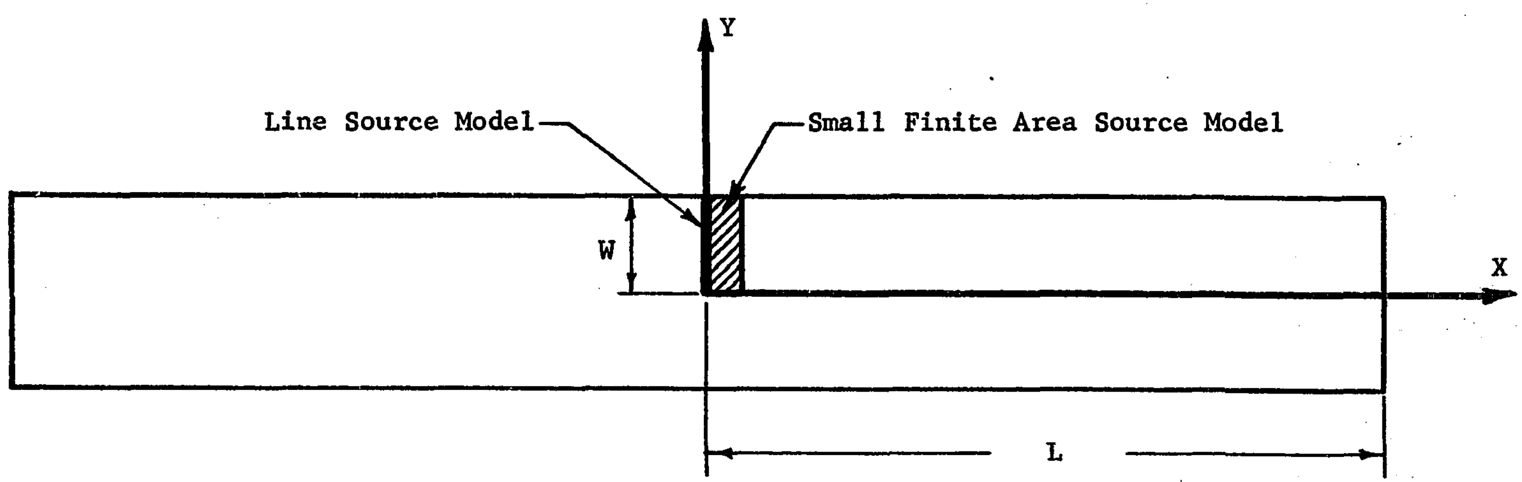

FIGURE 4-3 CENTERED COORDINATE SYSTEM FOR LONG RECTANGULAR SOURCE WITH SOURCE MODEL GEOMETRY

Photon releases from this line source model have three dimensional freedom of movement, and are followed in three dimensional space. Any interactions that occur are folded back into the positive quadrant of the Y-Z plane, immediately above the line source. The radial distribution of this folded mapping should be representative of that which exists at any axial location for the long rectangular source. The line source model is illustrated on Figure 4-3.

In order to test the validity of going from a small finite source model to the line source model, test programs were run. This comparative study of the source models is included in Appendix D. The results of the study confirm the fact that the line source does produce equivalent distribution of radial interactions.

When the source model is diminished to a line, there is no longer a need for a joint probability. Instead, uniform distribution along the line source dictates that the probability that an emission take place from a differential element of length, dy, would be

$$\frac{N(dy)}{N(W)} = \frac{dy}{W} = g(y)dy, \qquad 4.9$$

where N(dy) represents the number of photons released in the differential line increment, and N(W) represents the total number of emissions along the entire length of the source model.

This probability density function meets the probability fundamentals required of it in that

$$g(y) = \frac{1}{W} \geq 0 \quad \text{and} \quad \int_0^W \frac{dy}{W} = 1 \quad .$$

As a result, the related equation involving probability and the distribution function can be written as

$$P(0,y) = \int_0^y \frac{dy}{W} = F(y) = \frac{y}{W} \quad . \tag{4.10}$$

As would be expected, the elimination of one of the independent variables did not change the distribution function for the remaining variable.

A similar simplification is not possible for the circular source. The geometry of this source model is such that the area, and hence the photon emission, is concentrated toward the outer radius of the source. This distribution of area and emissions must be maintained in any model. Stockham (31) did diminish the area to a small sector in his research.

Direction of Emission

Now that a method of selecting emission points has been established, attention will be directed toward the question of what factors govern the direction of the emitted photon. In preparation for this analysis, a set of orthogonal cartesian axes is translated from the origin of the reference coordinate system to the established point of emission. The amount of translation in each coordinate direction was determined by the selection of the emission point. This concept of a translated axis system is used throughout this work and is illustrated on Figure 4-7.

The emission characteristics of a surface can be very involved. The energy leaving a surface configuration is usually composed of a term dependent on surface emittance and absolute temperature plus a term which sums the contribution of reflected energy from radiation incident on the surface. In general, both reflectance and emittance of a surface are functions of direction and wavelength. Love (1) devotes a chapter in his book to the radiative characteristics of surfaces.

It is not unusual to assume a gray diffuse surface as a model with which to work. One of the primary reasons for this assumption is the fact that it allows many practical problems to be modeled in a form tractable with existing methods of solution. The gray assumption implies that the radiosity characteristics are not a function of wavelength. The diffuse assumption, coupled with the choice of a black body, precludes any dependence of leaving radiation intensity on direction or reflectance.

For the purposes of this research the assumption of a diffuse, black body, source has been adopted. While this represents a limiting case for real surfaces, it allows the implications of various physical parameter changes to be studied.

With this specialization, the analysis of direction of emission can be initiated. A diffuse surface is defined as one with equal intensity of radiation in all directions. Intensity is defined as the radiating energy leaving a differential element of area on an imaginary plane within the time interval, t and t + dt, and having a direction of propagation contained in a differential solid angle, $d\omega$, whose central direction is normal to the imaginary plane. In order to fix the coordinate system used and indicate the physical aspects of this definition, Figure 4-4 has been included.

Now while the intensity is not a function of direction, the energy it characterizes certainly is. This can easily be visualized by imagining that one occupies a position directly over the source compared to a position off to one side. While the radiation will be as "bright" in either location, it is clear that the energy will be greater for the position immediately above the source.

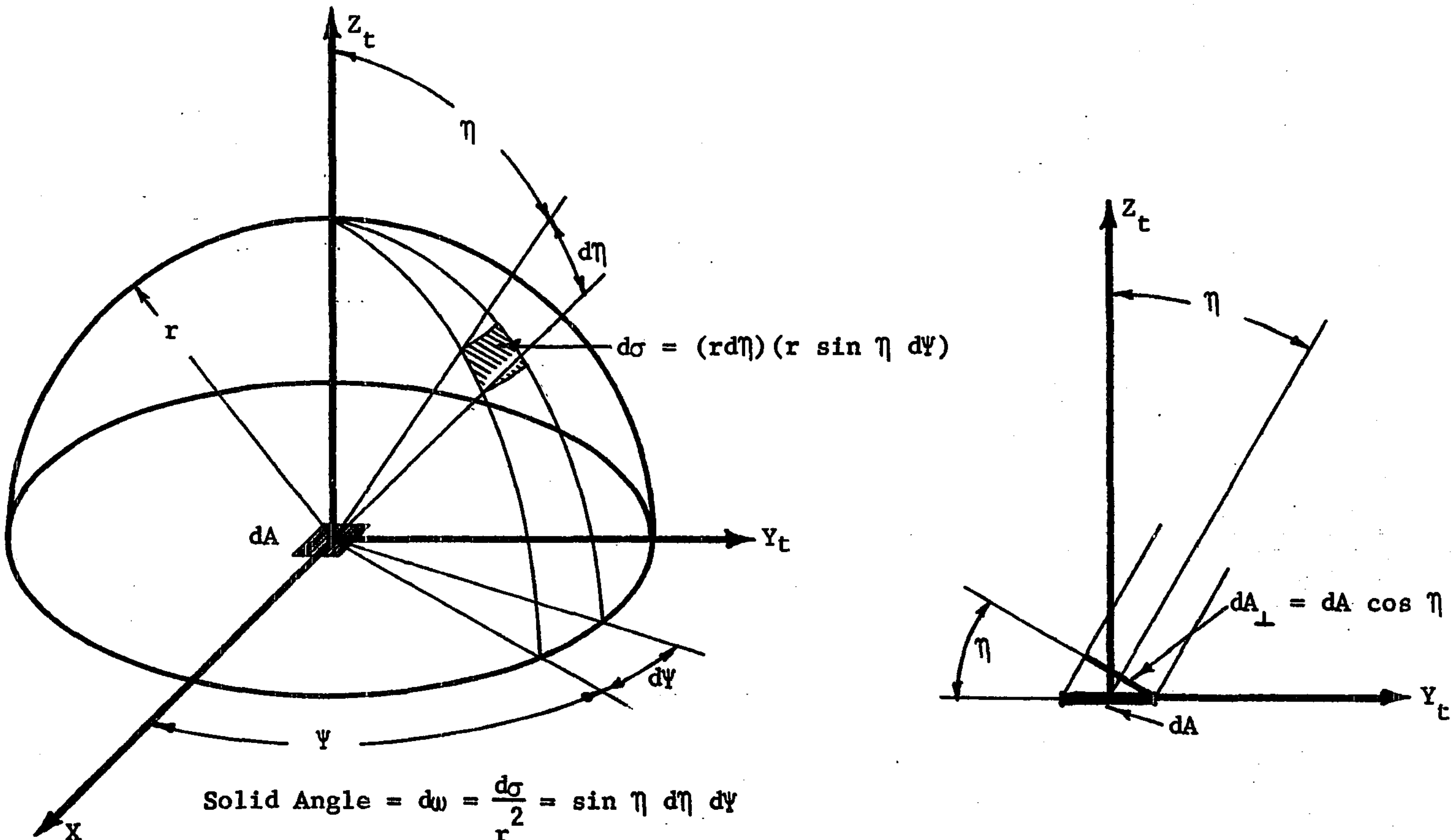

(a) (b)

FIGURE 4-4 GEOMETRY RELATED TO EMISSION FROM A DIFFUSE DIFFERENTIAL SURFACE

It should be noted that the imaginary plane through which the energy streams is perpendicular to the central direction of the solid angle. Figure 4-4b shows that for a fixed differential source area, dA, the imaginary area in the plane perpendicular to the central direction, $dA_{\perp} = dA \cos \eta$.

By appealing to the definition of intensity, the energy leaving through the differential solid angle, $d\omega$, is

$$E_{(d\omega)} = I \cdot dA \cos \eta \cdot dt \cdot \sin \eta \, d\eta d\Psi \quad . \qquad 4.11$$

The total energy leaving the differential surface, dA, could be expressed as

$$E_{(dA_t)} = \mathrm{FLUX} \cdot dA \cdot dt \quad . \qquad 4.12$$

For the diffuse case, where intensity is not a function of direction, the flux, q, can be written as

$$q = I \int_0^{2\pi} \int_0^{\frac{\pi}{2}} \sin \eta \cos \eta \, d\eta d\Psi = \pi I \quad . \qquad 4.13$$

The total energy leaving the differential area, dA, can be obtained by substituting the results of equation 4.13 into equation 4.12.

$$E_{(dA_t)} = \pi I \cdot dA \cdot dt \quad . \qquad 4.14$$

The previous developments can be summarized by saying that the number of photons, indicative of the energy, that escape through the surface of the hemisphere, in the differential surface element $d\sigma$, see Figure 4-4a, compared to the total number of photons released, is equal to the probability that a given photon released from the differential source area, dA, will escape through the differential area of the surrounding hemispherical surface, $d\sigma$. This verbal expression can be written in algebraic form as

$$\frac{N(d\sigma)}{N(dA_t)} = \frac{I \cdot dA \cdot dt \cdot \cos\eta \sin\eta \, d\eta d\Psi}{\pi I \cdot dA \cdot dt} , \qquad 4.15$$

or

$$\frac{\cos\eta \sin\eta \, d\eta d\Psi}{\pi} = p(\eta,\Psi) d\eta d\Psi \quad . \qquad 4.16$$

Appealing to the geometry given in Figure 4-4a, the angles are limited by

$$0 \le \eta \le \frac{\pi}{2} \qquad \text{and} \qquad 0 \le \Psi \le 2\pi \quad ,$$

and the fundamental rules of probability hold since

$$\frac{\cos\eta \sin\eta}{\pi} \ge 0 \qquad \text{and} \qquad \int_0^{2\pi} \int_0^{\frac{\pi}{2}} \frac{\cos\eta \sin\eta \, d\eta d\Psi}{\pi} = 1 \quad .$$

The variables in the joint probability density function given by equation 4.16 are statistically independent so that

$$p(\eta,\Psi) = f(\eta) \cdot g(\Psi) = 2 \sin\eta \cos\eta \cdot \frac{1}{2\pi} \quad . \qquad 4.17$$

As in a previous case, the factor of 2 in each individual density function is required so that the individual density functions also meet the fundamental probability rules. Following the procedures already established in the previous cases

$$P(0,\eta) = \int_0^{\eta} 2 \sin\eta \cos\eta \, d\eta = F(\eta)_E = \sin^2\eta \quad . \qquad 4.18$$

This distribution function can be rewritten as

$$F(\eta)_E = 1 - \cos^2\eta \qquad \text{or} \qquad \cos^2\eta = 1 - F(\eta)_E \quad .$$

Since the Monte Carlo method characterizes the distribution by a set of random numbers uniformly distributed between 0 and 1, the expression $1 - F(\eta)_E$ is simply another set of random numbers uniformly distributed between 0 and 1. Thus, $[1 - F(\eta)_E] = F'(\eta)_E$ can be considered as a new distribution function such that

$$F'(\eta)_E = \cos^2\eta \, . \qquad 4.19$$

The distribution function for the second variable in equation 4.17, Ψ, can be written as

$$P(0,\Psi) = \int_0^{\Psi} \frac{d\Psi}{2\pi} = F(\Psi)_E = \frac{\Psi}{2\pi} \, . \qquad 4.20$$

With the distribution functions known, it is now possible to generate a series of emissions whose directions properly reflect the probability density for a black diffuse source.

Photon Path Length

The photon has how been emitted from the surface and is moving in a known direction. The purpose of this section is to provide a means for determining how far the photon travels along this free path before it interacts with a particle of the aerosol. In other words, the distribution of photon free paths is sought.

A pencil of rays, passing through a particulate media, has its intensity attenuated with distance traveled because energy may be absorbed by the media or scattered outside the solid angle containing the pencil of rays. Figure 4-5 provides a physical description of this situation and sets up certain definitions for use in the development of the mathematical formulation.

The full equation of transfer, see Love (1), Sobolev (30), Sparrow and Cess (37), Kourganoff (38) or Chandraseknar (39), contains an emission term and a term to account for energy scattered into this pencil; however, the interest now is to be centered on the attenuation due to interactions. The attenuation of the ray in this circumstance is called extinction.

The decrease in intensity in traversing an incremental distance in a direction along the centerline of the ray is proportional to the energy,

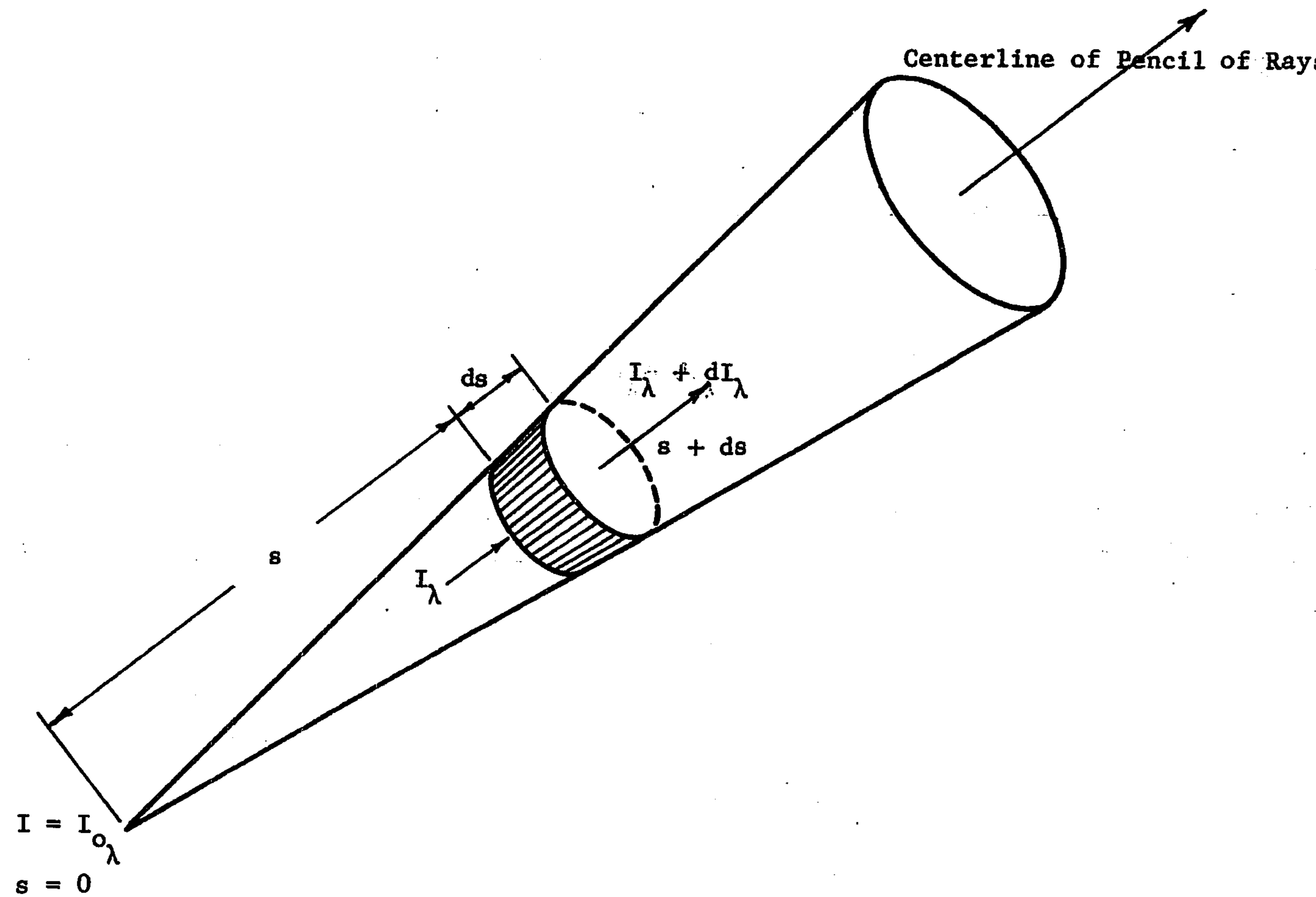

FIGURE 4-5 PHYSICAL DESCRIPTION AND DEFINITIONS FOR ATTENUATION OF INTENSITY

or the number of photons, entering the increment and to the distance of travel within the increment. The proportionality factor for the relationship is called attenuation coefficient, optical density, or volume extinction coefficient. The product of mass extinction coefficient and the mass density of the particulate medium being traversed is preferred by some, including Love (1).

Since this research has practical implications in the field of micrometeorology, the term optical density, designated as β_o, has been adopted for this work.

With this background the conservation of energy principle can be applied to the incremental volume shown in Figure 4-5. The resulting differential equation is

$$dI_\lambda = - \beta_o I_\lambda \, ds . \qquad 4.21$$

The subscript, λ, indicates that the equation is written for monochromatic radiation. Since the range of wavelengths providing direct energy transfer to the aerosol droplets has been limited to the interval between 7.5 and 13.5 microns, this work will assume that application of the above differential equation at a fixed wavelength of 10 microns will be a reasonable model for attenuation. The subscript will be dropped for convenience; however, a reminder will be inserted from time to time to assure that this assumption is not overlooked.

The optical density is considered to be a property of the medium and not a function of position or radiation intensity. With this factor in mind, the differential equation is amenable to separation of the variables in preparation for its solution.

$$\frac{dI}{I} = - \beta_o ds . \qquad 4.22$$

Direct integration leads to

$$\text{Ln } I = -\beta_o s + C \,. \qquad 4.23$$

From Figure 4-5, the initial condition is given that when $s = 0$, the intensity $I = I_o$. Using these conditions, the constant of integration can be evaluated as $C = \text{Ln } I_o$. Making this substitution in equation 4.23 leads to

$$\text{Ln } \frac{I}{I_o} = -\beta_o s \qquad \text{or} \qquad I = I_o e^{-\beta_o s} \,. \qquad 4.24$$

Substituting this formulation for its equivalent in equation 4.21 gives

$$dI = +\beta_o I_o e^{-\beta_o s} ds \,, \qquad 4.25$$

where the positive sign convention has been substituted in preparation for the developments that follow. The change in intensity reflects the positive number of photons that have suffered an interaction within the volume increment, from s to $s + ds$. The next step is to find the proportion of the photons that interact within this volume increment compared to the total original number of photons that entered the pencil of rays at $s = 0$. The original number of photons can be characterized by I_o. This development, in algebraic form is

$$\frac{dN(ds)}{N_t} = \frac{dI}{I_o} = \beta_o e^{-\beta_o s} ds = f(s) ds \,. \qquad 4.26$$

While this appears to be a probability density function, the fundamental rules must be applied. Optical density will always be a positive quantity, and by defining the distance, s, as having a range of definition which is strictly positive, the fundamentals are satisfied since

$$f(s) = \beta_o e^{-\beta_o s} \geq 0 \qquad \text{and} \qquad \int_0^{+\infty} \beta_o e^{-\beta_o s} ds = 1 \,,$$

for these restrictions.

Following the procedures that have been established by earlier examples, the probability distribution function can be written as

$$P(0,s) = \int_0^s \beta_o e^{-\beta_o s} ds = F(s) = -e^{-\beta_o s} + 1 \quad . \qquad 4.27$$

By line of argument similar to that used in the development of equation 4.19, it is possible to define a new distribution function such that

$$F'(s) = e^{-\beta_o s} \quad . \qquad 4.28$$

It is of some interest to establish the mean free path. To do this, the following line of development is considered. Accumulate the product of the number of photons that interact at a given distance and the distance of that interaction. Divide the above sum by the total number of original photons and the result will be a properly weighted mean free path (M.F.P.). In algebraic form

$$\text{M.F.P.} = \frac{\int_s sdN}{N_t} = \frac{\int_s sdI}{I_o} \quad . \qquad 4.29$$

Substituting for dI from equation 4.25 leads to

$$\text{M.F.P.} = \frac{\int_0^{+\infty} sI_o\beta_o e^{-\beta_o s} ds}{I_o} = \beta_o \int_0^{+\infty} se^{-\beta_o s} ds = \frac{1}{\beta_o} \quad . \qquad 4.30$$

Thus, the mean free path is the reciprocal of the optical density.

The Monte Carlo method can now be applied to the problem of finding the distance traveled by a photon before achieving an interaction with the particles of the aerosol. These free path lengths will be distributed, in a large number of trials, in keeping with the proper probability density function.

Extinction

At the end of the free path established by the last section, an interaction occurs. This interaction is one of the forms of extinction, either absorption or scattering. The fact that two possible outcomes are associated with this event leads to the conclusion that it is governed by discrete probability considerations. Appealing to the portion of this work on probability background, it is necessary to know the fraction of extinction interactions that result in each possible outcome in order to establish the probability of each outcome. The sum of the fractions encompassing the totality of possible outcomes, in this particular case two, must be unity according to probability fundamentals. Since only two outcomes are possible in the case being considered, the determination of the probability of either event is sufficient to fix that of the other.

The parameter which is found most frequently in the literature is the ratio of the scattering coefficient to the extinction coefficient, which is the same as the fraction of extinction interactions that result in the scattering outcome. This ratio does not have a commonly accepted name but is called albedo of a particle, see Sabolev (30), albedo for single scattering, see Chandrasekhar (39), or simply albedo, see Deirmendjian (7). Of course, the difference between this fraction and unity represents the fraction of interactions that are absorptions.

Thus, in order to generate the proper density distribution for this event, it is necessary simply to generate random numbers, uniformly distributed between 0 and 1, set them equal to the distribution function, and determine the outcome favorable to the event depicted by the random number. In other words, if the two outcomes are equally likely, the fraction of scatterings and absorptions would each be one half, and the distribution function would be one of equal steps. In this instance any random number below one half might be considered an absorption and any above one half would then be fixed as a scattering.

Once the type of extinction interaction is known, it will be necessary to perform certain analytical determinations for which a coordinate system is required. For this purpose, a set of cartesian orthogonal axes are translated to the point of the interaction from the reference axis system centered in the source. The origin of the translated system is at the point of the interaction.

Since the analysis of the two different types of extinction interaction are quite different for the most part, they are taken up separately. In any such separation it should be kept in mind that they do occur as the two possible outcomes of the interaction and are related in this manner.

Absorption

Extinction, as a result of absorption, is characterized by a photon being captured by the particle of the aerosol. The energy of the photon that is captured is transformed into some form of internal energy for the particle. In this research the aerosol is natural fog, and as a result, the internal energy transformation of the absorbed energy results in a small portion of the droplet volume being evaporated. This evaporation takes place at constant temperature, and for this reason the frequency of absorptions is indicative of the rate at which evaporation is occurring. The history of the photon is terminated at the point of absorption and the Monte Carlo solution is continued by returning to the source to initiate the release of another photon.

Scattering

In the event the interaction is determined to be a scattering, a rather more complicated analysis is required. Scattering can be defined as any change in direction of the incident photon. This change in direction can be caused by such factors as reflection, refraction, and diffraction. Love (1) and Sparrow and Cess (37) provide a good review of the fundamentals as well as a thorough discussion of the effect of scattering on the equation of transfer. Van De Hulst (10) and the work edited by Kerker (40) provide a more detailed study of the specifics involved in the scattering of electromagnetic waves.

Some definitions and assumptions are in order as a starting point. Coherent scattering, the condition that the scattered and incident radiation are at the same wavelength, is assumed to hold throughout this analysis. In keeping with other investigators, the effect of diffuse emission coupled with multiple reflections will be assumed to suppress polorization effects so that they can be neglected. Conservative scattering involves only particles with a real refractive index. In this case, the scattering coefficient is equal to the extinction coefficient and all photon interactions with particles are scatterings. While such scattering is not considered in the practical problems analyzed in this work, the computer programs written are general enough to be applied to the case of conservative scattering. Van De Hulst (10) reports that when the particles are more than three radii apart, a condition which is true for the natural aerosols studied in this research, the scattering function is not a function of the arrangement of the particles. In other words, the particles or droplets scatter independently of one another. For very low values of optical density, it would be possible to consider independent single scattering; however, the optical densities of interest in this research are such that the effects of multiple but independent scattering are used. The numerical information generated by the computer programs confirms the presence of multiple scattering. Since the medium through which the radiant energy is passing is homogeneous, the scattering is axially symmetric about the incident direction of the photon.

Isotropic scattering. The complexities of scattering analysis have led to simplifying assumptions which provide a means for attaining solutions to the equation of transfer. Isotropic scattering, which scatters incident intensity equally in all directions, is such an assumption. The validity of this assumption is tested in this work by carrying out numerical calculations involving isotropic scattering for comparison with other scattering functions. Rayleigh scattering, of special interest in molecular and very small particle distributions, is not investigated in this work. Stockham (31) calculated Rayleigh scattering for a particle cloud but found very little difference between it and isotropic scattering.

Since the scattered intensity is uniformly distributed in all directions, the amount of energy leaving the surface of an imaginary sphere, with the differential volume at its center, must be equal for equal surface areas. Figure 4-6 provides the geometrical background for the analysis that follows. From Figure 4-6 it can be seen that a differential surface element would have an area given by

$$d\sigma = r^2 \sin \eta_s \, d\eta_s \, d\Psi_s \quad . \qquad 4.31$$

In keeping with the methods of analysis used in previous cases, it can be said that the number of photons that will pass through this differen-

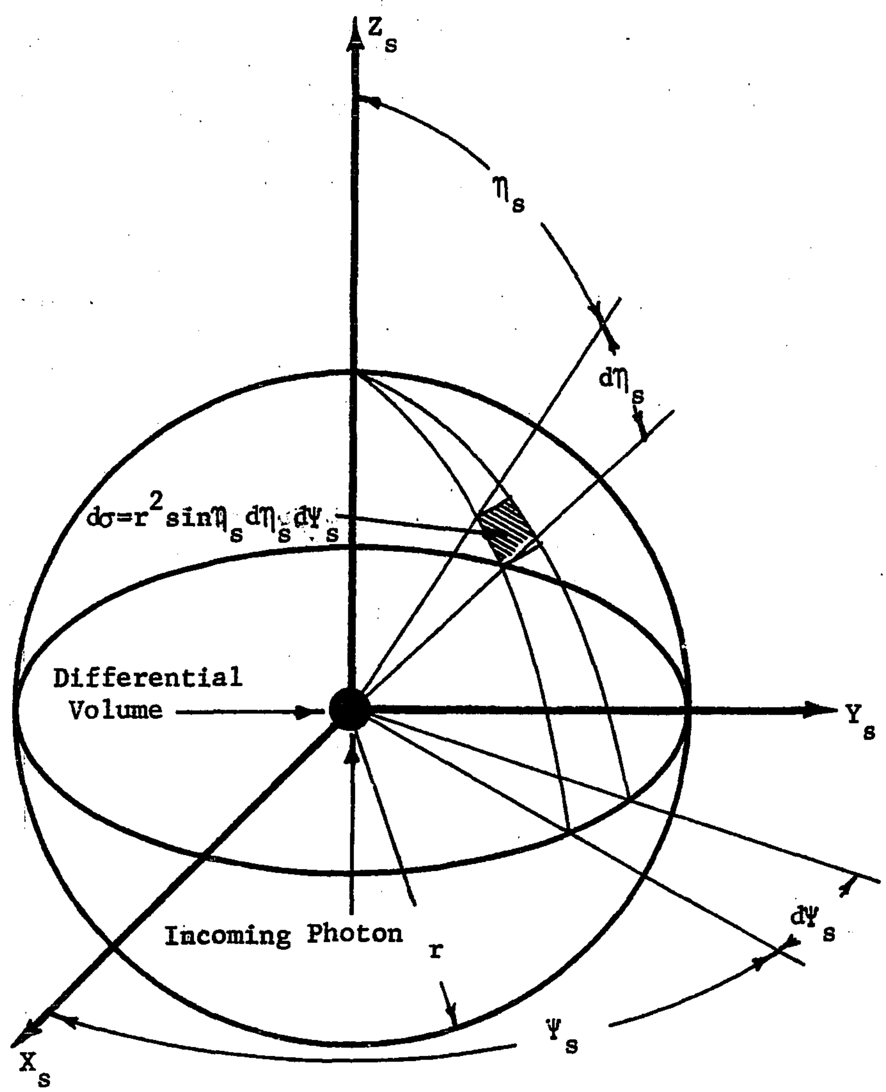

FIGURE 4-6 GEOMETRY RELATED TO ISOTROPIC SCATTERING

tial surface element, compared to the total energy passing through the surface of the sphere, will represent the probability that a given photon scattered from the differential volume will pass through the subject surface area element. This can be expressed in equation form as

$$\frac{N(d\sigma)}{N_t} = \frac{r^2 \sin \eta_s \, d\eta_s \, d\Psi_s}{4\pi r^2} = \frac{\sin \eta_s \, d\eta_s \, d\Psi_s}{4\pi} = p(\eta_s,\Psi_s) d\eta_s \, d\Psi_s \quad . \qquad 4.32$$

The polar angle has a range of definition such that $0 \leq \eta_s \leq \pi$. With this restriction, the probability fundamentals are satisfied by

$$p(\eta_s,\Psi_s) = \frac{\sin \eta_s}{4\pi} \geq 0 \quad \text{and} \quad \int_0^{2\pi} \int_0^{\pi} \frac{\sin \eta_s \, d\eta_s \, d\Psi_s}{4\pi} = 1 \quad .$$

Because of the statistical independence of the stochastic variables for this surface area element, it is possible to separate the joint probability density into the individual probability densities. For the range of definition of the variables involved, it is possible to show that the individual probability density functions satisfy all fundamental requirements since

$$f(\eta_s) = \frac{\sin \eta_s}{2} \geq 0 \qquad \text{and} \qquad \int_0^{\pi} \frac{\sin \eta_s}{2} \, d\eta_s = 1 \quad ,$$

as well as $g(\Psi_s) = \frac{1}{2\pi} \geq 0 \qquad \text{and} \qquad \int_0^{2\pi} \frac{d\Psi_s}{2\pi} = 1 \quad .$

With this background the necessary distribution functions can be constructed as

$$P(0,\eta_s) = \int_0^{\eta_s} \frac{\sin \eta_s}{2} \, d\eta_s = F(\eta_s)_I = -\frac{1}{2} \cos \eta_s + \frac{1}{2} \quad , \qquad 4.33$$

and

$$P(0,\Psi_s) = \int_0^{\Psi_s} \frac{d\Psi_s}{2\pi} = F(\Psi_s)_I = \frac{\Psi}{2\pi} \quad . \qquad 4.34$$

These distribution functions, when equated to a series of random numbers uniformly distributed between 0 and 1, will generate the appropriate probability density functions for the stochastic variables, η_s and Ψ_s, illustrated on Figure 4-6.

The previous development has used the scattering orthogonal cartesian coordinate system shown in Figure 4-6. The orientation of this coordinate system with respect to the translated and fixed reference coordinate systems was not required in the analysis of isotropic scattering. In fact, any orthogonal cartesian coordinate system with the same origin would lead to the same distribution of scattered energy. The actual orientation of the scattering coordinate system will be taken up in the section of this chapter on anisotropic scattering.

A differential volume, or droplet, emitting in a diffuse manner, would produce the same distribution of leaving energy as that resulting from isotropic scattering. The distribution functions for such emission would be defined in terms of a translated coordinate system with its origin at the point of emission. These distribution functions would be

$$F(\eta)_V = -\frac{1}{2}\cos\eta + \frac{1}{2} \quad , \qquad 4.35$$

and

$$F(\Psi)_V = \frac{\Psi}{2\pi} \quad , \qquad 4.36$$

where η is the polar angle measured in the translated coordinate system, and Ψ is the azimuthal angle in the same system. The equivalent nature of these distribution functions, coupled with the non-sensitive nature of the orientation of the coordinate system, can be used to advantage in constructing computer programs involving these radiative phenomena. The emission or re-emission from a differential volume is not considered in this work; however, isotropic scattering calculations have been based on the translated coordinate system in order to reduce calculation time.

Anisotropic scattering. As the name implies, this type of scattering shows a non-uniform distribution of scattered energy. Knowledge of the actual distribution of scattered energy is achieved by theoretical or empirical means. The applicable theoretical approach depends on the size parameter which is defined as the circumference of the scattering particle divided by the wavelength of the incident radiation. Considering the droplet sizes common to natural fog, and the wavelength model used in this research, the appropriate theoretical treatment is Mie theory.

The pioneering work of Gustav Mie on scattering from spherical particles is reported in Middleton (4), Van De Hulst (10), and others. Although it was originally a contribution to colloid chemistry, it has been the foundation for successful theoretical work on natural fog and haze. For a homogeneous cloud containing spheres of a single size, a monodispersion, the Mie solution for scattering distribution depends on the size parameter and the relative index of refraction of the spherical particles. Solutions are based on a monochromatic incident beam which is reasonably satisfied by the 10 micron wavelength model chosen for this work. Penndorf (8,9) has published some helpful background information and numerical data on the implementation at this theory for water droplets.

The fact that the natural aerosols are polydispersions, that is they contain a number of sizes of spheres even though they may be distributed isotropically, creates a problem in using Mie theory. Deirmendjian (7), using a realistic size distribution of particles, employed a superposition of Mie solutions for different droplet sizes to achieve a composite scattering function. This scattering function, which is empirically verified by Pritchard and Elliott (41), will be used as a model for this research.

It is believed that this scattering model is realistic since it combines the theoretical and empirical approaches in a complimentary manner.

Before displaying the functional form of this scattering function, more of the background required to understand the meaning and application of the scattering function will be developed. Up to this point the term scattering function has been used in a descriptive sense. Analytical work will demand an explicit definition in terms of a specific coordinate system, the scattering coordinate system. In order that scattering can be related to other photon events, it is necessary to fix the scattering coordinate system in some unique relationship to the translated and reference coordinate systems.

In keeping with the procedures established for photon tracing, the origin of a set of translated orthogonal cartesian axes is moved to the point of the scattering interaction. Imagine that second set of orthogonal cartesian axes, the scattering axis system, is fixed with the same origin but with the negative extension of the Z_s axis lying coincident with the path of the incoming photon. The coordinates and angles in the scattering coordinate system will all be subscripted with an s. While the Z_s axis is now fixed in space, the other axes can take on an infinite number of rotated positions. In order to fix these axes in such a way as to make analytical manipulations possible, the X_s-Y_s axis system is rotated about the Z_s axis until the X_s axis lies in the X_t-Y_t plane of the translated axis system with a common origin. The translated and scattering coordinate systems are now fixed in space, and analytical work can proceed. Figure 4-7 illustrates this combined system of related axes with a common origin.

With knowledge of the polar and azimuthal angles in the scattering coordinate system, it would be possible to transform any free path vector

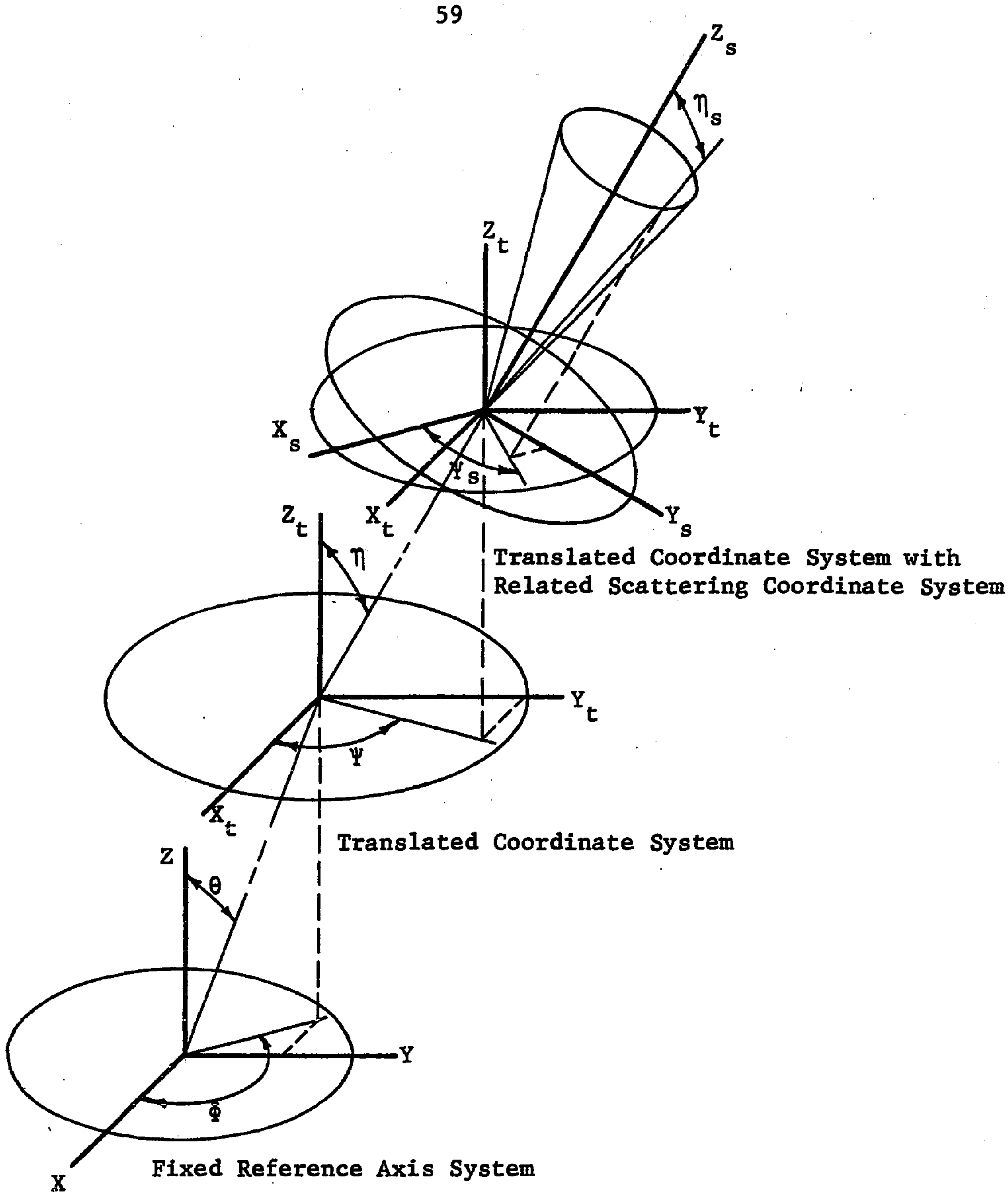

FIGURE 4-7 RELATED COORDINATE SYSTEMS USED IN THIS WORK

of known length, ℓ_s, into the three components x_s, y_s, and z_s in this coordinate system.

$$x_s = \ell_s \sin \eta_s \cos \Psi_s \,, \qquad 4.37$$

$$y_s = \ell_s \sin \eta_s \sin \Psi_s \,, \qquad 4.38$$

and

$$z_s = \ell_s \cos \eta_s \,, \qquad 4.39$$

where η_s is the polar angle in the scattering coordinate system and Ψ_s is the azimuthal angle as indicated on Figure 4-7.

The next operation requires that these components be further transformed into the components of the translated coordinate system with common origin. Such a transformation is made possible by the unique relationship established between the two systems. The y_s and z_s components, in general, will make a contribution to each coordinate component in the translated system; however, the x_s component lies in the X_t-Y_t plane of the translated axis system and makes no contribution to the z_t component. The requisite transformations are given by

$$x_t = x_s \sin \Psi + y_s \cos \eta \cos \Psi + z_s \sin \eta \cos \Psi \,, \qquad 4.40$$

$$y_t = -x_s \cos \Psi + y_s \cos \eta \sin \Psi + z_s \sin \eta \sin \Psi \,, \qquad 4.41$$

and

$$z_t = -y_s \sin \eta + z_s \cos \eta \,. \qquad 4.42$$

The angles η and Ψ are those which were defined in terms of the translated axis system for the incoming photon, illustrated on Figure 4-7. The components in the translated coordinate system can easily be converted to components in the fixed reference coordinate system.

The change in direction of the scattered photon can now be fixed by a knowledge of the polar and azimuthal angles of the scattered photon in the scattering coordinate system. The discussion which follows is centered on the scattering coordinate system with the understanding that transformation to any of the other related coordinate systems can be effected.

The intensity method of depicting the scattered energy is not uncommon. Because of the axially symmetric nature of the scattering, intensity as a function of polar angle is sufficient to establish the scattered energy distribution. The small droplet has radiant energy brought to it by photons. If the stream of photons is scattered by the element of volume represented by the droplet, the total energy scattered, collected over all possible directions, must equal the original incident energy because of conservation of energy principles.

The collection of scattered energy might be visualized in terms of the enumeration of energy escaping through an imaginary spherical shell with the scattering volume at its center. The physical picture for this concept is shown in Figure 4-6. The intensity leaving the imaginary spherical surface, which is the generating function for energy, is a function of polar angle and is axially symmetric about the forward direction. The scattered intensity is also a function of the incident energy. In applied work, conformity to some standard which is not dependent on incident energy is desirable. Normalized intensity, $\overline{I}(\eta_s)$, is a common standard in this regard and is defined to satisfy

$$\frac{1}{4\pi}\int_{\Omega}\overline{I}(\eta_s)\,d\omega = 1 \quad , \qquad 4.43$$

where $d\omega$ is the differential solid angle and Ω represents integration over all solid angles. The actual intensity is multiplied by an appropriate normalizing constant to bring about conformity with equation 4.43. Chandrasekhar (39) calls the reciprocal of this normalizing constant the average intensity.

This equation has the familiar look of a probability function. It sums the fractions of the incident energy that favor escape through the imaginary shell within the differential solid angle $d\omega$ located by the polar angle η_s. Since the fraction of incident energy favoring a given direction of scatter is analogous to the frequency with which incident photons will be scattered in that direction, the desired probability function has been formulated.

Because $d\omega = \sin \eta_s \, d\eta_s \, d\Psi_s$, equation 4.43 can be transformed to

$$\int_0^{2\pi} \int_0^{\pi} \frac{\bar{I}(\eta_s) \sin \eta_s}{4\pi} \, d\eta_s \, d\Psi_s = 1 \quad , \qquad 4.44$$

where η_s and Ψ_s are the scattering polar and azimuthal angles respectively. Since the probability density function in the integrand will be equal to or greater than zero, on the basis that the normalized intensity is equal to or greater than zero, the requisite probability fundamentals for a joint probability density function are met. Because the variables of this joint probability density function are statistically independent, they can be separated so that

$$p(\eta_s,\Psi_s) = \frac{\bar{I}(\eta_s) \sin \eta_s}{4\pi} = f(\eta_s) \cdot g(\Psi_s) = \frac{\bar{I}(\eta_s) \sin \eta_s}{2} \cdot \frac{1}{2\pi} \quad . \qquad 4.45$$

The individual probability density function for azimuthal angle has previously been shown to meet the required probability fundamentals. The distribution function for the equally likely azimuthal angle, representing axially symmetric scattering, can be written as

$$P(0,\Psi_s) = \int_0^{\Psi_s} \frac{d\Psi_s}{2\pi} = F(\Psi_s)_A = \frac{\Psi_s}{2\pi} \quad . \qquad 4.46$$

In the case of the probability density function associated with the polar angle, η_s, a somewhat more difficult situation exists in obtaining the related distribution function. This individual density function is equal to or greater than zero on the basis of restrictions already imposed on the joint function. Also,

$$\int_0^{\pi} \frac{\bar{I}(\eta_s)\sin\eta_s}{2}\, d\eta_s = 1$$

must be true in order that equation 4.44 be satisfied. In a symbolic way the probability distribution function for polar angle can be written according to the established format as

$$P(0,\eta_s) = \int_0^{\eta_s} \frac{\bar{I}(\eta_s)\sin\eta_s}{2}\, d\eta_s = F(\eta_s)_A \quad . \qquad 4.47$$

Unfortunately, the integral in equation 4.47 is not easily evaluated for most real normalized intensity functions. This difficulty has led various investigators to use different schemes to relate the probability distribution function of equation 4.47 to the specific polar angle to be generated as a random variable by the application of the Monte Carlo method. Stockham (31) used an area matching scheme to provide an adequate model for this integral. Schmidt (42) established a table of values for the integral and then employed a computer look-up scheme to interpolate the table. This work uses a somewhat different approach.

The starting point is to obtain an appropriate normalized intensity distribution curve such as that shown in Figure 4-8. With this curve, it is possible to evaluate the probability density function for polar angle, $\frac{\bar{I}(\eta_s)\sin\eta_s}{2}$, at as many specific values of polar angle as required to establish a smooth curve over the range of the polar angle. The probability density function for polar angle established by the previous step can be graphically integrated for increasing values of polar angle. The curve

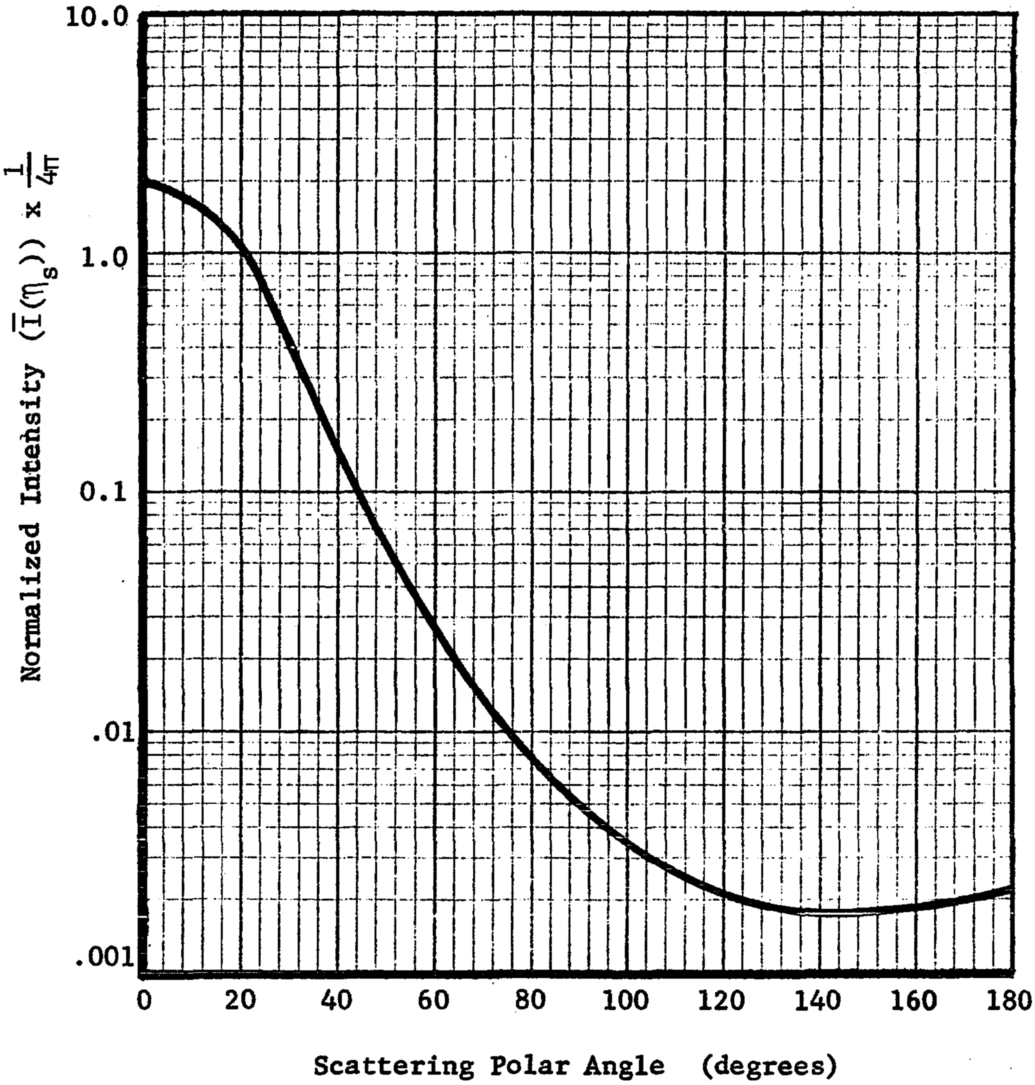

FIGURE 4-8 TYPICAL NORMALIZED INTENSITY DISTRIBUTION

generated in this way is the appropriate probability distribution function for polar angle. The probability distribution function that results from the application of this procedure to Figure 4-8, is illustrated on Figure 4-9.

For this research, the normalized intensity distribution curve comparable to Figure 4-8 is such that a simple mathematical expression can be used to provide a satisfactory approximation for the probability distribution function for scattering polar angle.

Now that the direction of the scattered photon can be established, it is essential to know how far it will go before achieving the next interaction with a particle of the aerosol. This is simply another application of the free path calculation already analyzed for the homogeneous aerosol model. The result of this analysis was reported as a probability distribution function by equation 4.28. In the event of an aerosol that is not homogeneous, a more difficult analysis would be required.

The distance traveled, coupled with the polar and azimuthal angles describing the path, can be transformed into components of the rectangular scattering coordinate system by equations 4.37, 4.38, and 4.39. These components, in turn, can be transformed into components in the related translated coordinate system with common origin by equations 4.40, 4.41, and 4.42. In this manner, the point at which the free path of the scattered photon is terminated can be established in terms of the fixed reference coordinate system.

Closure

All possible events in a photon history have now been analyzed individually. It is now possible to synthesize a typical history of a photon

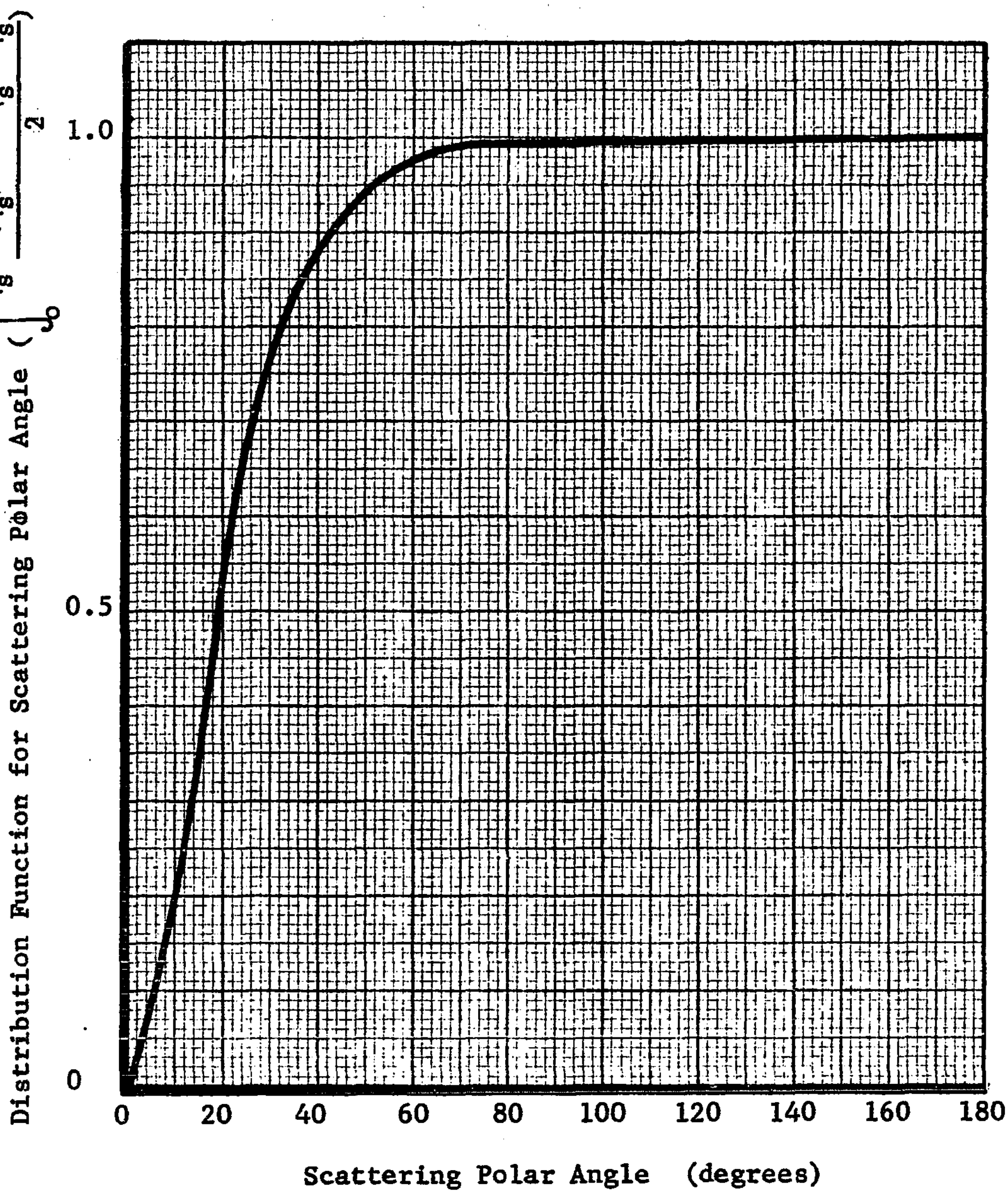

FIGURE 4-9 TYPICAL PROBABILITY DISTRIBUTION FUNCTION FOR SCATTERING POLAR ANGLE

from emission through a probable sequence of free paths and interactions until a history terminating event takes place. Only two events can cause the termination of a history, namely, an escape from the accounting shell or an absorption. Since an escape takes the photon to a spatial point where it is assumed that no significant contribution to the problem is possible, this type of termination is simply registered as an escape and a new photon history is initiated. In the case that the terminating event is an absorption within the accounting shell, it is relevant to ask where the absorption took place. The specific coordinates at the end of each free path have been calculated throughout the photon history with respect to the fixed reference coordinate system of the problem. The accounting shell has been established with reference to this same fixed coordinate system. For absorption interactions within the accounting shell, it would be possible to register individual coördinates for each such absorption. This type of data format would be very difficult to evaluate. To make evaluation more meaningful, the accounting shell was subdivided into subspaces or volumes, according to the discussion in Chapter II, and the subspace within which an absorption takes place can be determined. The absorptions within each subspace are counted until a sufficient number of them have taken place to cause their frequency of occurrence compared to original emissions to attain a steady value. This spatial absorption data can be used to obtain some interesting numerical results, pertinent in practical problems associated with natural aerosols.

CHAPTER V

AEROSOL MODEL

The analytical model just completed, coupled with the physical model developed in Chapter II, could be used to analyze a wide variety of aerosols and their radiative interactions. Since this study is predicated on natural fog as the aerosol, it is essential to develop specific information regarding its physical and optical properties. Given a correlated set of physical and optical properties, it would be possible to pose a number of problems for radiative transfer analysis.

The study of the physical and optical properties of natural fog has been of considerable interest to investigators for years. Best (43), Middleton (4), and Green and Lane (3) give concise historical reviews of work done in clouds and fog. Unfortunately, even these aerosols, although they have commanded considerable attention, have not yielded properties which can be used without considerable caution according to George (14), Green and Lane (3), and Wagman (12). Some of the reasons for this caution will become evident in the discussion which follows.

Although some investigators have made coordinated studies, physical and optical properties are often studied separately, even though it is recognized that they are related properties. aufm Kampe and Weickmann (44), in their paper concerning visibility and liquid content in clouds, along with the subsequent correspondence by Neiburger (45) and Fritz (46), point up the difficulties in relating physical and optical properties.

Physical Properties

The physical property of specific interest in this work is the liquid water content (LWC) of clouds and fog. One method of obtaining this information might involve the enumeration of water droplets and their sizes as found in a fixed volume of the aerosol. A second method might involve the collection of all moisture, both liquid and vapor, in a hygroscopic filtering device. If a fixed volume is filtered, the vapor contribution can be subtracted from the total through relative humidity considerations, leaving the liquid water content.

While the second, or composite, approach is conceded to be more accurate, it does not produce a physical picture of the distribution of this liquid as a finite number of droplets. For example, Shifrin is taken to task by Feigelson (47) for considering the water content as being physically modeled as a sheet of liquid through which the transfer process takes place. Because the actual transfer mechanism is dependent on the discrete droplets in the aerosol, this aspect of the liquid content will be pursued further.

Droplet Size Distribution

A considerable number of investigations have been made concerning the size distribution of fog and cloud water droplets. Best (43), Houghton (48), Houghton and Radford (20), Webb (49), Eldridge (50), and Thompson, Ward and Zinky (51) are representative publications on this aspect of the problem. In a general way the investigators agree that the distribution is unimodal in character and has a typical distribution curve similar to that shown on Figure 5-1.

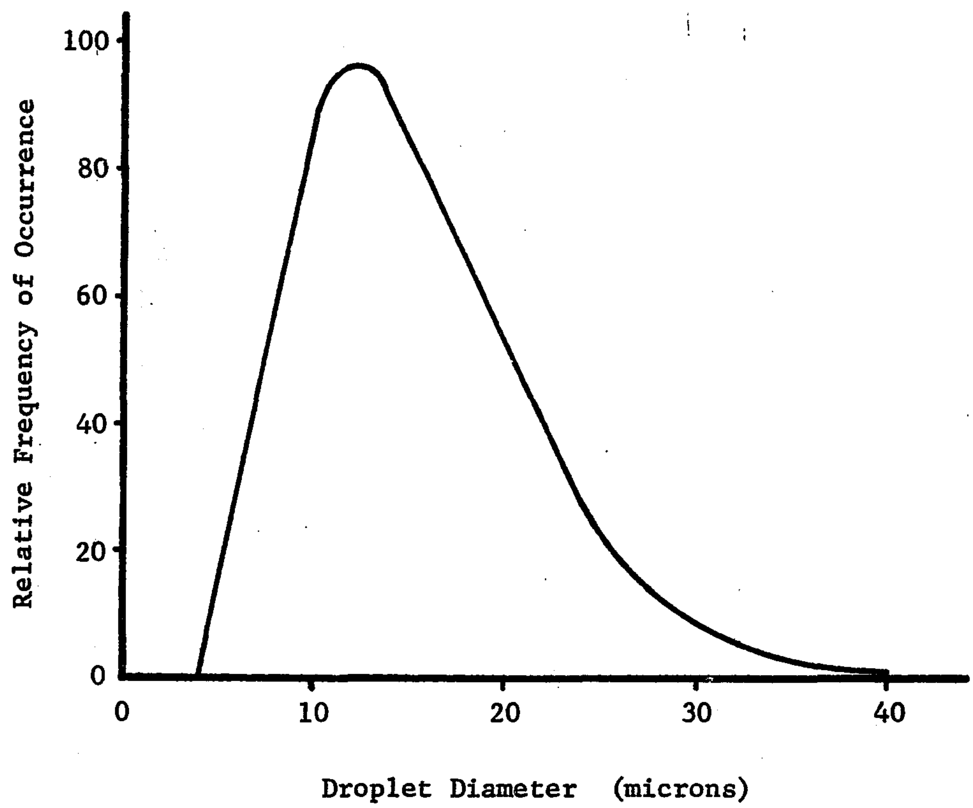

FIGURE 5-1 TYPICAL UNIMODAL SIZE DISTRIBUTION OF FOG DROPLETS

The work of Eldridge (50), and that attributed to Heverly and reported in Green and Lane (3), found large numbers of very small droplets not shown by other investigators; however, these small drops made no significant contribution to the total liquid water content.

Thompson, Ward and Zinky (51) have applied a hologram technique for imaging the interference patterns from natural fog droplets which can then be reproduced in such a way as to give three dimensional spatial assessment. This technique is quite new and can be expected to be improved further in subsequent experiments. Large sample volumes give good numbers of droplets for statistical meaning but the resolution of the system is better for small sample volumes.

There can be no question but that fogs and clouds are polydispersions. On the other hand, it is difficult to treat polydispersions analytically. Due to the shape of the typical size distribution curve, it is impossible to obtain a single characteristic radius that can be used in calculations. In a monodispersion, where the particles are all of a single size, it is possible to use the common radius of the droplets to represent and calculate such parameters as drop circumference, drop cross sectional area, and drop volume. In polydispersions three different radii would be required to represent these same parameters. The mean drop radius, the sum of all the individual drop radii divided by the number of drops, might be used to obtain a mean circumference. The mean radius for cross sectional area, the radius of a drop whose cross sectional area is equal to the average cross sectional area of all drops, can be used for calculations where the cross section of the drop is important, such as in certain optical considerations. The mean radius for volume, the radius corresponding to the drop whose volume is equal to the average drop volume, could be used to determine the total volume or weight of droplets. The differences which exist between these three mean radii will be a function of the specific size distribution curve for the subject droplets. Table 5-1 gives three specific examples which highlight the importance of the size distribution curve. The first example represents a maritime or seacoast fog, the second is from a cloud study, and the third is taken from a continental type fog.

TABLE 5-1

CHARACTERISTIC RADII FOR THREE POLYDISPERSED AEROSOLS

Numerical Mean Radius - μ	Mean Radius for Cross Section - μ	Mean Radius for Volume - μ	Reference
10.0	11.25	12.5	Houghton (48)
11.6	17.5	23.5	aufm Kampe (44)
3.5	4.2	4.8	Arnulf (19)

The first and last examples in Table 5-1 have been estimated on the basis of the size distribution curves contained in the subject references.

In summarizing the data available on radii characteristic of fogs and clouds, Table 5-2 is presented. The data for this table came from Green and Lane (3), Middleton (4), Elliott (25), and Thomson and others (51). The original investigator, whose data is reported, is given. The tabulation of additional data from other references would not materially alter the typical dimensions shown although individual cases might show significant variations. The cited references did not clarify the basis used in reporting the mean radius.

On the basis of the information in Table 5-2, a general picture of the sizes most common to fog droplets emerges. Maritime fogs have a somewhat larger characteristic drop size, perhaps due to the hygroscopic nuclei, and the continental fogs tend to have smaller droplets, probably due to the nuclei provided by industrial pollution. In spite of these differences, it seems that a reasonable range of droplet sizes chosen for various monodisperse fogs might be able to reflect the droplet sizes of greatest population in the polydispersions and thus provide reasonable fog models. Table 5-2 indicates that realistic monodisperse models might be made up of droplet sizes ranging from 4 to 10 microns in radius. Middleton (4) points out that monodisperse models used in theoretical calculations tend to confirm empirical properties for polydispersed natural fog.

TABLE 5-2

CHARACTERISTIC SIZES OF DROPLETS IN CLOUDS AND FOGS

Investigator	Peak Radius μ "most common"	Radius Range μ	Mean Radius μ	Comments
Diem in (3)	4.0-7.25	1 - 21		6 cloud types
Frith in (3)		to 15		50% LWC in 6-9
Kline in (3)		to 20	7	cloud
aufm Kampe in (3)		3 - 100		2 cloud types
Durbin in (3)	4 & 7.5			clouds
Bricard in (4)			4 - 10	4 cloud types
Houghton & Radford in (3,4)	4 - 10	1 - 50		maritime fog
Bricard in (3)	4 - 10			maritime fog
Heverly in (3)		1.75-7.5		continental fog
Elliott (25)	2 - 5			continental fog
Elliott (25)	10 - 20			maritime fog
Neiburger in (3)	7			Los Angeles fog
Thompson (51)	10			hologram

Droplet Number Density and Liquid Water Content

The next subject of interest in the category of physical properties is that of the number of droplets per unit volume of the aerosol. Green and Lane (3) consider this parameter to be of little significance due to the widely different types of fog and cloud which result from different nuclei. The relationship between nuclei, and condensation of droplets thereon, is a subject of some uncertainty. The coated slide and spider hair capture techniques used to determine size distributions are of little help in giving direct numerical values to number densities. In situ evaluation of number densities seems possible with the hologram technique, but it has not been used to provide a significant quantity of data in this field yet.

Houghton and Radford, as reported by Middleton (4), give a range of droplet number densities between 1 and 10 drops per cubic centimeter for typical maritime fogs. Eldridge (50) inferred number densities per cubic centimeter through infrared transmission studies; however, these studies resulted in number densities of several thousand for droplets below 1 micron in diameter. Such small droplets are shown to contribute very little liquid water content to the cloud, although their contribution to scattering is important.

Because of the difficulties of direct measurement of the number of droplets, perhaps a related parameter, namely liquid water content, might prove to be somewhat easier to establish in a general way. It could be used to some extent, in conjunction with characteristic droplet sizes, to establish the bounds of number density for monodisperse fog models.

Green and Lane (3) quote an upper bound of 1 gram per cubic meter which might be found in a thundercloud. Other investigators, such as Eldridge (50), have found considerably higher values of liquid content in some cloud formations. Perhaps the value of liquid water content might be used as a parameter for differentiating between cloud and fog. While on the subject, one difference between fog and cloud has been observed by many people. An ordinary fog allows some distance of visibility whereas a cloud formation, observed by an airplane passenger, will obscure the wing structure of the aircraft at a very short distance. Thus, poorer visibility and higher liquid water content are characteristic of some cloud types and are not considered to be the aerosol of interest in this study. Analysis of such aerosols is not precluded by the analytical or physical model chosen, but rather by the emphasis placed on the practical aspects of natural fog dissipation.

Many investigators, including Fiock and Dahl (24) and Feigelson (47), use a value of 0.5 gram per cubic meter as a target value that should be able to be dissipated by any fog dispersal system. Fiock and Dahl (24) give visibility data, taken from fog at Arcata, California, which converges to zero visibility when the liquid content reaches 1 gram per cubic meter. Houghton and Radford (22) state that their determinations of liquid water content for maritime fog never exceeded the value of 0.3 gram per cubic meter. These same investigators are quoted in Middleton (4) as placing fog in the range of liquid water content from 0.05 to 0.25 gram per cubic meter. They considered values above 0.5 gram per cubic meter as cloud structure.

This data on liquid water content is somewhat more cohesive in a general way than that of the number density. For this reason, a liquid water content between 0.05 and 0.25 gram per cubic meter is chosen as the primary region of interest in this work with a limited number of excursions to liquid water content values between 0.25 and 0.50 gram per cubic meter.

The above decision does not impose very restrictive limits on number density since a very large number of the smaller radius drops would be required to achieve the highest value of liquid water content. Houghton and Radford placed number densities above 50 drops per cubic centimeter in cloud structure. This limit seems a bit too restrictive in view of the numbers quoted by Webb (49) and Elliott (25). Appealing to these latter investigators, an arbitrary upper bound of 200 drops per cubic centimeter was adopted for this work.

Figure 5-2 illustrates the interrelationship between the various physical properties discussed and indicates the regions of primary and secondary interest.

Optical Properties

The optical properties that are of interest in this research include the extinction coefficient, with its constituent parts of absorption coefficient and scattering coefficient, as well as the scattering function relating the direction of scattered to incident radiation.

While the optical properties are not unrelated to the physical properties, one significant difference centers on the dependence of optical properties on the wavelength or frequency of the incident radiation. Usually such properties are discussed for the monochromatic case, or by means of gray assumptions properties are considered not to be frequency dependent. In this work it is assumed that monochromatic radiation at a wavelength of 10 microns characterizes the radiation throughout the "window" of direct radiative transfer to the droplets. The "window" extends from 7.5 to 13.5 microns approximately. Band absorption of the water vapor and carbon dioxide practically eliminates other frequencies in terms of a significant transfer of energy directly to the droplets. Figure 5-3 is a comparative

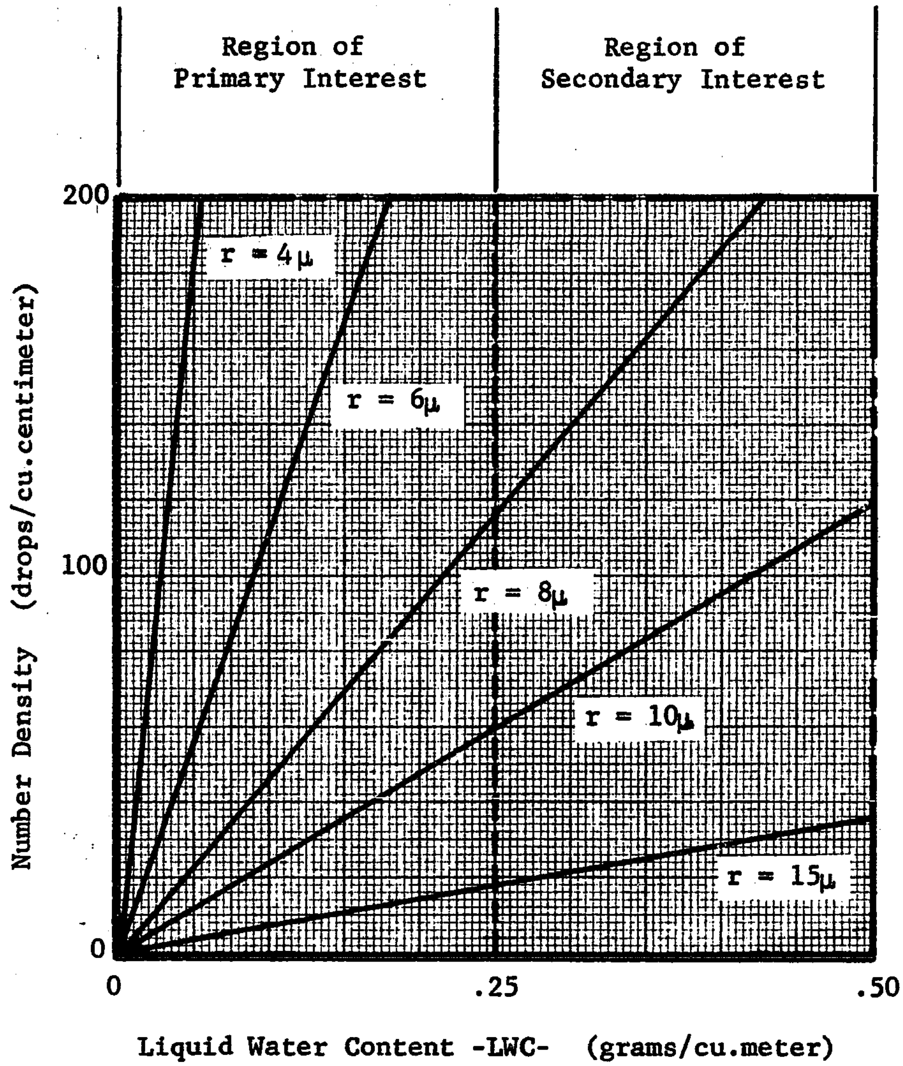

FIGURE 5-2 PHYSICAL PROPERTIES OF MONODISPERSE FOG MODELS

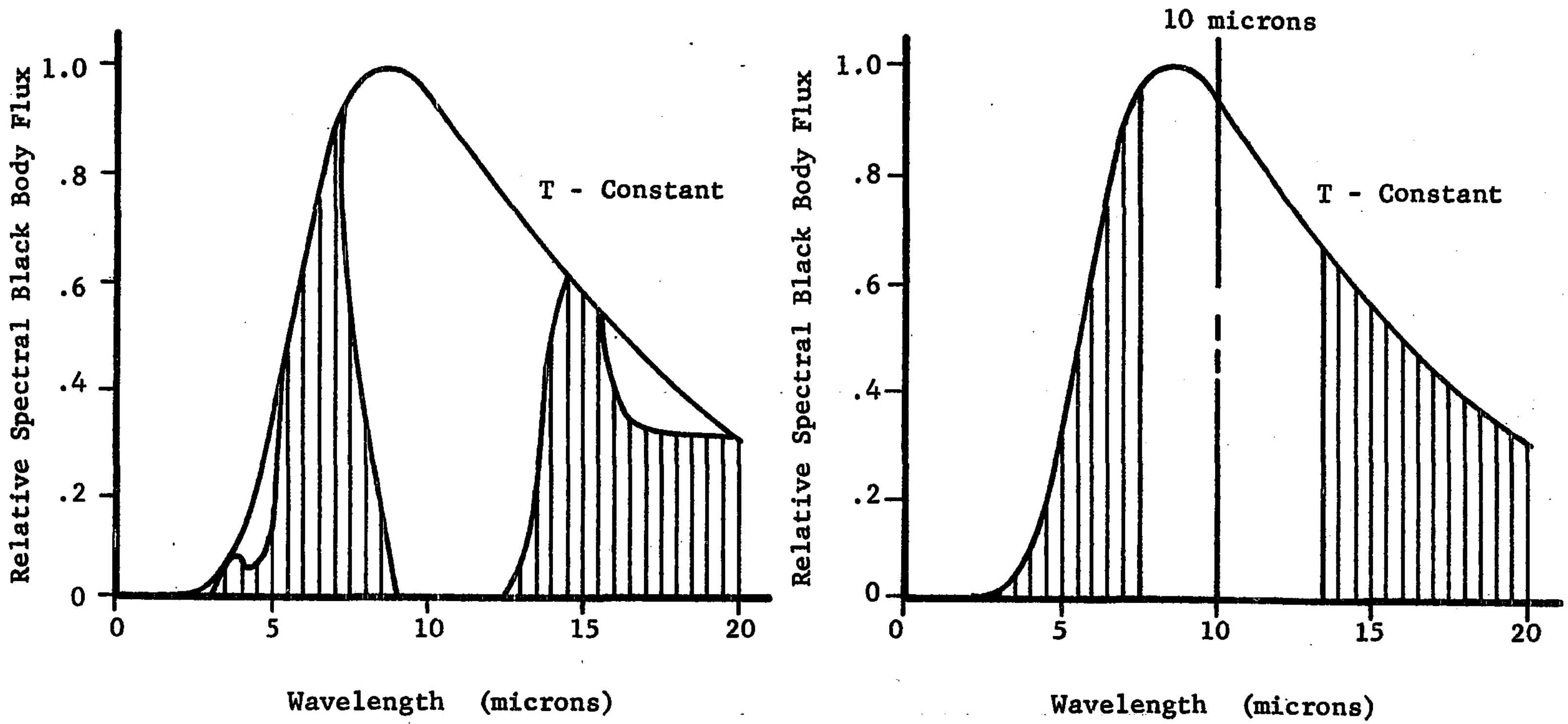

Actual Emission-Absorption Spectrum

Approximate Emission-Absorption Spectrum

NOTE: Shaded areas represent absorption by water vapor and carbon dioxide.

FIGURE 5-3 FLUX EMISSION SPECTRUM FROM BLACK SOURCE MODIFIED BY BAND ABSORPTION illustration showing the degree to which the fixed "window" of this study approximates the actual case. The emission curve is for a black source and represents the radiative flux emitted by such a source as a function of wavelength. The numerical data for absorption by carbon dioxide and water vapor on the actual curve was taken from Wolfe (52), and the illustrated information is confirmed by Kreith (53).

Since the properties for the single wavelength of 10 microns are considered to pertain to all radiation within the increment from 7.5 to 13.5 microns, the usual monochromatic subscripts will not be carried. Thus the problem has been converted to one of a quasi-monochromatic nature.

Optical Density

Having established a quasi-monochromatic model, attention is directed toward the extinction coefficient, or in meteorological terminology, the optical density, β_o. The extinction coefficient is actually the sum of the absorption and scattering coefficients.

Analytical work requires knowledge of the relative contributions of scattering and absorption. In some particulate media the particles have a real index of refraction which produces a special case of extinction. It is called conservative scattering since no absorption takes place and the extinction coefficient or optical density is equal to the scattering coefficient. When the particle has an electric conductivity, the index of refraction becomes complex and extinction includes the effects of both absorption and scattering. The selection of fog as the specific aerosol of interest, and the desire to disperse it by direct radiative transfer to the droplets, requires that the droplets absorb as well as scatter.

Without requiring that explicit values of extinction coefficient or optical density be known, it is possible to evaluate the relative contribution made by scattering and absorption. Most of the published information is available in the form of a parameter called albedo. Albedo is the ratio of the scattering coefficient to extinction coefficient. With absorbing particles, the numerical value of albedo is always less than unity. The difference between albedo and unity is the ratio of absorption coefficient to extinction coefficient. This ratio will be designated as absorption/extinction or abbreviated as abs/ext in this work.

Adaptations of the work of Centeno (54) have been used by many investigators, including Deirmendjian (7), to establish such parameters as albedo, as a function of wavelength, for water. Feigelson (47) gives some values of albedo based on independent investigations. These values are in substantial agreement with those quoted by Deirmendjian (7). Table 5-3 is a summary of this information.

TABLE 5-3

ABSORPTION/EXTINCTION FOR WATER DROPLETS

Wavelength-μ	Absorption/Extinction	References
10	.399	Deirmendjian (7)
6.05 - 16.6	.487 avg.	"
6.40 - 11.8	.30 avg.	Feigelson (47)
6.40 - 11.8	.37 avg.	Feigelson (Shifrin) (47)

Feigelson (47) used a value of absorption coefficient to extinction coefficient of 0.5 when his work was concentrated near the upper bound of the wavelength range given in Table 5-3. Since these cases are somewhat comparable to the wavelength increment being used in this research, the tabulated values, above, might be considered a bit low. On the basis of the values shown in Table 5-3, tempered by the comments just presented, a primary value of absorption coefficient to extinction coefficient, to be used in calculating radiative interactions with fog, was selected as 0.4. A secondary value to be used in a few comparative cases was established as 0.5.

It has been possible to select reasonable values for the ratio of absorption interactions to extinction interactions without the need to know explicit values for either coefficient. The next step is to establish representative explicit values for extinction coefficient or optical density. These values for optical density will be functions of droplet size and number density as well as a parameter called total Mie scattering coefficient for non-absorbing particles or transmission cross section for absorbing particles.

The literature contains a significant volume of information on total Mie scattering coefficient, defined as the total flux scattered by one particle in all directions divided by the flux incident on the geometrical cross section of the particle. This particular parameter is based on a real index of refraction, the conservative scattering or non-absorbing case, and is a function of the wavelength of the incident radiation as well as the index of refraction of the particle. Other terms are used to denote the total Mie scattering coefficient such as efficiency factor by Van De Hulst (10) and diffusion function by Houghton and Chalker as shown by Arnulf and others (19).

On the other hand, relatively little quantitative information is available for transmission cross section, which is analogous to total Mie scattering coefficient but applied to absorbing particles rather than non-absorbing particles. Transmission cross section is also a function of wavelength and index of refraction, which for the absorbing case is complex. Johnson and Terrell (55) have published quantitative information on transmission cross section for water droplets, and their data will be used in this research.

Because of the scarcity of data on absorbing particles, many investigations assume that the non-absorbing total Mie scattering coefficient can be used as a model for transmission cross section. This model is quite satisfactory when the ratio of the particle size to wavelength is sufficiently large, since transmission cross section, and total Mie scattering coefficient converge to the same numerical value in this instance.

Love (6) quotes from the work of Deirmendjian that the effect of a complex index of refraction is to damp out the oscillations in the intensity function or scattering function. The work of Johnson and Terrell (55), involving absorbing particles with a complex index of refraction, also referenced in Van De Hulst (10), indicates a similar damping action on total Mie scattering coefficient compared to transmission cross section.

In the present work, while applicable values of transmission cross section for absorbing water droplets are available, it was considered of some interest to determine the comparative agreement between transmission cross section and total Mie scattering coefficient. The range of particle sizes, coupled with the monochromatic incident radiation at a wavelength of 10 microns, might be expected to cause significant differences between these two parameters.

The work of Penndorf (8) is representative of the high quality of information that has been developed for the conservative scattering or non-absorbing case. The formula for volume extinction coefficient or optical density, subscripted with CS, for this case is

$$\beta_{CS} = N\sigma = N\pi r^2 K \ , \tag{5.1}$$

where β_{CS} = volume extinction coefficient (L^{-1}),

N = droplets per unit volume (L^{-3}),

σ = Mie scattering cross section (L^2),

r = droplet radius (L),

and K = total Mie scattering coefficient (dimensionless).

In the work of Johnson and Terrell for absorbing particles with complex refractive indices, the volume extinction coefficient or optical density, subscripted with an A, is

$$\beta_A = N\pi r^2 \sigma_t \ , \tag{5.2}$$

where β_A = volume extinction coefficient (L^{-1}),

N = droplets per unit volume (L^{-3}),

r = droplet radius (L),

and σ_t = transmission cross section (dimensionless).

The values of K and σ_t are functions of both the index of refraction of the particle and the size parameter α. This size parameter is defined as

$$\alpha = \frac{2\pi r}{\lambda} = \frac{\pi d}{\lambda} \ , \tag{5.3}$$

where r = radius of droplet (L),

and λ = wavelength of radiation (L).

In all of the equations that have just been written, it is necessary to use compatible length units when giving numerical identity to the parameters defined.

The work of Deirmendjian(7), at a wavelength of 10 microns, is used in this research as a primary reference to establish all optical properties of natural fog other than optical density or extinction coefficient. In order that optical density be established in a manner that is compatible with the other optical properties, it will be necessary to impose appropriate restrictions on the index of refraction of the particles. The specific example from the work of Johnson and Terrell (55) with complex refractive indices which afforded the best match with the complex index of Deirmendjian (7) was selected. A comparative refractive index for the conservative scattering case, involving the work of Penndorf (8) with real refractive indices, is taken as that index which is equal to the real portion of the complex refractive index of Deirmendjian (7). Table 5-4 gives a summary of these comparative indices.

TABLE 5-4

COMPARATIVE INDEX OF REFRACTION DATA

Deirmendjian (7)	1.212 - .0601i
Penndorf (8)	1.21 (interpolation)
Johnson & Terrell (55)	1.22 - .061i

In order to facilitate the calculation of optical density, the actual values of total Mie scattering coefficient and transmission cross section, based on the indices of refraction given in Table 5-4 and a wavelength of 10 microns, were plotted as illustrated on Figure 5-4. These curves cover the range of droplet radii already established. Since the size parameter defined by equation 5.3 is a function only of droplet radius for the monochromatic case, both the size parameter and droplet radius are illustrated as abscissae on Figure 5-4.

The optical density or extinction coefficient for absorbing droplets, given by equation 5.2, can now be calculated for known values of droplet radius and number density. Similar calculations for the non-absorbing case could be accomplished using equation 5.1. Considering the limits of

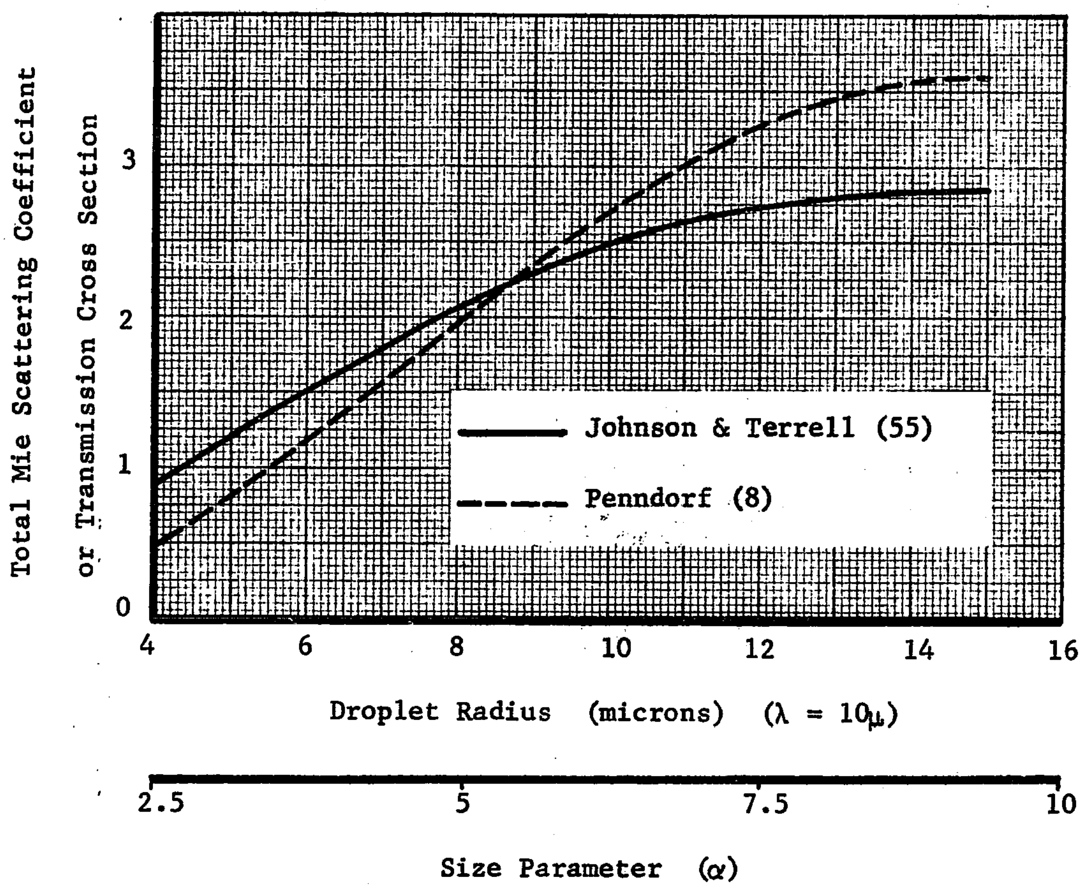

FIGURE 5-4 COMPARATIVE VALUES OF TOTAL MIE SCATTERING COEFFICIENT AND TRANSMISSION CROSS SECTION

investigation already imposed on droplet size and number density, the permissible values of optical density are bounded. Correlated values of these properties, based on the transmission cross section curve of Johnson and Terrell and thought to be representative of natural fog, are illustrated on Figure 5.5. An arbitraty upper limit of 80 km^{-1} for optical density was selected since it provided a reasonably full coverage of the range of physical properties established for fog models. A lower limit of 2.5 km^{-1} was selected since it represents haze, a lower limit for fog according to Middleton (4).

While the conservative scattering data based on the work of Penndorf (8) was not used in this research, the comparison shown on Figure 5-4 indicates that optical densities based on this model are in reasonably good agreement with those of absorbing droplets in the radius range from about 8 to 10 microns. For this work, optical density designated as β_o is synonymous with the optical density β_A calculated by equation 5.2.

Scattered Intensity Distribution

The only remaining optical property required to fix the aerosol model for numerical calculations is an appropriate scattering function. It is known that the scattered intensity distribution will be a function of wavelength, so it will be necessary to continue to impose the quasi-monochromatic radiation condition at a wavelength of 10 microns.

Isotropic scattering will be used for comparative purposes. These comparisons will tend to establish those aerosol models for which the isotropic scattering distribution is a reasonable approximation. The analytical form for the probability distribution function for this type of scattering has already been developed in Chapter IV.

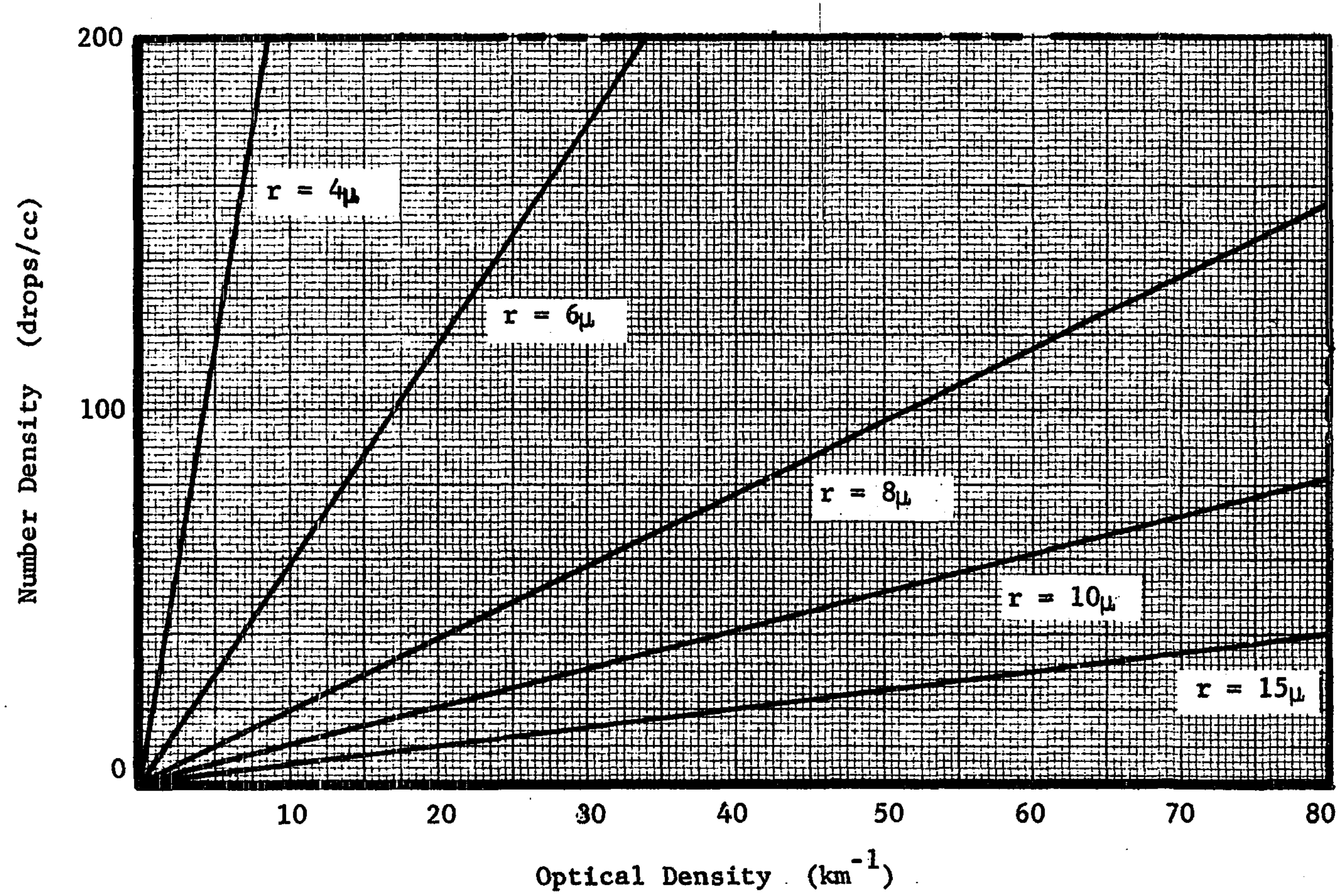

FIGURE 5-5 OPTICAL AND NUMBER DENSITIES BASED ON TRANSMISSION CROSS SECTIONS

General background literature for scattering can be found in texts such as Love (1) and Sparrow and Cess (37). Other references that have been found helpful are Love (6), Rochelle (11), Beattie (56) and Wheasler (57).

The contribution desired at this point is a scattering or intensity function, anisotropic in nature, which is a reasonable model for actual scattering from the water droplets in natural fog. This function should be verified by empirical scattering data, if possible.

The basic anisotropic scattering model used for this work is comparable to that developed by Deirmendjian (7) and empirically verified by Pritchard and Elliott (41). The contributions of the two perpendicularly polarized components are averaged for this work, and the resulting function is smoothed. Figure 5-6 illustrates the smoothed intensity distribution as a function of polar angle. The illustration is presented on a semilog plot which tends to mask the extreme degree of forward scatter and relative insignificance of back scatter. As indicated, the curve is drawn for a wavelength of 10 microns, a "most common" radius of 4 microns, and a number density of 100 droplets per cubic centimeter.

Most of the fog models analyzed in this work have droplets somewhat larger than the 4 microns of this example. On the other hand, the average droplet size for the example would be something larger that the "most common" radius, considering the usual distribution curve of droplet sizes. In a general way, for a given refractive index and wavelength, the scattered intensity will become increasingly unsymmetrical as the droplet size or size parameter is increased, favoring the forward direction. When the size parameter becomes very large, practically all scattered energy is concentrated in the forward direction, see Schmidt (42).

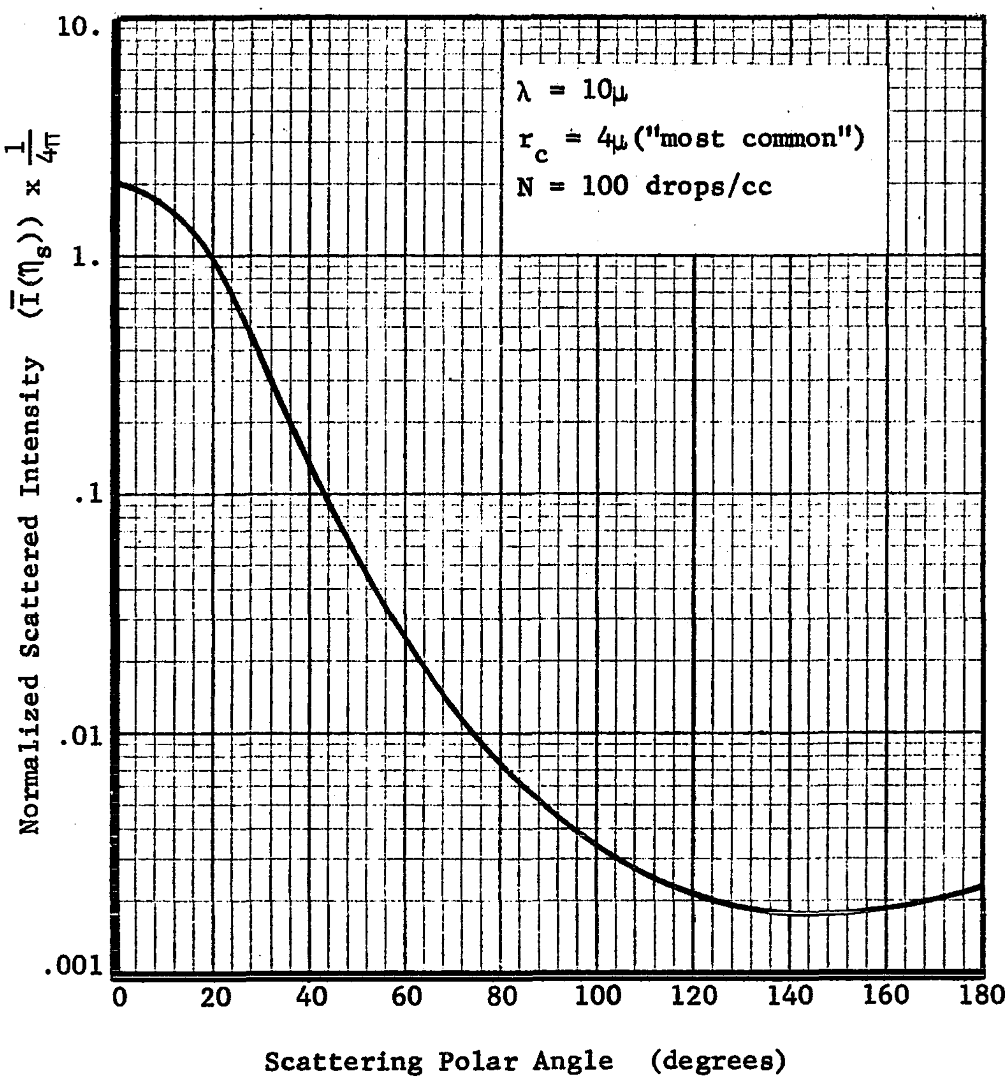

FIGURE 5-6 NORMALIZED INTENSITY DISTRIBUTION

The scattering function or intensity distribution curves for industrial haze, a lower limit for natural fog, given by Middleton (4), show this strong forward scattering along with a very weak back scatter. Pritchard and Elliott (41) show comparable empirical curves for scattering in light fog. This particular reference found that 56% of the total scattered energy was found in the range of polar angles between 0° and 20°, where 0° represents forward scatter. They also found that 18% of the energy was concentrated in the first two degrees of polar angle.

Because of the somewhat larger droplet sizes used for the fog models in this research compared to the model illustrated in Figure 5-6, and due to the empirical evidence supporting very strong forward scattering for natural fog, it might be argued that the scattering model chosen may be conservative in estimating forward scatter.

Appealing to the development of probability fundamentals related to scattering in Chapter IV, a properly normalized intensity function, $\bar{I}(\eta_s)$, comparable to the one illustrated on Figure 5-6, gives

$$\frac{1}{4\pi}\int_{\Omega} \bar{I}(\eta_s)d\omega = 1 \quad .$$

Expressing this equation in terms of the scattering polar and azimuthal angles, and breaking down the resulting expression in terms of the statistically independent variables, leads to

$$\int_0^{\pi} \frac{\bar{I}(\eta_s)\sin\eta_s}{2}\, d\eta_s = 1 \quad , \qquad 5.4$$

where $\frac{\bar{I}(\eta_s)\sin\eta_s}{2}$ is the probability density function for the scattering polar angle.

In the event the smoothed intensity function curve has not retained its normalization, the integral of equation 5.4 will evaluate to some constant other than unity. By multiplying both sides of the equation by an appropriate normalizing constant, the probability requirement can be met.

Following the procedure established in Chapter IV, the scattering polar angle density function, $\frac{[\bar{I}(\eta_s) \sin \eta_s]}{2}$, is evaluated for a large number of specific values of the polar angle, η_s. These numerical values are plotted and a smooth curve drawn through them to produce the function shown on Figure 5-7.

Graphical integration of the probability density function shown in Figure 5-7, for increasing values of polar angle, develops the probability distribution function for scattering polar angle. This graphical integration technique will produce discrete points on the probability distribution curve. A smooth curve, drawn through these points, gives the functional form of the probability distribution function for the polar scattering angle. Figure 5-8 illustrates the probability distribution function that results from the intensity distribution shown on Figure 5-6. The solid line represents this function.

The next step is to transform the graphical representation of this distribution function into an algebraic or tabular format. In this work, the algebraic format was chosen. A number of numerical techniques are available to serve as interpolating devices in a situation of this type; however, simple functions, well adapted to the Monte Carlo method were sought for this work. The result of this search is shown on Figure 5-8 as the dashed line. This dashed line is achieved by using two simple expressions in properly related ranges of the distribution function. These expressions are

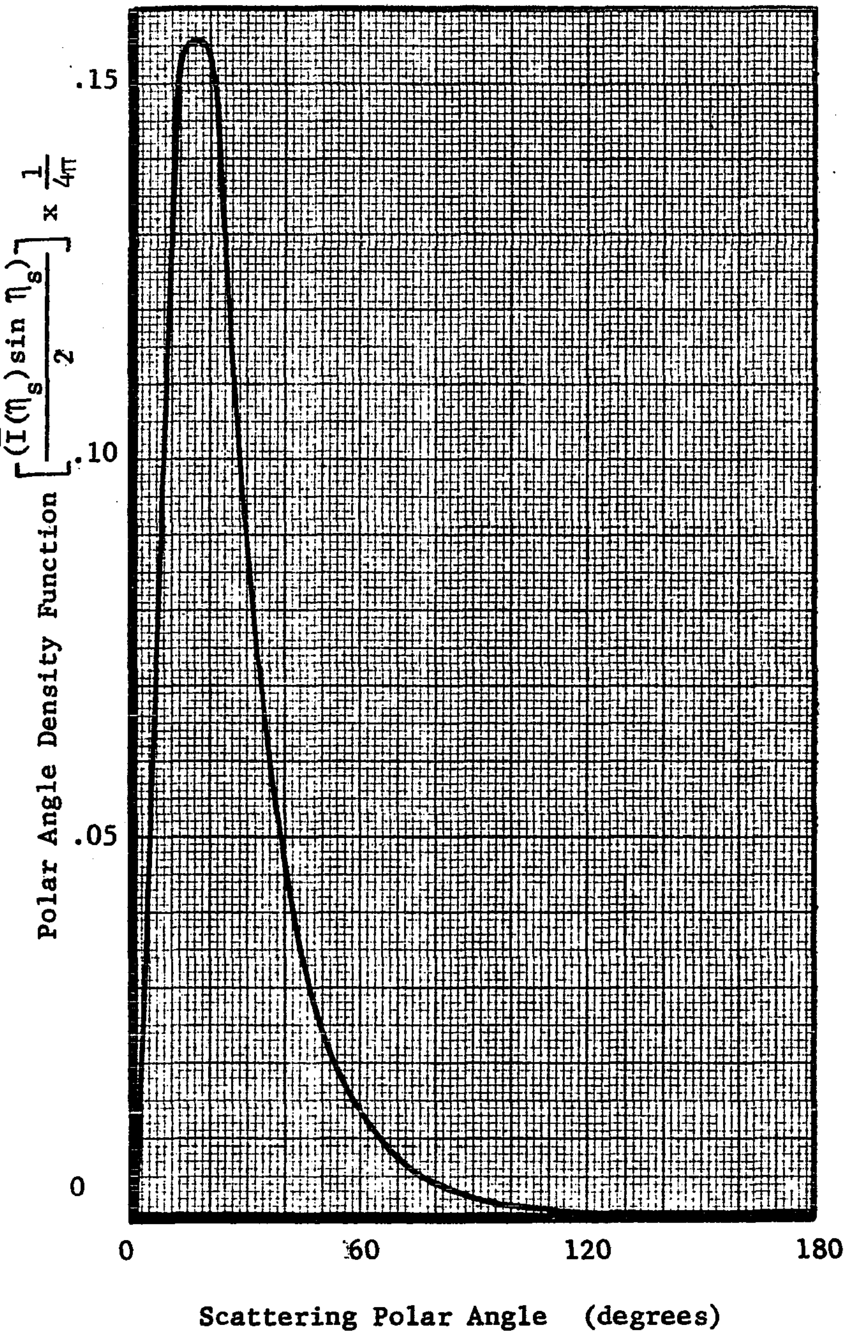

FIGURE 5-7 SCATTERING POLAR ANGLE PROBABILITY DENSITY FUNCTION

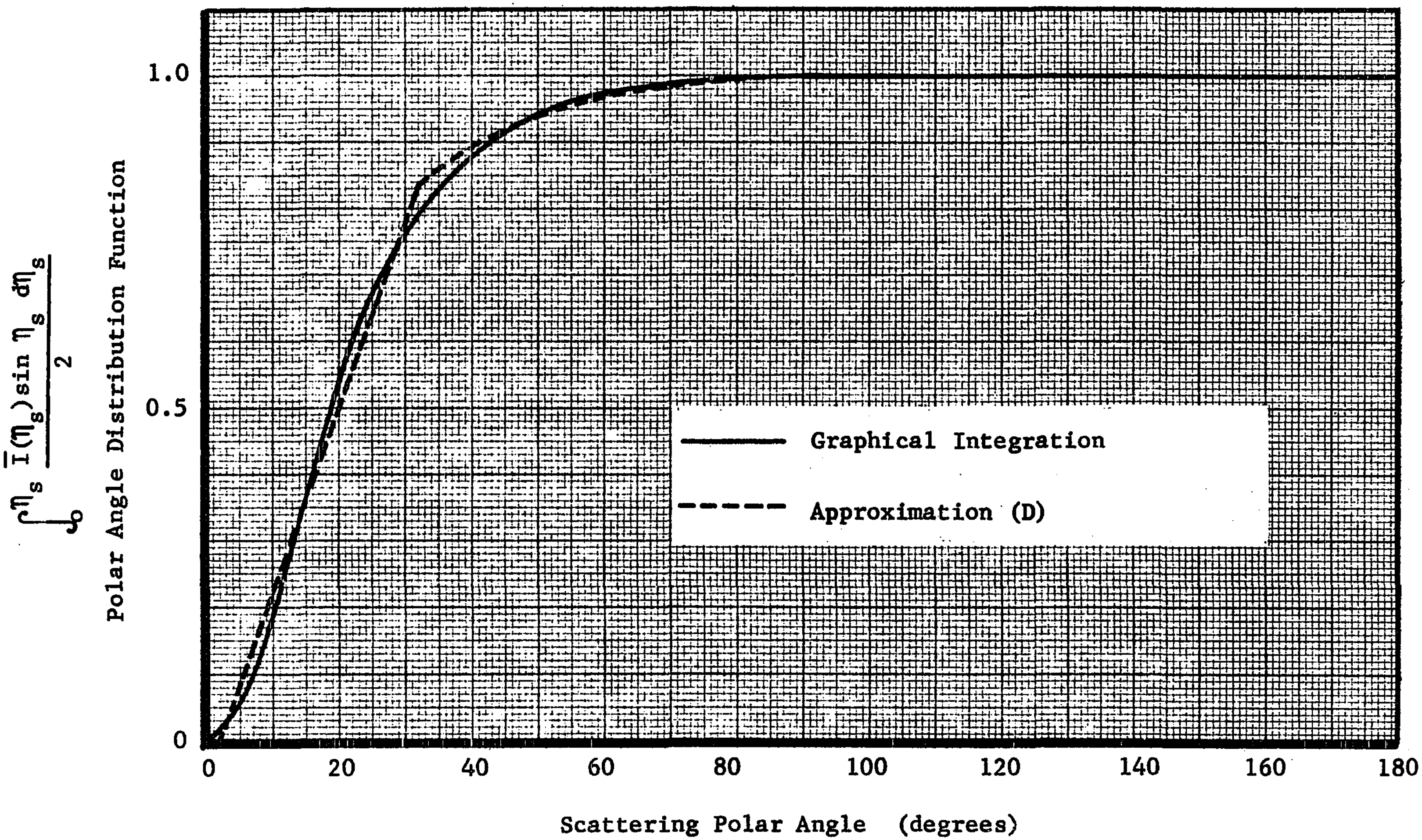

FIGURE 5-8 PROBABILITY DISTRIBUTION FUNCTION FOR SCATTERING POLAR ANGLE

$$F(\eta_s)_{D1} = \frac{\left(\frac{180\eta s}{\pi} - 2\right)}{36.1} \qquad \text{for } 0 \le F(\eta_s) \le .83 \,, \tag{5.5}$$

and

$$F(\eta_s)_{D2} = 1 - \exp\left(\frac{10\eta s}{\pi}\right) \qquad \text{for } .83 < F(\eta_s) \le 1.0 \,. \tag{5.6}$$

where the polar angle is measured in radians.

Because this particular scattering model may be conservative in forward scattering, for reasons previously discussed, a simple distribution function favoring stronger forward scattering but otherwise retaining a strong functional resemblence to the distribution function of Figure 5-8 was developed. The mathematical expression for this strong forward scattering is

$$F(\eta_s)_F = 1 - \exp\left(-\frac{13.5\eta_s}{\pi}\right) \,, \tag{5.7}$$

where the polar angle, η_s, is measured in radians.

The functional form for this strong forward scattering is shown on Figure 5-9. The isotropic scattering distribution function is also shown on Figure 5-9. The distribution function achieved by graphical integration, as well as its approximation, shown on Figure 5-8, fall between the limits established by the two simple distribution functions depicted on Figure 5-9; however, much closer to the strong forward scattering function. The distribution function for the equally likely azimuthal angle was developed in Chapter 4.

Strong forward scattering, designated (F), isotropic scattering, designated (I), and the approximation shown on Figure 5-8, designated (D), are all subjected to numerical calculations in this research.

Closure

On the basis of the material developed in this chapter, the physical and optical properties of monodisperse aerosols, used to represent models of natural fog, have been established in terms of reasonable limits.

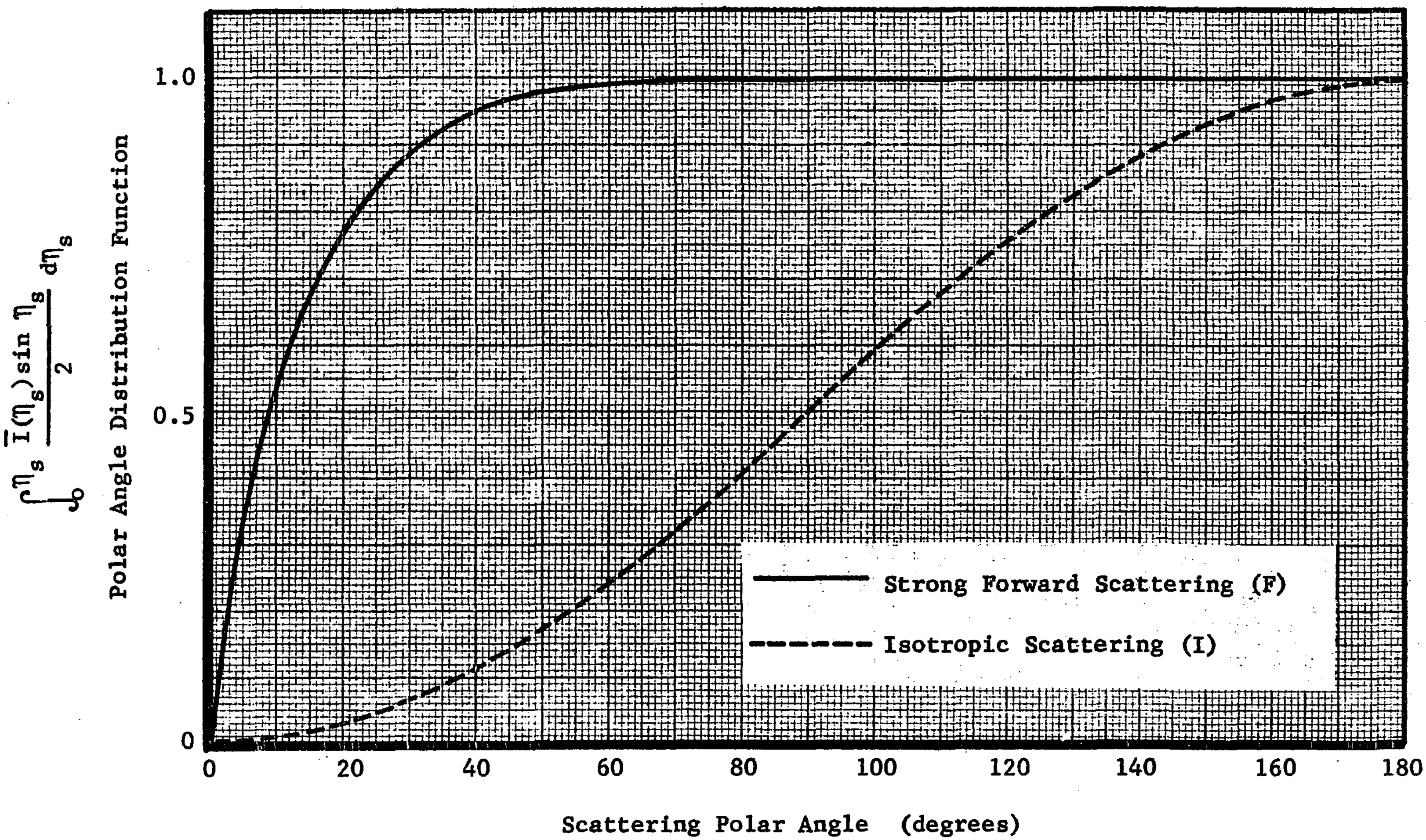

FIGURE 5-9 PROBABILITY DISTRIBUTION FUNCTIONS FOR SCATTERING POLAR ANGLE

The following list of properties are considered representative of those which might be characteristic of natural fog. All possible combinations from this list have not been analyzed; however, a reasonable cross section is analyzed in order to provide meaningful conclusions.

Tabulated Physical and Optical Properties for Fog Models

Droplet Radius (microns)	4, 6, 8, and 10
Number Density (drops/cc)	not to exceed 200
Liquid Water Content (LWC) (gram/cu.meter)	
a. Primary Zone	0.05 to 0.25
b. Secondary Zone	0.25 to 0.50
Absorption Coefficient/Extinction Coefficient	
a. Primary Value	0.40
b. Secondary Value	0.50
Index of Refraction	1.212 - .0601i
Optical Density (β_o) (km^{-1})	2.5 to 80.0

Scattering Function

a. Strong Forward Scattering (F)

$$F(\eta_s)_F = 1 - \exp\left(-\frac{13.5\eta_s}{\pi}\right)$$

b. Approximation (Deirmendjian) (D)

$$F(\eta_s)_{D1} = \frac{\left(\frac{180\eta_s}{\pi} - 2\right)}{36.1} \quad \text{for } 0 \le F(\eta_s) \le .83$$

$$F(\eta_s)_{D2} = 1 - \exp\left(-\frac{10\eta_s}{\pi}\right) \quad \text{for } .83 < F(\eta_s) \le 1.0$$

c. Isotropic Scattering (I)

$$F(\eta_s)_I = -\frac{1}{2}\cos\eta_s + \frac{1}{2}$$

Droplet Heat of Vaporization (Btu/lb)	1065.6
Droplet Temperature (^oF)	50

CHAPTER VI

NUMERICAL RESULTS

Introduction

The stage has now been set such that specific problems can, when properly posed, be subjected to numerical analysis through the probabilistic analytical methods previously discussed. It remains to define specific problems in explicit terms so that the proper numerical structure can be generated.

The computer programs, which have been included in Appendix H, provide the means for following photons from the source through a sequence of probable paths that eventually lead to a termination of each photon history. In this work, a termination is brought about when a photon is absorbed by a water droplet or when the photon has moved to a spatial location outside the boundaries of the accounting shell. In the event of an absorption, the energy transfer is used to provide the heat of vaporization required for droplet evaporation. This evaporation of droplets is fundamental to the thermal dissipation of fog. Considering the practical emphasis of this work on fog dispersal, it is clear that the energy absorbed by the droplets will be the basic information sought.

The objective of the computer programs is to determine the spatial distribution of absorption interactions within the accounting envelope. The aerosol properties which will effect this distribution are the optical density, the ratio of absorption to extinction interactions, and the type of scattering associated with the aerosol particles. Knowledge of the absorptions that take place in a given spatially fixed volume compared to the original emissions from the source which go directly to the droplets will produce a ratio of the energy absorbed in the volume to that emitted by the source in the "window" wavelength increment. This ratio can be utilized to determine the rate at which energy is being converted to the evaporation of droplets within the spatially fixed volume. With knowledge of the total liquid water contained in the subject volume, it is possible to calculate the time required, at the specific transfer rate, to evaporate all the liquid therein. This last statement might be considered as a general expression of the problem for which numerical results are reported in this chapter.

Numerical Definition of Problem

The geometry associated with the sources has already been discussed in Chapter II. The temperatures which are to be considered are conditioned by the practical implication that the source represents an airport runway or a landing pad. The source must be restricted to temperatures that are within the structural limitations of the material of composition and which are not detrimental to people who might be required to work in the immediate vicinity. In addition, the source must be able to work at the prescribed temperature for long periods of time, perhaps continuously.

Two sources are to be studied, namely, a long rectangular source and a circular source. Emphasis will be placed on the long rectangular source. The reference coordinate system for each source model is centered in the respective areas as shown in Figures 2-1 and 2-3. Symmetrical accounting envelopes, shown in these same figures, when complemented by the base plane, including the source, represent the boundary conditions for photon escape. The subdivision of the accounting envelope into spatially fixed volumes, called subspaces in this work, is indicated on Figure 2-2.

The radiative properties of a source are fixed by its temperature and surface characteristics. For the numerical results which follow, the source has been assumed to emit as a diffuse black body which is a limiting case for the gray diffuse assumption made in Chapter II.

The energy which is transferred directly to the droplet for evaporative action is restricted to the wavelength interval between 7.5 and 13.5 microns. The radiation is considered to be modeled by monochromatic radiation at a wavelength of 10 microns. The fraction of the total energy emitted by the source which is contained within this wavelength "window" has been investigated for a series of source temperatures and is given in some detail in Appendix E.

Tables 6-1 and 6-2 summarize the source and accounting envelope characteristics for which numerical results are sought.

Aerosol

Specific information pertinent to this aspect of the problem was thoroughly discussed in Chapter V. In order to be assured that practical limits of the properties of natural fog have been included in these numerical studies, a representative cross section has been chosen for analysis. Optical densities representing the optically thin case of 2.5 km^{-1} and increasing in increments to the optically thicker case of 80 km^{-1} have been investigated. Absorption coefficient to extinction coefficient ratios of 0.4 and 0.5, anisotropic scattering functions of two forward scattering

TABLE 6-1

LONG RECTANGULAR SOURCE MODEL

Source Width	50 meters
Source Length	2500 meters
Accounting Shell Diameter	250 meters
Accounting Subspace Volumes	See Appendix F
Source Temperature	600^{o}R or $333\text{-}1/3^{o}$K
Source Emittance	1.0
Window Emission Fraction	0.4030

TABLE 6-2

CIRCULAR SOURCE MODEL

Source Diameter	50 meters
Accounting Hemisphere Diameter	250 meters
Accounting Subspace Volumes	See Appendix F
Source Temperature	600^{o}R or $333\text{-}1/3^{o}$K
Source Emittance	1.0
Window Emission Fraction	0.4030

types, (F) and (D), as well as isotropic scattering, (I), have been coupled with realistic values of the other aerosol properties in order to provide an inclusive coverage of the radiative parameters.

Table 6-3 presents a summary of the cases studied and gives page numbers on which associated tabular or illustrated numerical information can be found.

Numerical Results

The objectives of this chapter will be achieved by reporting the numerical information on the spatial distribution of absorption interactions and exposing the practical implications of this absorption information with regard to evaporative fog dissipation.

The spatial distribution of absorption interactions has been deposited, due to its bulk, in Appendix F. This information is in tabular form and gives the fraction of original emissions that are absorbed in each subspace of the accounting envelope. A legend, explaining the format of this data, is included in Appendix F. This information has been indexed according to the source model used. The page numbers, for various sets of radiative parameters, are given in Table 6-3 and repeated in Table F-3.

While this absorption information represents a fundamental finding of this research, its usefulness can be greatly enhanced by transforming it into parameters which give greater practical insight. In other words, this spatial distribution of absorption interactions represents a foundation on which to build numerical calculations of other parameters having stronger practical implications.

Table 6-4 is a representative example of the tabulated absorption information found in Appendix F.

TABLE 6-3

AEROSOL MODELS STUDIED

SOURCE	OPT.DENS. β_o - km^{-1}	RADIUS μ	NO.DENS. cc^{-1}	ABS/EXT	SCAT.FUN.	PAGE NO.
Rect.	2.5	4	55	.4	(F)	113,201
Rect.	2.5	4	55	.4	(I)	202
Rect.	5.0	6	30	.4	(F)	114,140 149,203
Rect.	5.0	6	30	.4	(I)	149,204
Rect.	5.0	6	30	.5	(F)	140,205
Rect.	7.5	6	45	.4	(F)	115,206
Rect.	7.5	6	45	.4	(I)	207
Rect.	7.5	6	45	.4	(D)	208
Rect.	7.5	6	45	.5	(F)	209
Rect.	10.0	6	60	.4	(F)	111,141 150,210
Rect.	10.0	6	60	.4	(I)	150,211
Rect.	10.0	6	60	.4	(D)	212
Rect.	10.0	6	60	.5	(F)	141,213
Rect.	15.0	6	90	.4	(F)	116,157 214
Rect.	15.0	6	90	.4	(I)	215
Rect.	15.0	6	90	.4	(D)	157,216
Rect.	15.0	6	90	.5	(F)	217
Rect.	20.0	6	120	.4	(F)	117,142 151,218
Rect.	20.0	6	120	.4	(I)	151,219
Rect.	20.0	6	120	.4	(D)	220
Rect.	20.0	6	120	.5	(F)	142,221 222,223

TABLE 6-3 (continued)

SOURCE	OPT.DENS. β_o - km^{-1}	RADIUS μ	NO.DENS. cc^{-1}	ABS/EXT	SCAT.FUN.	PAGE NO.
Rect.	25.0	8	60	.4	(F)	118,224
Rect.	25.0	8	60	.4	(I)	225
Rect.	25.0	8	60	.5	(F)	226
Rect.	30.0	8	72	.4	(F)	119,227
Rect.	30.0	8	72	.5	(F)	228
Rect.	40.0	8	96	.4	(F)	120,143 152,229
Rect.	40.0	8	96	.4	(I)	152,230
Rect.	40.0	8	96	.5	(F)	143,231
Rect.	50.0	8	120	.4	(F)	121,232
Rect.	50.0	8	120	.5	(F)	233
Rect.	60.0	10	60	.4	(F)	122,234
Rect.	60.0	10	60	.5	(F)	235
Rect.	80.0	10	96	.4	(F)	123,144 153,236
Rect.	80.0	10	96	.4	(I)	153,237
Rect.	80.0	10	96	.5	(F)	144,238
Circ.	5.0	6	30	.4	(F)	124,239 259
Circ.	7.5	6	45	.4	(F)	125,240
Circ.	10.0	6	60	.4	(F)	126,145 154,241
Circ.	10.0	6	60	.4	(I)	154,242
Circ.	10.0	6	60	.5	(F)	145,243

TABLE 6-3 (continued)

SOURCE	OPT.DENS. β_o- km^{-1}	RADIUS μ	NO.DENS. cc^{-1}	ABS/EXT	SCAT.FUN.	PAGE NO.
Circ.	15.0	6	90	.4	(F)	127,244
Circ.	15.0	6	90	.4	(I)	245
Circ.	15.0	6	90	.4	(D)	246
Circ.	20.0	6	120	.4	(F)	128,247 259
Circ.	24.0	15	15	.4	(F)	129,155 248
Circ.	25.0	8	60	.4	(I)	155,249
Circ.	50.0	8	120	.4	(F)	130,250 259
Circ.	80.0	10	96	.4	(F)	131,156 251
Circ.	80.0	10	96	.4	(I)	156,252

Example Problem

In order to discern the relationship of the absorption information to the practical problem of fog dissipation, a parameter of relative evaporation time for droplets, located at various permissible sites in the accounting envelope, was chosen. Spatial points having equal relative evaporation time are called isochronic points. Lines or surfaces connecting such points are called relative isochrons, or simply isochrons. In order to show the orderly process required to transform the absorption data to relative isochrons, a typical example is considered to be the most direct and informative.

The example used is that of the long rectangular source with physical dimensions and accounting envelope dimensions, as well as other source characteristics, given in Table 6-1. This particular source model will be coupled with the aerosol model given in Table 6-3 having an optical density of 10 km^{-1}, a droplet radius of 6 microns, a number density of 60 drops per cubic centimeter, an absorption to extinction ratio of 0.4, and a scattering function of the strong forward scattering type, (F).

The spatial distribution of the absorption interactions for this example case can be found in Appendix F; however, for convenience, this table has been reproduced as Table 6-4. The columns of this table represent the six rays of the cross section of the accounting envelope and are arranged from left to right according to their position above the horizontal. The rows of data, ten in number, represent the radial increments which define the specific subspaces. The rows are arranged from top to bottom to represent the radial increments from the center of the source outward. Figure 2-2 is a physical representation of these accounting subspace features.

The numerical data in this table represents the fraction of the photons that, having been emitted from the source in the emission "window" of interest in this work, terminate their histories by an absorption within the specific subspace. The number of photons emitted from the source can be considered to characterize the total energy emitted in the "window" wavelength increment, hereafter called window energy or window emission. Thinking in these terms, the fraction of emitted photons that are absorbed within any given subspace is representative of the fraction of the window energy that is converted, through absorption, to the evaporation of droplets within the designated subspace. The window energy emitted by the source is determined by the source size and the surface characteristics and temperature.

Thus, the absorption tables provide essential information about the energy absorbed in each subspace when the emission characteristics of the

TABLE 6-4

RADIANT HEAT TRANSFER FROM LONG RECTANGULAR SOURCE

54,997	Histories	Anisotropic Scattering (F)
25,000	Absorptions	Optical Density - 10 km^{-1}
37,623	Scatterings	Absorption/Extinction - .4

FRACTION OF ORIGINAL EMISSIONS ABSORBED IN EACH SUBSPACE

.006291	.005800	.005455	.005873	.005000	.004691
.015437	.013219	.011037	.010564	.009746	.010619
.005037	.009728	.011929	.011873	.011146	.011546
.002782	.006419	.008891	.010873	.011492	.010837
.002364	.006255	.007564	.009946	.011237	.010746
.001546	.005218	.007255	.008928	.009891	.011328
.001927	.004891	.006691	.008600	.009055	.010819
.001255	.003855	.005800	.007637	.008855	.008819
.001146	.003800	.005346	.006782	.008655	.008746
.001182	.003800	.006328	.006709	.007946	.008000

source are known.

Each subspace contains droplets of water for the aerosol model being studied in this example. The aerosol is considered to be isotropic and contains a monodispersion of droplets. With these assumptions in mind, it is possible to determine the liquid water content of the aerosol per unit volume. Since the volumes of the individual subspaces are determined by the geometry of the accounting envelope, it is possible to determine the liquid water content of each subspace. A knowledge of the liquid water content of a given subspace leads to the determination of the heat required to evaporate it.

It is clear that knowing the rate of window energy release from the source, the subsequent portion if this energy absorbed in a given subspace, and the amount of energy required to evaporate the liquid water contained in the specific subspace, should provide a basis for determining the time required to accomplish the evaporation. The calculations outlined in this paragraph were carried out for each subspace in the example problem. The individual volumes of the subspaces can be found in Appendix F. The resulting relative evaporation times for the individual subspaces are given on Table 6-5. The format for this table is the same as that described for Table 6-4.

A further transformation of the relative evaporation time information given in Table 6-5 was considered useful and informative. It is assumed that the properties of the subspace are sufficiently uniform so that the properties and characteristics of the subspace can be considered to act at a point. This point is considered to be the center of gravity of the subspace cross section. Following this approach, the values in Table 6-5 can be plotted along each ray line represented by the columns in Table 6-5.

TABLE 6-5 RADIANT HEAT TRANSFER FROM LONG RECTANGULAR SOURCE

54,997 Histories	Anisotropic Scattering (F)	Number Density - 60 cc^{-1}
25,000 Absorptions	Optical Density - 10 km^{-1}	Droplet Radius - 6 microns
37,623 Scatterings	Absorption/Extinction - .4	Source Temperature - 600^{o}R

RELATIVE TIME IN MINUTES TO EVAPORATE DROPLETS IN EACH SUBSPACE

4.135740	4.485855	4.769561	4.430097	5.203588	5.546357
5.056286	5.904672	7.072016	7.388663	8.008811	7.350393
25.826828	13.372710	11.520527	10.956770	11.671429	11.267087
65.465698	28.372910	20.484268	16.750275	15.848053	16.805923
99.053131	37.435913	30.957382	23.543289	20.838440	21.790588
185.121277	54.848129	39.448303	32.056168	28.935135	25.264633
175.523300	69.154236	50.550507	39.329468	37.353210	31.262909
310.971680	101.237183	67.287827	51.102448	44.073349	44.253235
385.955566	116.396072	82.735748	65.217468	51.104019	50.572296
418.224365	130.089737	78.119659	73.683289	62.212540	61.792648

This illustration plots the relative evaporation time as a function of radial position. A smooth curve is drawn through the points. This smooth curve is used as the interpolating device for this data. Interpolation of the smooth curve gives the radial location where the relative evaporation time is equal to 10, 15, 30, 60 minutes or any other selected time value within the range of the curve.

A plot of the type just discussed is illustrated in Figure 6-1. This illustration is for the typical case along ray number four in Table 6-5.

Points depicting an equal value of relative evaporation time along each of the six rays could be connected. The resulting line is the relative isochron that was mentioned earlier. Since the symmetry of the problems being investigated allow "folding" into a two dimensional format, the relative isochrons appear as lines on polar plots illustrating this parameter. Actually these lines also represent the generating line for a surface, so that it would be permissible to talk in terms of isochronic surfaces. Figure 6-2 is a polar plot of the relative isochrons of 10, 15, 30, and 60 minutes for the specific example problem being analyzed.

Closure

Curves illustrating relative isochrons could be drawn for all cases given in Table 6-3. Rather than display all of these cases in this particular format, a representative sample of such plots has been included at the end of this chapter. These curves are intended to be used for comparative purposes. For this reason, all of them have been standardized in terms of the scattering function, (F), and the ratio of absorption coefficient to extinction coefficient, 0.4. The parameter that is changing from illustration to illustration is the optical density. Some illustrations

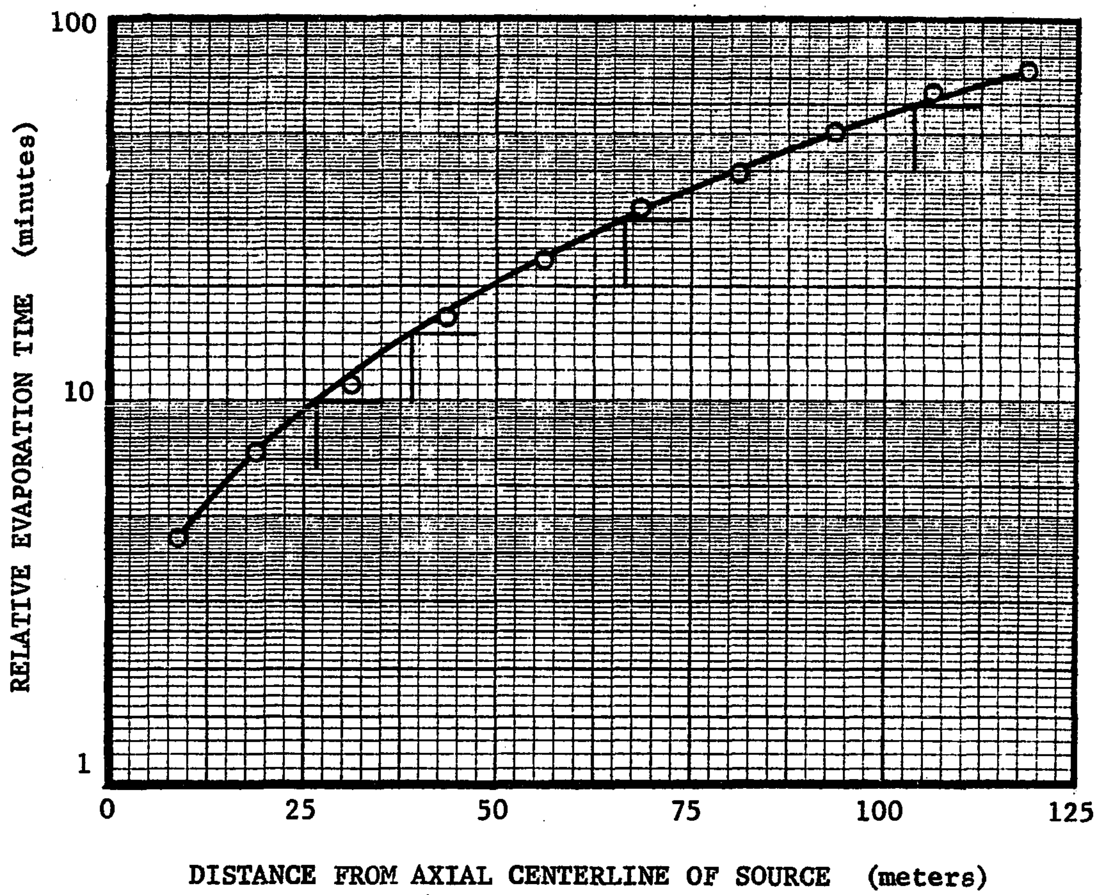

LEGEND:

Optical Density - 10 km^{-1} Absorption/Extinction - 0.4

Droplet Radius - 6 microns Scattering Function - (F)

Source Temperature - 600^{o}R Number Density - 60 drops/cc

FIGURE 6-1 RELATIVE EVAPORATION TIME CURVE ALONG RAY FOUR

RELATIVE ISOCHRONS FOR RADIATIVE EVAPORATION OF DROPLETS BY A LONG RECTANGULAR SOURCE

54,997 Histories	Anisotropic Scattering (F)
25,000 Absorptions	Optical Density - 10.0 km^{-1}
37,623 Scatterings	Absorption/Extinction - 0.4

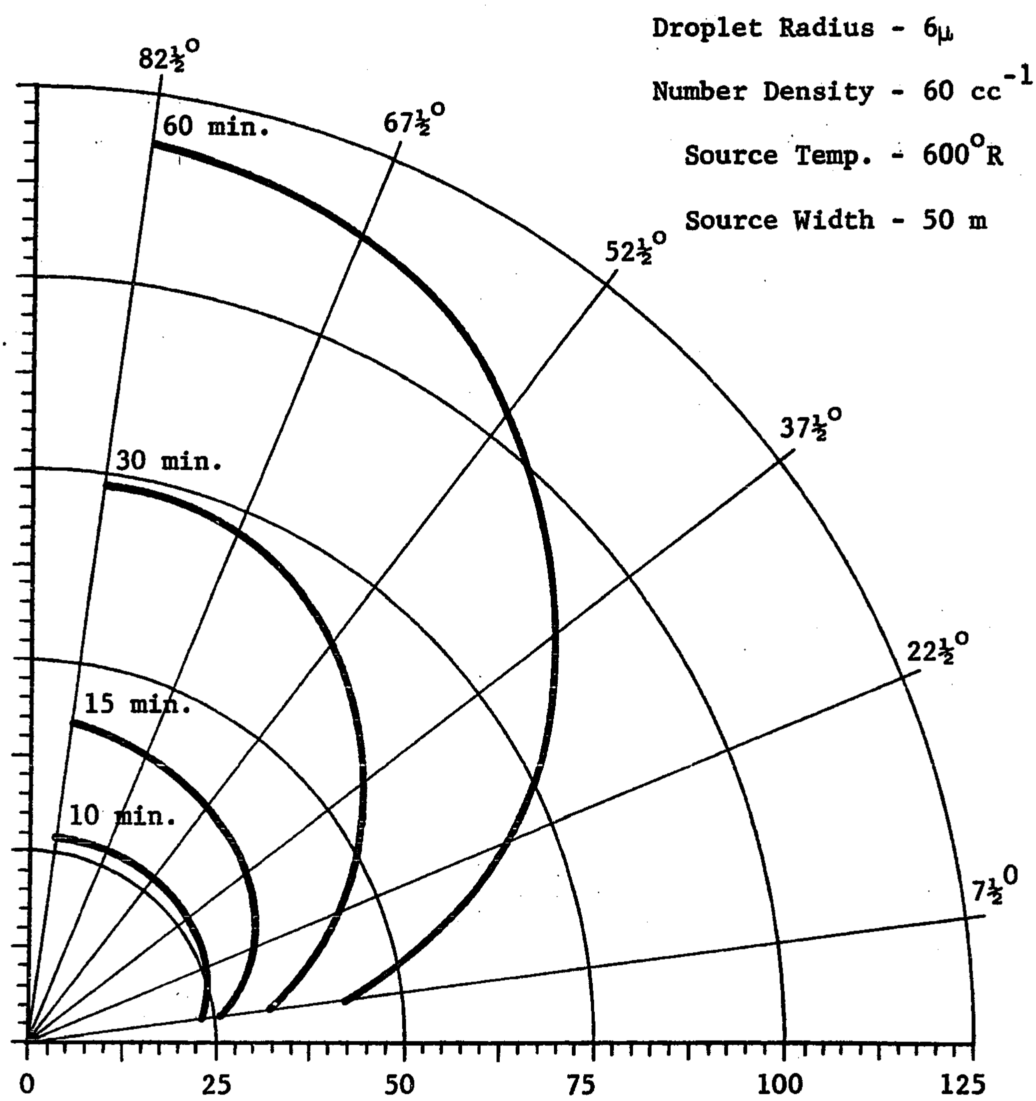

DISTANCE FROM AXIAL CENTERLINE OF SOURCE (meters)

FIGURE 6-2

have been included for each source model.

The effect of optical density is apparent. Further comparisons, involving changes in various radiative parameters, will be taken up in Chapter VII.

While interpretation and analysis of the numerical results of this research will be taken up in Chapter VII, it is necessary to inject a word of caution at this point.

Interpretation of the isochronic curves of this chapter must be undertaken with considerable care in order that these curves are not misunderstood.

The data represented is based on the physical and optical properties of the aerosol remaining constant during the evaporation process. This is not a good assumption in terms of the real situation. In the actual case of evaporation, or fog dissipation, gradual changes in the physical and optical properties of the aerosol will take place with time. The dissipation will be progressive, from the source outward, and the optical density at any location will tend to decrease with time, in the absence of diffusion or mixing.

The relative isochrons do not represent the progressive boundaries of the evaporation process as a function of time. They do represent those spatial locations having a common constant relative evaporation time, considering the radiative parameters remain fixed at their initial conditions.

Attention is directed to Chapter VII which summarizes, compares, and interprets the numerical findings that have been reported in this chapter.

RELATIVE ISOCHRONS FOR RADIATIVE EVAPORATION OF DROPLETS BY A LONG RECTANGULAR SOURCE

343,008	Histories	Anisotropic Scattering	(F)
50,000	Absorptions	Optical Density - 2.5 km^{-1}	
74,281	Scatterings	Absorption/Extinction - 0.4	

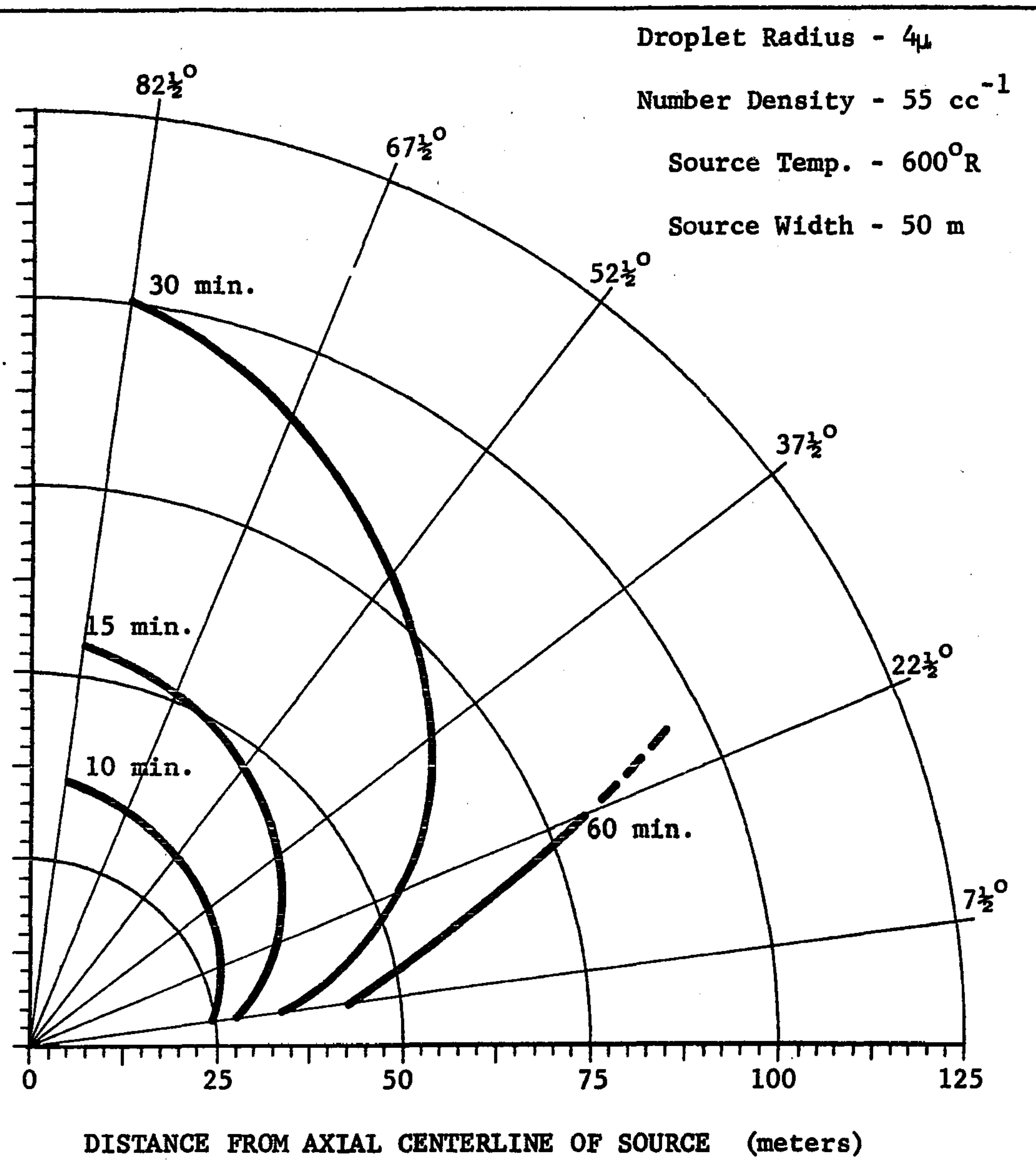

FIGURE 6-3

RELATIVE ISOCHRONS FOR RADIATIVE EVAPORATION OF DROPLETS BY A LONG RECTANGULAR SOURCE

93,962 Histories	Anisotropic Scattering (F)
25,000 Absorptions	Optical Density - 5.0 km^{-1}
37,606 Scatterings	Absorption/Extinction - 0.4

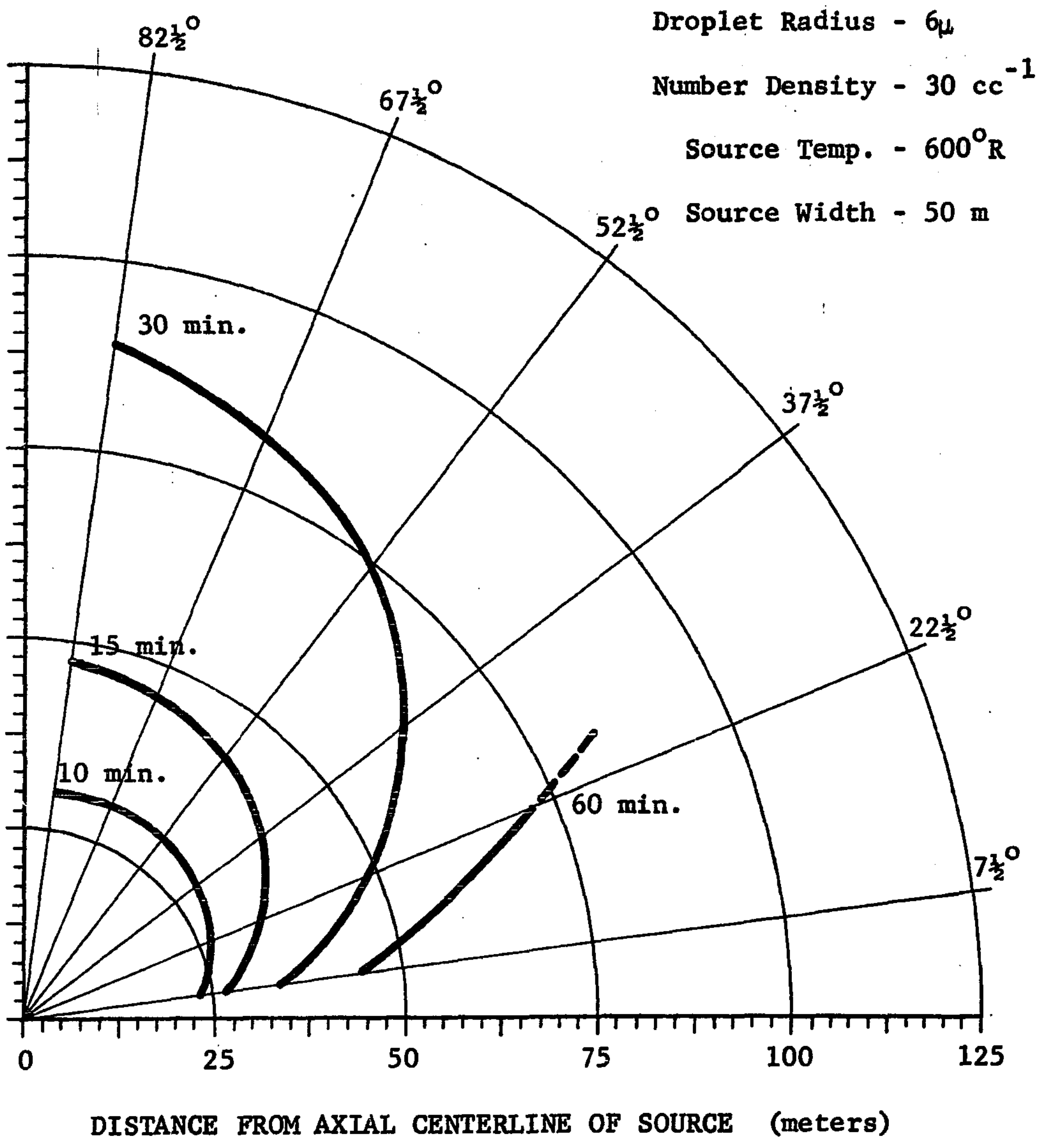

FIGURE 6-4

RELATIVE ISOCHRONS FOR RADIATIVE EVAPORATION OF DROPLETS BY A LONG RECTANGULAR SOURCE

135,174 Histories		Anisotropic Scattering (F)
50,000 Absorptions		Optical Density - 7.5 km^{-1}
74,614 Scatterings		Absorption/Extinction - 0.4

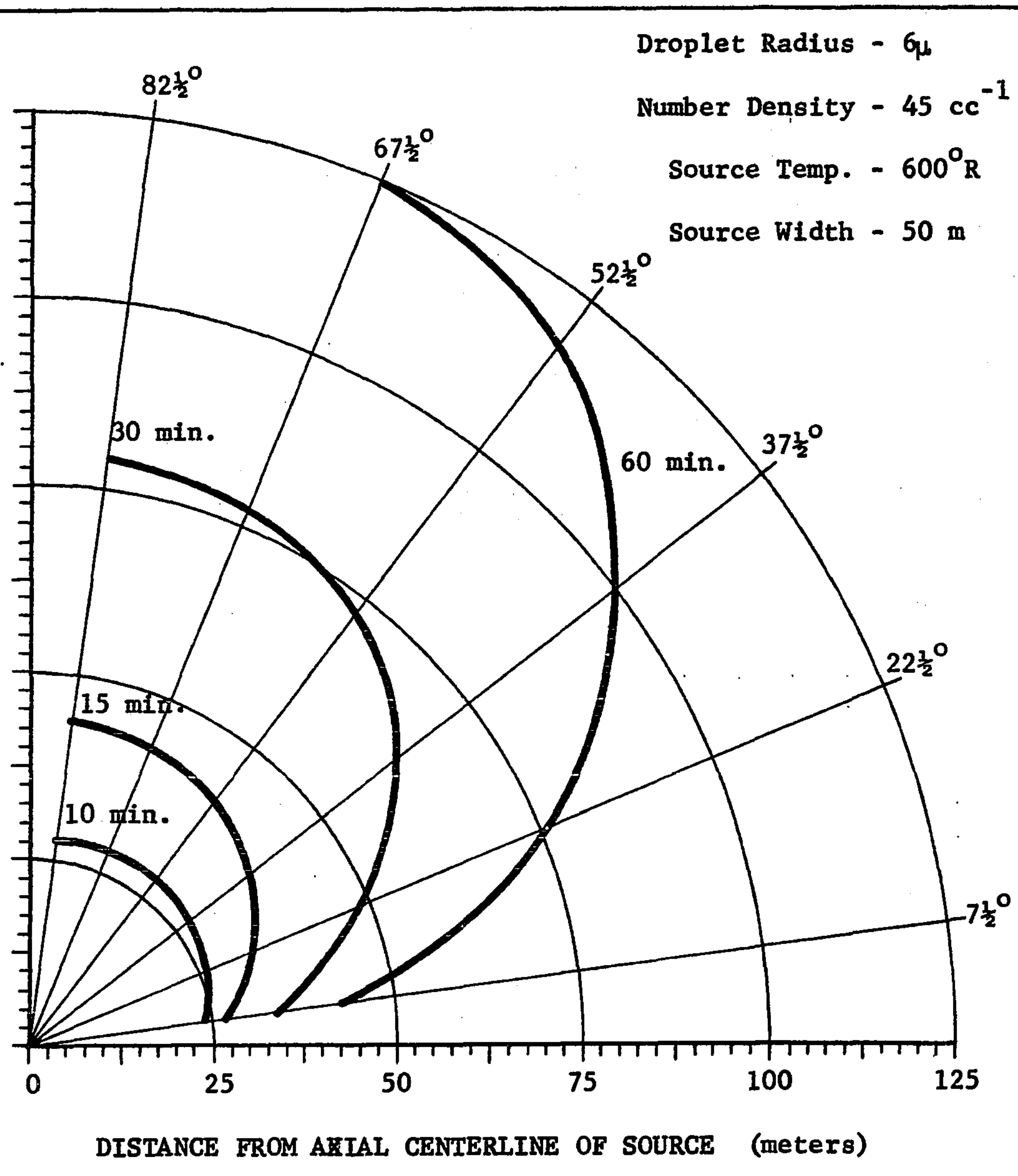

FIGURE 6-5

RELATIVE ISOCHRONS FOR RADIATIVE EVAPORATION OF DROPLETS BY A LONG RECTANGULAR SOURCE

84,209	Histories	Anisotropic Scattering (F)
50,000	Absorptions	Optical Density - 15.0 km^{-1}
74,769	Scatterings	Absorption/Extinction - 0.4

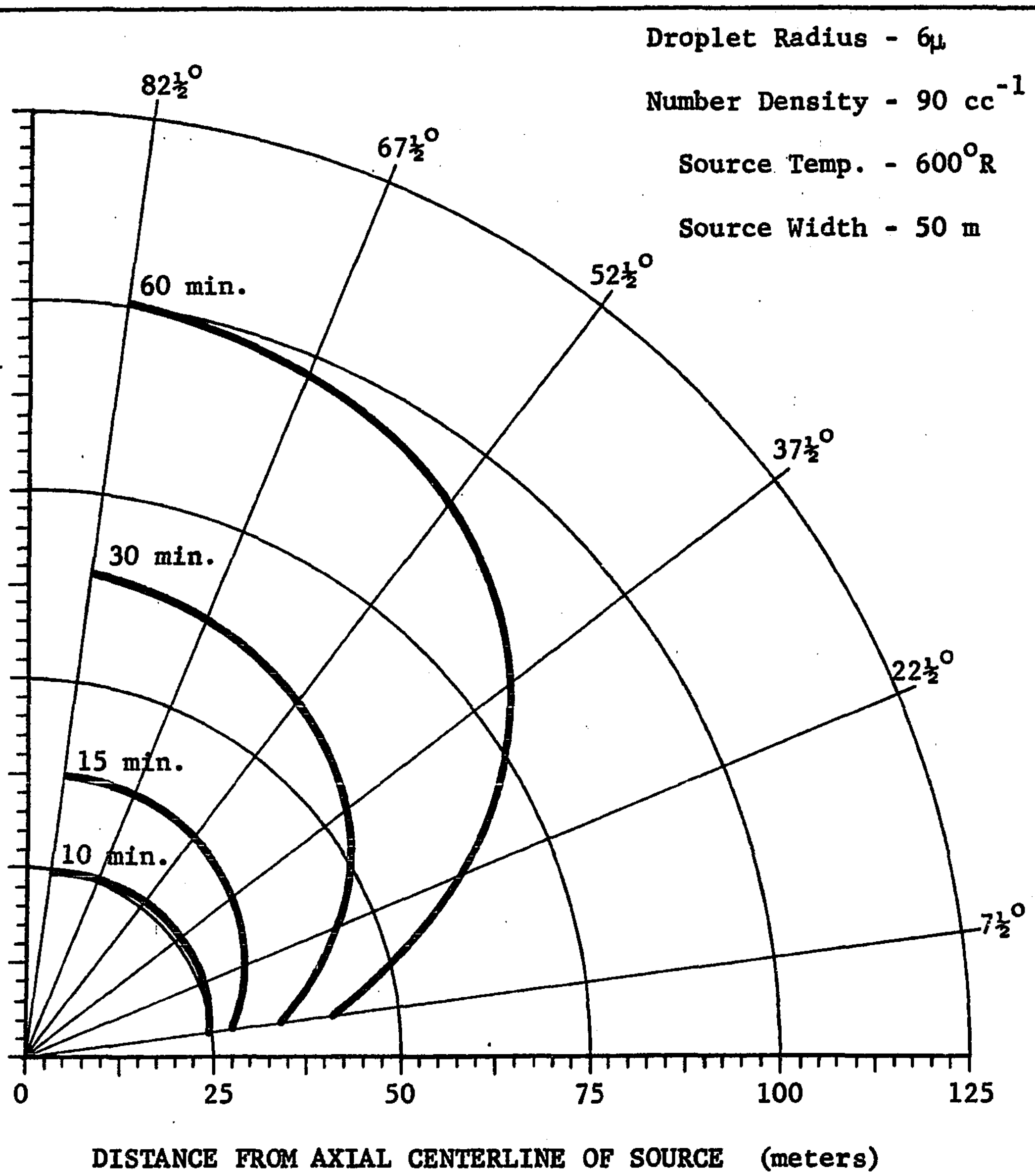

FIGURE 6-6

RELATIVE ISOCHRONS FOR RADIATIVE EVAPORATION OF DROPLETS BY A LONG RECTANGULAR SOURCE

36,118 Histories	Anisotropic Scattering (F)
25,000 Absorptions	Optical Density - 20.0 km^{-1}
37,595 Scatterings	Absorption/Extinction - 0.4

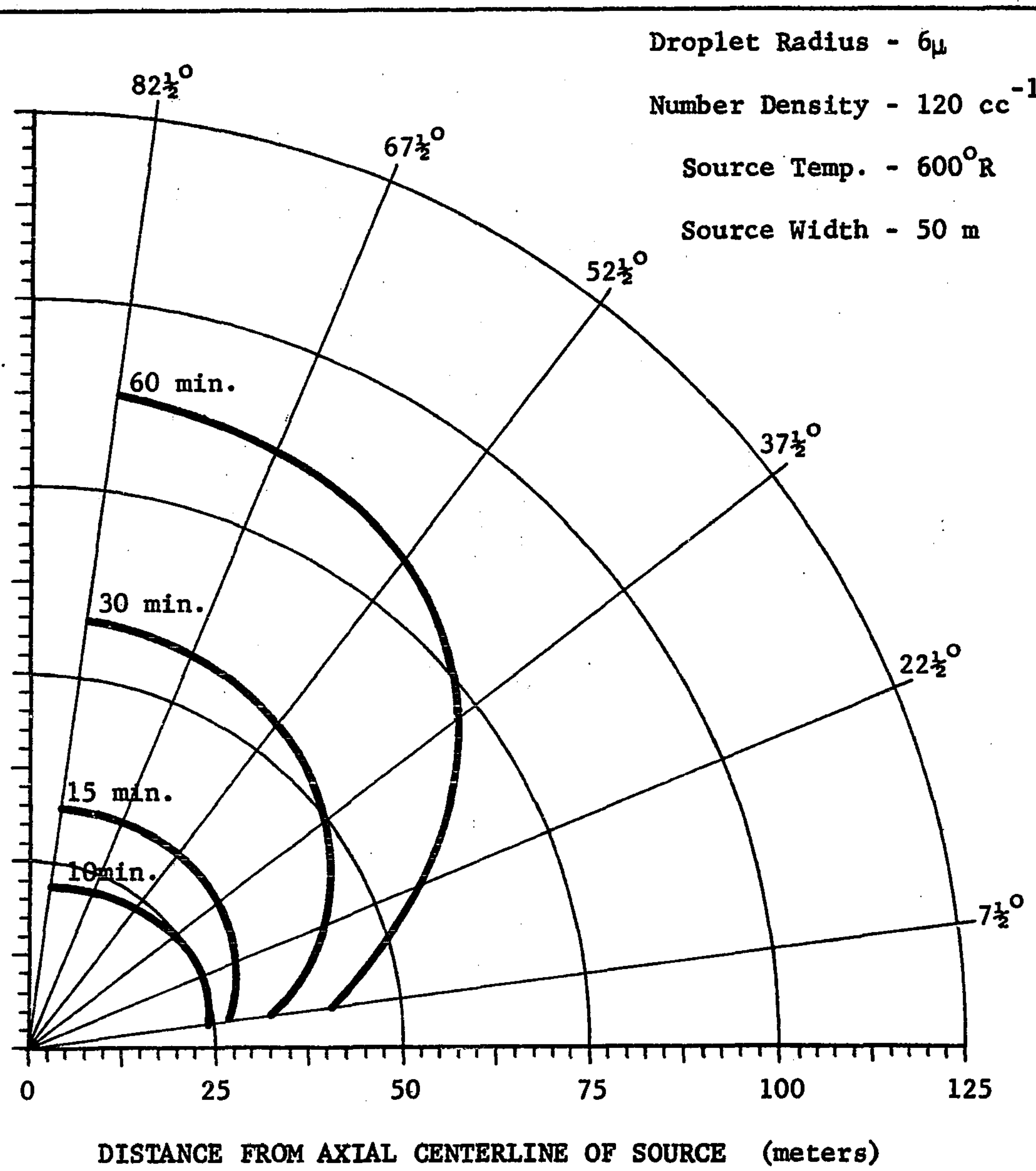

FIGURE 6-7

RELATIVE ISOCHRONS FOR RADIATIVE EVAPORATION OF DROPLETS BY A LONG RECTANGULAR SOURCE

64,751	Histories	Anisotropic Scattering (F)
50,000	Absorptions	Optical Density - 25.0 km^{-1}
74,812	Scatterings	Absorption/Extinction - 0.4

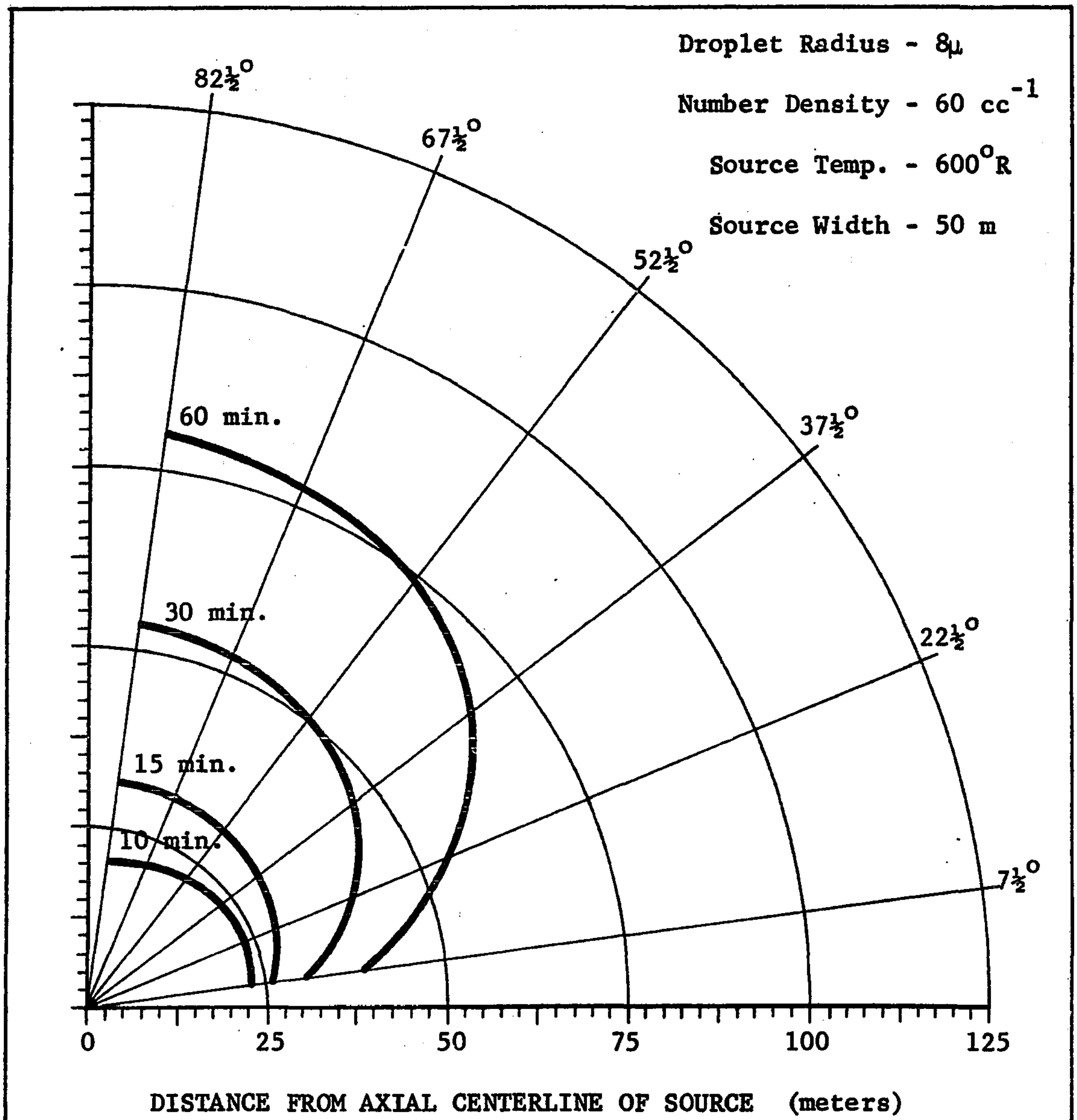

FIGURE 6-8

RELATIVE ISOCHRONS FOR RADIATIVE EVAPORATION OF DROPLETS BY A LONG RECTANGULAR SOURCE

60,569	Histories	Anisotropic Scattering (F)
50,000	Absorptions	Optical Density - 30.0 km^{-1}
75,023	Scatterings	Absorption/Extinction - 0.4

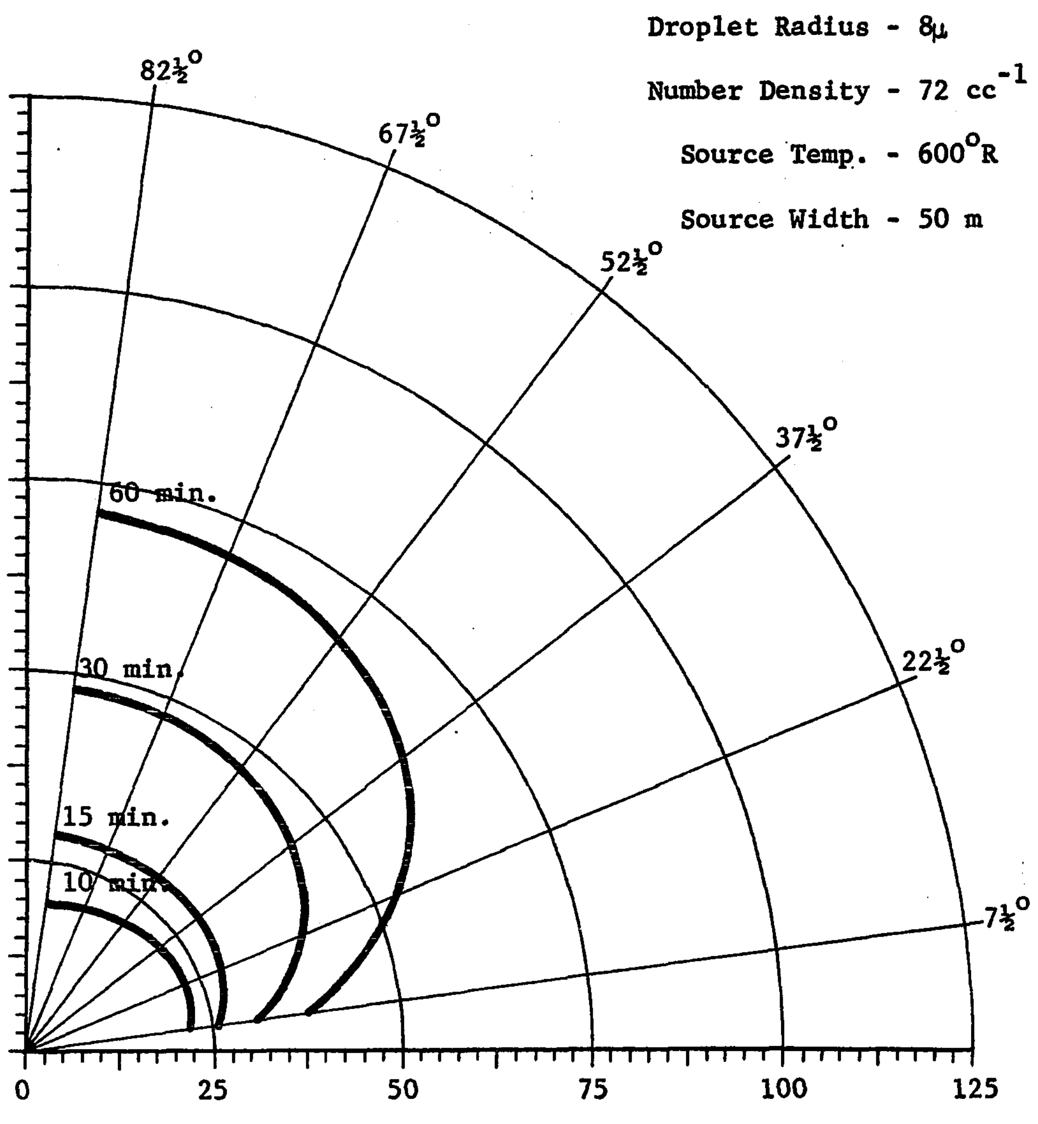

FIGURE 6-9

RELATIVE ISOCHRONS FOR RADIATIVE EVAPORATION OF DROPLETS BY A LONG RECTANGULAR SOURCE

55,609 Histories	Anisotropic Scattering (F)
50,000 Absorptions	Optical Density - 40.0 km^{-1}
74,755 Scatterings	Absorption/Extinction - 0.4

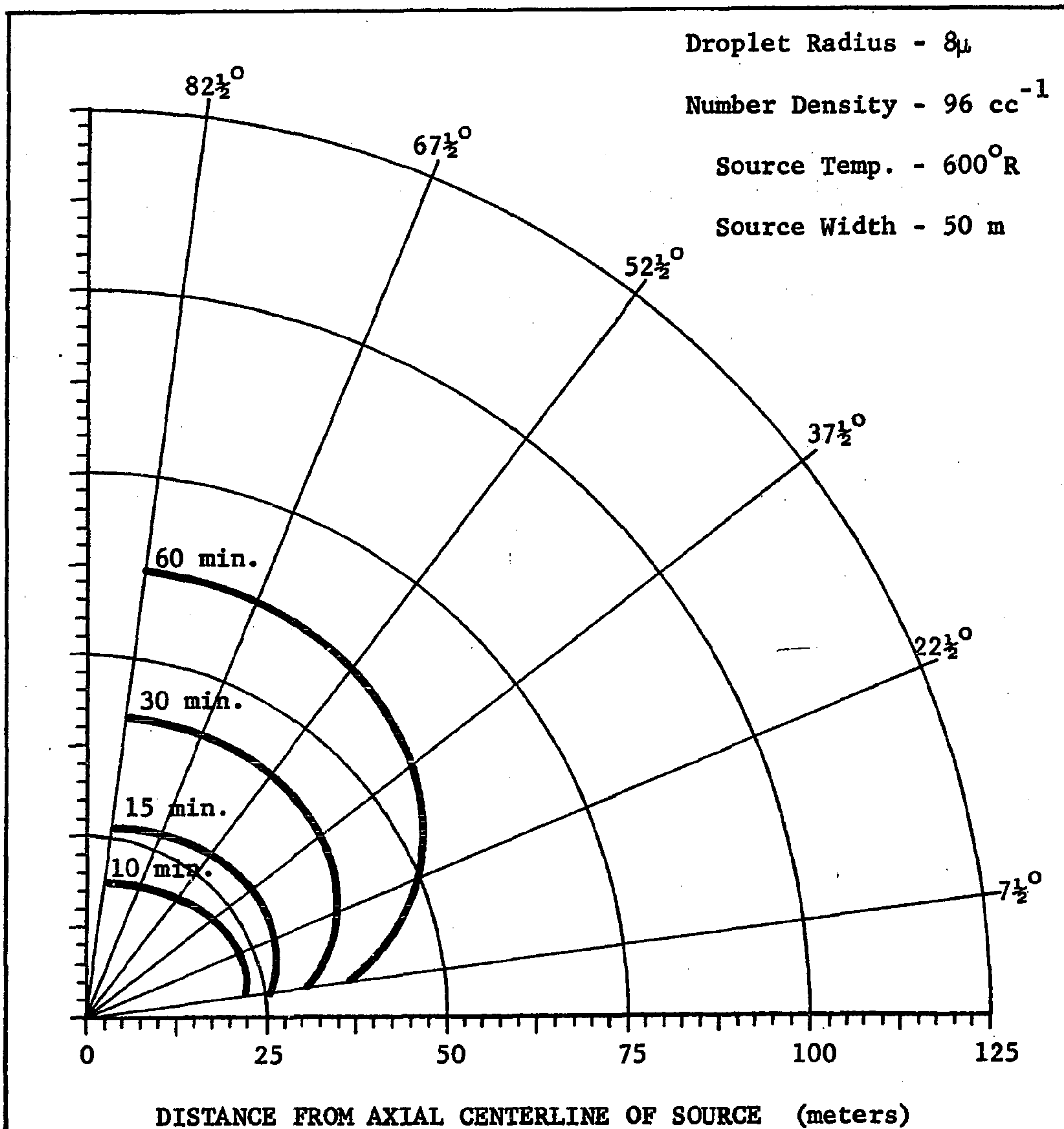

FIGURE 6-10

RELATIVE ISOCHRONS FOR RADIATIVE EVAPORATION OF DROPLETS BY A LONG RECTANGULAR SOURCE

26,640 Histories	Anisotropic Scattering (F)
25,000 Absorptions	Optical Density - 50.0 km^{-1}
37,229 Scatterings	Absorption/Extinction - 0.4

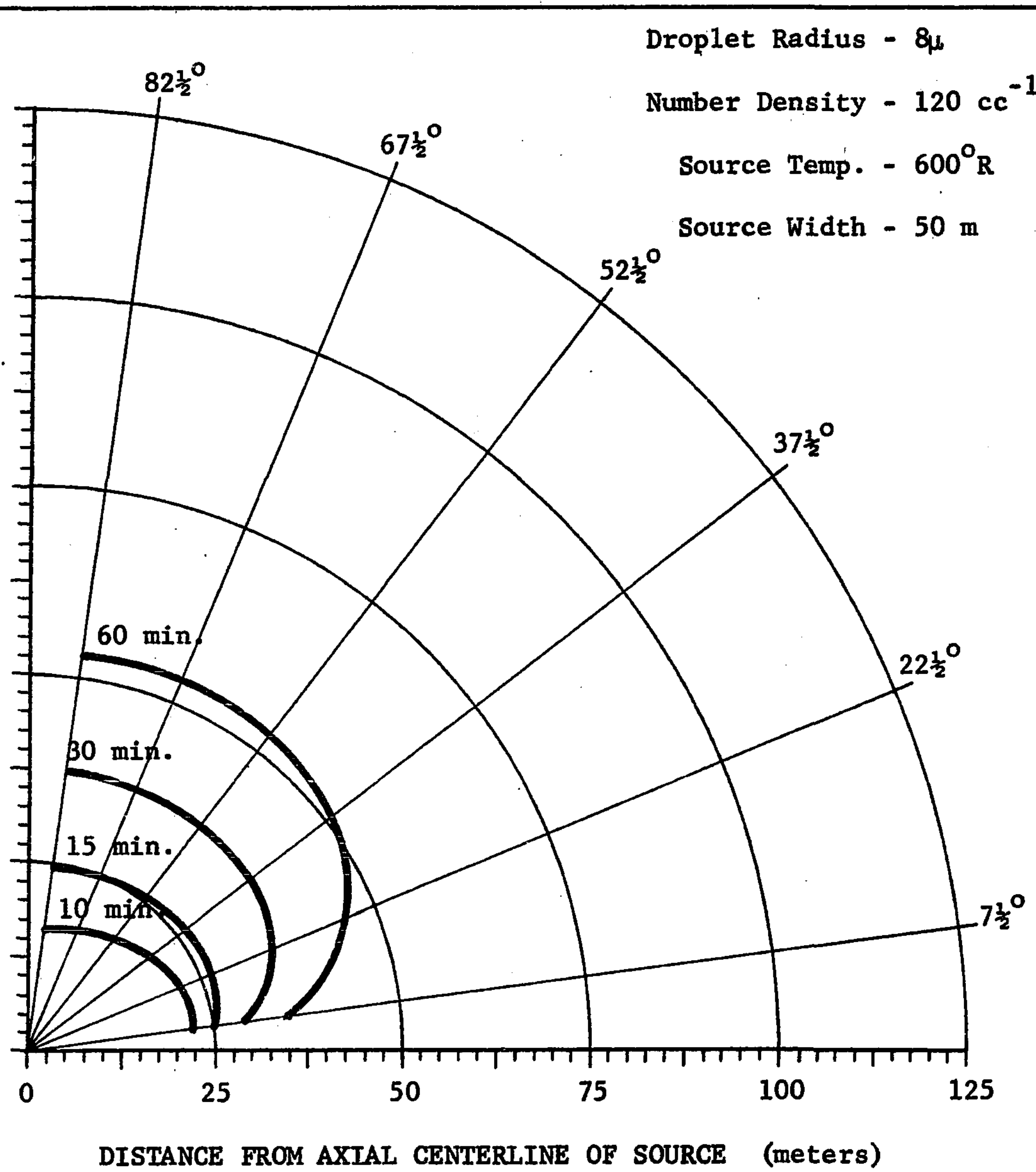

FIGURE 6-11

RELATIVE ISOCHRONS FOR RADIATIVE EVAPORATION OF DROPLETS BY A LONG RECTANGULAR SOURCE

52,002 Histories	Anisotropic Scattering (F)
50,000 Absorptions	Optical Density - 60.0 km^{-1}
75,122 Scatterings	Absorption/Extinction - 0.4

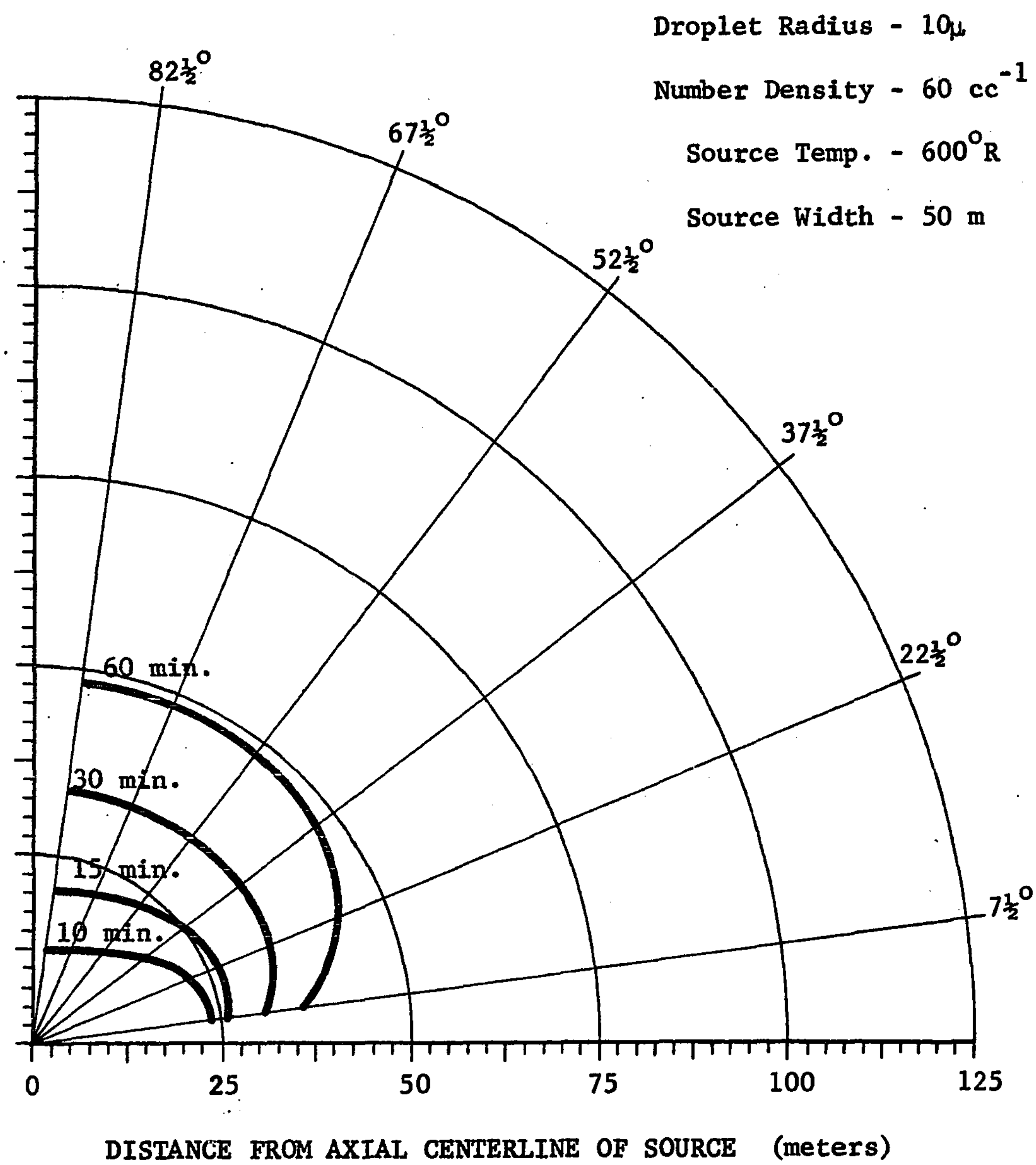

FIGURE 6-12

RELATIVE ISOCHRONS FOR RADIATIVE EVAPORATION OF DROPLETS BY A LONG RECTANGULAR SOURCE

50,921	Histories	Anisotropic Scattering (F)
50,000	Absorptions	Optical Density - 80.0 km^{-1}
74,922	Scatterings	Absorption/Extinction - 0.4

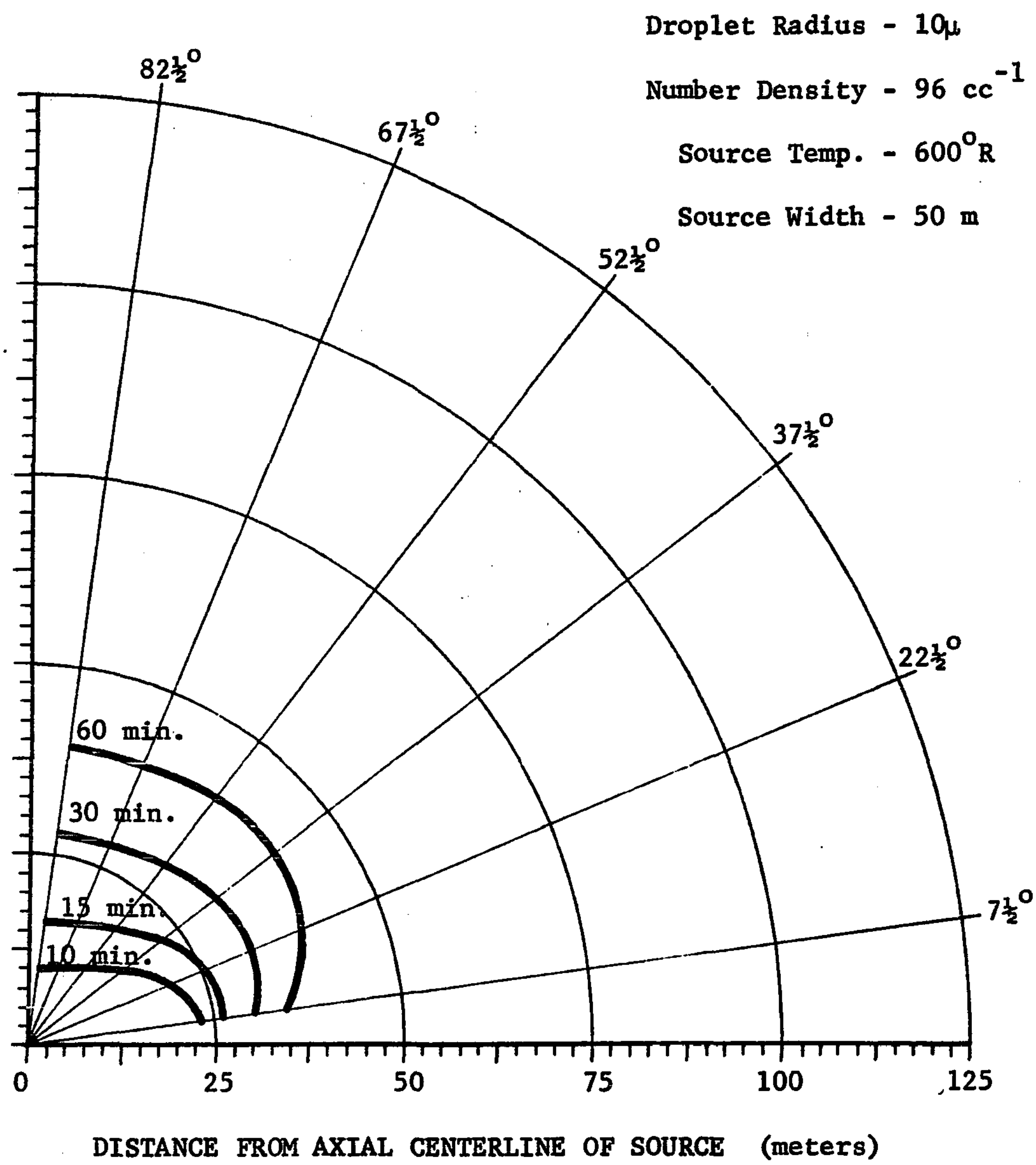

FIGURE 6-13

RELATIVE ISOCHRONS FOR RADIATIVE EVAPORATION OF DROPLETS BY A CIRCULAR SOURCE

112,984 Histories	Anisotropic Scattering (F)
25,000 Absorptions	Optical Density - 5.0 km^{-1}
37,186 Scatterings	Absorption/Extinction - 0.4

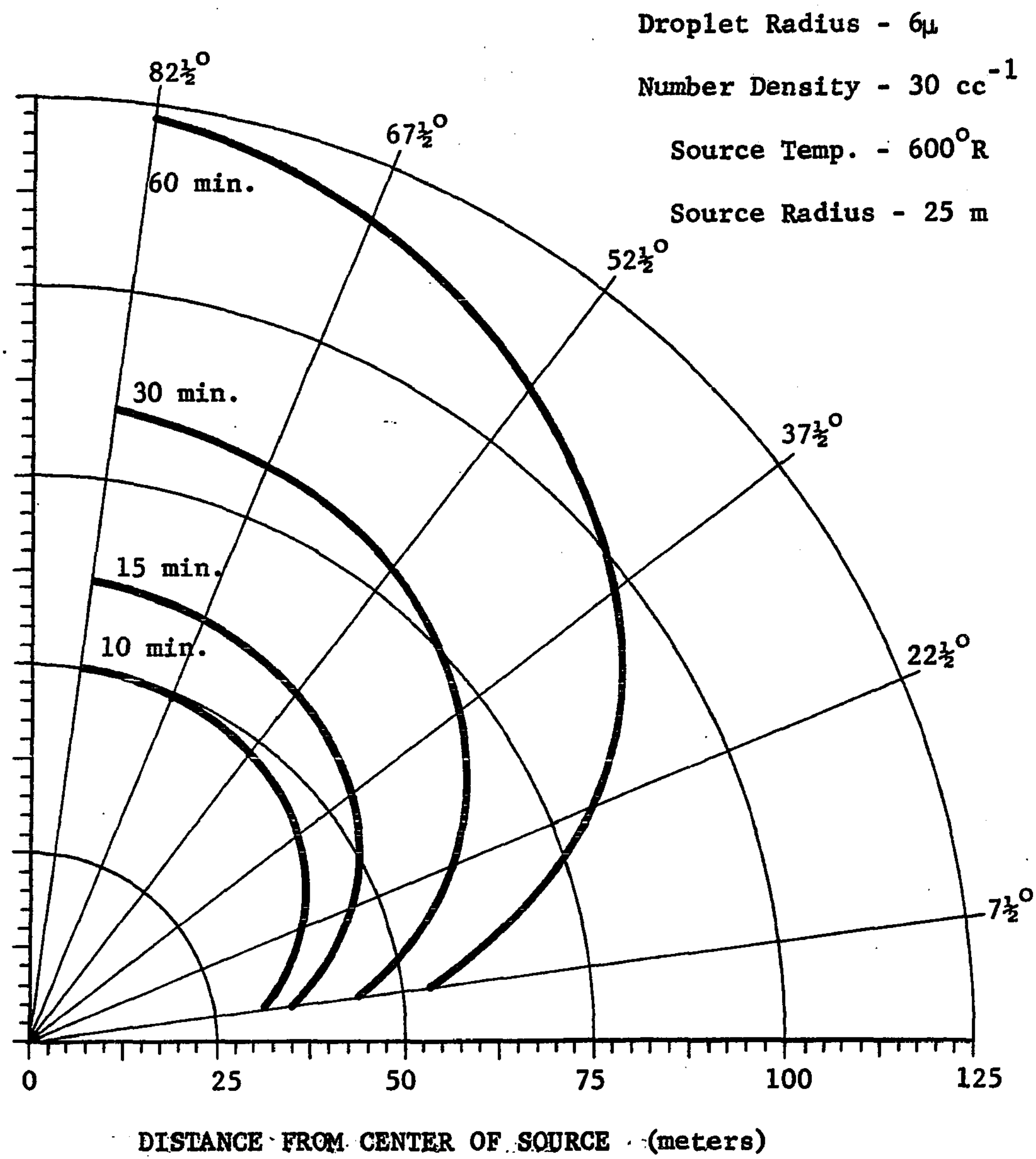

FIGURE 6-14

RELATIVE ISOCHRONS FOR RADIATIVE EVAPORATION OF DROPLETS BY A CIRCULAR SOURCE

80,758 Histories	Anisotropic Scattering (F)
25,000 Absorptions	Optical Density - 7.5 km^{-1}
37,520 Scatterings	Absorption/Extinction - 0.4

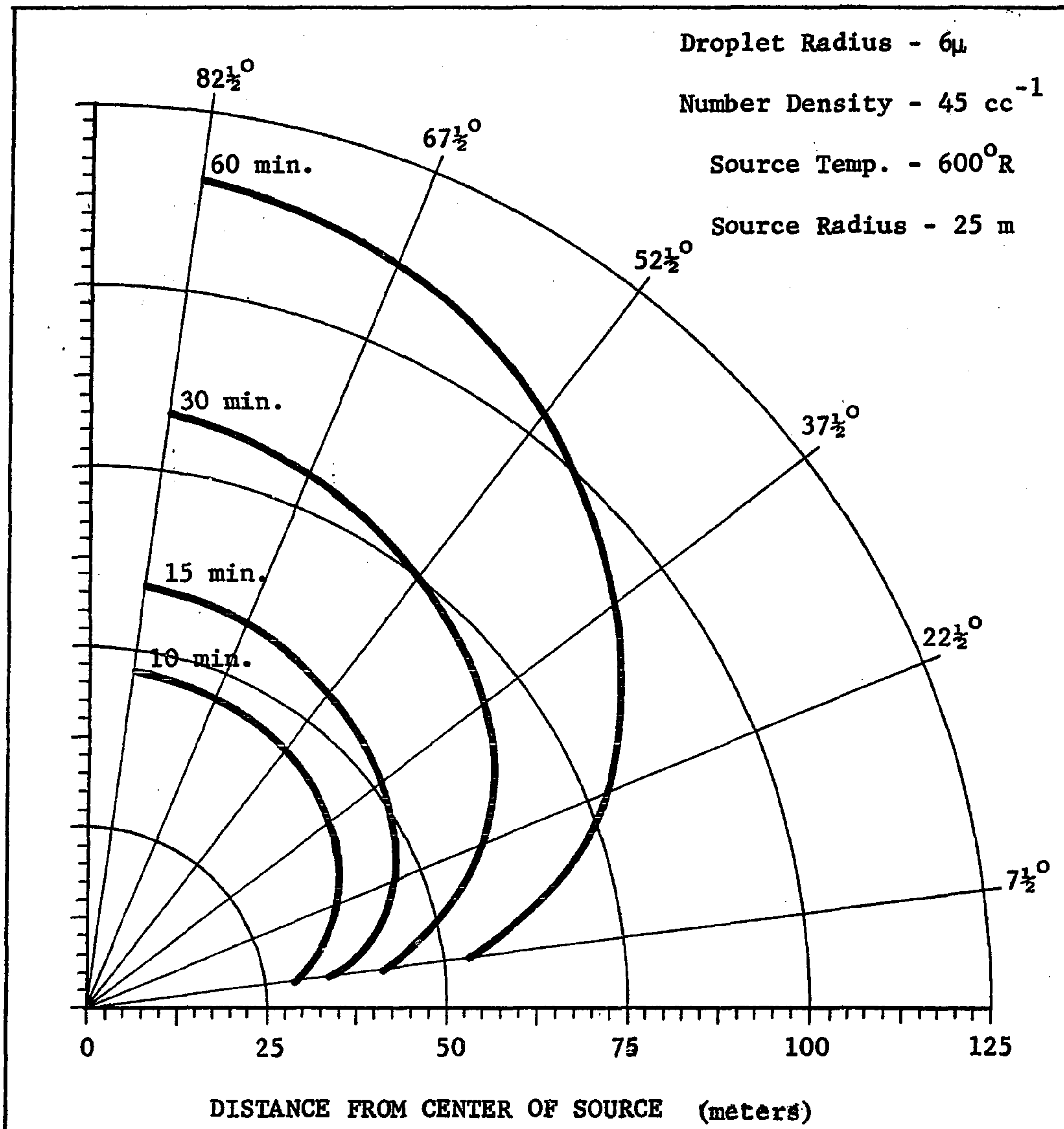

FIGURE 6-15

RELATIVE ISOCHRONS FOR RADIATIVE EVAPORATION OF DROPLETS BY A CIRCULAR SOURCE

63,799	Histories	Anisotropic Scattering (F)
25,000	Absorptions	Optical Density - 10.0 km^{-1}
37,176	Scatterings	Absorption/Extinction - 0.4

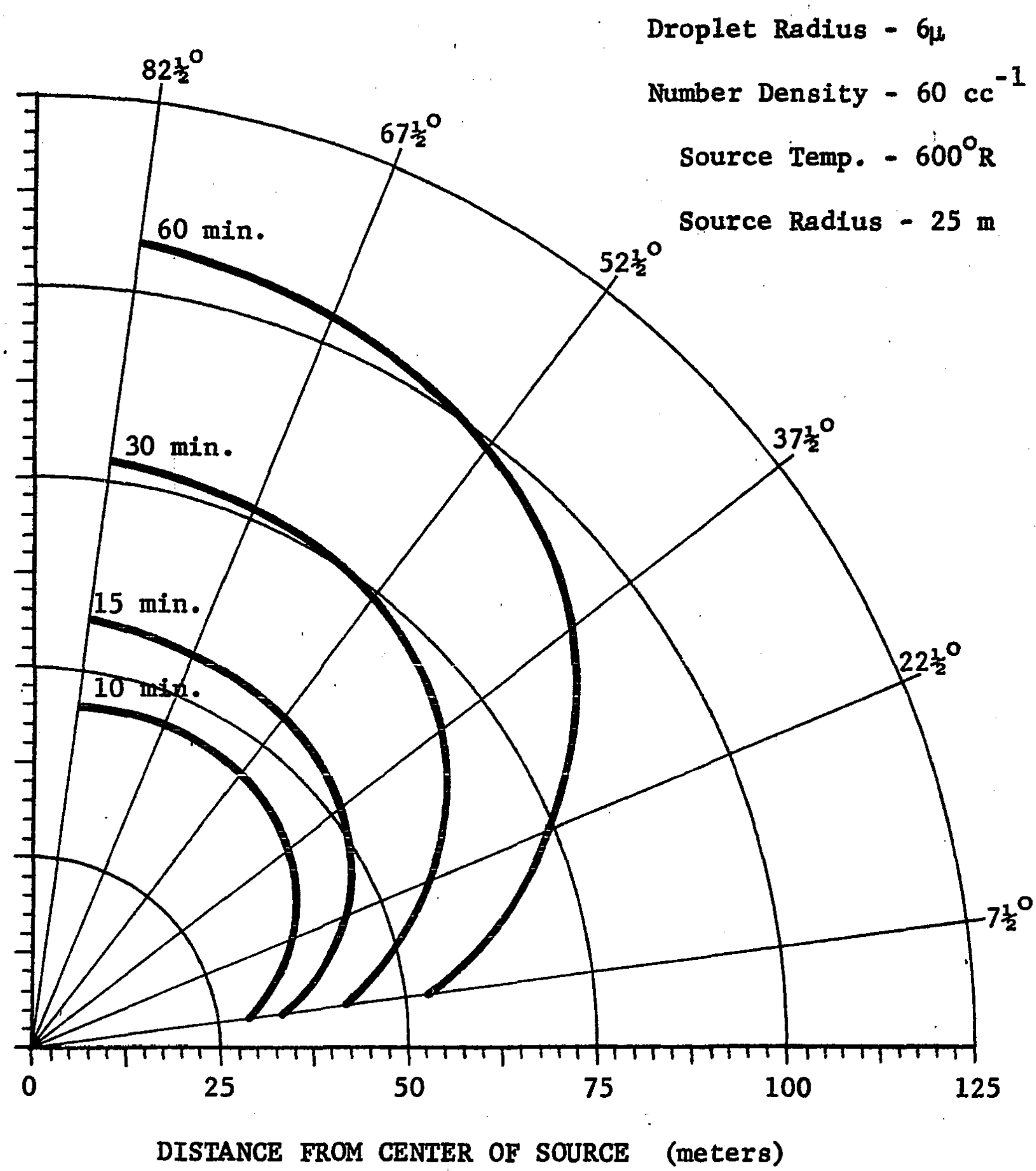

FIGURE 6-16

RELATIVE ISOCHRONS FOR RADIATIVE EVAPORATION OF DROPLETS BY A CIRCULAR SOURCE

47,503 Histories	Anisotropic Scattering (F)
25,000 Absorptions	Optical Density - 15.0 km^{-1}
37,393 Scatterings	Absorption/Extinction - 0.4

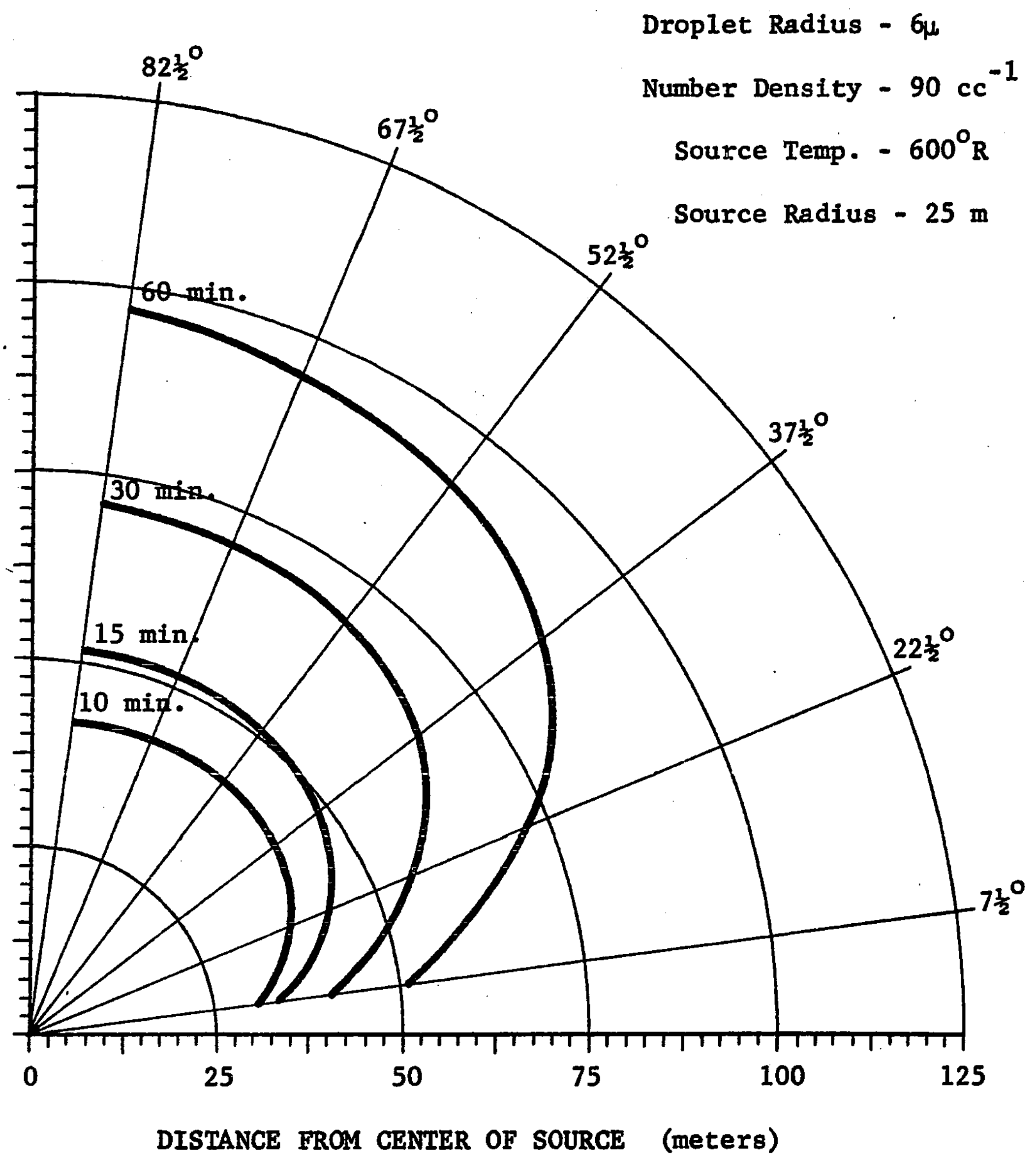

FIGURE 6-17

RELATIVE ISOCHRONS FOR RADIATIVE EVAPORATION OF DROPLETS BY A CIRCULAR SOURCE

39,777 Histories	Anisotropic Scattering (F)
25,000 Absorptions	Optical Density - 20.0 km^{-1}
37,292 Scatterings	Absorption/Extinction - 0.4

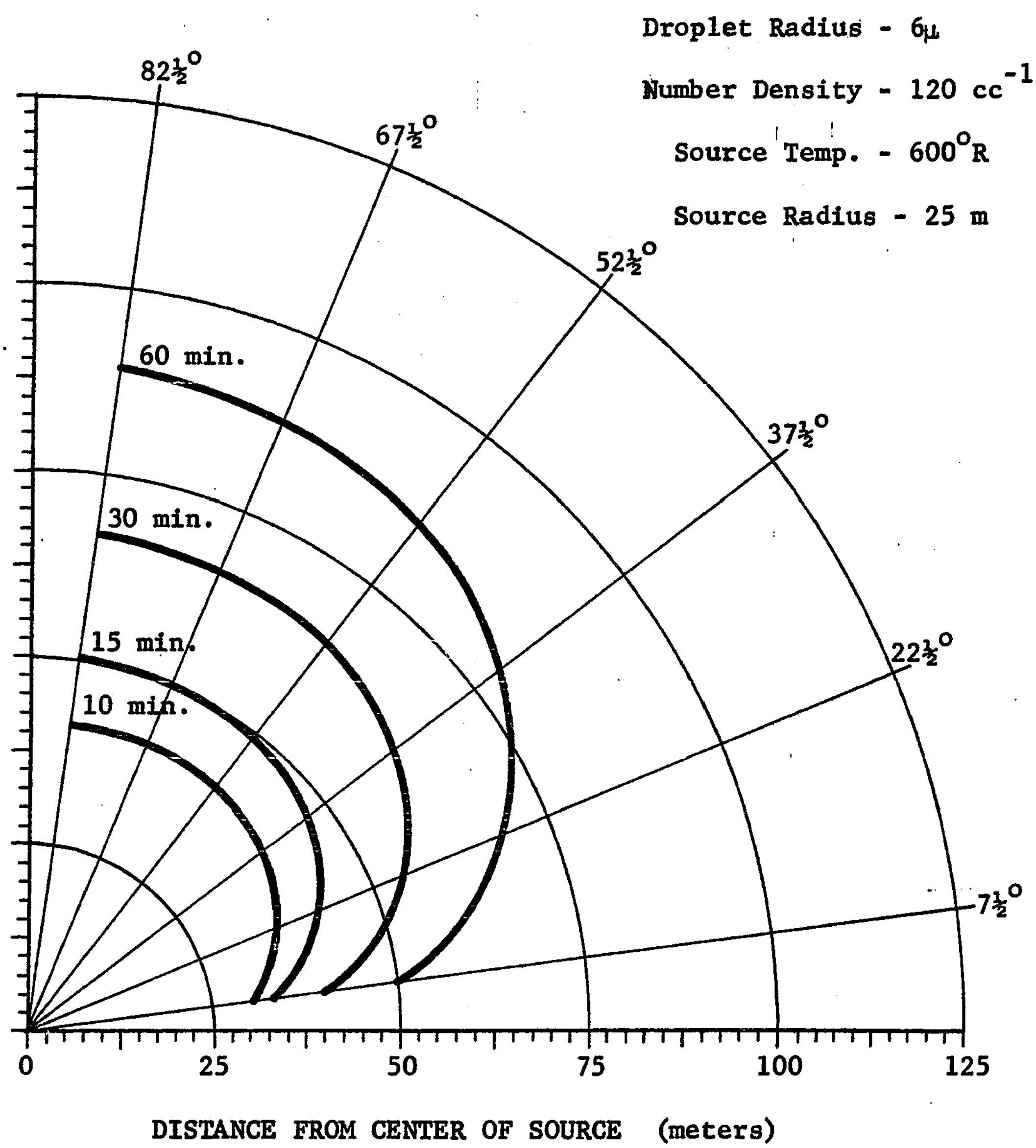

FIGURE 6-18

RELATIVE ISOCHRONS FOR RADIATIVE EVAPORATION OF DROPLETS BY A CIRCULAR SOURCE

35,805	Histories	Anisotropic Scattering	(F)
25,000	Absorptions	Optical Density - 24.0 km^{-1}	
37,268	Scatterings	Absorption/Extinction - 0.4	

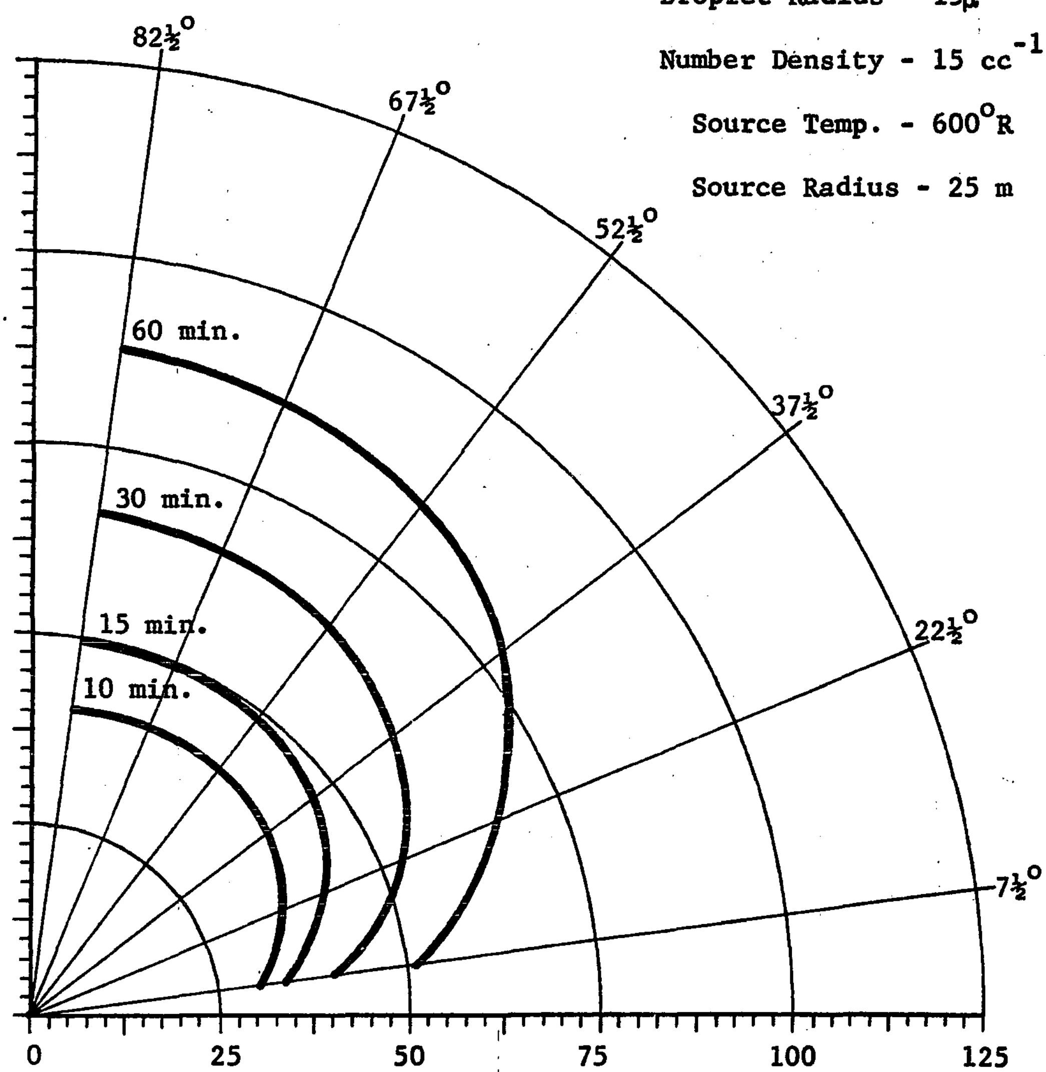

FIGURE 6-19

RELATIVE ISOCHRONS FOR RADIATIVE EVAPORATION OF DROPLETS BY A CIRCULAR SOURCE

27,352	Histories	Anisotropic Scattering (F)
25,000	Absorptions	Optical Density - 50.0 km^{-1}
37,339	Scatterings	Absorption/Extinction - 0.4

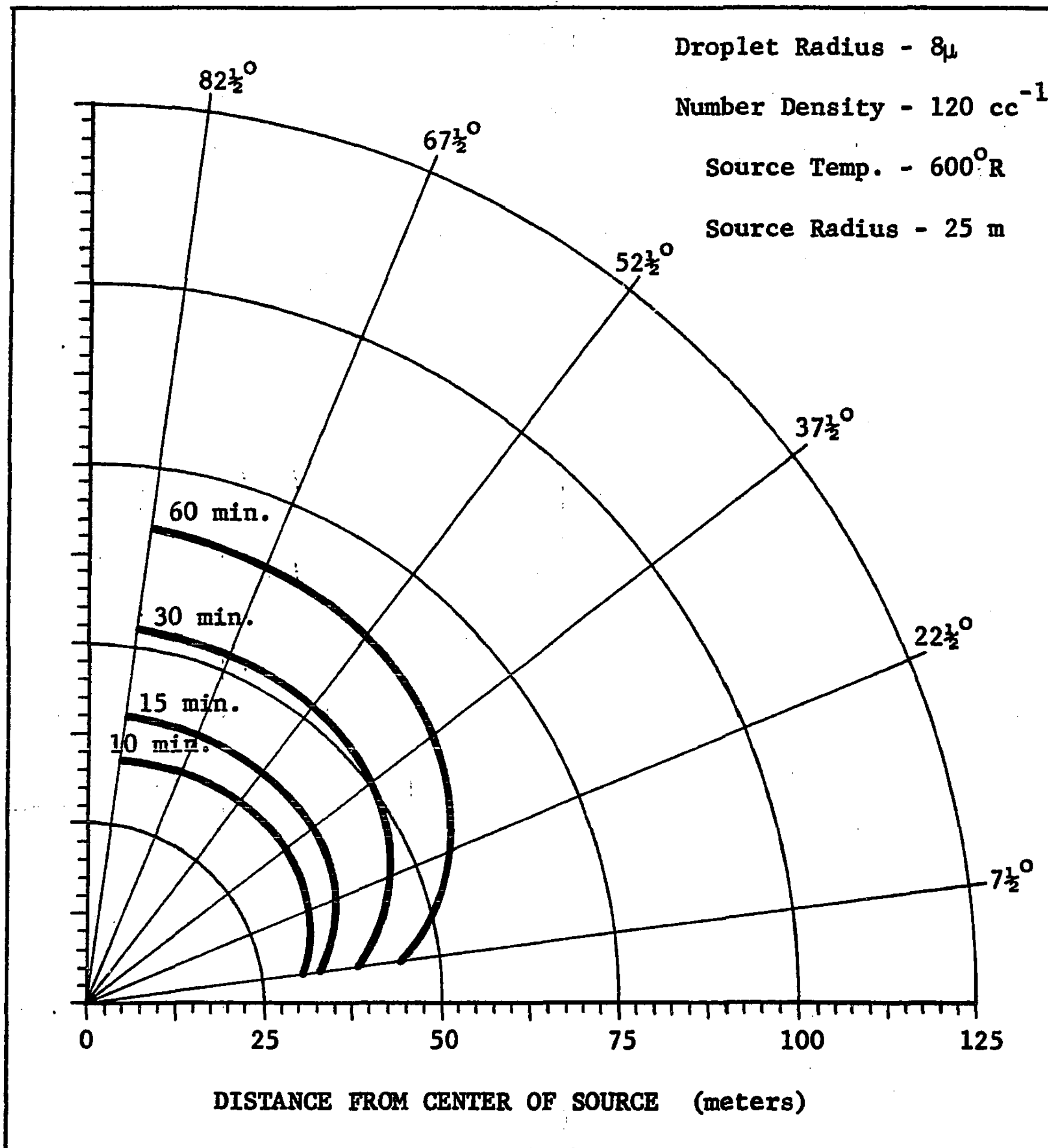

FIGURE 6-20

RELATIVE ISOCHRONS FOR RADIATIVE EVAPORATION OF DROPLETS BY A CIRCULAR SOURCE

25,604 Histories	Anisotropic Scattering (F)
25,00 Absorptions	Optical Density - 80.0 km^{-1}
37,275 Scatterings	Absorption/Extinction - 0.4

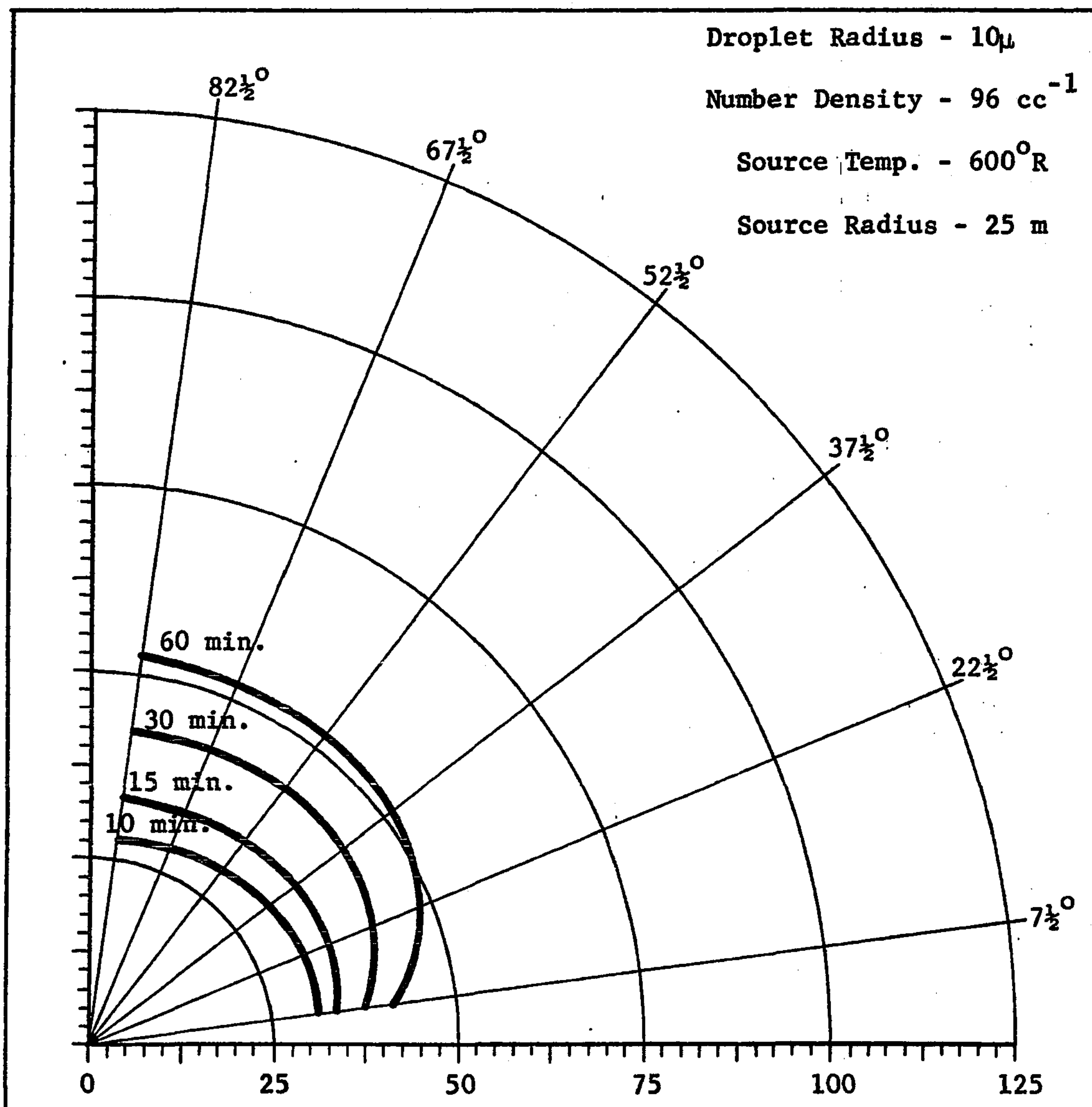

FIGURE 6-21

CHAPTER VII

COMPARATIVE ANALYSIS OF NUMERICAL RESULTS

Chapter VI introduced the format of the absorption data contained in Appendix F and has shown how this information can be transformed for presentation as an isochronic curve.

The tables of absorption data contain legends which summarize the numbers of photon histories and other major interaction events. These legends are able to provide some general insight into the complex problem being studied in this work. The absorption data, which were generated by the computer programs of Appendix H, were based on the collection of either 25,000 or 50,000 total absorptions. One case was run for 100,000 absorptions in order to check the convergence of the absorption data to a stable numerical result. The output from this check program confirmed the validity of the numerical data obtained for the 25,000 and 50,000 absorptions runs. It should be pointed out that a greater number of absorptions does add to the confidence in the statistical result as indicated in Appendix B.

The number of histories required to produce the requisite number of absorptions diminished rapidly with increasing optical density. For the long rectangular source, at an optical density of 2.5 km^{-1}, 343,008 histories were required to produce 50,000 absorptions, while at an optical density of 80 km^{-1}, it required only 50,921 histories to achieve the 50,000 absorptions level.

Since only absorptions or escapes can terminate a photon history, the numbers just cited support the observation that a large number of photons escaped in the optically thin case. The mean free path of a photon was established in Chapter IV as being equal to the reciprocal of the optical density. For the optically thin case, optical density of 2.5 km^{-1}, the mean free path would be 400 meters. This distance is well in excess of the imaginary bounding surface of the accounting shell; therefore, a significant portion of the photons emitted from the source will escape without any radiative interaction with the aerosol. The optically thicker case, optical density of 80 km^{-1}, would have a mean free path of only 12.5 meters. This case would provide a number of radiative interactions with the surrounding aerosol before a photon could travel a sufficient distance to escape. Since 40 or 50 percent of all interactions are absorptions, the optically thick case would strongly favor this history terminating event over an escape from the shell.

The discussion just completed is graphically illustrated by the fact that there were 293,008 escapes for the optically thin case and only 921 escapes for the optically thick case. Both cases involved a total of 50,000 absorptions.

The escape information contained in the legend is not broken down although it would be simple to modify the computer programs so that escapes could be categorized as base plane escapes, side or shell escapes, or in the case of the long rectangular source, end escapes. Except for collecting information on end escapes, the present work simply lumped the remaining escapes into a single category.

The work of Stockham (25) provides some insight into this problem of escape distribution. While the geometry for the work of this reference is not identical to that used in this research, it is similar enough to allow some conclusions with regard to base plane escapes. Stockham was interested in the number of photons, having been emitted from a black circular source and scattered by a cylindrical particle cloud, that struck the base plane containing the source. The number of photons striking the base plane was significantly greater for all cases using isotropic scattering as compared to a forward type scattering function. This increase in base plane hits was evident both within the cloud and at base plane locations outside the cloud. In spite of the differences in geometry, the similarities are such that it seems certain that the base plane escapes are increased by the use of isotropic scattering as compared to forward scattering for the physical models of this research. The logic of this conclusion is easily established in a conceptual way by noting that the emission from the source is always in a direction away from the base plane. With forward scattering the original sense of direction is altered least; therefore, it would be anticipated that there would be fewer base plane escapes.

End escapes have not been listed for the long rectangular source cases even though this parameter was collected for all runs. The results indicated that such losses were insignificant. They were nonexistent in all but four case studies where thay amounted to 20 losses out of 343,008 emissions, 4 losses out of 93,962 emissions, 1 loss out of 89,486 emissions, and 3 losses out of 77,950 emissions. All of these losses were for the optically thin cases with optical densities of 2.5 or 5 km^{-1}.

The number of scatterings listed in the legend should bear a fixed relationship to the number of absorptions. The sum of the absorptions and scatterings represent the total extinction interactions. The ratio of absorption interactions to scattering interactions should be either 1./1.5

or 1./1. depending on whether the ratio of the absorption coefficient to extinction coefficient is 0.4 or 0.5. The numerical information generated on the number of scatterings and absorptions falls within about 1% of the expected values. This result is considered to be a confirmation that the probabilistic analytical model is operating satisfactorily.

The computer facilities at the University of Oklahoma generated sufficient photon histories to produce 25,000 absorptions in about 25 minutes for the optically thicker cases and in about 45 minutes for the optically thinner cases.

The isochronic curves, displayed in Chapter VI, were all drawn for an absorption coefficient to extinction coefficient ratio of 0.4 and for the forward scattering function designated (F). The purpose in doing this was to establish a family of standard curves, one for each value of optical density, so that comparisons with cases involving changes in the problem parameters would be facilitated. The curves themselves are of interest in comparing the effects of optical density on the position and shape of the relative isochrons.

The general shape of the relative isochrons would be expected to reflect the symmetry of the physical model and its emission distribution. In this respect, the findings of this work are intuitively reasonable. However, any attempt to try to explain specific shape characteristics soon meets with difficulty due to the complex nature of the radiative interactions with the aerosol. It is the very complicated nature of these interactions that led to the probabilistic analytical approach selected for this work. In all cases involving either source configuration, there is a shrinking of the relative isochrons toward the source as the optical density of the aerosol is increased. This shrinking might have been anticipated in view of the decreasing length of photon mean free path.

The differences in shape for relative isochrons, brought about by a change in source geometry, for a given optical density, tend to be sympathetic to the distribution of emissions from the source and the geometry of collection imposed by the accounting envelope and its subspace volumes. The fact that the cross section of the accounting shell is the same for either source tends to hide the fact that the volumes of the subspaces are quite different.

The temporal boundaries of the dissipating fog and the spatial location of the relative isochrons are not synonymous. In actual thermal dissipation, the physical and optical properties of the aerosol would be changing at any spatial location with time. The rate of change in aerosol properties would be greatest at locations near the source. These locations would tend to be cleared of their fog in a relatively short period of time and would subsequently represent volumes filled with a medium transparent to the radiation in the wavelength interval providing direct heat transfer to the droplets. Thus, emitted photons would be able to penetrate to locations more distant from the source, and direct energy exchange with the droplets at these more distant locations would be enhanced. For the reasons developed above, the relative isochrons could be considered as conservative estimates of the boundaries of the thermally dissipating fog in the absence of diffusion activity within the aerosol.

Before presenting the comparative illustrations of this chapter, a somewhat oversimplified conceptual discussion of the interaction events between photons emitted from the source and the droplets of the surrounding aerosol should prove helpful. The energy exchange at any small spatially fixed volume is a function of the number density of photons at that location and the fraction of interactions that are energy transferring absorptions. An important parameter in this discussion is the mean free path length of the photon, which along with the other physical and optical properties of the aerosol is considered to remain constant during the generation of numerical results for each example problem. When a relative isochron, considered as an imaginary surface through which photons pass, is located at a distance from the source that is much shorter than the mean free path length of the emitted photons, the photon number density is high. The rate of evaporation along the isochronic surface could be improved in this instance by increasing the fraction of interactions that are absorptions or by increasing the number density of photons. When the relative isochron is located at a distance from the source that is much greater than the mean free path length of the emitted photons, any photon that reaches the vicinity of the isochronic surface will probably have suffered several interactions enroute. Since many of these interactions are history terminating absorptions, the number of surviving photons that pass through the isochronic surface could be very small. Improved energy exchange in this situation might be enhanced most by increasing the photon number density at this spatial location. Because of its importance in evaluating the information on the comparative illustrations, the mean free path length has been made a part of the legend information on each illustration.

The format for the comparative curves in this chapter is somewhat different than that used for the relative isochrons in Chapter VI. Instead of using a polar plot, the radial distance of the relative isochron from the source is the ordinate on a rectangular plot with the angle above the horizontal as abscissa. This type of comparative illustration was chosen because it maintained good separation of lines. This separation should reduce the possible confusion of lines that would exist on a polar plot for the optically thicker cases.

Now that the family of comparative isochronic curves has been established from Chapter VI, it is of interest to change some of the radiative parameters and observe the subsequent changes generated in the positions of the relative isochrons. The first comparison will involve the ratio of absorption coefficient to extinction coefficient. As indicated in the tabular absorption data, Appendix F, this parameter was investigated for numerical values of 0.4 and 0.5 for a large number of optical densities, all using the same forward scattering function, (F), as that for the set of standard comparative isochronic curves. For this reason it is possible to make direct comparisons with individual relative isochrons from the standard curves which were drawn for an absorption coefficient to extinction coefficient ratio of 0.4. Several comparisons, involving only the change in the ratio of absorption interactions, for the long rectangular source model, spanning the range of optical densities investigated in this work have been illustrated. Figures 7-1 through 7-5 provide this comparison for increasing values of optical density. Figure 7-6 is a similar curve for a single case involving the circular source.

These illustrations show that for the limiting case involving a low value of optical density or high value of photon mean free path length, and a relative isochron near the source compared to mean free path length (see the 15 minute isochron on Figure 7-1), the increased rate of absorption interactions is beneficial. This is due to the high number density of the photons in the vicinity of this isochronic surface and the increased number of interactions with the aerosol droplets that are absorptions.

These absorptions mean that more energy is being made available to evaporate liquid at the spatial location depicted by the isochronic surface and as a result, this surface expands to a new radial location which encompasses the additional liquid water required to accommodate the increased energy transfer through droplet evaporation.

The other limiting case for these illustrations involves a high value of optical density or a short photon mean free path length, and a relative isochron remote from the source compared to the length of the mean free path. The 60 minute isochron on Figure 7-5 is an example of this situation. In this case, most photons that reach the isochronic surface will have encountered several interactions enroute. If a higher proportion of these interactions are history terminating absorptions, the number of photons that survive to reach the isochronic surface may be so small that the higher rate of absorption interactions cannot make up for the depleted supply of photons. In this case the local rate of energy exchange may be decreased thus requiring a shrinking of the isochronic surface to a new radial position where the energy transfer rate and the droplet evaporation requirements are in equilibrium.

The intermediate cases, involving locations and aerosol properties between these limiting cases, are subject to varying degrees of the same descriptive arguments used to explain the results for the limiting cases.

Figure 7-6 is a single example for the circular source at a low value of optical density. The comparative results shown on this illustration are similar to those indicated for a low optical density aerosol model with the long rectangular source (see Figure 7-2).

The next series of comparative illustrations involves the changes in spatial location of the relative isochrons brought about by changes in the

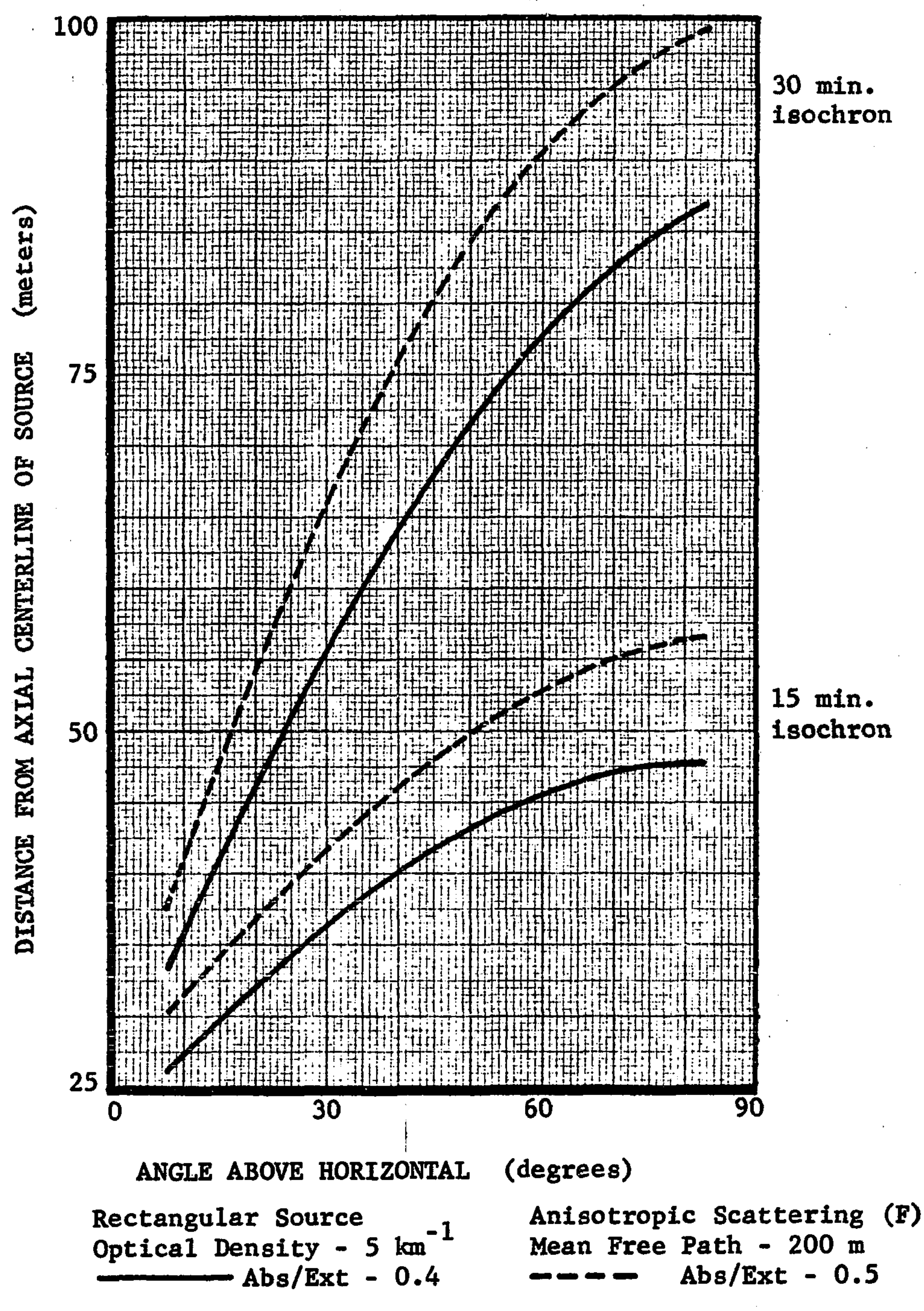

FIGURE 7-1 COMPARATIVE LOCATIONS OF RELATIVE ISOCHRONS

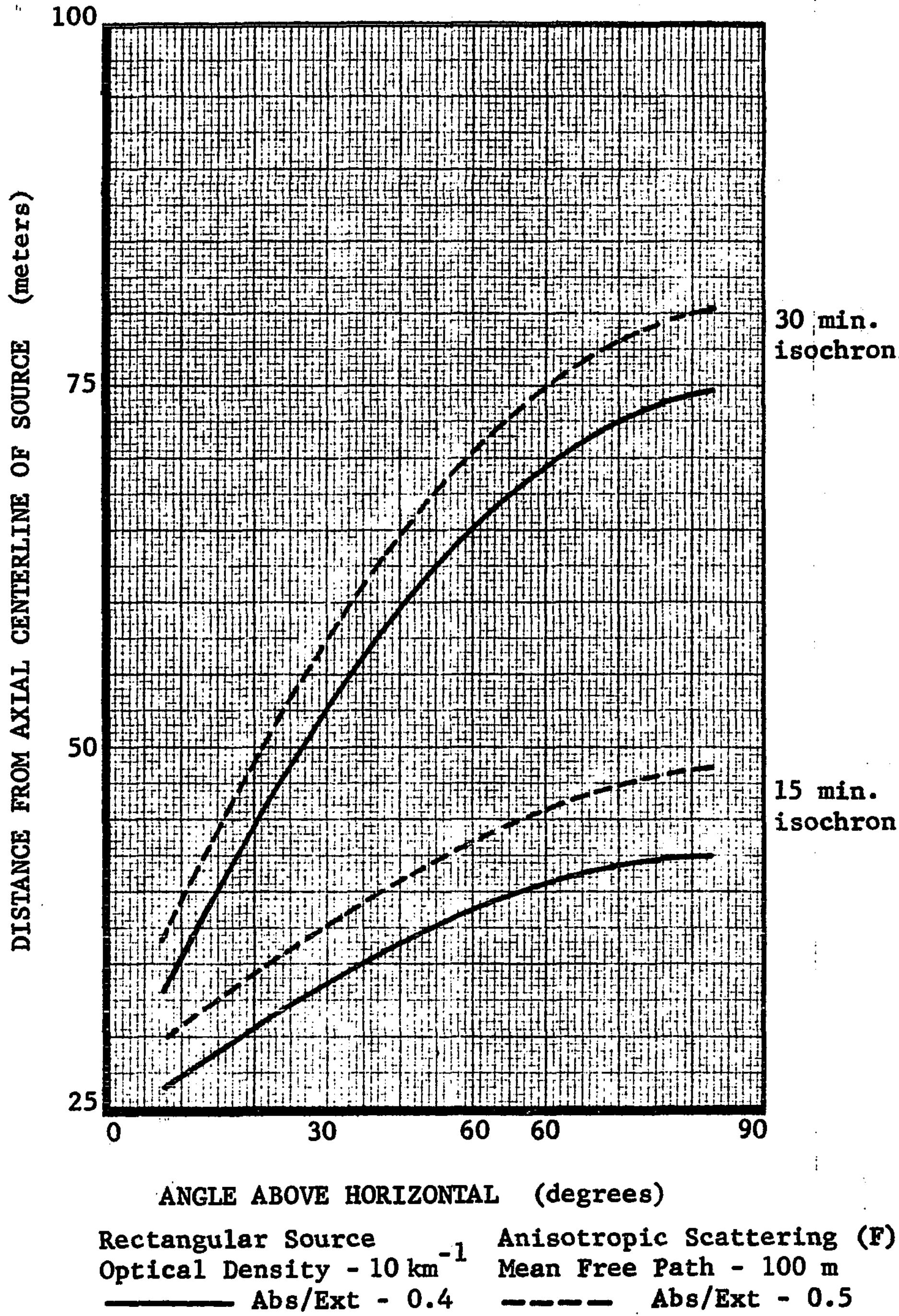

FIGURE 7-2 COMPARATIVE LOCATIONS OF RELATIVE ISOCHRONS

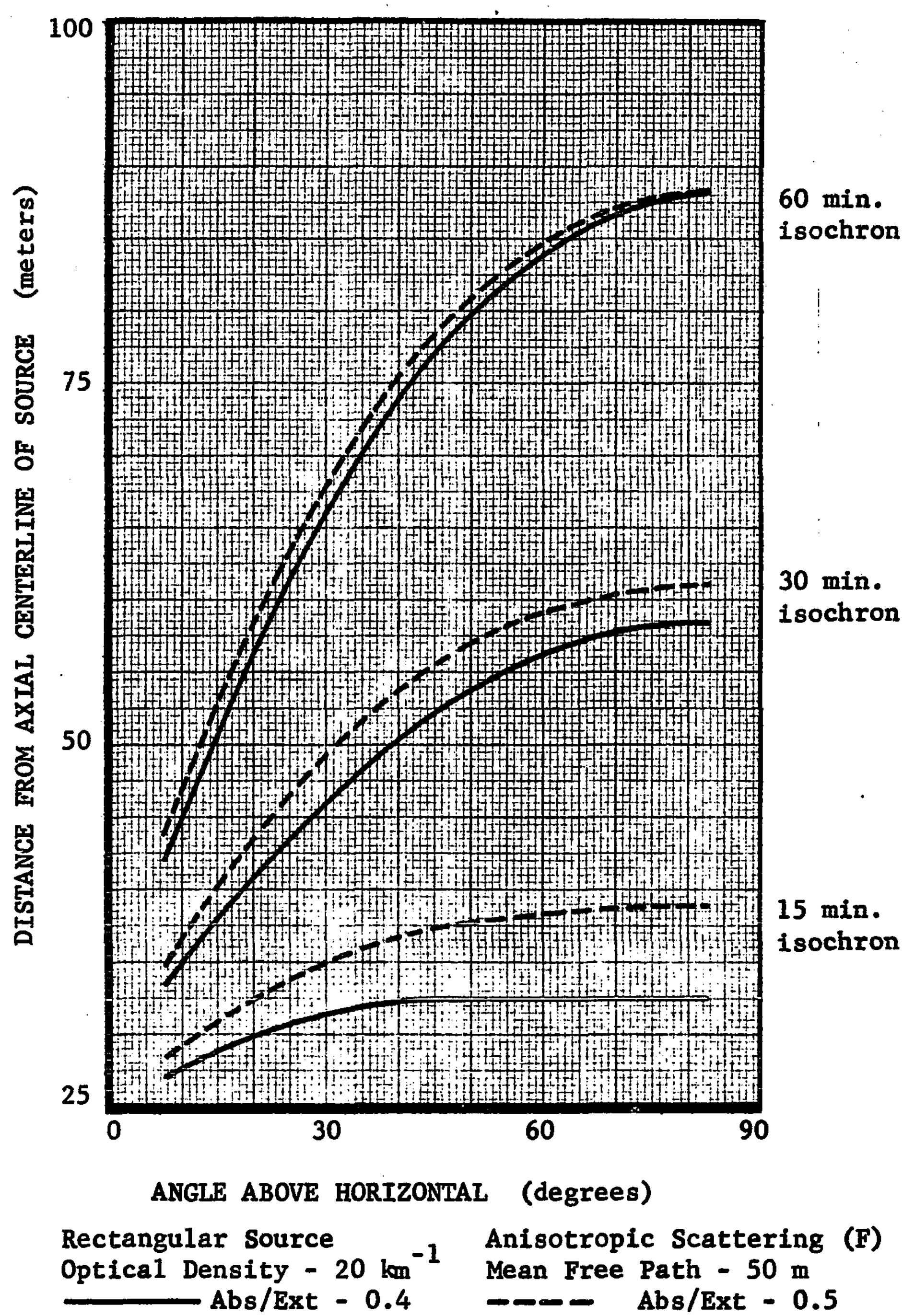

FIGURE 7-3 COMPARATIVE LOCATIONS OF RELATIVE ISOCHRONS

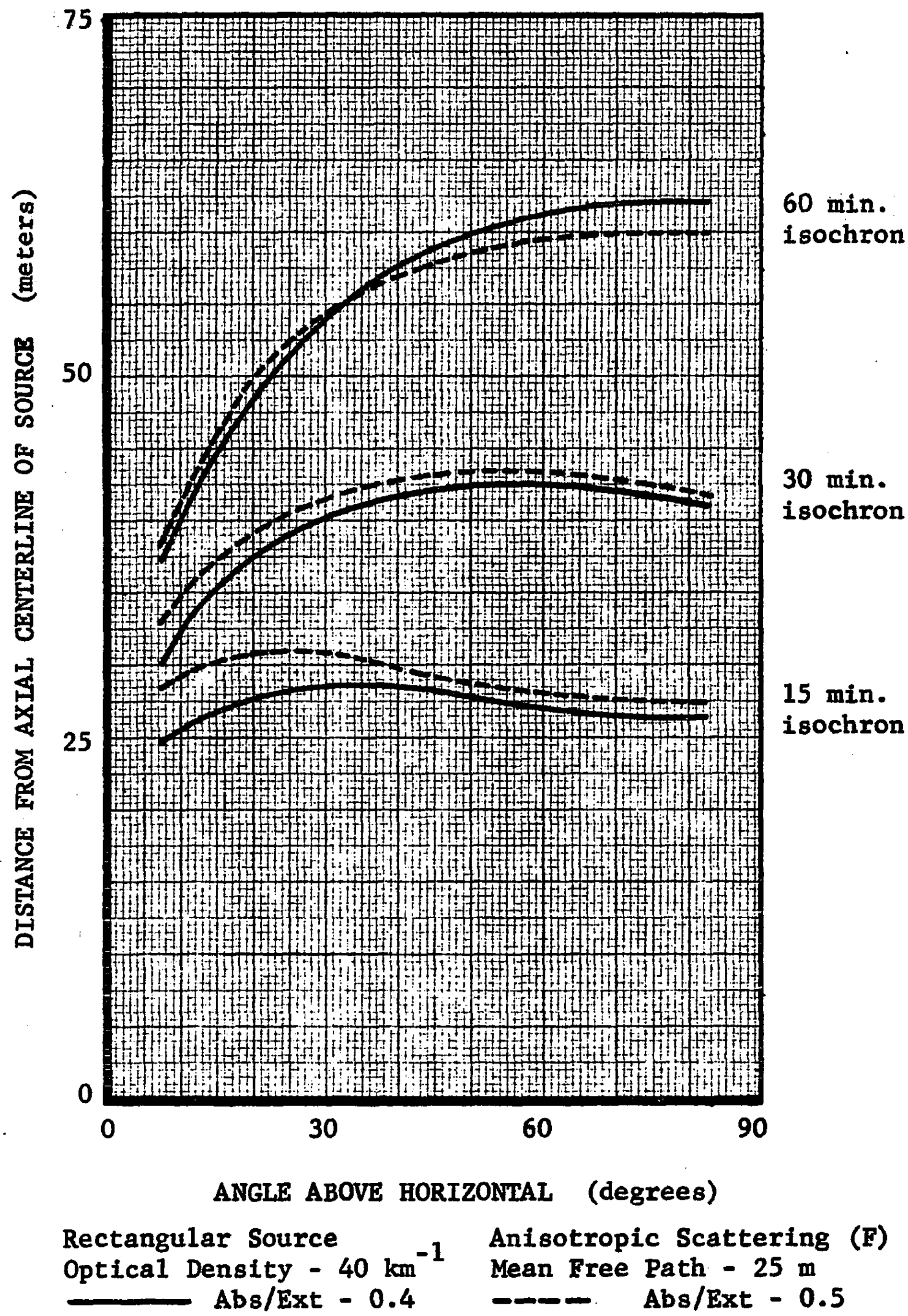

FIGURE 7-4 COMPARATIVE LOCATIONS OF RELATIVE ISOCHRONS

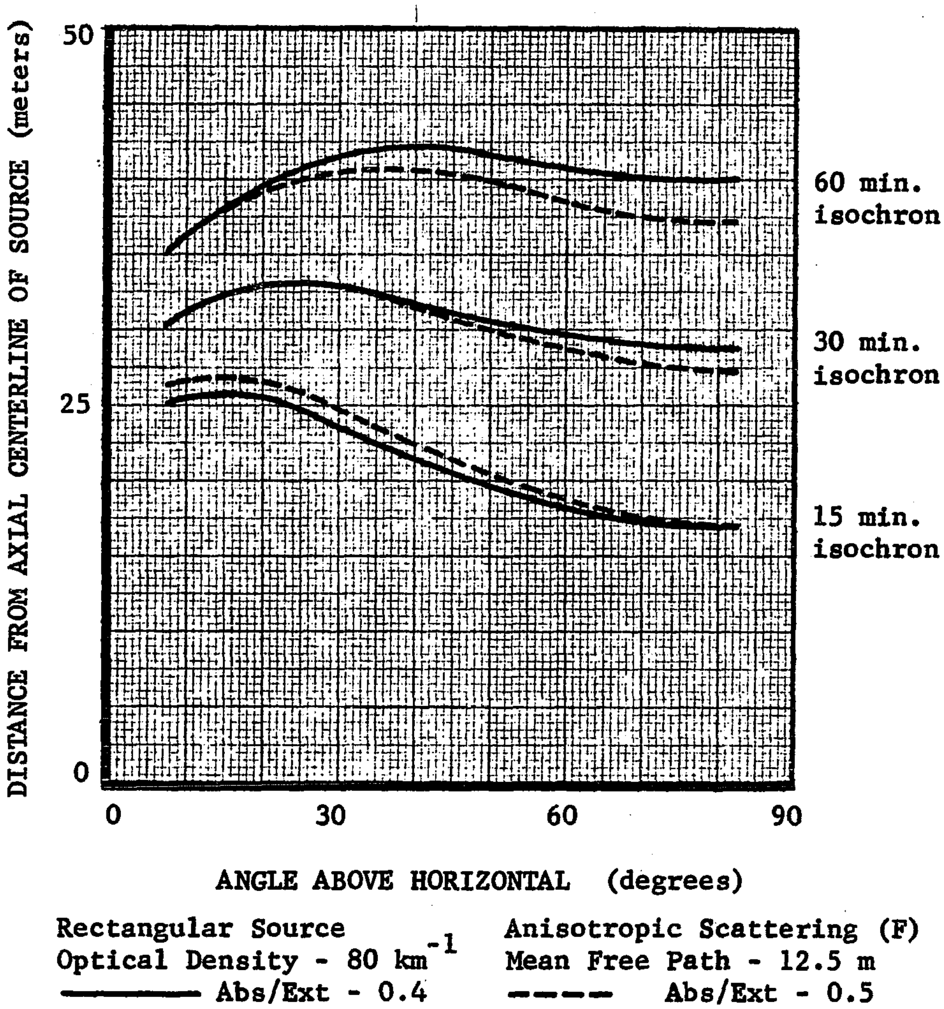

FIGURE 7-5 COMPARATIVE LOCATIONS OF RELATIVE ISOCHRONS

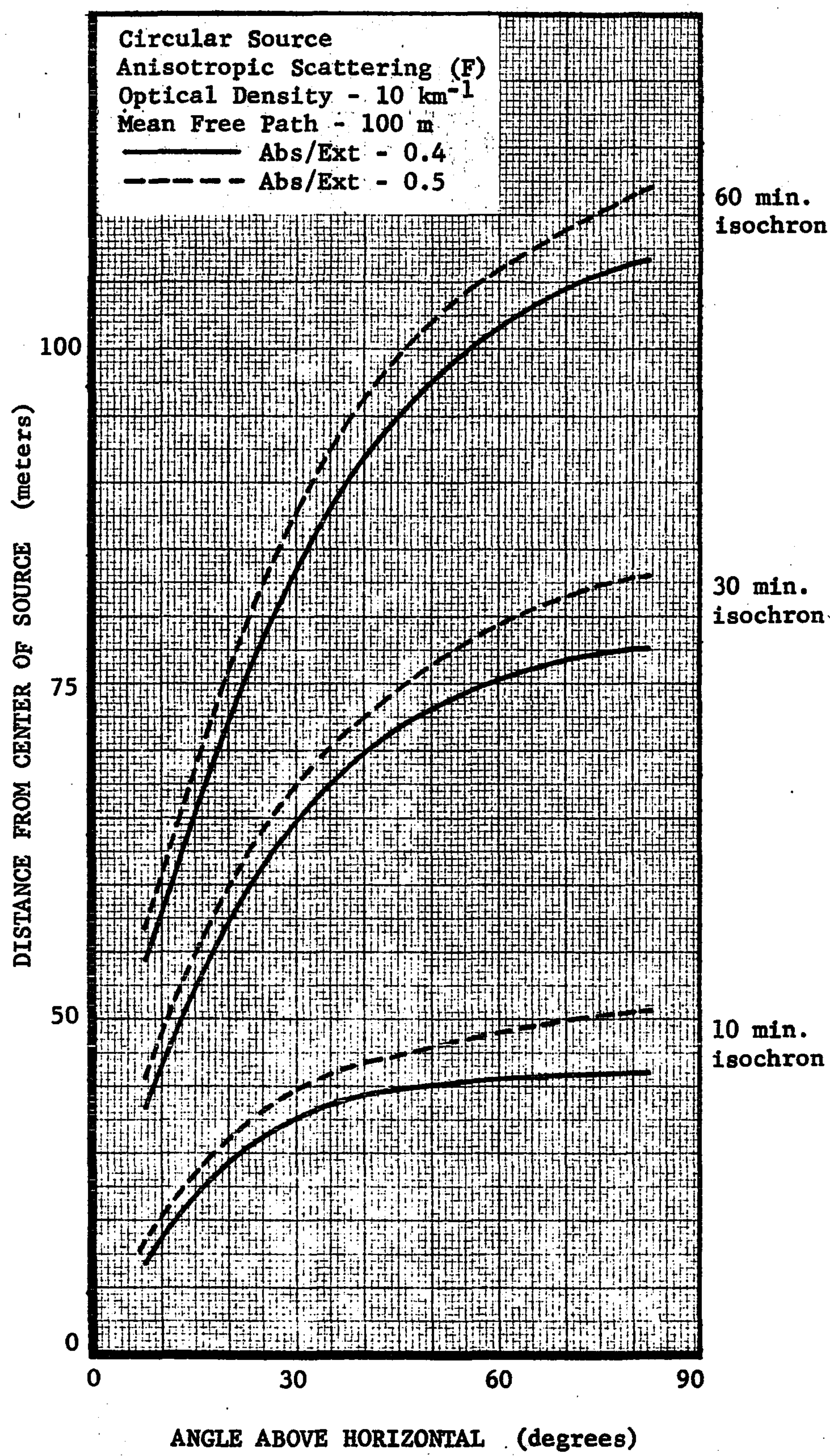

FIGURE 7-6 COMPARATIVE LOCATIONS OF RELATIVE ISOCHRONS

scattering function. The standard for this comparison will be the same isochronic curves, found in Chapter VI, which have been used in the preceding study involving the ratio of absorption interactions. These standard curves were drawn for the strong forward scattering function, (F), and for an absorption coefficient to extinction coefficient ratio of 0.4. Figures 7-7 through 7-14 represent comparisons between isotropic scattering, (I), and anisotropic scattering, (F), with an absorption coefficient to extinction coefficient ratio of 0.4. These comparative figures are arranged in increasing values of optical density. Figures 7-7 through 7-11 and Figure 7-15 are for the long rectangular source and Figures 7-12 through 7-14 are for the circular source.

It has already been noted that isotropic scattering increases the number of escapes through the base plane due to the fact that this type of scattering favors backward and forward scattering equally.

As before, the discussion will center on the limiting cases. For low values of optical density or long photon mean free path length, the relative isochrons near the source compared to the mean free path length (see the 15 minute isochron on Figure 7-7) are moved to increased radial locations under the influence of isotropic scattering. This improvement is due to the fact that the back scattered photons from isotropic scattering will increase the number density of photons in the vicinity of the isochronic surface and this increase leads to more absorptions. The greater number of absorptions is indicative of an increase in energy transfer at this location and as a result the isochronic surface expands to encompass more liquid water to utilize this energy for droplet evaporation.

For the limiting case involving a high value of optical density or a short photon mean free path, and a relative isochron in a remote location relative to the mean free path length, the 60 minute isochron of Figure 7-11 is used. In this case each photon will probably encounter several scattering interactions with the droplets of the aerosol before reaching the subject isochronic surface. Since the isotropic scattering function shows an equal preference for forward and backward scattering, this scattering model would make it more difficult for photons to reach a remote location as compared to the strong forward scattering model which tends to maintain a more nearly straight line of photon travel. Thus, the reduced number of photons reaching the remote isochronic surface with isotropic scattering will cause the surface to shrink toward the source until a position of equilibrium between energy transfer and evaporation requirements is reached.

Intermediate cases can be subjected to varying degrees of the same type of analysis just developed for the limiting cases.

Figures 7-12 through 7-14 represent similar comparisons involving isotropic scattering for the circular source with its hemispherical accounting shell. This particular accounting envelope has a large proportion of its volume, consequently liquid water, concentrated near the base plane. The subspaces generated by a given polar angle increment near the vertical are very small and contain only a small portion of the liquid water in the accounting envelope. Isotropic scattering has already been shown to favor keeping higher photon number densities in the vicinity of the base plane than would be expected with forward scattering. This tendency causes more interactions and energy transfer to take place in the vicinity of the base plane with a subsequent beneficial expansion of the relative isochrons near the horizontal. The question of why the forward scattering function is better for subspaces near the vertical is more complicated. These subspaces have greater linear extent in the vertical direction than in any lateral direction. Photons emitted from the diffuse plane source, favor being emitted in directions toward the vertical. If these photons continue to move in nearly the same direction after a scattering, their opportunity to eventually be absorbed in one of the subspaces near the vertical will be enhanced. Strong forward scattering will tend to maintain a similar direction of motion after scattering. Isotropic scattering, on the other hand, will tend to favor more lateral motion on the part of the scattered photon. This lateral motion will provide greater opportunity for the photon to be scattered outside the relatively small solid angle which defines a given subspace near the vertical.

Since the scattering function derived by Deirmendjian (7) has been used as the basis for developing practical scattering functions for use with natural fog, it is of interest to know how it compares with the strong forward scattering function for a fixed ratio of absorption coefficient to extinction coefficient of 0.4. For this comparison, the approximate analytical expression, developed in Chapter V and designated (D), was used. The difference in the spatial distribution of absorptions was small when this scattering function, (D), was compared to the strong forward scattering function (F). This might have been expected due to the strong resemblence of the probability distribution functions for these cases. Figure 7-15 has been included in this chapter as an example of the excellent agreement between the two scattering functions (D) and (F). Figure 7-15 tends to confirm the fact that the points for the approximate function (D), though almost identical with those of the strong forward scattering function (F), slightly favor the position that would be taken by a comparative isotropic scattering isochron. This would be expected from the relative shapes of their probability distribution functions.

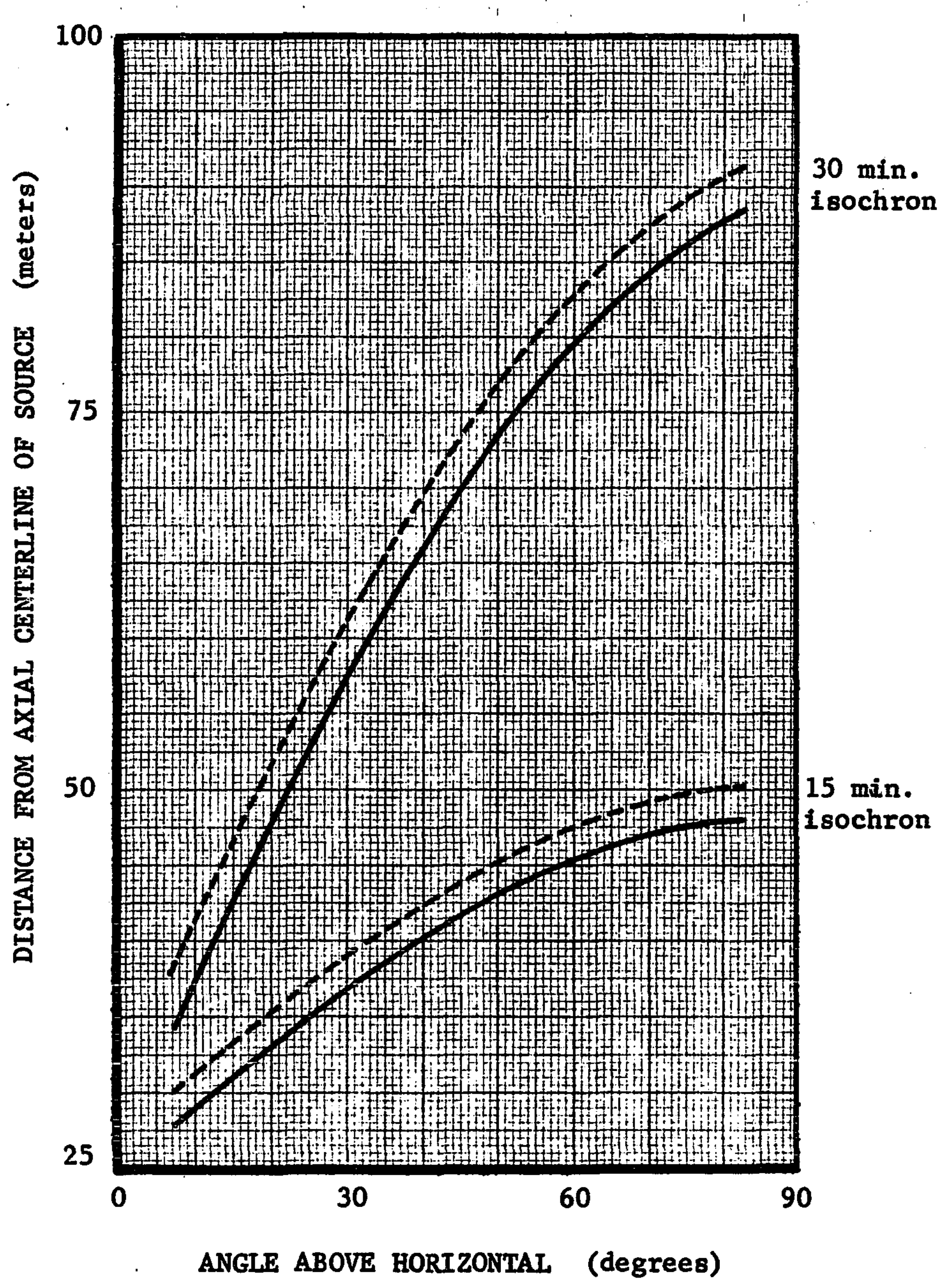

Rectangular Source
Optical Density - 5 km^{-1}
Mean Free Path - 200 m

Absorption/Extinction - 0.4
——— Anisotropic Scattering (F)
– – – – Isotropic Scattering (I)

FIGURE 7-7 COMPARATIVE LOCATIONS OF RELATIVE ISOCHRONS

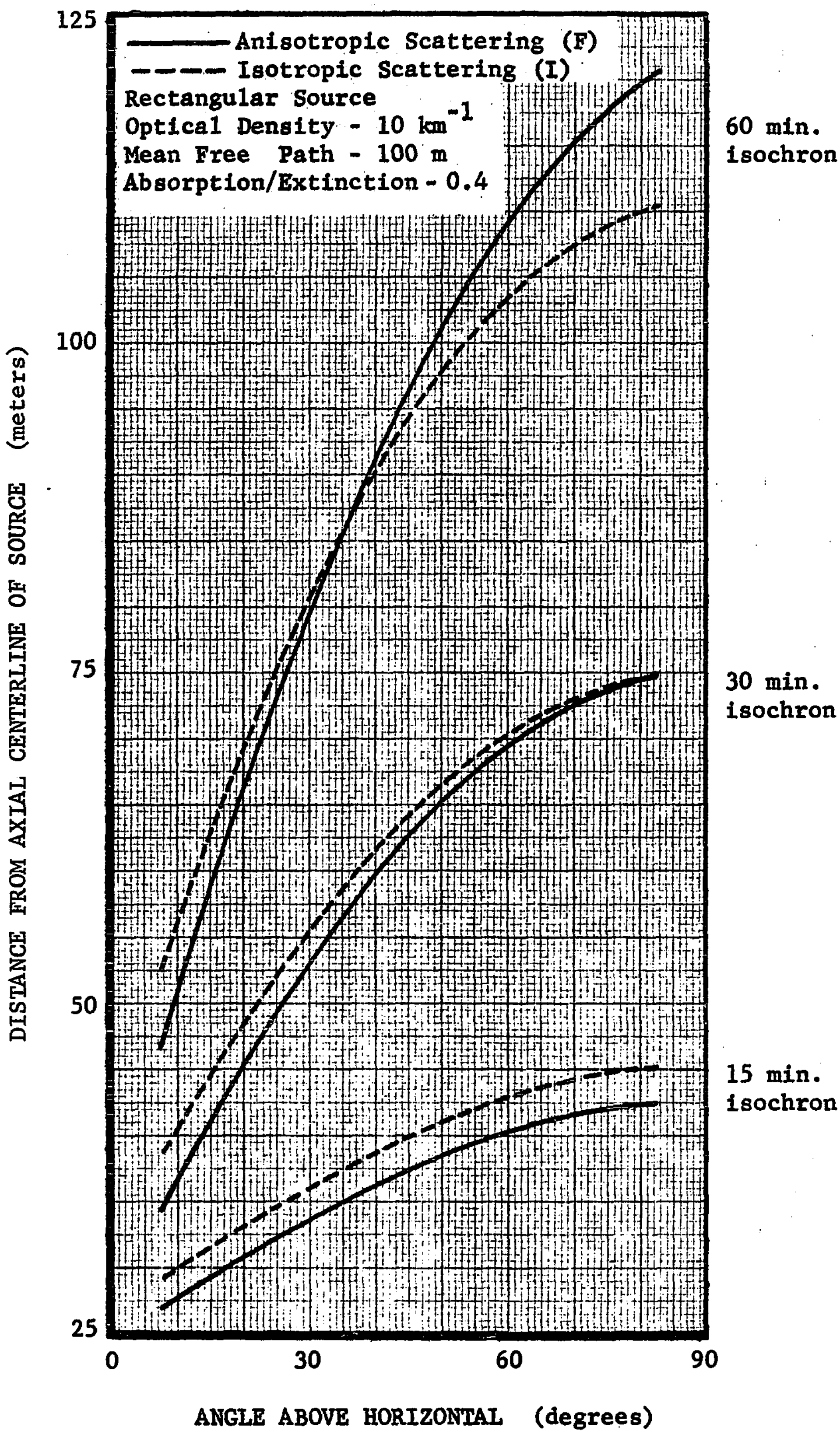

FIGURE 7-8 COMPARATIVE LOCATIONS OF RELATIVE ISOCHRONS

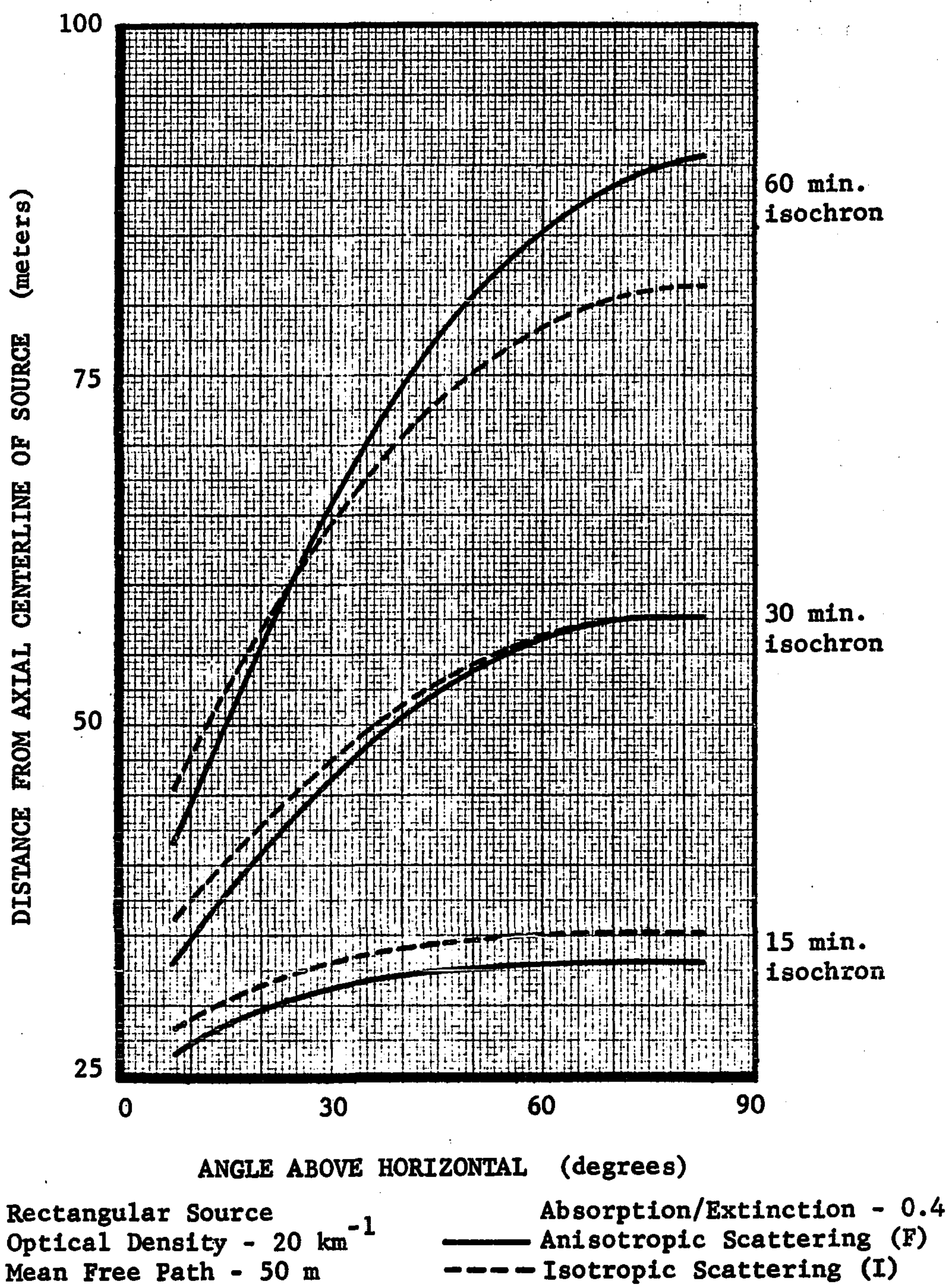

FIGURE 7-9 COMPARATIVE LOCATIONS OF RELATIVE ISOCHRONS

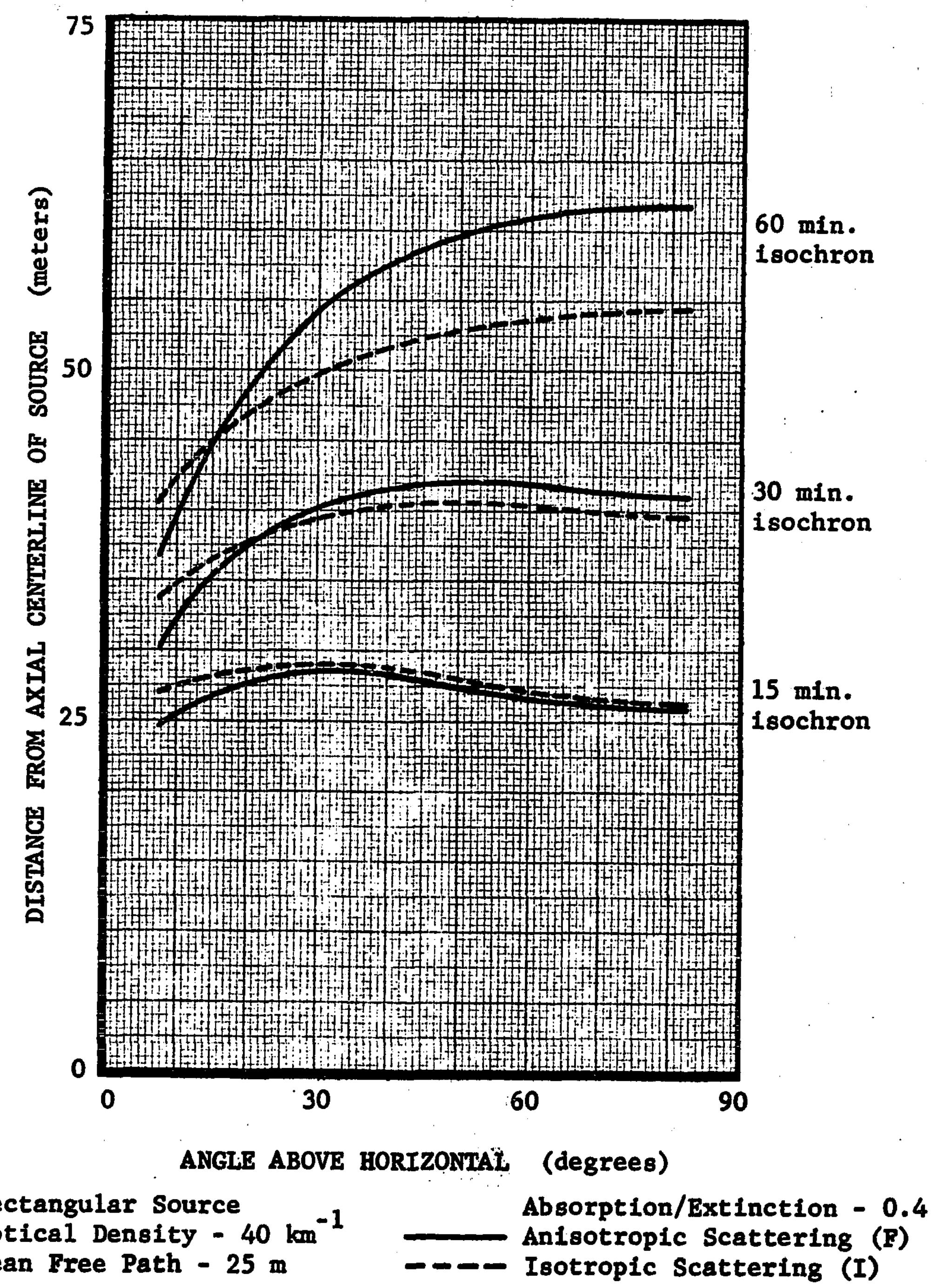

FIGURE 7-10 COMPARATIVE LOCATIONS OF RELATIVE ISOCHRONS

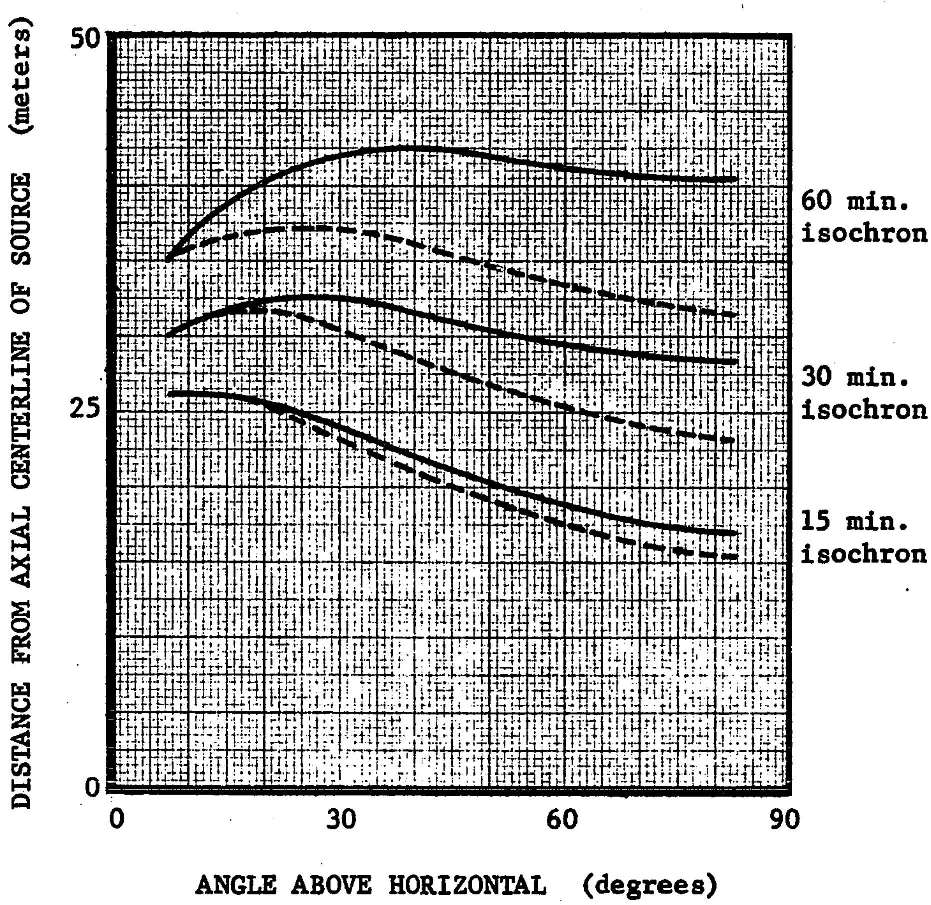

Rectangular Source
Optical Density - 80 km^{-1}
Mean Free Path - 12.5 m

Absorption/Extinction - 0.4
——— Anisotropic Scattering (F)
- - - - Isotropic Scattering (I)

FIGURE 7-11 COMPARATIVE LOCATIONS OF RELATIVE ISOCHRONS

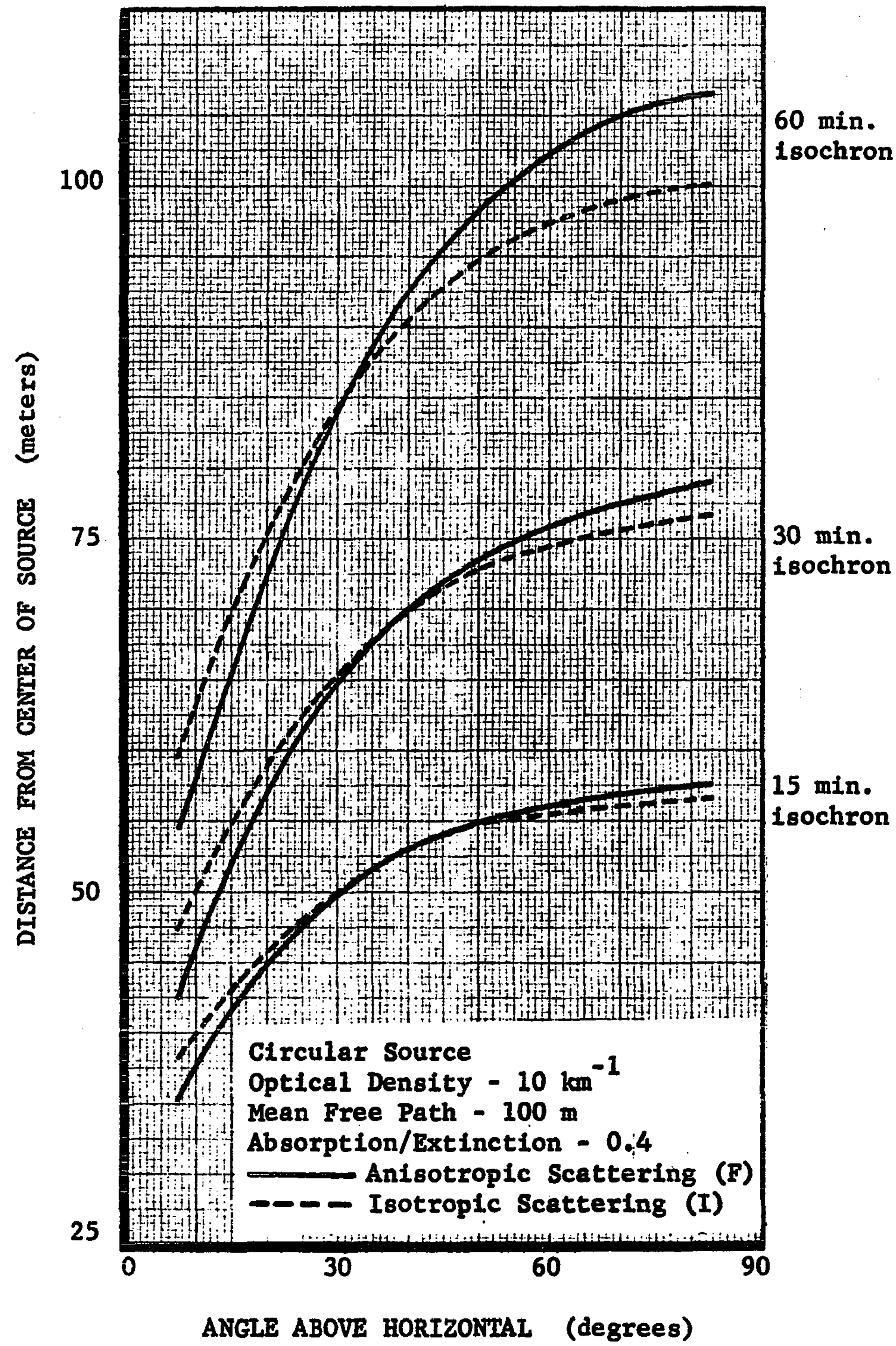

FIGURE 7-12 COMPARATIVE LOCATIONS OF RELATIVE ISOCHRONS

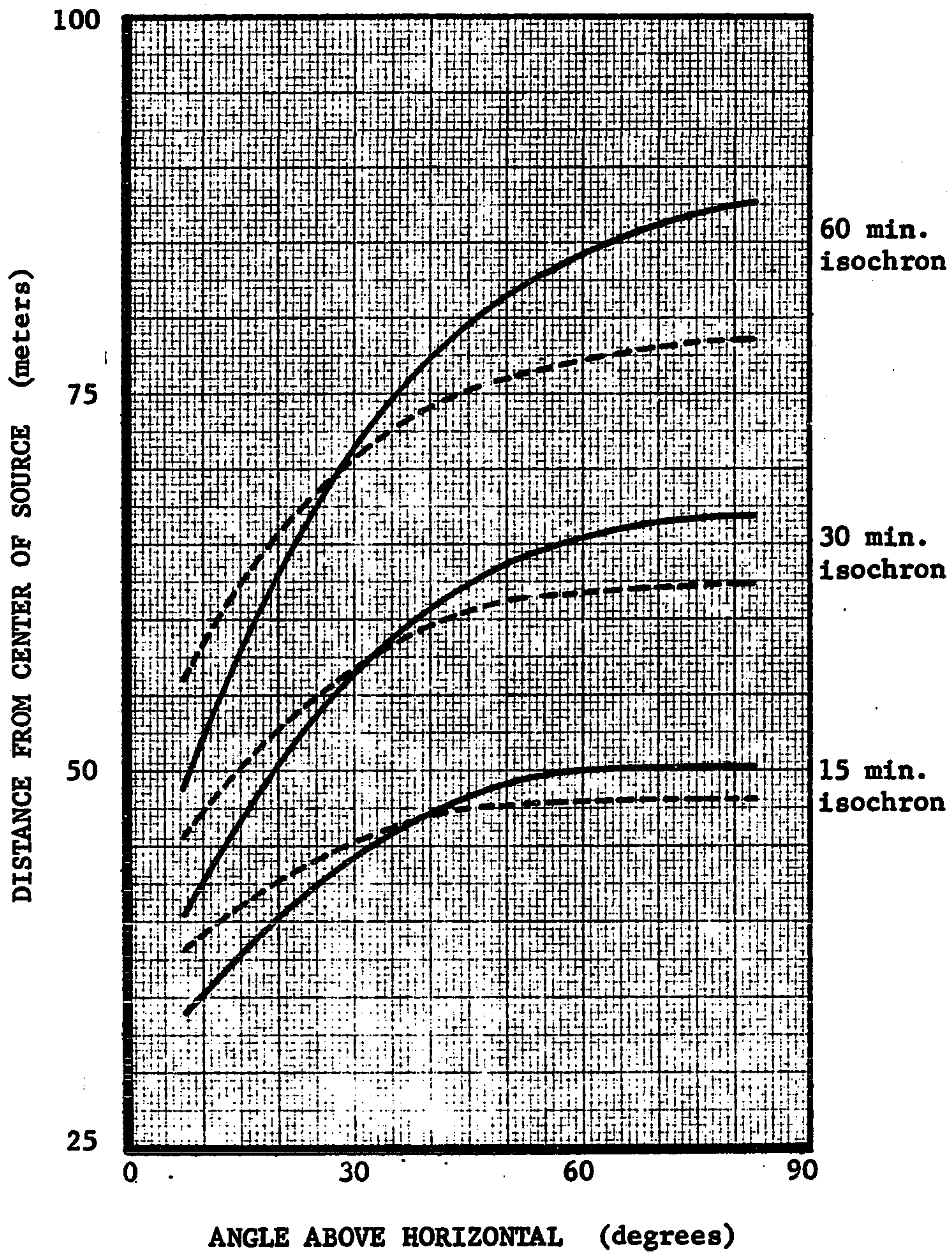

Circular Source   Mean Free Path - 40 m   Abs/Ext - 0.4
Optical Density - 24 km^{-1} (F)   ——— Anisotropic Scattering (F)
Optical Density - 25 km^{-1} (I)   - - - - Isotropic Scattering (I)

FIGURE 7-13   COMPARATIVE LOCATIONS OF RELATIVE ISOCHRONS

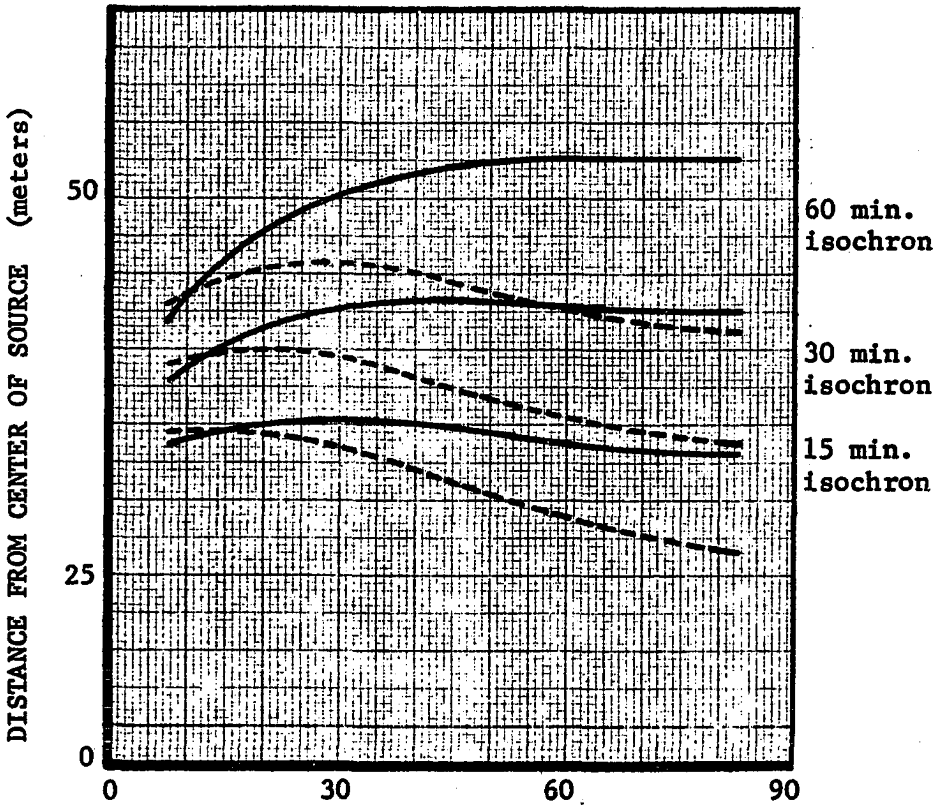

Circular Source
Optical Density - 80 km^{-1}
Mean Free Path - 12.5 m

Absorption/Extinction - 0.4
——— Anisotropic Scattering (F)
– – – – Isotropic Scattering (I)

FIGURE 7-14 COMPARATIVE LOCATIONS OF RELATIVE ISOCHRONS

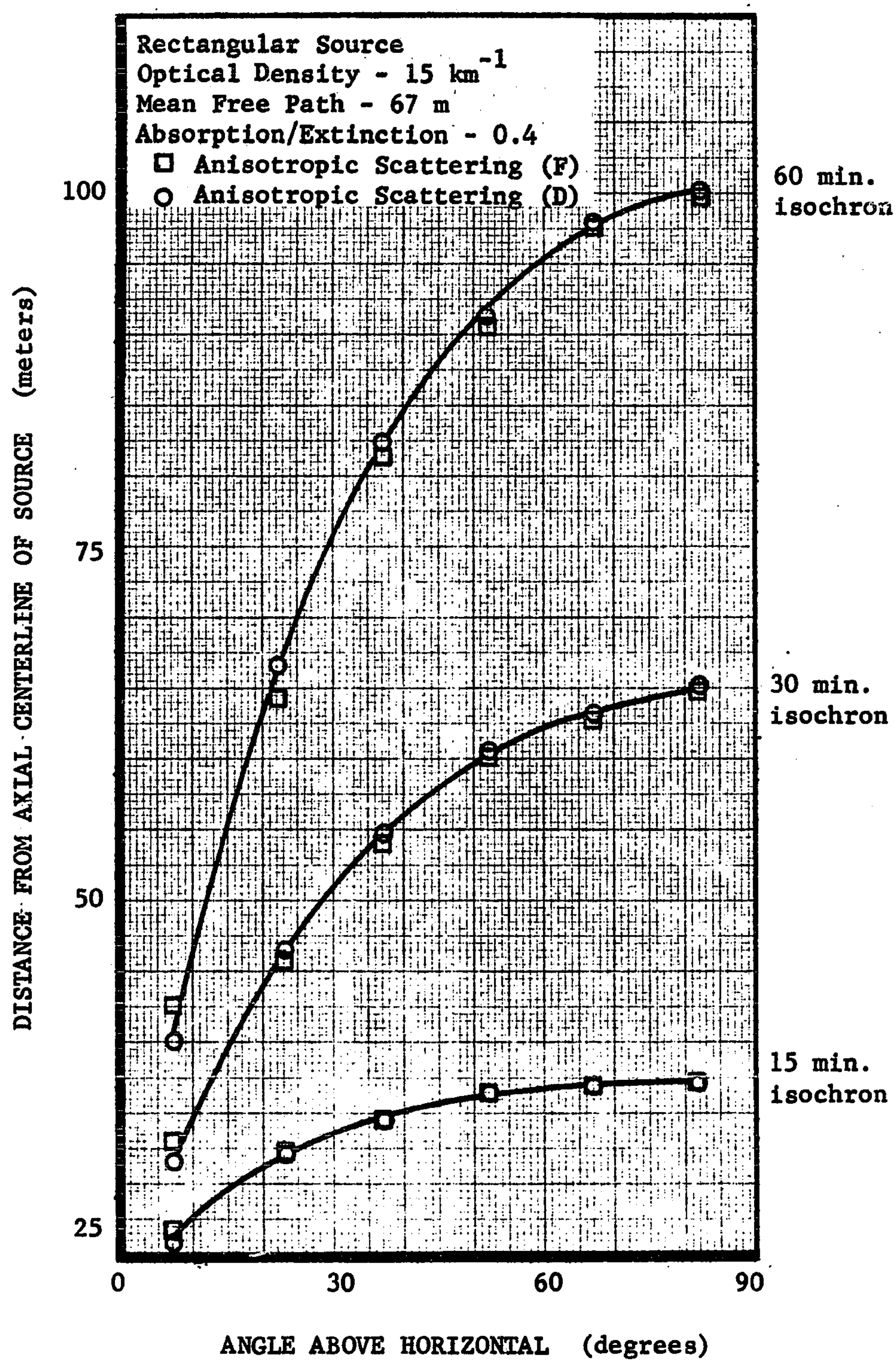

FIGURE 7-15 COMPARATIVE LOCATIONS OF RELATIVE ISOCHRONS

Closure

Attention should be called to the work reported in Appendix G since it is related to the material just discussed. In this related study the droplet was considered as a surface, and a configuration factor approach was used to attempt to determine evaporation time for a droplet in a given location above a circular source. In summary, this approach gave reasonably good agreement for the optically thin cases. The conservatism of the approach tended to reduce the value of the actual surface of the droplet for locations near the source, and hence, the relative time curve is high for locations near the source.

It would be natural to consider the effect of source temperature on the positions of the relative isochrons. The energy which is emitted by the black source used in this study is a function of the fourth power of the temperature and the fraction of the total emitted energy that passes through the energy window. In order to simplify the comparison between different source temperatures, the above factors have been combined in such a way as to provide a correction factor for use with the isochronic curves. Since the correction factor is a multiplicative one, it is only necessary to multiply the time value of a given isochron by this correction in order to determine the new time value for that isochron. The position of the isochron stays the same, but the time specifying it is modified to reflect the new source temperature. Figure 7-16 is the graphic form of this temperature correction function. For example, at a temperature of $800^{\circ}R$, the correction factor is about 0.327. This means that the comparative standard isochrons, as well as all other relative isochrons developed thus far in this work, would have their constant time values reduced by this correction factor. A 60 minute relative isochron would

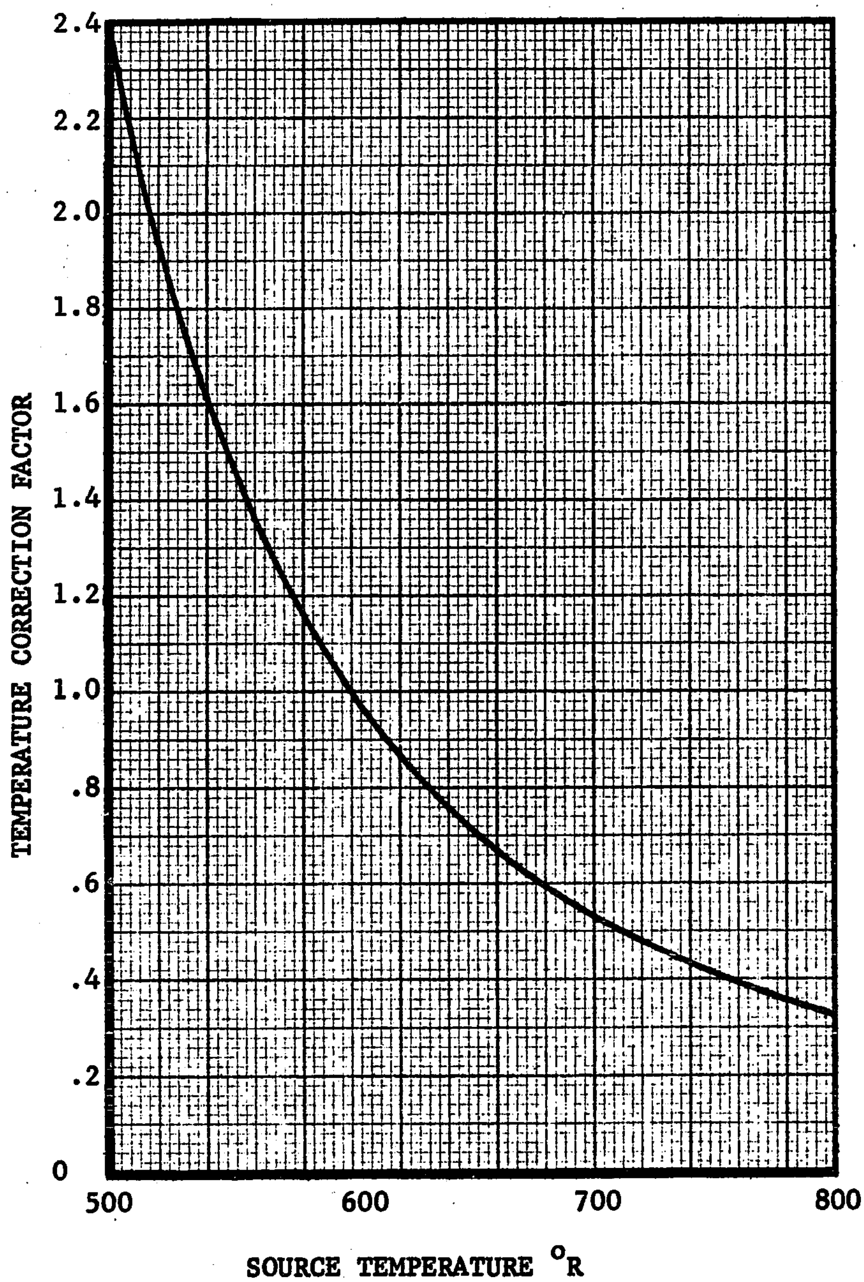

FIGURE 7-16 BLACK BODY SOURCE TEMPERATURE CORRECTION FOR USE WITH RELATIVE ISOCHRONS

become a (60 x 0.327) minute isochron, or about a 20 minute isochron.

The purpose of this chapter has been to compare the effects that changes in the principle radiative parameters have on the spatial distribution of absorption interactions. These comparisons have been illustrated for a number of cases. While an exhaustive discussion of all aspects of the trends has not been undertaken, the fundamental differences have been exposed.

CHAPTER VIII

SUMMARY AND CONCLUSION

The objectives of this work were to determine the spatial distribution of radiative interactions for a finite areal source radiating to a semi-infinite aerosol and to gain insight into the implications of these findings with regard to using this type of source geometry for dissipating natural fog.

The physical model chosen reflected the practical aspect of the problem with a long rectangular or circular source surrounded by an imaginary shell within which the radiative interactions were to be assessed.

Due to the complexity of the problem, involving absorption and multiple scattering, a probabilistic analytical model was established. This analytical model employed a Monte Carlo method to follow photons, released from the source, through probable paths and interactions in the surrounding aerosol. The history of the interactions, specifically the absorption interactions, was established in terms of its spatial distribution within the accounting shell. The computer program used to implement the Monte Carlo method was constructed such that many of the parameters, including geometry and aerosol properties, could be changed to reflect other radiative conditions.

The aerosol models selected for analysis were carefully worked out on the basis of information available in the literature. The optical and physical properties are believed to represent values characteristic of natural fog.

The spatial distribution of absorption interactions was determined for a large number of cases reflecting both aerosol properties and source geometry.

The spatial absorption data was transformed to relative evaporation time curves for the water droplets. These relative evaporation times have been illustrated as isochronic curves where lines of equal relative evaporation time are called isochrons. The development and use of the isochronic curves is particularly helpful in providing understanding and insight regarding the dissipation of fog. Many comparative illustrations were developed using this parameter.

Because the analysis has been based on the radiative parameters remaining fixed at their initial conditions, the practical implications must be considered more in terms of their qualitative rather than quantitative value.

The relative isochrons depict locations where complete evaporation would have taken place at the rate of exchange established by the intitial conditions of the radiative parameters. The actual dissipation of fog will be a gradual and progressive process in terms of improving visibility. Ashley and Douglas (58) provide an informative discussion of visibility through natural fog at various wavelengths in the infrared. The rate at which the droplets are being evaporated will determine the rate at which optical density is decreasing and visibility is increasing. Additional work in this important area is required and would receive partial support from the existing work of Luchak and Langstroth (59) and Langstroth and others (60), and the related work of Johnson (61).

A related problem involves the physical movement of the aerosol during the heating period. This movement can be brought about by convection, turbulence, and wind. While these diffusion factors have not been made a part of this research, some background work has been done and is available as a starting point for further work. Among the references involved are such typical examples as Townsend (62), Deacon (63) and Herring (64). Additional related areas which would be of interest involve the forces which act on the droplets. Saxton and Ranz (65) report their studies on thermal forces, and Orr and Keng (66) have prepared a paper on photophoretic effects. Current publications in meteorology continue to have material in this general area.

Associated with the research reported here is the problem of vertical heat flux and flux divergence in fog. Some work has been done in these aspects of the problem, and it is reported in such references as Elliott (67), Funk (68), and Munn (2).

While the emphasis of this work has been placed on dissipating fog which has already formed, the actual development and evolution of fog might provide information of value on its dissipation. As an example, a heated runway might be maintained continuously, and in this way the dissipating action of the radiant energy could act on the fog during the formative period.

Another aspect of the problem that has not been investigated in this study is the matter of relative humidity and its effect on droplet evaporation. It is known that a decrease in relative humidity is helpful to fog dissipation. Additional work on the coordinated activity of heating droplets directly in the wavelength interval between 7.5 and 13.5 microns, and using the energy at all other wavelengths to heat the air and reduce its relative humidity, would be of interest.

The temperature of the source was discussed somewhat in Chapter VII. The practical limits of temperature are related to the ability of the structural material to withstand elevated temperatures for long periods of time. Practical considerations involving personnel and aerodynamic problems associated with landing are also of interest. The structural ability of concrete to withstand high temperatures for long periods of time is not well documented. Additional work in this area would be required to support the design of an actual system. Some studies, such as those by Saemann and Washa (69) and those of Heiskell, Black, Crew, and Lee (70), are available. The temperatures posed in this research have purposely been held to moderate levels.

The temperature of the source has been considered isothermal in this study. Practical attainment of this ideal situation would be enhanced by the source material having a high thermal conductivity. The thermal conductivity of concrete can be improved by the inclusion of metallic aggregates. Davis, Browne and Witter (71) give some physical properties of concrete augmented with this type of aggregate. Another use of concrete of this same general type is in the shielding of atomic energy plants. Davis (72) gives a summary of the important characteristics of concrete developed for this purpose. The conductive heat transfer from the heating elements through the concrete to the surface and the resulting surface temperature distribution is treated in such references as Jakob (73) and Ingersoll and Zobel (74).

Practical design criteria and overall feasibility might be established or confirmed by large scale laboratory experiments, comparable to those reported by Pilié and others (75) for fog seeding.

Any complex problem can be expanded quickly to include related problems. In such cases the problem is usually broken down into segments for analysis. When sufficient information has been developed on the individual segments, a coordinated solution can frequently be synthesized. The work reported in this research represents a contribution to an important segment of the complex problem of radiative interactions between a finite areal source and a surrounding semi-infinite aerosol. The direct energy exchange between the finite source and the droplets of the semi-infinite aerosol has been investigated on the basis of carefully developed parameters and reasonable assumptions. The findings indicate a significant rate of exchange, and the practical implications exposed by this research are appealing enough to invite further investigation both analytical and empirical.

LIST OF REFERENCES

1. Love, T. J., Radiative Heat Transfer, Charles Merrill Books Inc., Columbus, Ohio, 1968

2. Munn, R. E., Descriptive Micrometeorology, Academic Press, New York, 1966

3. Green, H. L. and Lane, W. R., Particulate Clouds: Dusts, Smokes and Mists, D. Van Nostrand Company, Inc., Princeton, New Jersey, 1957

4. Middleton, W. E. K., Vision Through the Atmosphere, University of Toronto Press, Toronto, Canada, 1952

5. Schuster, A., "Radiation Through a Foggy Atmosphere," The Astrophysical Journal, Vol. XXI, No. 1, January 1905, pp. 1-22

6. Love, T. J., "An Investigation of Radiant Heat Transfer in Absorbing, Emitting, and Scattering Media," USAF Aeronautical Research Laboratories Report ARL 63-3, Wright-Patterson AFB, Ohio, January 1963

7. Deirmendjian, D., in Electromagnetic Scattering, M. Kerker, editor, The Macmillan Company, New York, 1963

8. Penndorf, R., "Research on Aerosol Scattering in the Infrared, Scientific Report No. 1, Results of an Approximation Method to the Mie Theory for Colloidal Spheres," USAF Geophysics Research Directorate, Air Force Cambridge Research Center, Air Research and Development Command, RAD-TR-59-36, Bedford, Mass., September 1959

9. Penndorf, R., "Research on Aerosol Scattering in the Infrared, Scientific Report No. 2, Mie Scattering in the Forward Area," USAF Geophysics Research Directorate, Air Force Cambridge Research Center, Air Research and Development Command, RAD-TR-60-10, Bedford, Mass., February 1960

10. Van De Hulst, H. C., Light Scattering by Small Particles, John Wiley and Sons, Inc., New York, 1957

11. Rochelle, W. C., "Review of Thermal Radiation from Liquid and Solid Propellant Rocket Exhausts," NASA TM X-53579, George C. Marshall Space Flight Center, Huntsville, Alabama, February 1967

12. Wagman, J., "Current Problems in Atmospheric Aerosol Research," The International Journal of Air and Water Pollution, Vol. 10, No. 11-12, November-December 1966, pp. 777-782

13. ________, Journal of the Air Pollution Control Association, Vol. 17, No. 9, September 1967

14. George, J. J., Fog: Compendium of Meteorology, American Meteorological Society, Boston, Massachusetts, 1951

15. Belyaev, V. I. and Pavlova, I. S., "On the Possibility of Influencing the Weather by Artificial Dissipation of Cloudiness," Bulletin of the Academy of Sciences, USSR, Geophysics Series 1, American Geophysical Union, 1962, pp. 129-133

16. Hicks, J. R., "Improving Visibility Near Airports During Periods of Fog." Journal of Applied Meteorology, Vol. 6, No. 1, February 1967, pp. 39-42

17. Downie, C. S. and Smith R. B., "Thermal Techniques for Dissipating Fog from Aircraft Runways," USAF AFCRC-TN-58-477, Geophysics Research Directorate, Air Force Cambridge Research Center, Air Research and Development Command, Bedford, Mass., 1958

18. Robertson, G. W., "Low Temperature Fog at the Edmonton Airport as Influenced by Moisture from Combustion of Natural Gas," Quarterly Journal of the Royal Meteorological Society, Vol. 81, 1954, pp. 190-197

19. Arnulf, A. J., Bricard, J., Cure, E., and Veret, C., "Transmission by Haze and Fog in the Spectral Region 0.35 to 10 Microns," Journal of the Optical Society of America, Vol. 47, No. 6, June 1957, pp. 491-498

20. Houghton, H. G. and Radford, W. H., "On the Measurement of Drop Size and Liquid Water Content in Fogs and Clouds," Papers in Physical Oceanography and Meteorology, Massachusetts Institute of Technology and Woods Hole Oceanographic Institution, Vol. VI, No. 4, 1938

21. Humphreys, W. J., Fogs and Clouds, The Williams and Wilkins Company, Baltimore, Md., 1926

22. Houghton, H. G. and Radford, W. H., "On the Local Dissipation of Natural Fog," Papers in Physical Oceanography and Meteorology, Massachusetts Institute of Technology and Woods Hole Oceanographic Institution, Vol. VI, No. 3, October 1938

23. Pilié, R. J., "Investigation of Warm Fog Properties and Fog Modification Concepts," Project Fog Drops, NASA CR-368, Cornell Aeronautical Laboratory, Inc., Buffalo, New York

24. Fiock, E. F. and Dahl, A. I., "Fog Dispersion by Radiant Tubes," National Bureau of Standards Report No. 1914, 1952

25. Elliott, W. P., Air Force Cambridge Research Laboratories, Bedford, Mass., Personal communication during Seminar at University of Oklahoma.

26. Parzen, E., Modern Probability Theory and Its Applications, John Wiley and Sons, Inc., New York, 1960

27. Uspensky, J. V., Introduction to Mathematical Probability, McGraw-Hill Book Company, Inc., New York, 1937

28. Kovach, L. D., Computer Oriented Mathematics, Holden-Day, San Francisco, 1964

29. Froberg, C. E., Introduction to Numerical Analysis, Addison-Wesley Publishing Company, Inc., Reading, Mass., 1965

30. Sobolev, V. V., A Treatise on Radiative Transfer, D. Van Nostrand Company, Inc., Princeton, New Jersey, 1963

31. Stockham, L. W., "Radiative Heat Transfer from a Finite Cylindrical Particle Cloud," Ph.D. dissertation, University of Oklahoma, 1967

32. Howell, J. R. and Perlmutter, M., "Monte Carlo Solution of Thermal Transfer Through Radiant Media Between Gray Walls," Transactions of the ASME, February 1964, pp. 116-122

33. Perlmutter, M. and Howell, J. R., "Radiant Transfer from Gray Gas Between Concentric Cylinders Using Monte Carlo," Journal of Heat Transfer, May 1964, pp. 169-179

34. Howell, J. R., Strite, M. K. and Renkel, H., "Heat Transfer Analysis of Rocket Nozzles Using Very High Temperature Propellants," AIAA Journal, Vol. 3, No. 4, April 1965, pp. 669-673

35. Corlett, R. C., "Direct Monte Carlo Calculation of Radiative Heat Transfer in Vacuum," Transactions of the ASME, November 1966, pp. 376-382

36. Campbell, P. M., "Monte Carlo Method for Radiative Transfer," International Journal of Heat and Mass Transfer, Vol. 10, No. 4, 1967, pp. 519-527

37. Sparrow, E. M. and Cess, R. D., Radiation Heat Transfer, Brooks/Cole Publishing Company, Belmont, California, 1966

38. Kourganoff, V., Basic Methods in Transfer Problems, Dover Publications, Inc., New York, 1963

39. Chandrasekhar, S., Radiative Transfer, Dover Publications, Inc., New York, 1960

40. Kerker, M., editor, Electromagnetic Scattering, The Macmillan Company, New York, 1963

41. Pritchard, B. S. and Elliott, W. G., "Two Instruments for Atmospheric Optics Measurements," Journal of the Optical Society of America, Vol. 50, No. 3, March 1960, pp. 191-202

42. Schmidt, R. N., "Infrared Diffuse Reflector Coating," unpublished progress report, USAF, AF 33 (615)-5305, October 1966

43. Best. A. C., "Drop-Size Distribution in Cloud and Fog." Quarterly Journal of the Royal Meteorological Society, Vol. 77, 1951, pp. 418-426

44. aufm Kampe, H. J. and Weickmann, H. K., "Trabert's Formula and the Determination of the Water Content in Clouds," Journal of Meteorology, Vol. 9, June 1952, pp 167-171

45. Neiburger, M., "Further Comments on Visibility and Liquid Content in Cloud," Journal of Meteorology, Vol. 11, February 1954, pp. 80-81

46. Fritz, S., "Small Drops, Liquid Water Content and Transmission in Clouds," Journal of Meteorology, Vol. 11, October 1954, pp. 428-429

47. Feigelson, E. M., in A Collection of Articles on Dynamic Meteorology, I. A. Kibel, editor, American Geophysical Union, Consultants Bureau, New York, 1960, pp. 73-104

48. Houghton, H. G., "The Size and Size Distribution of Fog Particles," Physics, Vol. 2, June 1932, pp. 467-475

49. Webb, W. L., "Particulate Counts in Natural Clouds and Fogs," Journal of Meteorology, Vol. 13, April 1956, pp. 203-206

50. Eldridge, R. G., "Measurements of Cloud Drop-Size Distributions," Journal of Meteorology, Vol. 14, February 1957, pp. 55-59

51. Thompson, B. J., Ward, J. H. and Zinky, W. R., "Application of Hologram Techniques for Particle Size Analysis," Applied Optics, Vol. 6, March 1967, pp. 519-526

52. Wolfe, W. L., editor, Handbook of Military Infrared Technology, U.S. Government Printing Office, Washington, D. C., 1965

53. Kreith, F., Radiation Heat Transfer for Spacecraft and Solar Power Plant Design, International Textbook Company, Scranton, Penn., 1962

54. Centeno V, M., "The Refractive Index of Liquid Water in the Near Infra-Red Spectrum," Journal of the Optical Society of America, Vol. 31, March 1941, pp. 244-247

55. Johnson, J. C. and Terrell, J. R., "Transmission Cross Sections for Water Spheres Illuminated by Infrared Radiation," Journal of the Optical Society of America, Vol. 45, No. 6, June 1955, pp. 451-454

56. Beattie, J. F., "Angular Distribution of Scattered Intensity from Various Aerosols," Ph.D. dissertation, University of Oklahoma, 1965

57. Wheasler, R. A., "Measurement of Angular Distribution of Scattered Monochromatic Intensity from an Aerosol Containing Particles of Irregular Size and Shape for Wavelengths in the Infrared," Ph.D. dissertation, University of Oklahoma, 1964

58. Ashley, A. and Douglas, C. A., "Can Infrared Improve Visibility Through Fog?" Illuminating Engineering, Vol. LXI, No. 4, April 1966, pp. 243-250

59. Luchak, G., and Langstroth, G. O., "Applications of Diffusion Theory to Evaporation from Droplets and Flat Surfaces," Canadian Journal of Research, Vol. 28, Sec. A, 1950, pp. 574-579

60. Langstroth, G. O., Diehl, C. H. H. and Winhold, E. J., "The Evaporation of Droplets in Still Air," Canadian Journal of Research, Vol. 28, Sec. A, 1950, pp. 580-595

61. Johnson, J. C., "Measurement of the Surface Temperature of Evaporating Water Drops," Journal of Applied Physics, Vol. 21, January 1950, pp. 22-23

62. Townsend, A. A., "Natural Convection in the Earth's Boundary Layer," Quarterly Journal of the Royal Meteorological Society, No. 88, 1962, pp. 51-56

63. Deacon, E. L., "Vertical Diffusion in the Lowest Layers of the Atmosphere," Quarterly Journal of the Royal Meteorological Society, No. 75, 1949, pp. 89-103

64. Herring, J. R., "Some Analytical Results in the Theory of Thermal Convection," Journal of the Atmospheric Sciences, Vol. 23, November 1966, pp. 672-677

65. Saxton, R. L. and Ranz, W. E., "Thermal Force on an Aerosol Particle in a Temperature Gradient," Journal of Applied Physics, Vol. 23, No. 8, August 1952, pp. 917-923

66. Orr, C., Jr., and Keng, E. Y. H., "Photophoretic Effects in the Stratosphere," Journal of the Atmospheric Sciences, Vol. 21, September 1964, pp. 475-478

67. Elliott, W. P., "The Height Variation of Vertical Heat Flux Near the Ground," Quarterly Journal of the Royal Meteorological Society, No. 90, 1964, pp. 260-265

68. Funk, J. P., "Radiative Flux Divergence in Radiation Fog," Quarterly Journal of the Royal Meteorological Society, No. 75, 1962, pp. 233-249

69. Saemann, J. C. and Washa, G. W., "Variation of Mortar and Concrete Properties with Temperature," Journal of the American Concrete Institute, Vol. 29, No. 5, November 1957, pp. 385-395

70. Heiskell, R. H., Black, R. H., Crew, R. J. and Lee, H., "Elevated Temperatures of Portland Cement Mixtures Related to Surface Removal," Journal of the American Concrete Institute, Vol. 29, No. 7, January 1958, pp. 591-603

71. Davis, H. S., Browne, F. L. and Witter, H. C., "Properties of High Density Concrete Made with Iron Aggregate," Journal of the American Concrete Institute, Vol. 27, No. 7, March 1956, pp. 705-726

72. Davis, H. S., "High-Density Concrete for Shielding Atomic Energy Plants," Journal of the American Concrete Institute, Vol. 29, No. 11, May 1958, pp. 965-977

73. Jakob, M., Heat Transfer, Volumes I and II, John Wiley and Sons, Inc., New York, 1964 printing

74. Ingersoll, L. R., Zobel, O. J., and Ingersoll, A. C., Heat Conduction with Engineering and Geological Applications, McGraw-Hill Book Company, Inc., New York, 1948

75. Pilié, R. J., Kocmond, W. C., and Jiusto, J. E., "Warm Fog Suppression in Large-Scale Laboratory Experiments," Science, Vol. 157, September 1967, pp. 1319-1320

76. Eckert, E. R. G. and Drake, R. M., Heat and Mass Transfer, McGraw-Hill Book Company, Inc., New York, 1959

77. Hamilton, D. C., and Morgan, W. R., "Radiant-Interchange Configuration Factors," NACA TN 2836, 1952

APPENDICES

APPENDIX A

END LOSS FROM CYLINDRICAL ACCOUNTING SHELL

In order to test the validity of the assumption that end loss can be neglected for a long rectangular source, a program involving typical photon interaction with the aerosol was initiated for different source and accounting shell lengths. The reference coordinate system remained centered in the source, and all emissions were initiated from the line source fixed as a portion of the Y axis. The length of the actual long rectangular source, and with it the accounting shell, was reduced symmetrically with respect to this coordinate system such that the reference coordinate system remained centered axially. This modification of length should assure end losses which are equally distributed between the two ends. The losses calculated with this program were considered to be twice those that would be experienced for the practical case where the source is unsymmetrically located, being near one end and, as a simultaneous result, more remote from the other end, for a long rectangular source. The half-width of the source was 25 meters and the radius of the accounting shell was 125 meters.

Two different aerosol models were used. Both of the models were selected from cases which are optically thin, and each had a strong forward scattering function, (F), and an absorption coefficient to extinction coefficient ratio of 0.4. It was felt that these parameters would assure fewer interactions which might tend to reduce end losses. The results of these two cases were quite consistent. A total of 2500 original emissions were initiated, and the photon histories were followed until terminated by an absorption or an escape. The escapes were divided into end escapes and other escapes.

An end loss was considered to have occurred only when it was determined that the photon would have had an interaction within the extended limits of the accounting shell, except that the interaction would have been beyond the end plane of the actual accounting shell. Thus, a number of photons might have penetrated the end plane, but because they also penetrated either the base plane or the cylindrical surface of the accounting shell before coming to the end of their probable path, they were not considered as end losses in terms of a lost interaction.

Figure A-1 depicts these end losses for the optical densities of 5 km^{-1} and 10 km^{-1}. The ordinates have been labeled in both the number of losses registered for 2500 original histories and as a percent of the original histories. The values for this illustration represent the end losses from a single end.

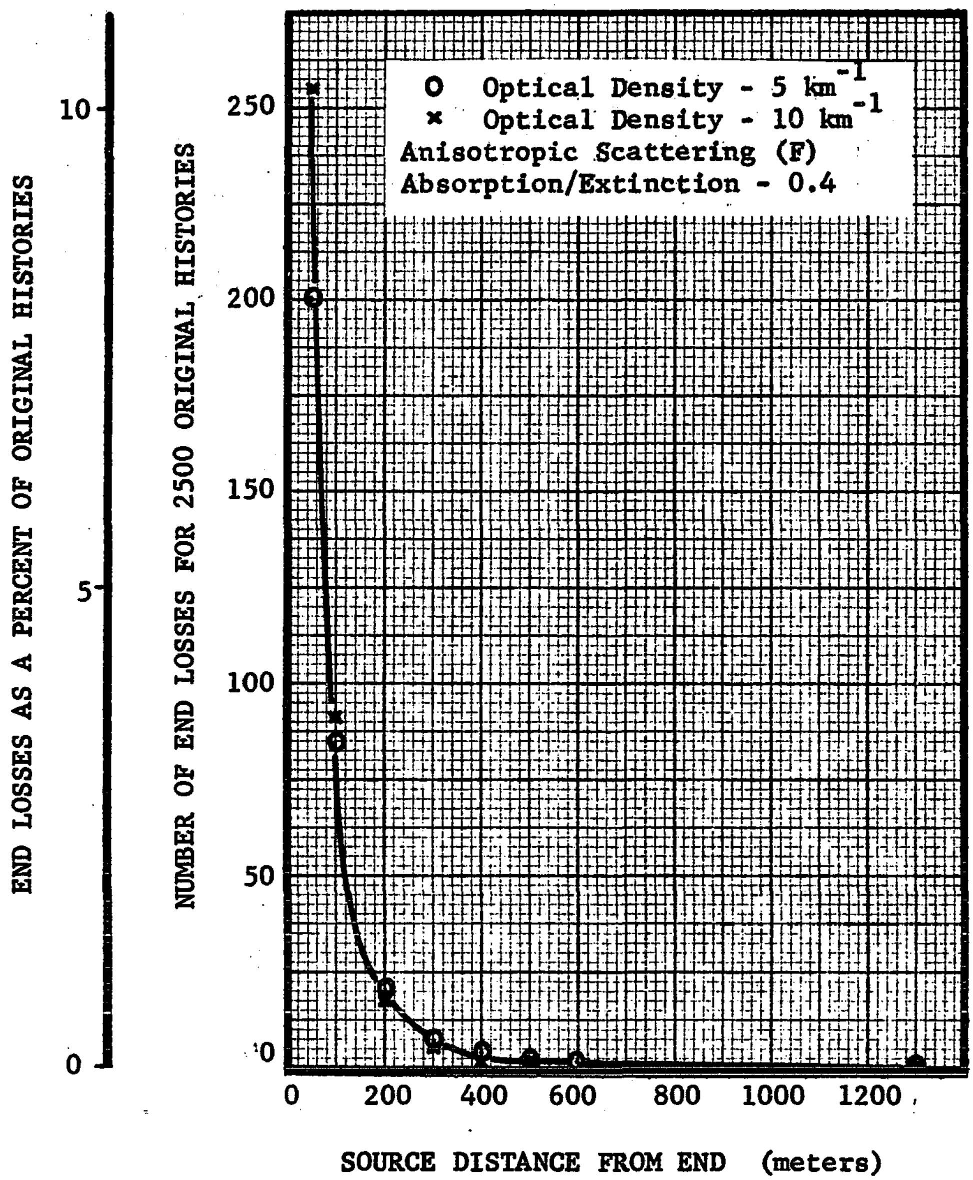

FIGURE A-1 PHOTON INTERACTIONS LOST THROUGH END OF CYLINDRICAL ACCOUNTING ENVELOPE FOR LONG RECTANGULAR SOURCE

APPENDIX B

CONVERGENCE OF NUMERICAL RESULTS USING MONTE CARLO METHODS

It was mentioned in Chapter II that the subdivision of the accounting envelope will effect the number of photon histories required for the frequency of interaction within a given subspace to reach a stable value. Having selected the disposition of the subspaces of the accounting envelope, it remains to determine the number of original emissions required to achieve this stable frequency of photon interaction with the aerosol.

In order to determine the requisite number of histories, or perhaps a better measure would be the number of photon interactions such as absorptions, a series of trial programs was run with increasing numbers of original emissions and interactions. The numerical result desired involves the relative time required to evaporate the water droplets of a monodisperse and isotropic aerosol contained in each subspace of the accounting envelope. This numerical result is a function of the volume of the particular subspace and the ratio of absorptions within that subspace compared to the number of original emissions.

Figure B-1 is a representation of this relative time for droplet evaporation from the subspaces along ray number 3, for the circular source, with the optical density of the aerosol being 10 km^{-1}. The strong forward scattering function (F) and an absorption coefficient to extinction coefficient ratio of 0.4 were used for this numerical example. The source

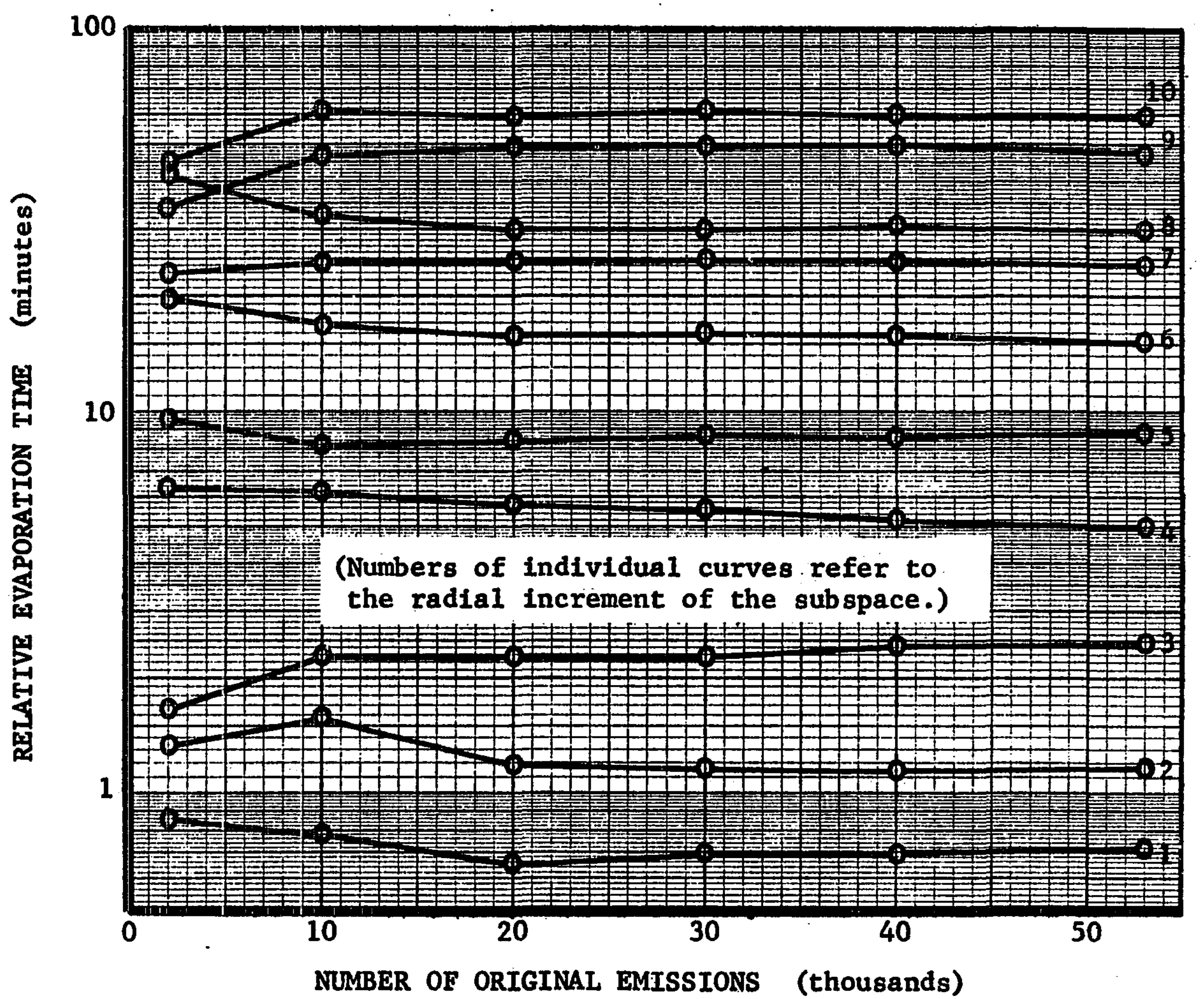

FIGURE B-1 CONVERGENCE TO STABLE RELATIVE EVAPORATION TIMES FOR DROPLETS IN DESIGNATED SUBSPACES LOCATED ALONG RAY THREE FOR THE CIRCULAR SOURCE radius was 25 meters with an accounting shell radius of 125 meters. This illustration is a typical case, and while it might be argued that the other rays would result in a somewhat different convergence picture, all other rays were checked and were found to give similar, though not identical, patterns of convergence.

Problem parameters, such as optical density or extinction coefficient, can create certain problems with regard to the spatial distribution of radiative interactions and can cause some concern regarding the convergence to a stable numerical result. Photon mean free path considerations cause most interactions to take place close to the source for optically thick cases, and conversely, the optically thin cases exhibit a tendency to produce more interactions at some distance from the source. The practical emphasis in this work suggests that the subspaces of greatest interest, in either case, will tend to have good interaction density. For this reason, the convergence problem created by different optical densities did not cause difficulties in this research.

Campbell (36) has suggested that the statistical error will be reduced by taking a series of 4000 original emissions for each of ten different starting numbers for the generation of random numbers and then averaging the results. This method was programmed and compared to a second program which used a single number to start the generation of random numbers and then carried out a series of 40,000 original emissions. The ten different starting numbers required by the averaging method were taken from the Monte Carlo work of Stockham (31). The starting number for the case of 40,000 original emissions was the same as that used in this research. The numerical results of the two methods, namely the time required to evaporate

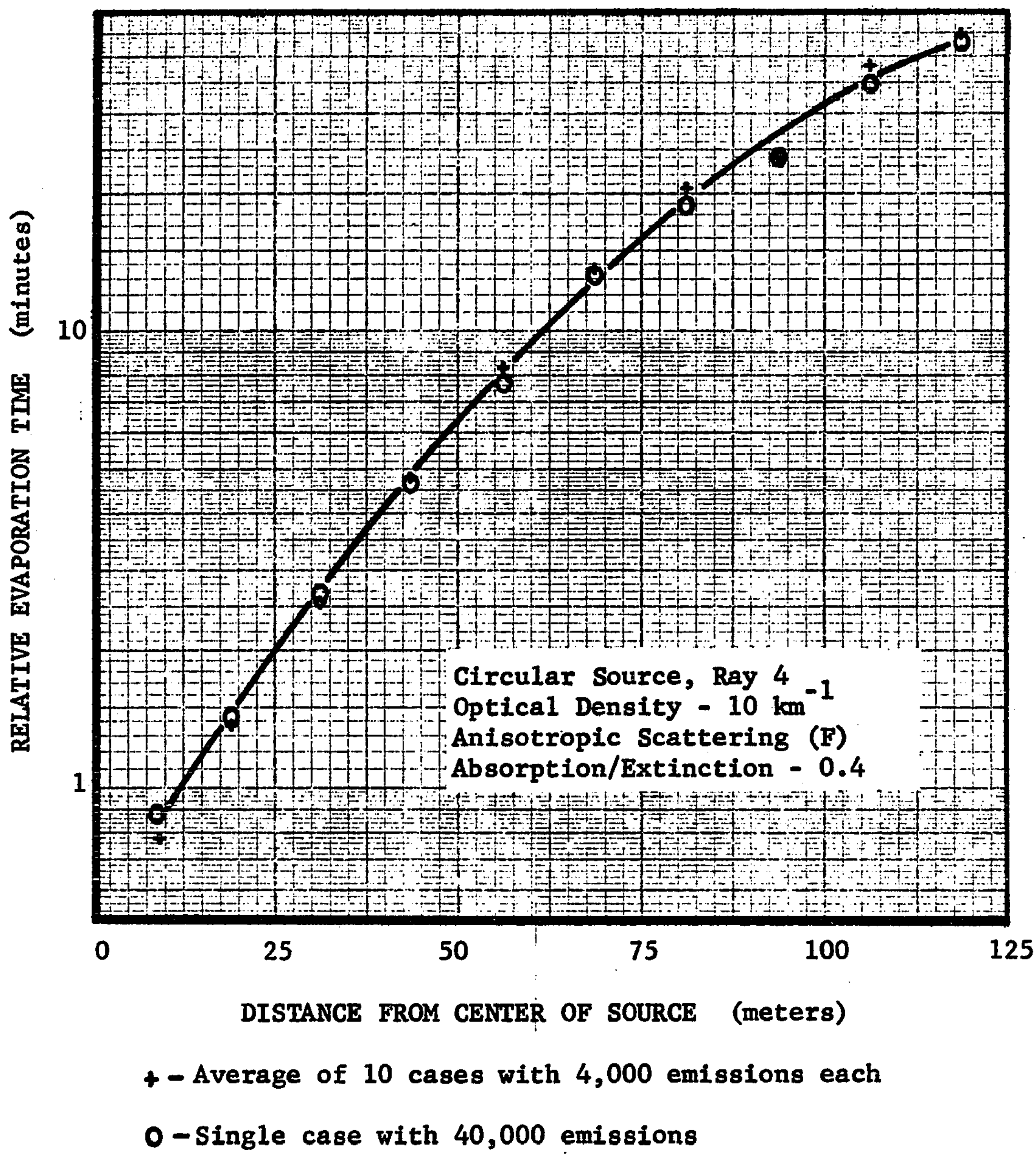

FIGURE B-2 COMPARISON OF TWO DIFFERENT MONTE CARLO METHODS droplets in the subspaces along ray number 4 for the same circular source, and aerosol model previously established in this appendix have been plotted for comparison on Figure B-2.

Since no advantage could be discerned for the somewhat more involved averaging method of Campbell, all cases in this research have been calculated with a large number of original emissions, using a single starting number for the random number generating subroutine.

On the basis of studies reported in this section, it was determined that satisfactory convergence could be achieved with a total of 25,000 absorptions distributed among the subspaces of the accounting envelope. Because of the somewhat better computer run times on the IBM 360/50 computer at the University of Missouri at Rolla, a majority of the runs for the rectangular source were for 50,000 absorptions.

One particular case, involving the rectangular source, was run for 25,000 absorptions, 50,000 absorptions, and 100,000 absorptions. While some data scatter was obvious for an individual subspace, the best fit curves for relative time data along a given ray were in excellent agreement.

For the cases involving 25,000 absorptions, the probability that the fraction of absorptions in a given subspace is within 10% of the correct value is 63% for a fraction of .005, 89% for a fraction of .01, and 99% for a fraction of .1. For the cases involving 50,000 absorptions, the probability that the fraction is within 10% of the correct value is 74% for a fraction of .005, 97.5% for a fraction of .01, and greater than 99% for a fraction of .1.

APPENDIX C

RANDOM NUMBER GENERATION

Since the generation of random numbers, uniformly distributed between 0 and 1, is such an important aspect of the Monte Carlo method, it was considered desirable to test the output of the computer subroutine to be used for this purpose. A word of caution is in order due to the small finite size of the sample output being analyzed. Only when the collection of random numbers becomes very large can it be expected to approach the ideal distribution. For this reason, the data which follows in this section cannot be judged on the specific basis that one set of random numbers is better than another, but rather should be considered as empirical evidence of the proper functioning of the random number generating subroutine.

The only control exerted by the programmer using the subject subroutine is the selection of the first integer starting number for the subroutine. The particular subroutine used in this research was recommended by the manufacturer of the computing system, and the instructions regarding the selection of a starting number simply say that any odd integer number of nine or fewer digits is satisfactory. While it was reassuring to be using a recommended random number generator, it was of some interest to test the subroutine with a few different starting numbers.

Since computing was done at the University of Oklahoma and at the University of Missouri at Rolla, it was also of some interest to establish the compatability of the subroutine with both computer systems. For this purpose, identical photon tracing programs were initiated at both facilities. The outputs of these programs were identical, and this was considered as a confirmation of the compatibility of the subroutine with the computer systems.

All experiments with the random number generating subroutine were conducted at the University of Oklahoma. A number of experiments, intended as reasonable simulations of the actual use of the subroutine, were run, and the outputs were visually inspected for certain characteristics. Because the inspection was visual, it is possible that some human error may be present in the results reported here.

Experiments

The subroutine was used to generate random numbers sequentially in five groups, repeating the sequence 500 times. In this manner a total of 2500 random numbers was generated. Three different starting numbers were used to initiate the operation of the subroutine. These starting numbers have been given code designations in Table C-1 in order to simplify the display of tabular results which follow.

TABLE C-1

STARTING NUMBERS

Code	Starting Number
A	73759153
B	53579173
C	100003

Randomness

One of the simple tests of randomness involves the distribution of the digits themselves between odd and even digits. The results of this test, applied to the first 1000 digits generated by the subroutine, are shown in Table C-2.

TABLE C-2

ODD AND EVEN DISTRIBUTION OF DIGITS

Starting Number	Odd Digits	Even Digits
A	516	484
B	511	489
C	480	520

A second test might be to consider the distribution of odd and even digits for every eight digit generated. This test was made for the first 1000 digits generated by the subroutine, and the results are shown in Table C-3.

TABLE C-3

ODD AND EVEN DISTRIBUTION OF EVERY EIGHTH DIGIT

Starting Number	Odd Digits	Even Digits
A	66	59
B	67	58
C	60	65

Distribution

The distribution of the generated random numbers should be uniform between 0 and 1, and further, the mean value of the generated numbers should be 0.50. The program included a calculation of the mean value of the random numbers generated in each of the five groups and also the overall mean value for all groups.

The mean values achieved for the five groups, using the three different starting numbers are shown in Table C-4.

TABLE C-4

MEAN VALUES OF GENERATED RANDOM NUMBERS

	A	B	C
Group 1	.4643	.5124	.5199
Group 2	.5119	.5291	.5029
Group 3	.4694	.5108	.4876
Group 4	.5128	.5283	.5089
Group 5	.4890	.4908	.4997
Overall Average	.4895	.5143	.5038

In order to test the uniformity of distribution in the range from 0 to 1, ten intervals of equal size were established. Visual inspection of the first 2500 random numbers generated, 500 in each of five groups, was used to determine the number of random numbers that fell in each of the intervals. Table C-5 is the representation of this information for starting number A. The data for other starting numbers was evaluated and provided similar distribution.

TABLE C-5

UNIFORMITY OF DISTRIBUTION BETWEEN 0 AND 1

	Interval									
	0-.1	.1-.2	.2-.3	.3-.4	.4-.5	.5-.6	.6-.7	.7-.8	.8-.9	.9-1.
Group 1	64	46	63	54	45	58	49	46	46	37
Group 2	55	57	45	44	34	43	50	63	50	60
Group 3	53	63	56	48	53	53	52	33	46	44
Group 4	36	53	60	41	57	48	42	57	51	54
Group 5	48	51	51	53	50	58	42	41	49	51
Totals	256	270	275	240	239	260	235	240	242	246

Closure

In closing this section is should be reiterated that the display of numerical data has been intended to show that the random number generating subroutine has performed properly. It is not intended that comparisons be made to establish one starting number as being better than another. In fact, the finite size of the sample inspected precludes any conclusions of this type.

Starting number A was used in the research computer programs. The ratio of scattered to absorbed photons was used to monitor the performance of the random number generator throughout the production runs.

APPENDIX D

COMPARISON OF LINE AND AREA SOURCE FOR RECTANGULAR CASE

In Chapter II it was argued that uniform distribution of radiative interactions in the axial direction for the long rectangular source would allow the real case to be modeled by selecting a small but representative area somewhere near the axial center of the long real source such that the symmetry arguments supporting the uniform axial distribution would hold true. It was further postulated that if the small finite area represented a satisfactory source model, then in a limiting operation this area could be shrunk to a line source. In spite of the seeming validity of this line of reasoning, it was of some interest to investigate the matter numerically to be assured that the line source would in fact produce the same radial distribution of radiative interactions as the finite area source.

A computer program was set up for initiating and accounting for photon histories from a finite area source, 25 meters in the Y direction by 1 meter in the X direction for the centered coordinate system shown in Figure 2-1. The line source program was set up with a line source located along the Y axis and 25 meters in length, a dimension equal to the half width of the real source. The two programs were run for 20,000 photon histories, and the resulting radial distribution of radiative interactions was developed in terms of the relative times required to evaporate the water droplets contained in the various subspaces of the accounting envelope.

Figure D-1 is an illustration of the findings of this study along ray number 4, for an aerosol with an optical density of 10 km^{-1}, a strong forward scattering function (F), and an absorption coefficient to extinction coefficient ratio of 0.4. The accounting shell was 2500 meters long with a radius of 125 meters. This diagram is typical of those for the other rays.

Because of the assurance afforded by this study, the actual cases for the long rectangular source were run with the line source model. Because of the limited number of original emissions for which the test cases were developed, a third set of points for a computer run of 54,997 original histories, representing 25,000 absorptions, has been incorporated in Figure D-1 in order to support the validity of the other numerical data.

It was thought that the reduction to a line source, since it would reduce the required calculations to find an emission point, might result in some saving of computer time. The time saving was very small, a matter of seconds, and was not considered as a significant saving since the computer run times usually equalled or exceeded one half hour for 25,000 absorptions.

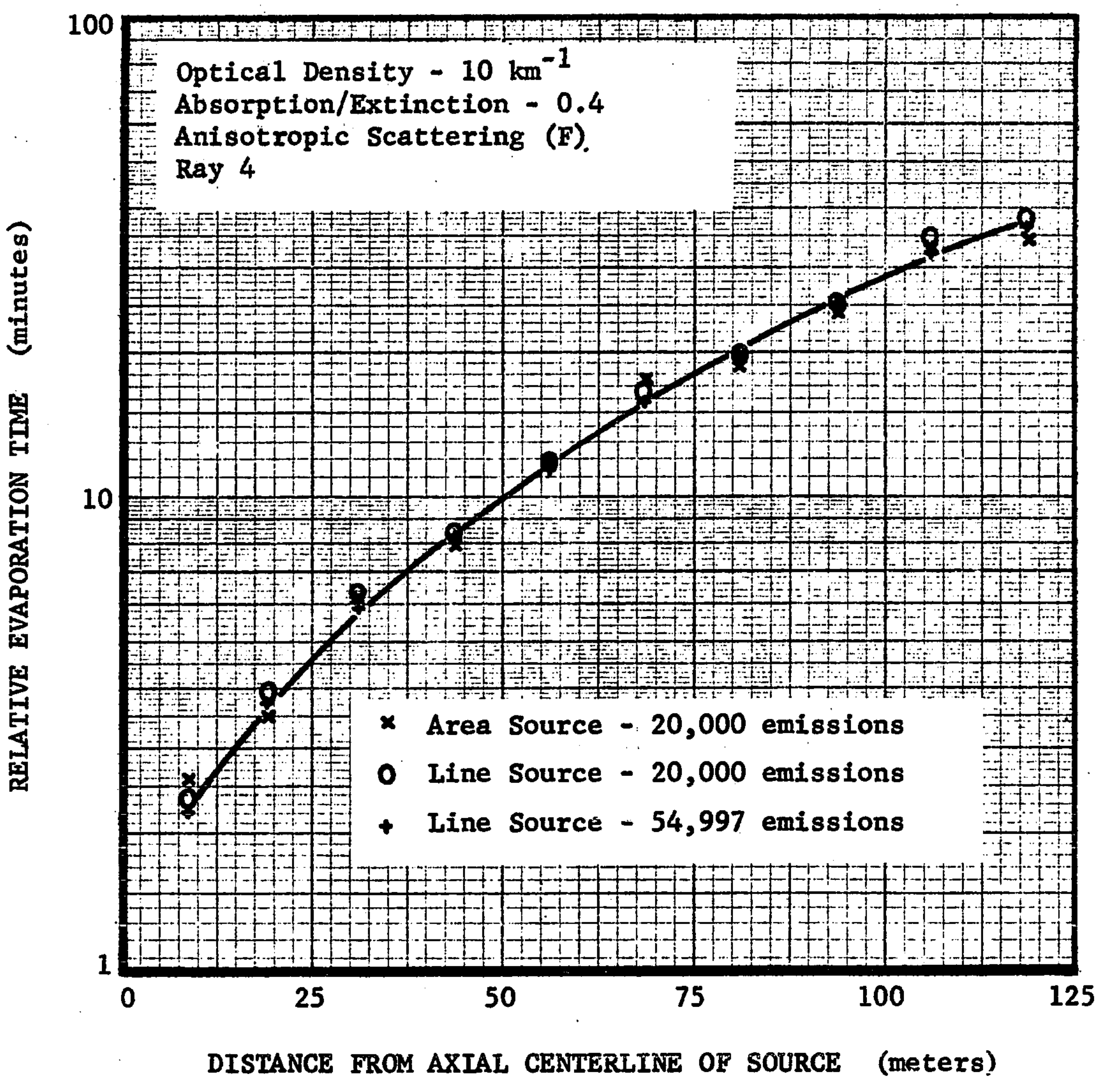

FIGURE D-1 COMPARISON OF MONTE CARLO RESULT FOR SMALL AREA AND LINE SOURCE APPROXIMATIONS FOR LONG RECTANGULAR SOURCE

APPENDIX E

EFFICIENCY OF "WINDOW" RADIATION

The emission of energy from an ideal black body source will increase with temperature. The spectral emission curve, which confirms the increase in total flux emission, also provides an illustration of the fact that the wavelength at which the greatest rate of emission takes place, moves toward shorter wavelengths as the source temperature is increased.

Since this work is interested in the direct heat transfer to the droplets of an aerosol in the wavelength interval or "window" from 7.5 to 13.5 microns, it is of some interest to know the fraction of the total emitted black body flux that is emitted through the "window". In this work, the ratio of the emission through the "window" to that over all wavelengths, is called the efficiency of "window" radiation.

Figure E-1 gives graphic evidence of the increased total emission, as well as the increase in flux emitted through the "window", with increasing temperature. The area under the spectral flux curve represents the flux emitted.

The fraction of the total emitted flux that passes through the "window" is not obvious from Figure E-1. For this reason Figure E-2 has been included to illustrate this parameter.

From the illustrations of this section, it can be seen that the emission temperatures which produce the most efficient use of the wavelength

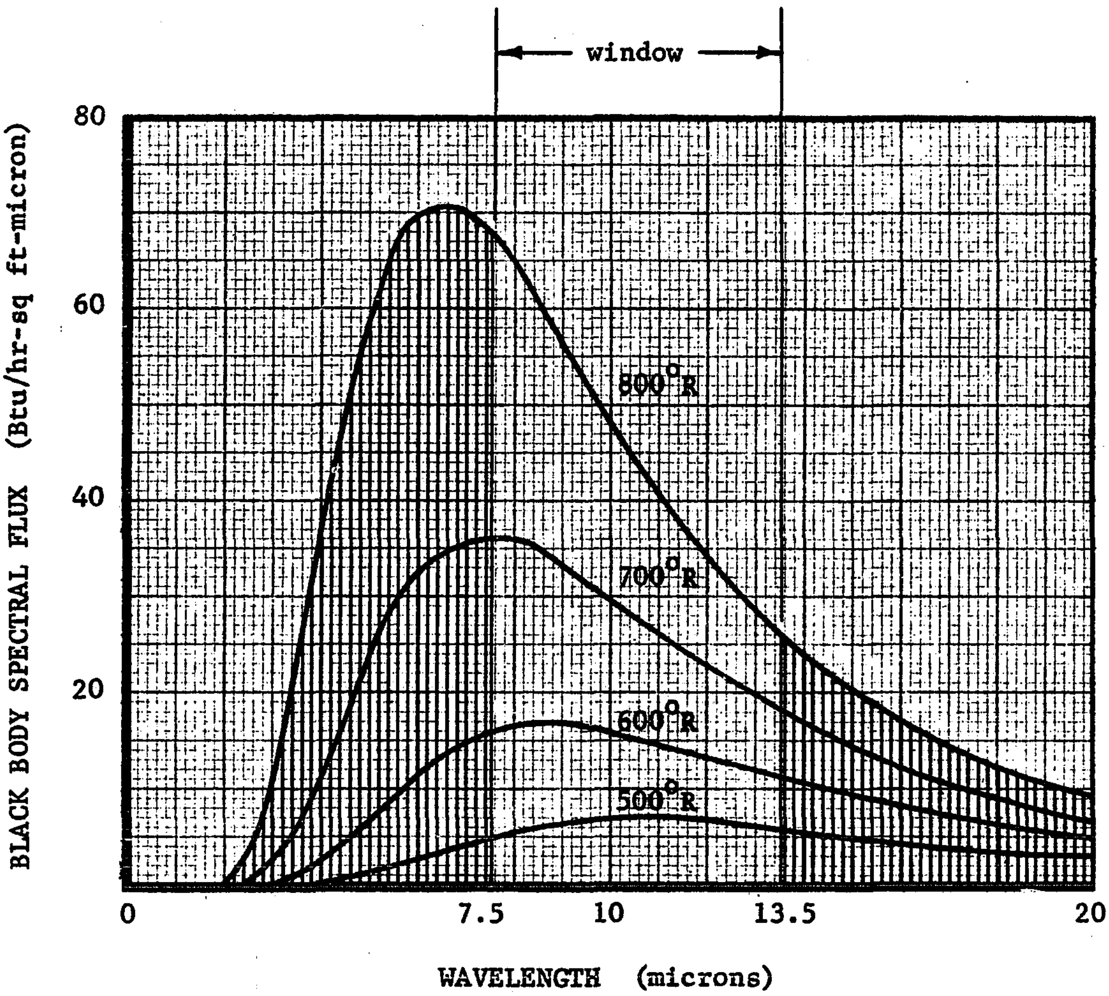

FIGURE E-1 BLACK BODY SPECTRAL FLUX DISTRIBUTION FOR VARIOUS SOURCE TEMPERATURES

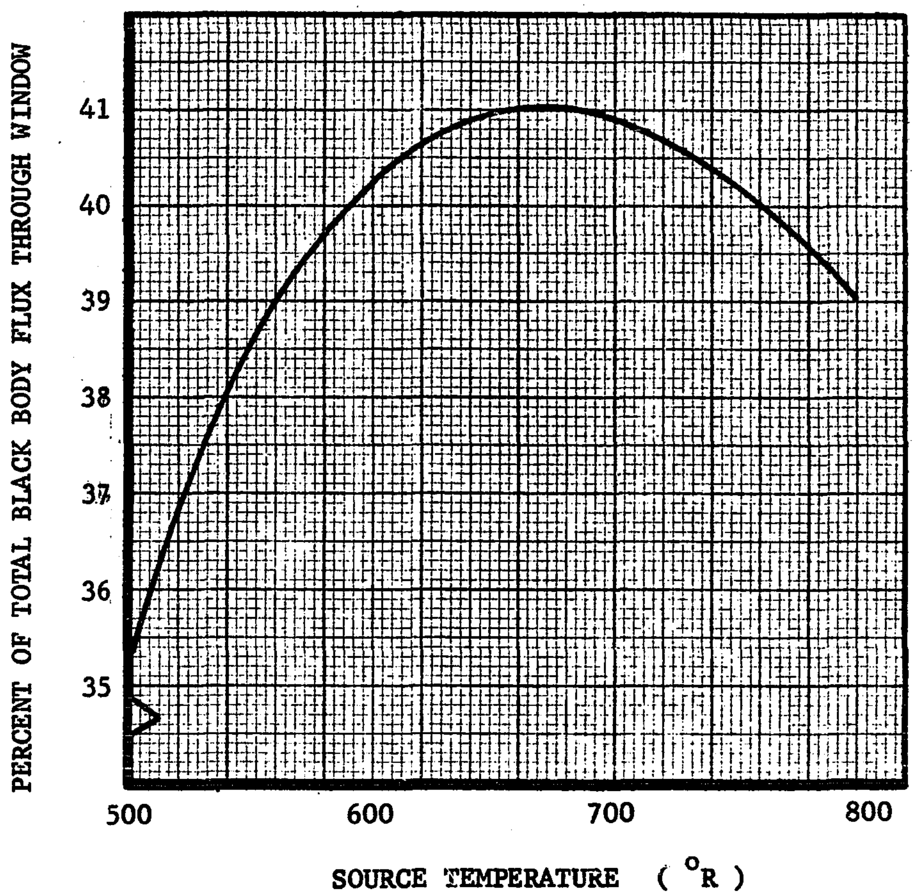

FIGURE E-2 PERCENT OF TOTAL BLACK BODY FLUX EMITTED THROUGH THE WAVELENGTH WINDOW FROM 7.5 TO 13.5 MICRONS interval of interest in this work are complimentary to the practical fog dispersal aspects of the problem being studied.

Practical combinations of black body source temperature and "window" efficiency have been related in such a way as to produce a correction curve, Figure 7-16, for use with the relative isochron curves of Chapters VI and VII. This allows the findings of these chapters to be extended to various possible source temperatures.

APPENDIX F

SPATIAL ABSORPTION DATA

The tables of spatial distribution of absorption interactions included in this section represent the fundamental findings of this research work. It is this information, properly transformed, that has been displayed and discussed in Chapters VI and VII. The numerical studies in these chapters do not exhaust the use to which this absorption data can be applied. For this reason, the data has been deposited here for possible additional use in radiative interaction studies.

Tables F-1 and F-2 have been included in order to make this section complete. These tables contain the volumes, in cubic meters, of the subspace volumes of the accounting envelopes for the long rectangular source and the circular source.

The tabluated data is arranged as a matrix of six columns and ten rows. The columns represent data for the rays numbered 1 thru 6, and the rows represent data for the radial increments numbered 1 thru 10. A partial cross section view of the accounting envelope is shown in Figure F-1 in order to provide a physical concept of the subdivision.

In the absorption tables, the use of anisotropic scattering (F) represents the use of the strong forward scattering function, whereas anisotropic scattering (D) is the designation for the use of the approximation to the scattering function of Deirmendjian (7). Both of these scattering functions were developed in Chapter V.

All other requisite information is contained in the legend on the related table.

The tables of absorption data have been arranged in two groups. The first group contains data for the long rectangular source and has been arranged according to increasing values of optical density. The second group contains information related to the circular source and has also been arranged in terms of increasing optical density.

Table F-3, preceding the absorption tables, represents a summary of the cases covered and can be used as an index for finding desired absorption information.

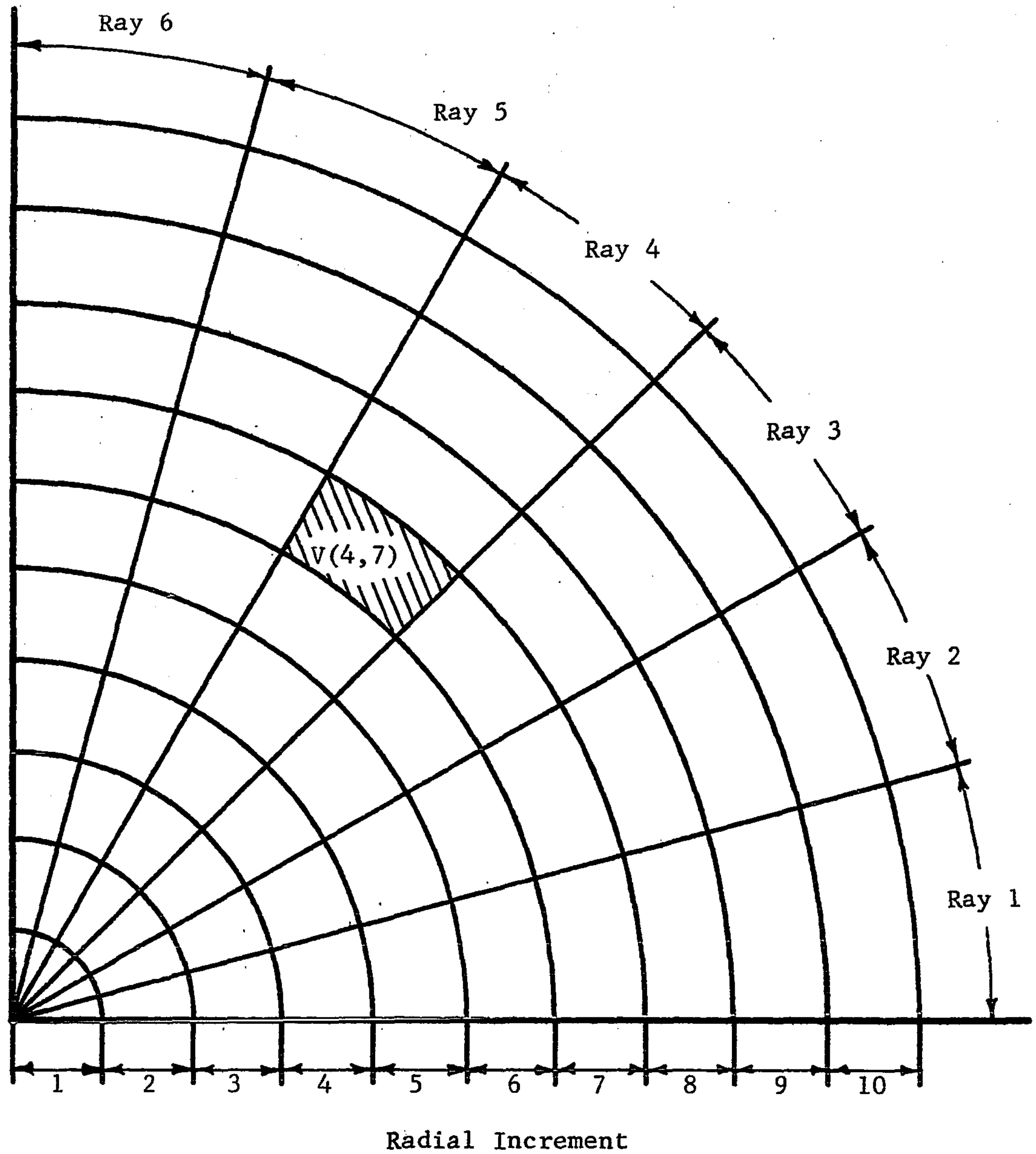

FIGURE F-1 SUBDIVISION OF ACCOUNTING ENVELOPE CROSS SECTION INTO SIXTY SUBSPACES

TABLE F-1

SUBSPACE VOLUMES FOR THE ACCOUNTING ENVELOPE SURROUNDING THE CIRCULAR SOURCE (CU.METERS)

Source Diameter - 50 meters　　Accounting Hemisphere Diameter - 250 meters

1058.72	986.58	847.19	650.07	408.65	139.38
7411.07	6906.02	5930.35	4550.52	2860.58	975.69
20115.77	18744.92	16096.66	12351.40	7764.42	2648.29
39172.81	36503.26	31346.13	24052.71	15120.18	5157.19
64582.20	60181.06	51678.76	39654.49	24927.86	8502.40
96343.94	89778.25	77094.50	59156.70	37187.46	12683.91
134458.00	125295.00	107593.44	82559.31	51899.00	17701.71
178924.44	166731.13	143175.56	109862.44	69062.44	23555.83
229743.19	214086.75	183840.81	141066.00	88677.81	30246.25
286914.13	267361.56	229589.25	176169.94	110745.13	37772.96

TABLE F-2

SUBSPACE VOLUMES FOR THE ACCOUNTING ENVELOPE SURROUNDING THE LONG RECTANGULAR SOURCE PER METER OF LENGTH (CU.METERS/METER)

Source Width - 50 meters   Accounting Envelope Diameter - 250 meters

6.54	6.54	6.54	6.54	6.54	6.54
19.61	19.61	19.61	19.61	19.61	19.61
32.68	32.68	32.68	32.68	32.68	32.68
45.75	45.75	45.75	45.75	45.75	45.75
58.82	58.82	58.82	58.82	58.82	58.82
71.90	71.90	71.90	71.90	71.90	71.90
84.97	84.97	84.97	84.97	84.97	84.97
98.04	98.04	98.04	98.04	98.04	98.04
111.11	111.11	111.11	111.11	111.11	111.11
124.18	124.18	124.18	124.18	124.18	124.18

TABLE F-3

INDEX TO TABULATED SPATIAL ABSORPTION DATA

SOURCE	OPT.DENS. km^{-1}	RADIUS μ	NO.DENS. cc^{-1}	ABS/EXT	SCAT.FUN.	PAGE NO.
Rect.	2.5	4	55	0.4	(F)	201
Rect.	2.5	4	55	0.4	(I)	202
Rect.	5.0	6	30	0.4	(F)	203
Rect.	5.0	6	30	0.4	(I)	204
Rect.	5.0	6	30	0.5	(F)	205
Rect.	7.5	6	45	0.4	(F)	206
Rect.	7.5	6	45	0.4	(I)	207
Rect.	7.5	6	45	0.4	(D)	208
Rect.	7.5	6	45	0.5	(F)	209
Rect.	10.0	6	60	0.4	(F)	210
Rect.	10.0	6	60	0.4	(I)	211
Rect.	10.0	6	60	0.4	(D)	212
Rect.	10.0	6	60	0.5	(F)	213
Rect.	15.0	6	90	0.4	(F)	214
Rect.	15.0	6	90	0.4	(I)	215
Rect.	15.0	6	90	0.4	(D)	216
Rect.	15.0	6	90	0.5	(F)	217
Rect.	20.0	6	120	0.4	(F)	218
Rect.	20.0	6	120	0.4	(I)	219
Rect.	20.0	6	120	0.4	(D)	220
Rect.	20.0	6	120	0.5	(F)	221,222,223

TABLE F-3 (continued)

SOURCE	OPT.DENS. km^{-1}	RADIUS μ	NO.DENS. cc^{-1}	ABS/EXT	SCAT.FUN.	PAGE NO.
Rect.	25.0	8	60	0.4	(F)	224
Rect.	25.0	8	60	0.4	(I)	225
Rect.	25.0	8	60	0.5	(F)	226
Rect.	30.0	8	72	0.4	(F)	227
Rect.	30.0	8	72	0.5	(F)	228
Rect.	40.0	8	96	0.4	(F)	229
Rect.	40.0	8	96	0.4	(I)	230
Rect.	40.0	8	96	0.5	(F)	231
Rect.	50.0	8	120	0.4	(F)	232
Rect.	50.0	8	120	0.5	(F)	233
Rect.	60.0	10	60	0.4	(F)	234
Rect.	60.0	10	60	0.5	(F)	235
Rect.	80.0	10	96	0.4	(F)	236
Rect.	80.0	10	96	0.4	(I)	237
Rect.	80.0	10	96	0.5	(F)	238

TABLE F-3 (continued)

SOURCE	OPT.DENS. km^{-1}	RADIUS μ	NO.DENS. cc^{-1}	ABS/EXT	SCAT.FUN.	PAGE NO.
Circ.	5.0	6	30	0.4	(F)	239
Circ.	7.5	6	45	0.4	(F)	240
Circ.	10.0	6	60	0.4	(F)	241
Circ.	10.0	6	60	0.4	(I)	242
Circ.	10.0	6	60	0.5	(F)	243
Circ.	15.0	6	90	0.4	(F)	244
Circ.	15.0	6	90	0.4	(I)	245
Circ.	15.0	6	90	0.4	(D)	246
Circ.	20.0	6	120	0.4	(F)	247
Circ.	24.0	15	15	0.4	(F)	248
Circ.	25.0	8	60	0.4	(I)	249
Circ.	50.0	8	120	0.4	(F)	250
Circ.	80.0	10	96	0.4	(F)	251
Circ.	80.0	10	96	0.4	(I)	252

RADIANT HEAT TRANSFER FROM LONG RECTANGULAR SOURCE

343,008 HISTORIES

50,000 ABSORPTIONS

74,281 SCATTERINGS

ANISOTROPIC SCATTERING (F)

OPTICAL DENSITY = 2.5 (1/KM)

ABSORPTION/EXTINCTION = 0.4

FRACTION OF ORIGINAL EMISSIONS ABSORBED IN EACH SUBSPACE

.001554	.001443	.001297	.001399	.001239	.001396
.003892	.003283	.002924	.002912	.002942	.002875
.001507	.002691	.003152	.003149	.003443	.003557
.000697	.002163	.002857	.003052	.003428	.003904
.000557	.001738	.002875	.003399	.003227	.003528
.000487	.001399	.002338	.003326	.003385	.003359
.000475	.001347	.002058	.002764	.003729	.003469
.000656	.001499	.002163	.002583	.003251	.003522
.000711	.001487	.002417	.002755	.002921	.003633
.000650	.001376	.002391	.003070	.003099	.003370

RADIANT HEAT TRANSFER FROM LONG RECTANGULAR SOURCE

334,459	HISTORIES		ISOTROPIC SCATTERING (I)
50,000	ABSORPTIONS		OPTICAL DENSITY = 2.5 (1/KM)
74,591	SCATTERINGS		ABSORPTION/EXTINCTION = 0.4

FRACTION OF ORIGINAL EMISSIONS ABSORBED IN EACH SUBSPACE

.001683	.001498	.001325	.001372	.001301	.001375
.004162	.003367	.003062	.002873	.002993	.002891
.001641	.002828	.003265	.003411	.003382	.003654
.000894	.002257	.002927	.003178	.003546	.003956
.000750	.001860	.003038	.003403	.003337	.003651
.000634	.001504	.002592	.003462	.003498	.003501
.000613	.001414	.002192	.002712	.003696	.003397
.000753	.001573	.002162	.002413	.003435	.003693
.000888	.001621	.002473	.002640	.002834	.003704
.000721	.001298	.002275	.002876	.002805	.003238

RADIANT HEAT TRANSFER FROM LONG RECTANGULAR SOURCE

93,962 HISTORIES ANISOTROPIC SCATTERING (F)

25,000 ABSORPTIONS OPTICAL DENSITY = 5 (1/KM)

37,606 SCATTERINGS ABSORPTION/EXTINCTION = 0.4

FRACTION OF ORIGINAL EMISSIONS ABSORBED IN EACH SUBSPACE

.003054	.002714	.002586	.002618	.002363	.002373
.007897	.006449	.005821	.005470	.005481	.005438
.002629	.005204	.005694	.006077	.006513	.006119
.001618	.003384	.005034	.006130	.006268	.006684
.001266	.003086	.004693	.005864	.005939	.007003
.001000	.002565	.004523	.005449	.006641	.006641
.001213	.002469	.003746	.004959	.006300	.005907
.001298	.003001	.004395	.004959	.005140	.006141
.001064	.002554	.004363	.005619	.005013	.006503
.000734	.002022	.003501	.005524	.005907	.005438

RADIANT HEAT TRANSFER FROM LONG RECTANGULAR SOURCE

89,486 HISTORIES	ISOTROPIC SCATTERING (I)
25,000 ABSORPTIONS	OPTICAL DENSITY = 5 (1/KM)
37,415 SCATTERINGS	ABSORPTION/EXTINCTION = 0.4

FRACTION OF ORIGINAL EMISSIONS ABSORBED IN EACH SUBSPACE

.003118	.002727	.002905	.002682	.002347	.002615
.008783	.006884	.006034	.005766	.005923	.005800
.003095	.005889	.006671	.006738	.006627	.006638
.002090	.004056	.005599	.006504	.006928	.006861
.001933	.003509	.005029	.006046	.006459	.007521
.001564	.002771	.004693	.006001	.006928	.006996
.001643	.002984	.004291	.004984	.006549	.005900
.001766	.002917	.004459	.004649	.005330	.006537
.001240	.002514	.004157	.004895	.004761	.005990
.000972	.002000	.002872	.005085	.005085	.005062

RADIANT HEAT TRANSFER FROM LONG RECTANGULAR SOURCE

77,950	HISTORIES	ANISOTROPIC SCATTERING	(F)
25,000	ABSORPTIONS	OPTICAL DENSITY = .5	(1/KM)
24,888	SCATTERINGS	ABSORPTION/EXTINCTION = 0.5	

FRACTION OF ORIGINAL EMISSIONS ABSORBED IN EACH SUBSPACE

.004105	.003541	.003643	.003348	.002989	.003079
.009660	.008608	.007620	.006620	.006851	.007107
.003323	.006132	.007004	.007197	.007787	.007377
.002155	.004310	.006325	.007415	.007915	.008416
.001681	.003874	.005593	.007235	.007287	.008275
.001155	.002951	.005311	.006684	.007620	.007659
.001450	.003182	.004670	.006055	.006748	.007261
.001527	.003323	.005234	.005978	.005863	.007543
.001129	.003105	.004516	.006042	.006068	.007248
.000770	.002399	.003489	.006235	.006774	.006260

RADIANT HEAT TRANSFER FROM LONG RECTANGULAR SOURCE

135,174 HISTORIES — ANISOTROPIC SCATTERING (F)

50,000 ABSORPTIONS — OPTICAL DENSITY = 7.5 (1/KM)

74,614 SCATTERINGS — ABSORPTION/EXTINCTION = 0.4

FRACTION OF ORIGINAL EMISSIONS ABSORBED IN EACH SUBSPACE

.004638	.004239	.004054	.003632	.004172	.003803
.011999	.009454	.008855	.008175	.007916	.007701
.004690	.007997	.008019	.008715	.008737	.008996
.002042	.005186	.007250	.008633	.009351	.009506
.001642	.004402	.006340	.007975	.008522	.009144
.001746	.004587	.006325	.007709	.008352	.009085
.001406	.003640	.005349	.007546	.008308	.008611
.001243	.003573	.004794	.005630	.007324	.008167
.001487	.003839	.004920	.006710	.006562	.007538
.000969	.002745	.004794	.006658	.007102	.007390

RADIANT HEAT TRANSFER FROM LONG RECTANGULAR SOURCE

128,703 HISTORIES — ISOTROPIC SCATTERING (I)

50,000 ABSORPTIONS — OPTICAL DENSITY = 7.5 (1/KM)

74,676 SCATTERINGS — ABSORPTION/EXTINCTION = 0.4

FRACTION OF ORIGINAL EMISSIONS ABSORBED IN EACH SUBSPACE

.004747	.004506	.004281	.004056	.004211	.004180
.012525	.010295	.009705	.009036	.008803	.008345
.005439	.008407	.009192	.009308	.009728	.009860
.002929	.005765	.007677	.008951	.010147	.010404
.002525	.005221	.006464	.008764	.009471	.009751
.002447	.005027	.006363	.008407	.008384	.009565
.001865	.004064	.005384	.006954	.008485	.008764
.001709	.003768	.004810	.005734	.007498	.008353
.001632	.003559	.004778	.006029	.006480	.007747
.001414	.002222	.003768	.005928	.006092	.006566

RADIANT HEAT TRANSFER FROM LONG RECTANGULAR SOURCE

135,290 HISTORIES	ANISOTROPIC SCATTERING (D)
50,000 ABSORPTIONS	OPTICAL DENSITY = 7.5 (1/KM)
74,657 SCATTERINGS	ABSORPTION/EXTINCTION = 0.4

FRACTION OF ORIGINAL EMISSIONS ABSORBED IN EACH SUBSPACE

.004561	.004147	.004051	.003614	.004139	.003725
.012085	.009365	.008973	.008160	.008116	.007554
.004516	.007953	.007894	.008648	.008700	.009092
.001996	.005152	.007340	.008796	.009136	.009712
.001685	.004324	.006201	.008279	.008315	.008818
.001678	.004524	.006335	.007990	.008219	.009417
.001382	.003600	.005366	.007185	.008456	.008700
.001197	.003807	.004797	.005477	.007488	.007835
.001338	.003858	.005048	.006608	.006586	.007754
.001035	.002994	.004494	.006615	.007244	.007502

RADIANT HEAT TRANSFER FROM LONG RECTANGULAR SOURCE

114,526 HISTORIES

50,000 ABSORPTIONS

50,131 SCATTERINGS

ANISOTROPIC SCATTERING (F)

OPTICAL DENSITY = .7.5 (1/KM)

ABSORPTION/EXTINCTION = 0.5

FRACTION OF ORIGINAL EMISSIONS ABSORBED IN EACH SUBSPACE

.006086	.005335	.004960	.004488	.004977	.004654
.014110	.011814	.010190	.009963	.009561	.009290
.005431	.009404	.010155	.010216	.010609	.010836
.002358	.006287	.008531	.010635	.011002	.010915
.002096	.005466	.007981	.009631	.010006	.010696
.001973	.005361	.007273	.008976	.009587	.010810
.001668	.004383	.005955	.008557	.010347	.009544
.001467	.004401	.005841	.006837	.008094	.008924
.001598	.004200	.005553	.007815	.007623	.008880
.001100	.003178	.005265	.007492	.008164	.008033

RADIANT HEAT TRANSFER FROM LONG RECTANGULAR SOURCE

54,997 HISTORIES

25,000 ABSORPTIONS

37,623 SCATTERINGS

ANISOTROPIC SCATTERING (F)

OPTICAL DENSITY = 10 (1/KM)

ABSORPTION/EXTINCTION = 0.4

FRACTION OF ORIGINAL EMISSIONS ABSORBED IN EACH SUBSPACE

.006291	.005800	.005455	.005873	.005000	.004691
.015437	.013219	.011037	.010564	.009746	.010619
.005037	.009728	.011292	.011873	.011146	.011546
.002782	.006419	.008891	.010873	.011492	.010837
.002364	.006255	.007564	.009946	.011237	.010746
.001546	.005218	.007255	.008928	.009891	.011328
.001927	.004891	.006691	.008600	.009055	.010819
.001255	.003855	.005800	.007637	.008855	.008819
.001146	.003800	.005346	.006782	.008655	.008746
.001182	.003800	.006328	.006709	.007946	.008000

RADIANT HEAT TRANSFER FROM LONG RECTANGULAR SOURCE

52,654 HISTORIES

25,000 ABSORPTIONS

37,508 SCATTERINGS

ISOTROPIC SCATTERING (I)

OPTICAL DENSITY = 10 (1/KM)

ABSORPTION/EXTINCTION = 0.4

FRACTION OF ORIGINAL EMISSIONS ABSORBED IN EACH SUBSPACE

.006628	.005660	.006039	.006096	.005299	.005546
.016903	.014130	.012858	.010882	.010408	.011832
.007236	.009971	.012155	.012364	.012478	.013066
.004406	.008261	.009572	.011699	.012459	.012649
.003532	.007122	.008546	.010427	.012022	.011129
.002754	.006381	.007103	.008774	.010427	.011699
.002108	.004786	.006628	.008413	.009496	.010503
.002222	.003646	.005717	.007616	.008527	.008850
.001481	.003722	.004691	.006077	.007483	.007483
.001121	.003096	.004273	.005299	.005831	.007217

RADIANT HEAT TRANSFER FROM LONG RECTANGULAR SOURCE

109,853 HISTORIES — ANISOTROPIC SCATTERING (D)

50,000 ABSORPTIONS — OPTICAL DENSITY = 10 (1/KM)

75,098 SCATTERINGS — ABSORPTION/EXTINCTION = 0.4

FRACTION OF ORIGINAL EMISSIONS ABSORBED IN EACH SUBSPACE

.006281	.005480	.005125	.005344	.005025	.004552
.015757	.013026	.011361	.010168	.009895	.010150
.005471	.009540	.010587	.011606	.011488	.011597
.002886	.006554	.009012	.010978	.011342	.011306
.002421	.005972	.007519	.010368	.011424	.011461
.001593	.005198	.007437	.008721	.009768	.010824
.001666	.005025	.007082	.008557	.009012	.010077
.001538	.003951	.005862	.008311	.008866	.009194
.001429	.003405	.005862	.006627	.008839	.009085
.001083	.003814	.006026	.006399	.007674	.008530

RADIANT HEAT TRANSFER FROM LONG RECTANGULAR SOURCE

47,481 HISTORIES

25,000 ABSORPTIONS

25,088 SCATTERINGS

ANISOTROPIC SCATTERING (F)

OPTICAL DENSITY = .10 (1/KM)

ABSORPTION/EXTINCTION = 0.5

FRACTION OF ORIGINAL EMISSIONS ABSORBED IN EACH SUBSPACE

.007982	.007013	.006466	.006276	.006150	.005918
.019229	.015901	.013648	.012847	.012110	.012026
.006023	.012173	.013290	.013374	.013163	.013205
.003517	.008403	.010404	.012595	.013395	.012974
.002654	.006466	.008151	.010741	.012637	.012742
.001938	.005960	.008319	.010109	.012005	.011415
.002001	.005560	.007708	.010236	.010931	.011183
.001622	.004360	.006255	.009625	.010762	.009920
.001179	.004086	.006276	.007603	.009604	.009962
.001095	.004318	.006908	.007456	.008066	.008593

RADIANT HEAT TRANSFER FROM LONG RECTANGULAR SOURCE

84,209 HISTORIES — ANISOTROPIC SCATTERING (F)

50,000 ABSORPTIONS — OPTICAL DENSITY = 15 (1/KM)

74,769 SCATTERINGS — ABSORPTION/EXTINCTION = 0.4

FRACTION OF ORIGINAL EMISSIONS ABSORBED IN EACH SUBSPACE

.009536	.008538	.007683	.007553	.007149	.006757
.023133	.018763	.016245	.015058	.014132	.013965
.007719	.014037	.014785	.015865	.015533	.015545
.003396	.009940	.012410	.014535	.014440	.015960
.003111	.007410	.010367	.013526	.014357	.014476
.002387	.006294	.009025	.010854	.012540	.012849
.001900	.005843	.008776	.010711	.011353	.012291
.001520	.004750	.008586	.009880	.010094	.011103
.001425	.004121	.007006	.008621	.010023	.009892
.001294	.003931	.005771	.007256	.008788	.008954

RADIANT HEAT TRANSFER FROM LONG RECTANGULAR SOURCE

82,976 HISTORIES — ISOTROPIC SCATTERING (I)

50,000 ABSORPTIONS — OPTICAL DENSITY = 15 (1/KM)

74,921 SCATTERINGS — ABSORPTION/EXTINCTION = 0.4

FRACTION OF ORIGINAL EMISSIONS ABSORBED IN EACH SUBSPACE

.010148	.009376	.008617	.008472	.007436	.008460
.026273	.020211	.017909	.016282	.015318	.015872
.010232	.015149	.017017	.017427	.017571	.017174
.005652	.010678	.013064	.015065	.016113	.016957
.004001	.007954	.010690	.013148	.014293	.015667
.003145	.006448	.009461	.010160	.012727	.012678
.002567	.005941	.008340	.008978	.010376	.012003
.002169	.004640	.006725	.008219	.008954	.010184
.001675	.003194	.005062	.006424	.007412	.008075
.001567	.002398	.003326	.004953	.006219	.006339

RADIANT HEAT TRANSFER FROM LONG RECTANGULAR SOURCE

83,958 HISTORIES — ANISOTROPIC SCATTERING (D)

50,000 ABSORPTIONS — OPTICAL DENSITY = 15 (1/KM)

74,457 SCATTERINGS — ABSORPTION/EXTINCTION = 0.4

FRACTION OF ORIGINAL EMISSIONS ABSORBED IN EACH SUBSPACE

.009445	.008742	.007587	.007408	.006908	.006741
.023416	.018712	.016997	.015401	.014614	.014209
.007623	.014043	.014900	.015412	.015996	.015424
.003478	.009945	.012602	.014460	.014364	.015877
.002990	.007563	.010386	.013185	.014388	.014472
.002251	.006491	.008540	.011268	.012530	.012566
.001882	.006027	.008850	.010636	.010779	.012280
.001548	.004943	.008445	.009624	.010839	.011530
.001441	.004157	.006694	.008576	.010124	.009695
.001334	.003966	.006015	.006718	.009374	.009124

RADIANT HEAT TRANSFER FROM LONG RECTANGULAR SOURCE

74,379 HISTORIES — ANISOTROPIC SCATTERING (F)

50,000 ABSORPTIONS — OPTICAL DENSITY = 15 (1/KM)

49,860 SCATTERINGS — ABSORPTION/EXTINCTION = 0.5

FRACTION OF ORIGINAL EMISSIONS ABSORBED IN EACH SUBSPACE

.012611	.009936	.009532	.008887	.008510	.008470
.029040	.023111	.019616	.018043	.016927	.016295
.009599	.017707	.017344	.018594	.018527	.018137
.004047	.011603	.014144	.016470	.016900	.017155
.003092	.008618	.012167	.014950	.016134	.015461
.002232	.007314	.009331	.012288	.013606	.014211
.002286	.006790	.009398	.011589	.011899	.012598
.001398	.005203	.007811	.009868	.010984	.011146
.001748	.004450	.006763	.008497	.010729	.010339
.001412	.004114	.005808	.007704	.009438	.009653

RADIANT HEAT TRANSFER FROM LONG RECTANGULAR SOURCE

36,118 HISTORIES — ANISOTROPIC SCATTERING (F)

25,000 ABSORPTIONS — OPTICAL DENSITY = 20 (1/KM)

37,595 SCATTERINGS — ABSORPTION/EXTINCTION = 0.4

FRACTION OF ORIGINAL EMISSIONS ABSORBED IN EACH SUBSPACE

.012736	.011684	.009801	.009137	.009109	.008915
.031563	.023894	.021319	.017471	.016861	.018440
.010272	.017526	.018855	.019215	.017858	.018218
.004541	.011407	.014397	.017498	.018827	.018716
.003710	.008888	.011601	.014480	.013954	.016169
.002575	.007946	.011047	.013345	.014370	.013511
.002104	.005454	.009109	.011324	.012431	.013511
.001910	.005316	.007780	.010217	.011933	.011379
.001661	.004707	.006811	.009441	.009607	.009940
.001744	.003572	.005565	.007725	.008832	.010244

RADIANT HEAT TRANSFER FROM LONG RECTANGULAR SOURCE

36,588 HISTORIES — ISOTROPIC SCATTERING (I)

25,000 ABSORPTIONS — OPTICAL DENSITY = 20 (1/KM)

37,398 SCATTERINGS — ABSORPTION/EXTINCTION = 0.4

FRACTION OF ORIGINAL EMISSIONS ABSORBED IN EACH SUBSPACE

.013830	.012326	.010933	.010687	.010905	.009675
.035203	.025828	.023368	.020143	.019460	.019569
.013064	.018831	.020253	.019542	.021346	.021045
.006696	.012326	.014677	.018175	.019323	.018531
.004619	.009949	.012436	.014376	.014376	.016508
.003362	.006997	.010905	.011670	.012600	.013584
.002624	.004619	.006942	.009484	.010331	.011479
.001667	.003662	.006013	.007133	.009293	.008855
.002023	.002842	.004810	.005548	.006888	.007817
.001175	.002979	.003608	.004346	.005630	.006396

RADIANT HEAT TRANSFER FROM LONG RECTANGULAR SOURCE

71,882 HISTORIES

50,000 ABSORPTIONS

75,185 SCATTERINGS

ANISOTROPIC SCATTERING (D)

OPTICAL DENSITY = 20 (1/KM)

ABSORPTION/EXTINCTION = 0.4

FRACTION OF ORIGINAL EMISSIONS ABSORBED IN EACH SUBSPACE

.012827	.010837	.010211	.009432	.009390	.008430
.031037	.024192	.020770	.018809	.016861	.018196
.009849	.017974	.018989	.019490	.019142	.019059
.004633	.011268	.014830	.017459	.017863	.017946
.003297	.009001	.011825	.014162	.015442	.016277
.002574	.007178	.011533	.013800	.013300	.014663
.001906	.005773	.009057	.011088	.013439	.013007
.001906	.005467	.007665	.010003	.011672	.011811
.001850	.004619	.007151	.008792	.009627	.010837
.001711	.004201	.006246	.007679	.008319	.009210

RADIANT HEAT TRANSFER FROM LONG RECTANGULAR SOURCE

32,495	HISTORIES	ANISOTROPIC SCATTERING (F)
25,000	ABSORPTIONS	OPTICAL DENSITY = 20 (1/KM)
24,882	SCATTERINGS	ABSORPTION/EXTINCTION = 0.5

FRACTION OF ORIGINAL EMISSIONS ABSORBED IN EACH SUBSPACE

.014987	.013448	.011509	.011232	.011633	.010155
.038437	.028404	.024096	.021172	.020588	.020157
.010617	.021573	.021542	.022834	.021142	.021696
.005262	.012956	.017910	.020126	.020434	.019942
.003539	.009878	.013725	.016618	.017110	.017357
.002000	.008309	.012033	.014772	.014741	.014741
.002216	.005939	.009386	.011971	.012310	.014833
.001908	.005262	.007817	.010155	.012033	.011109
.001723	.003908	.006155	.009325	.009017	.009725
.001539	.004062	.005170	.008494	.009601	.009017

RADIANT HEAT TRANSFER FROM LONG RECTANGULAR SOURCE

65,084 HISTORIES — ANISOTROPIC SCATTERING (F)

50,000 ABSORPTIONS — OPTICAL DENSITY = 20 (1/KM)

50,331 SCATTERINGS — ABSORPTION/EXTINCTION = 0.5

FRACTION OF ORIGINAL EMISSIONS ABSORBED IN EACH SUBSPACE

.015073	.013890	.011815	.011646	.011324	.010141
.037936	.028363	.025152	.021818	.020958	.020435
.011155	.021526	.021695	.022079	.021587	.021403
.005501	.013214	.017608	.019360	.020727	.019652
.003350	.010079	.012768	.017147	.017024	.018084
.002658	.007913	.011785	.013736	.014550	.014458
.002351	.006069	.009311	.011462	.012737	.014212
.001936	.005378	.007974	.009803	.011385	.011308
.001644	.004102	.006853	.009065	.009280	.010187
.001398	.003857	.005501	.007775	.008620	.008420

RADIANT HEAT TRANSFER FROM LONG RECTANGULAR SOURCE

130,127 HISTORIES	ANISOTROPIC SCATTERING (F)
100,000 ABSORPTIONS	OPTICAL DENSITY = 20 (1/KM)
100,577 SCATTERINGS	ABSORPTION/EXTINCTION = 0.5

FRACTION OF ORIGINAL EMISSIONS ABSORBED IN EACH SUBSPACE

.015400	.013671	.011896	.011919	.011035	.010474
.038224	.028403	.024791	.022639	.020857	.020526
.011612	.021625	.022278	.021940	.021548	.021564
.005180	.012864	.017076	.018605	.020319	.019804
.003235	.009921	.012910	.016276	.017199	.017675
.002613	.008038	.011512	.013886	.015154	.015093
.002213	.006025	.009199	.011666	.012795	.013756
.001883	.005464	.008069	.009629	.011143	.011742
.001668	.004181	.006916	.008845	.009260	.010029
.001214	.004119	.005787	.007762	.008484	.008868

RADIANT HEAT TRANSFER FROM LONG RECTANGULAR SOURCE

64,751 HISTORIES	ANISOTROPIC SCATTERING (F)
50,000 ABSORPTIONS	OPTICAL DENSITY = 25 (1/KM)
74,812 SCATTERINGS	ABSORPTION/EXTINCTION = 0.4

FRACTION OF ORIGINAL EMISSIONS ABSORBED IN EACH SUBSPACE

.015150	.013961	.011845	.011737	.011660	.010764
.038625	.028834	.025529	.022054	.021266	.021266
.012602	.020401	.022332	.023397	.022115	.020756
.005189	.012926	.016262	.018594	.019830	.020772
.003645	.009390	.014641	.016108	.016849	.016880
.002981	.007243	.011120	.013977	.015027	.014872
.002317	.006255	.009869	.011320	.012865	.013405
.001853	.005513	.008432	.009405	.011506	.012000
.001745	.005019	.006625	.009004	.009575	.010486
.001390	.003722	.005544	.007367	.008185	.008185

RADIANT HEAT TRANSFER FROM LONG RECTANGULAR SOURCE

68,095 HISTORIES — ISOTROPIC SCATTERING (I)

50,000 ABSORPTIONS — OPTICAL DENSITY = 25 (1/KM)

75,112 SCATTERINGS — ABSORPTION/EXTINCTION = 0.4

FRACTION OF ORIGINAL EMISSIONS ABSORBED IN EACH SUBSPACE

.017813	.015052	.013466	.013746	.012835	.012027
.043337	.031544	.028372	.023805	.023394	.022292
.015978	.022307	.023408	.023893	.023996	.022792
.007534	.014025	.016565	.018210	.020325	.020662
.004714	.009663	.013276	.014862	.015522	.015948
.003275	.006300	.008870	.011205	.012864	.013746
.002599	.004450	.007064	.007725	.009619	.010691
.002085	.003980	.005096	.006403	.007710	.008238
.001513	.002423	.004244	.004685	.005375	.005859
.000910	.002027	.002658	.003334	.003613	.004347

RADIANT HEAT TRANSFER FROM LONG RECTANGULAR SOURCE

59,791 HISTORIES — ANISOTROPIC SCATTERING (F)

50,000 ABSORPTIONS — OPTICAL DENSITY = 25 (1/KM)

49,928 SCATTERINGS — ABSORPTION/EXTINCTION = 0.5

FRACTION OF ORIGINAL EMISSIONS ABSORBED IN EACH SUBSPACE

.018581	.016073	.014952	.014300	.013296	.013163
.048235	.034905	.029386	.026409	.025255	.023816
.014501	.024050	.024937	.024803	.025087	.023900
.005870	.015253	.018414	.021190	.021124	.022027
.003479	.010988	.015052	.016524	.017110	.018548
.003044	.007677	.011423	.013464	.015036	.015353
.002040	.006339	.009550	.011607	.012360	.013296
.002091	.005369	.007877	.009316	.010453	.010503
.001706	.004248	.005937	.007627	.007877	.009366
.001171	.003629	.005185	.006556	.007710	.007208

RADIANT HEAT TRANSFER FROM LONG RECTANGULAR SOURCE

60,569 HISTORIES

50,000 ABSORPTIONS

75,023 SCATTERINGS

ANISOTROPIC SCATTERING (F)

OPTICAL DENSITY = 30 (1/KM)

ABSORPTION/EXTINCTION = 0.4

FRACTION OF ORIGINAL EMISSIONS ABSORBED IN EACH SUBSPACE

.018161	.017187	.013901	.013555	.013901	.012911
.045535	.033301	.028860	.024930	.023956	.024633
.014248	.022024	.024732	.025426	.023989	.023742
.005481	.014562	.017633	.019862	.020357	.020555
.004028	.010038	.014892	.016939	.018244	.018640
.003087	.008602	.011375	.013621	.015734	.016048
.002163	.006670	.009592	.011293	.013192	.013654
.001948	.005812	.007611	.009246	.010055	.011243
.001321	.003847	.006290	.007925	.008437	.009394
.001403	.003616	.005514	.006720	.006637	.007231

RADIANT HEAT TRANSFER FROM LONG RECTANGULAR SOURCE

56,673 HISTORIES	ANISOTROPIC SCATTERING (F)
50,000 ABSORPTIONS	OPTICAL DENSITY = 30 (1/KM)
49,941 SCATTERINGS	ABSORPTION/EXTINCTION = 0.5

FRACTION OF ORIGINAL EMISSIONS ABSORBED IN EACH SUBSPACE

.021386	.019921	.017380	.017080	.016286	.015228
.056217	.040301	.034637	.029485	.027315	.027156
.016833	.026415	.027332	.027844	.026573	.026027
.006246	.015404	.019957	.022621	.021015	.022639
.003705	.010499	.015351	.017539	.018122	.019427
.003106	.007923	.011593	.013904	.014716	.014875
.002364	.006211	.008928	.010693	.011452	.012069
.001747	.004676	.006546	.008099	.009581	.009511
.001218	.003758	.005064	.006723	.007676	.007852
.001147	.002929	.004252	.005576	.005805	.006317

RADIANT HEAT TRANSFER FROM LONG RECTANGULAR SOURCE

55,609 HISTORIES — ANISOTROPIC SCATTERING (F)

50,000 ABSORPTIONS — OPTICAL DENSITY = 40 (1/KM)

74,755 SCATTERINGS — ABSORPTION/EXTINCTION = 0.4

FRACTION OF ORIGINAL EMISSIONS ABSORBED IN EACH SUBSPACE

.024079	.020356	.018486	.017497	.017191	.016310
.059487	.041450	.036181	.030427	.028718	.028341
.017389	.027406	.027945	.027406	.026057	.026560
.006618	.016184	.020770	.021867	.022982	.022245
.004064	.011149	.015519	.016346	.017965	.020482
.003021	.007840	.011527	.013433	.014260	.014710
.002068	.006150	.008919	.011095	.010592	.012192
.001331	.004981	.006078	.008236	.009495	.009207
.001421	.003345	.005539	.006815	.007643	.007337
.000953	.002697	.004046	.004981	.005934	.005808

RADIANT HEAT TRANSFER FROM LONG RECTANGULAR SOURCE

63,241 HISTORIES — ISOTROPIC SCATTERING (I)

50,000 ABSORPTIONS — OPTICAL DENSITY = 40 (1/KM)

75,168 SCATTERINGS — ABSORPTION/EXTINCTION = 0.4

FRACTION OF ORIGINAL EMISSIONS ABSORBED IN EACH SUBSPACE

.027451	.023924	.021458	.020446	.018184	.017821
.067440	.046694	.036717	.033254	.030234	.029996
.021442	.029142	.027846	.027909	.025189	.026644
.007543	.015243	.017536	.019070	.019212	.018690
.004949	.007637	.010816	.011954	.013551	.013267
.002736	.005218	.007321	.007748	.008460	.009456
.001724	.003052	.004570	.004981	.005250	.006452
.000870	.001486	.002767	.003194	.003763	.003985
.000474	.001091	.001708	.002040	.001866	.002941
.000316	.000601	.000933	.001091	.001502	.001771

RADIANT HEAT TRANSFER FROM LONG RECTANGULAR SOURCE

53,312 HISTORIES   ANISOTROPIC SCATTERING (F)

50,000 ABSORPTIONS   OPTICAL DENSITY = 40 (1/KM)

49,923 SCATTERINGS   ABSORPTION/EXTINCTION = 0.5

FRACTION OF ORIGINAL EMISSIONS ABSORBED IN EACH SUBSPACE

.029055	.024497	.022078	.020577	.020671	.019095
.072535	.050795	.040216	.034808	.032751	.030593
.021121	.031269	.032019	.029431	.027161	.027367
.006265	.017801	.021083	.023203	.022809	.022959
.004052	.010748	.015081	.015475	.017257	.017257
.002851	.007447	.010429	.012192	.012849	.012793
.001819	.005421	.007147	.008553	.009191	.010598
.001407	.003939	.005365	.007315	.006940	.007822
.000844	.002870	.004164	.005008	.005852	.005777
.000769	.002082	.002926	.003920	.004239	.004314

RADIANT HEAT TRANSFER FROM LONG RECTANGULAR SOURCE

26,640 HISTORIES — ANISOTROPIC SCATTERING (F)

25,000 ABSORPTIONS — OPTICAL DENSITY = 50 (1/KM)

37,229 SCATTERINGS — ABSORPTION/EXTINCTION = 0.4

FRACTION OF ORIGINAL EMISSIONS ABSORBED IN EACH SUBSPACE

.029692	.026201	.020383	.020008	.019069	.019782
.073461	.049174	.040465	.034159	.031869	.032658
.020796	.031344	.030143	.030030	.028791	.027665
.007320	.016592	.021959	.022072	.024324	.023911
.004129	.011449	.014715	.015090	.018056	.018168
.002590	.007808	.010135	.013589	.011974	.013363
.001839	.004617	.007845	.008821	.010285	.009122
.001464	.003341	.005068	.006757	.007545	.007282
.000863	.002778	.004279	.005255	.005556	.005668
.000713	.001989	.003003	.003829	.003529	.004054

RADIANT HEAT TRANSFER FROM LONG RECTANGULAR SOURCE

51,738 HISTORIES — ANISOTROPIC SCATTERING (F)

50,000 ABSORPTIONS — OPTICAL DENSITY = 50 (1/KM)

50,127 SCATTERINGS — ABSORPTION/EXTINCTION = 0.5

FRACTION OF ORIGINAL EMISSIONS ABSORBED IN EACH SUBSPACE

.036240	.030461	.025822	.025668	.023851	.021435
.088639	.058062	.045363	.038811	.034153	.033612
.024547	.035255	.033322	.030558	.028722	.029089
.006784	.016912	.022111	.021609	.021995	.021242
.004040	.010534	.013433	.014535	.015559	.015366
.002319	.006514	.008814	.010457	.010418	.011481
.001450	.004330	.006243	.007209	.007538	.007229
.001198	.003035	.003866	.004793	.005992	.005624
.000541	.002145	.002957	.003556	.004040	.004136
.000483	.001701	.002416	.002648	.002590	.002957

RADIANT HEAT TRANSFER FROM LONG RECTANGULAR SOURCE

52,002 HISTORIES ANISOTROPIC SCATTERING (F)

50,000 ABSORPTIONS OPTICAL DENSITY = .60 (1/KM)

75,122 SCATTERINGS ABSORPTION/EXTINCTION = 0.4

FRACTION OF ORIGINAL EMISSIONS ABSORBED IN EACH SUBSPACE

.035576	.029691	.025576	.023922	.021595	.021941
.085151	.056248	.043883	.038287	.034268	.033422
.022865	.034672	.033460	.029826	.030460	.028653
.007384	.017384	.020595	.021384	.022230	.022595
.003981	.010942	.015269	.015269	.015172	.016269
.002461	.006365	.009500	.011403	.012423	.010827
.001385	.003981	.006077	.007288	.008538	.007904
.000942	.003115	.004808	.005250	.005596	.006077
.000827	.001865	.003096	.003692	.003750	.004288
.000596	.001211	.002096	.002558	.003000	.002615

RADIANT HEAT TRANSFER FROM LONG RECTANGULAR SOURCE

50,999 HISTORIES	ANISOTROPIC SCATTERING (F)
50,000 ABSORPTIONS	OPTICAL DENSITY = 60 (1/KM)
50,083 SCATTERINGS	ABSORPTION/EXTINCTION = 0.5

FRACTION OF ORIGINAL EMISSIONS ABSORBED IN EACH SUBSPACE

.042766	.035216	.030530	.028765	.024824	.024216
.103080	.065197	.049138	.040511	.036667	.036373
.027157	.037138	.035334	.029922	.030138	.027667
.007059	.016883	.020373	.019981	.020255	.019549
.003726	.009608	.011961	.013216	.013687	.013628
.001922	.005647	.007471	.008569	.009412	.008432
.001216	.003392	.004843	.005431	.005922	.005941
.000784	.002314	.003216	.003824	.003824	.004373
.000510	.001902	.002137	.002490	.002275	.002843
.000392	.000980	.001275	.001549	.001569	.001392

RADIANT HEAT TRANSFER FROM LONG RECTANGULAR SOURCE

50,921 HISTORIES	ANISOTROPIC SCATTERING (F)
50,000 ABSORPTIONS	OPTICAL DENSITY = 80 (1/KM)
74,922 SCATTERINGS	ABSORPTION/EXTINCTION = 0.4

FRACTION OF ORIGINAL EMISSIONS ABSORBED IN EACH SUBSPACE

.046032	.037745	.031775	.029222	.026629	.026099
.108462	.065651	.050176	.041555	.037666	.035506
.027827	.039512	.034190	.031284	.029418	.029222
.007384	.017223	.020110	.020247	.018755	.019206
.003319	.008739	.011528	.012195	.013079	.011665
.001787	.004890	.007364	.007895	.008130	.008366
.001060	.002749	.004320	.004694	.005165	.004890
.000766	.001669	.002632	.002906	.003574	.003103
.000393	.001159	.001512	.001591	.002023	.002003
.000196	.000962	.001100	.001237	.001100	.001257

RADIANT HEAT TRANSFER FROM LONG RECTANGULAR SOURCE

62,060 HISTORIES — ISOTROPIC SCATTERING (I)

50,000 ABSORPTIONS — OPTICAL DENSITY = 80 (1/KM)

75,155 SCATTERINGS — ABSORPTION/EXTINCTION = 0.4

FRACTION OF ORIGINAL EMISSIONS ABSORBED IN EACH SUBSPACE

.054995	.041653	.034225	.031792	.027908	.027022
.121656	.068804	.049065	.039865	.033258	.030648
.030406	.034386	.027071	.023171	.019207	.016855
.006413	.010200	.011215	.009861	.009314	.008186
.002224	.003690	.004141	.004077	.003980	.004496
.000532	.001354	.001982	.001644	.001821	.001692
.000226	.000596	.000741	.000838	.000822	.000918
.000097	.000322	.000387	.000290	.000403	.000274
.000048	.000064	.000193	.000145	.000048	.000177
.000000	.000016	.000064	.000048	.000064	.000081

RADIANT HEAT TRANSFER FROM LONG RECTANGULAR SOURCE

50,488 HISTORIES   ANISOTROPIC SCATTERING (F)

50,000 ABSORPTIONS   OPTICAL DENSITY = .80 (1/KM)

50,178 SCATTERINGS   ABSORPTION/EXTINCTION = 0.5

FRACTION OF ORIGINAL EMISSIONS ABSORBED IN EACH SUBSPACE

.054746	.044941	.036484	.033731	.029512	.028918
.131378	.074810	.055795	.041535	.038326	.036682
.031096	.040227	.035216	.028680	.026422	.024778
.007012	.015687	.017668	.017450	.016024	.015449
.003011	.007606	.009448	.009943	.009983	.009289
.001347	.004100	.005546	.005407	.005427	.005685
.000733	.002436	.002931	.002773	.003149	.003347
.000495	.001188	.001525	.001684	.001842	.001604
.000198	.000733	.000931	.000832	.001010	.001030
.000059	.000436	.000535	.000515	.000416	.000574

RADIANT HEAT TRANSFER FROM CIRCULAR SOURCE

112,984 HISTORIES — ANISOTROPIC SCATTERING (F)

25,000 ABSORPTIONS — OPTICAL DENSITY = .5 (1/KM)

37,186 SCATTERINGS — ABSORPTION/EXTINCTION = 0.4

FRACTION OF ORIGINAL EMISSIONS ABSORBED IN EACH SUBSPACE

.002363	.001673	.001336	.000876	.000620	.000195
.010718	.007789	.004948	.003585	.002266	.000743
.005027	.007337	.007497	.005169	.002930	.001142
.002399	.005434	.006417	.005187	.003248	.001496
.001956	.005178	.005797	.005532	.003921	.001159
.001620	.004540	.005762	.005240	.003744	.001372
.001673	.004222	.005541	.005054	.003691	.001257
.001655	.004576	.005691	.005479	.003425	.001407
.001443	.004257	.005523	.004956	.003691	.001372
.001381	.003788	.005222	.005160	.003346	.001248

RADIANT HEAT TRANSFER FROM CIRCULAR SOURCE

80,758 HISTORIES　　ANISOTROPIC SCATTERING (F)

25,000 ABSORPTIONS　　OPTICAL DENSITY = 7.5 (1/KM)

37,520 SCATTERINGS　　ABSORPTION/EXTINCTION = 0.4

FRACTION OF ORIGINAL EMISSIONS ABSORBED IN EACH SUBSPACE

.003566	.002340	.001820	.001238	.000830	.000186
.016605	.011231	.008111	.005287	.002947	.000941
.007417	.010364	.009225	.007603	.004185	.001560
.003244	.008049	.008878	.007851	.005312	.002105
.002860	.006711	.008160	.007925	.005448	.001709
.002501	.006848	.008445	.007677	.005139	.001895
.002477	.005523	.007392	.006538	.005337	.001635
.002229	.005461	.007628	.007145	.005114	.001721
.001907	.005126	.007157	.006810	.004953	.001808
.002031	.005176	.006699	.006897	.004792	.001795

RADIANT HEAT TRANSFER FROM CIRCULAR SOURCE

63,799 HISTORIES — ANISOTROPIC SCATTERING (F)

25,000 ABSORPTIONS — OPTICAL DENSITY = 10 (1/KM)

37,176 SCATTERINGS — ABSORPTION/EXTINCTION = 0.4

FRACTION OF ORIGINAL EMISSIONS ABSORBED IN EACH SUBSPACE

.003981	.003182	.002335	.001630	.000972	.000376
.022571	.014734	.010204	.006959	.004060	.001317
.009608	.013276	.013088	.009922	.005941	.001991
.004859	.010596	.012148	.010094	.007492	.002179
.003793	.008856	.011724	.009608	.006599	.002147
.003370	.007759	.010251	.009028	.006536	.002477
.002147	.007194	.009091	.008574	.006301	.002304
.002539	.007727	.009702	.008872	.006473	.002179
.002602	.005596	.007947	.008182	.005549	.002304
.002288	.005408	.007837	.008072	.005533	.001771

RADIANT HEAT TRANSFER FROM CIRCULAR SOURCE

61,990 HISTORIES　　　　ISOTROPIC SCATTERING (I)

25,000 ABSORPTIONS　　　　OPTICAL DENSITY = 10 (1/KM)

37,394 SCATTERINGS　　　　ABSORPTION/EXTINCTION = 0.4

FRACTION OF ORIGINAL EMISSIONS ABSORBED IN EACH SUBSPACE

.003968	.003291	.002404	.001694	.001145	.000226
.022681	.014293	.010776	.007259	.004388	.001484
.010518	.015148	.013083	.009421	.006453	.002097
.006098	.012131	.012292	.010405	.007356	.002533
.004872	.009792	.011841	.010131	.007082	.002452
.004630	.008872	.009792	.009308	.006437	.002339
.003952	.007598	.009340	.009324	.005694	.002468
.003872	.007614	.009018	.008405	.005727	.002242
.003662	.006549	.008114	.007598	.004436	.001920
.002775	.005017	.006904	.006437	.004436	.001500

RADIANT HEAT TRANSFER FROM CIRCULAR SOURCE

54,503 HISTORIES — ANISOTROPIC SCATTERING (F)

25,000 ABSORPTIONS — OPTICAL DENSITY = 10 (1/KM)

25,064 SCATTERINGS — ABSORPTION/EXTINCTION = 0.5

FRACTION OF ORIGINAL EMISSIONS ABSORBED IN EACH SUBSPACE

.004954	.004092	.003321	.002055	.001248	.000459
.027650	.018017	.012953	.008623	.004825	.001725
.011724	.016678	.015889	.011339	.007926	.002404
.005541	.012917	.013981	.012164	.008183	.002220
.004183	.010623	.013816	.011632	.008000	.002275
.003725	.009192	.011265	.010110	.007101	.003156
.002807	.008458	.010476	.009743	.007321	.002660
.002826	.007596	.010293	.010458	.006862	.002220
.003009	.006990	.009853	.008899	.005945	.002624
.002110	.006403	.008825	.008642	.005926	.001780

RADIANT HEAT TRANSFER FROM CIRCULAR SOURCE

47,503 HISTORIES — ANISOTROPIC SCATTERING (F)

25,000 ABSORPTIONS — OPTICAL DENSITY = .15 (1/KM)

37,393 SCATTERINGS — ABSORPTION/EXTINCTION = 0.4

FRACTION OF ORIGINAL EMISSIONS ABORBED IN EACH SUBSPACE

.006063	.004463	.003705	.002526	.001495	.000653
.032798	.021072	.016715	.010336	.006547	.002147
.013768	.020693	.018020	.014357	.008799	.002484
.006652	.014841	.015831	.013873	.008673	.003179
.004547	.011957	.014989	.012631	.008168	.003347
.004463	.009873	.013936	.012041	.008484	.002737
.003726	.008799	.012504	.011683	.007747	.003031
.003663	.008063	.011515	.010484	.007052	.002821
.003326	.008336	.010547	.009663	.006568	.002589
.002505	.006884	.009389	.009810	.006589	.002126

RADIANT HEAT TRANSFER FROM CIRCULAR SOURCE

46,670 HISTORIES — ISOTROPIC SCATTERING (I)

25,000 ABSORPTIONS — OPTICAL DENSITY = 15 (1/KM)

37,394 SCATTERINGS — ABSORPTION/EXTINCTION = 0.4

FRACTION OF ORIGINAL EMISSIONS ABSORBED IN EACH SUBSPACE

.006064	.004843	.003921	.002978	.001500	.000471
.033212	.021663	.016177	.011313	.006857	.002100
.015556	.022563	.018663	.014228	.008914	.002721
.009192	.016199	.017656	.013992	.009171	.003128
.006214	.013049	.014892	.013306	.008099	.003493
.006664	.011506	.013178	.013006	.008207	.002700
.005442	.010135	.012942	.011035	.007435	.002421
.005185	.008378	.010735	.009471	.006750	.002421
.004114	.007328	.008764	.008121	.005485	.001800
.003621	.006342	.007349	.006492	.004650	.001864

RADIANT HEAT TRANSFER FROM CIRCULAR SOURCE

47,589 HISTORIES

25,000 ABSORPTIONS

37,455 SCATTERINGS

ANISOTROPIC SCATTERING (D)

OPTICAL DENSITY = 15 (1/KM)

ABSORPTION/EXTINCTION = 0.4

FRACTION OF ORIGINAL EMISSIONS ABSORBED IN EACH SUBSPACE

.005758	.004434	.003719	.002648	.001471	.000588
.033117	.021328	.016138	.010233	.006262	.002143
.013659	.020299	.018282	.013848	.008805	.002501
.006577	.014856	.016159	.013722	.008826	.003089
.004812	.011809	.014331	.012398	.008216	.003404
.004119	.010065	.014205	.012104	.008910	.002438
.003593	.009057	.012230	.011725	.008111	.002858
.003509	.008111	.011410	.010318	.007250	.002858
.003425	.007922	.010612	.009876	.006934	.002564
.002438	.007397	.009666	.009393	.006640	.002164

RADIANT HEAT TRANSFER FROM CIRCULAR SOURCE

39,777 HISTORIES — ANISOTROPIC SCATTERING (F)

25,000 ABSORPTIONS — OPTICAL DENSITY = 20 (1/KM)

37,292 SCATTERINGS — ABSORPTION/EXTINCTION = 0.4

FRACTION OF ORIGINAL EMISSIONS ABSORBED IN EACH SUBSPACE

.007768	.006059	.004651	.003117	.002313	.000955
.041657	.028082	.020012	.013400	.007793	.002715
.017749	.027327	.023607	.018051	.009377	.003570
.007567	.018277	.020137	.016844	.011338	.003771
.006411	.013324	.017372	.014883	.010081	.003319
.005028	.012268	.015285	.014657	.009226	.003293
.004601	.011615	.014707	.013249	.009377	.002916
.004249	.009453	.012092	.011489	.007869	.002489
.003821	.007919	.011489	.010383	.007190	.003193
.003168	.006662	.009754	.010056	.007014	.002464

RADIANT HEAT TRANSFER FROM CIRCULAR SOURCE

35,805 HISTORIES

25,000 ABSORPTIONS

37,268 SCATTERINGS

ANISOTROPIC SCATTERING (F)

OPTICAL DENSITY = 24 (1/KM)

ABSORPTION/EXTINCTION = 0.4

FRACTION OF ORIGINAL EMISSIONS ABSORBED IN EACH SUBSPACE

.009077	.007541	.005446	.003687	.002542	.000950
.049825	.033459	.023153	.015445	.008854	.003100
.020640	.030499	.026812	.019411	.011423	.004161
.009021	.019774	.023516	.019439	.012987	.003994
.006480	.015501	.019718	.016255	.011646	.004301
.005279	.013210	.017484	.016087	.011535	.003463
.005446	.011367	.015724	.014411	.008854	.003351
.003547	.009328	.012596	.012456	.008881	.003156
.003212	.008546	.011060	.010641	.007736	.002765
.002988	.008211	.010585	.008323	.006982	.002346

RADIANT HEAT TRANSFER FROM CIRCULAR SOURCE

36,130 HISTORIES — ISOTROPIC SCATTERING (I)

25,000 ABSORPTIONS — OPTICAL DENSITY = .25 (1/KM)

36,971 SCATTERINGS — ABSORPTION/EXTINCTION = 0.4

FRACTION OF ORIGINAL EMISSIONS ABSORBED IN EACH SUBSPACE

.010047	.008331	.006228	.003820	.002878	.001273
.055715	.036064	.024301	.016025	.009881	.002851
.026764	.033878	.029034	.020897	.011929	.004567
.013590	.023554	.023305	.019596	.011652	.004179
.010379	.016828	.020869	.016939	.010075	.003598
.008469	.013534	.015223	.013313	.008719	.003294
.007556	.011680	.011597	.011542	.007362	.002823
.005203	.008995	.010241	.008580	.006061	.002104
.003681	.007224	.008276	.007224	.004539	.001688
.003017	.005397	.005591	.005536	.003183	.001246

RADIANT HEAT TRANSFER FROM CIRCULAR SOURCE

27,352 HISTORIES — ANISOTROPIC SCATTERING (F)

25,000 ABSORPTIONS — OPTICAL DENSITY = 50 (1/KM)

37,339 SCATTERINGS — ABSORPTION/EXTINCTION = 0.4

FRACTION OF ORIGINAL EMISSIONS ABSORBED IN EACH SUBSPACE

.018719	.013747	.011443	.007531	.004643	.001645
.103210	.059996	.039485	.025483	.013747	.004533
.040290	.051331	.039887	.028225	.016781	.005703
.013966	.028554	.030820	.024934	.016269	.006179
.008592	.019267	.023033	.020035	.013893	.004643
.006106	.015026	.018134	.016452	.011370	.003693
.003766	.010018	.013674	.012760	.009286	.002888
.002742	.008445	.009689	.008921	.006727	.002303
.002084	.006362	.007166	.008263	.004789	.001828
.001718	.005082	.006288	.005009	.005009	.001828

RADIANT HEAT TRANSFER FROM CIRCULAR SOURCE

25,604 HISTORIES — ANISOTROPIC SCATTERING (F)

25,000 ABSORPTIONS — OPTICAL DENSITY = .80 (1/KM)

37,275 SCATTERINGS — ABSORPTION/EXTINCTION = 0.4

FRACTION OF ORIGINAL EMISSIONS ABSORBED IN EACH SUBSPACE

.027574	.022145	.015232	.009998	.006366	.002265
.156460	.083112	.050305	.031714	.017263	.005273
.051789	.064521	.048860	.032026	.018981	.006327
.014334	.032065	.032495	.024488	.014646	.004921
.007225	.016482	.020270	.016599	.011522	.003476
.004179	.011600	.013240	.010780	.007538	.002578
.002421	.007968	.008866	.006874	.004882	.001953
.001523	.004452	.005780	.004491	.003398	.001172
.001250	.003398	.003749	.003125	.001836	.001094
.001055	.001836	.002656	.002187	.001250	.000547

RADIANT HEAT TRANSFER FROM CIRCULAR SOURCE

31,059 HISTORIES — ISOTROPIC SCATTERING (I)

25,000 ABSORPTIONS — OPTICAL DENSITY = .80 (1/KM)

37,335 SCATTERINGS — ABSORPTION/EXTINCTION = 0.4

FRACTION OF ORIGINAL EMISSIONS ABSORBED IN EACH SUBSPACE

.032680	.023053	.016549	.010883	.006439	.001706
.171094	.087060	.048585	.028526	.014263	.004121
.060079	.059371	.042854	.023858	.013072	.003606
.016453	.024663	.020542	.014617	.007727	.001964
.007083	.010754	.010432	.006085	.003413	.001320
.002962	.004636	.004443	.003348	.002383	.000483
.001320	.001739	.002125	.001320	.001095	.000451
.000644	.000934	.000837	.000805	.000386	.000032
.000258	.000354	.000451	.000290	.000258	.000000
.000064	.000097	.000161	.000064	.000097	.000032

APPENDIX G

CONFIGURATION FACTOR APPROACH TO DROPLET HEAT TRANSFER

For comparative purposes, it was considered worthwhile to evaluate direct heat transfer to a droplet on the basis of a differential surface exchanging energy with a finite surface, for the case of the circular source.

A significant problem arises in attempting to define the surface of the droplet as seen from different locations on the finite surface, or source, for different permissible droplet locations. In order to avoid this difficulty, a simplifying assumption was made for defining the droplet surface. This assumption defines the droplet surface as the cross sectional area of the droplet oriented perpendicular to the radius vector from the center of the finite source to the center of the droplet. Such an assumption should provide a conservative estimate of the actual surface. This definition also provides the essential information on the orientation of the assumed differential surface to the finite surface.

Using the method of superposition described by Sparrow and Cess (37), it is possible to describe the configuration factor of the differential droplet area, in any spatial location, as a function of two known cases. The first case is where the differential area is parallel to the X-Y plane, and the second case is where the differential area is parallel to the X-Z plane. A physical picture of these cases, as well as a general description of the geometry for the development that follows, is given in Figure G-1.

It should be noted that because of the symmetry in this example, it is possible to consider locations of the differential surface described in terms of the coordinates in the Y-Z plane.

The method of superposition states that the configuration factor from the droplet to the source is given by

$$F_{dA_d-A_s} = |\lambda_d| \; F_{dA_d-A_s}(0,-1,0) + |\gamma_d| \; F_{dA_d-A_s}(0,0,-1) \quad , \qquad \text{G.1}$$

where λ_d and γ_d are the direction cosines of the unit normal to the differential surface as defined for the droplet. The absolute value signs insure that the superposition is an additive procedure. The value $F_{dA_d-A_s}$ (0,-1,0) refers to the configuration factor for a differential area whose surface normal lies parallel to the negative direction of the Y axis. The configuration factor, $F_{dA_d-A_s}(0,0,-1)$, refers to the case where the differential area lies overhead such that the unit normal to the surface lies parallel to the negative direction of the Z axis.

λ_d represents the direction cosine for the Y component of the surface normal, and γ_d represents the direction cosine for the Z component. Since the location of the differential area is restricted to the upper right hand quadrant of the Y-Z plane, the direction cosines are taken in such a way that the absolute value signs can be removed. The direction cosines are

$$\lambda_d = \cos \eta \qquad \text{G.2}$$

and

$$\gamma_d = \sin \eta \ , \qquad \text{G.3}$$

where η is the angle, measured in a counterclockwise direction, between the Y axis and the radius vector to the differential area. This situation is illustrated on Figure G-1.

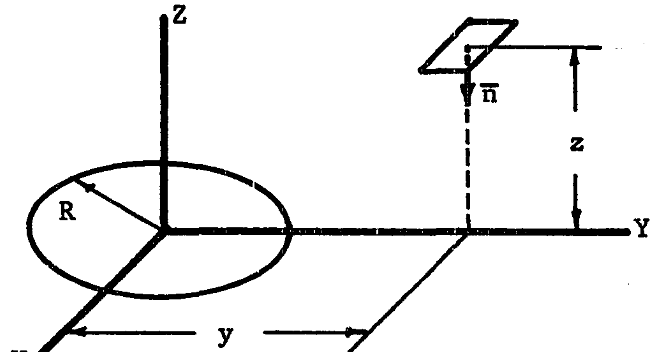

Geometry for Configuration Factor $F_{dA_d-A_s}(0,0,-1)$

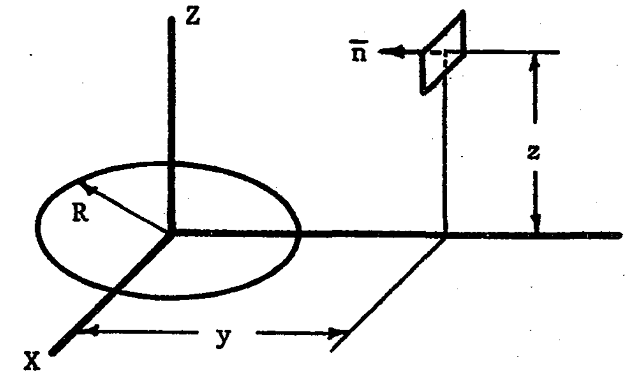

Geometry for Configuration Factor $F_{dA_d-A_s}(0,-1,0)$

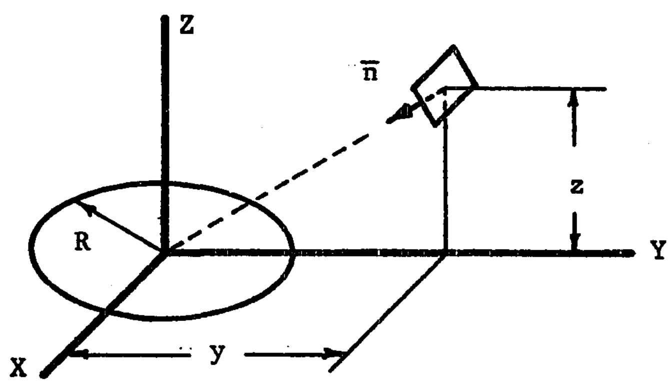

Geometry for General Configuration Factor Case

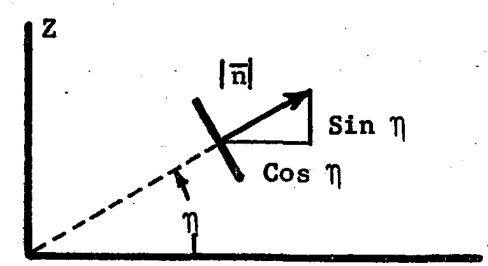

Absolute Value Direction Cosines

FIGURE G-1 GEOMETRY FOR USE WITH CONFIGURATION FACTOR SUPERPOSITION METHOD

The configuration factor components on the right hand side of equation G.1 are known and can be found in such references as Sparrow and Cess (37), Kreith (53), Eckert and Drake (76), and Hamilton and Morgan (77). Within the framework of the geometry established in Figure G-1, these configuration factors can be written as follows:

$$F_{dA_d-A_s}(0,0,-1) = \frac{1}{2}\left[1 - \frac{U - 2S^2T^2}{\sqrt{U^2 - 4S^2T^2}}\right], \qquad \text{G.4}$$

where $S = Z/Y$, $T = R/Z$ and $U = 1 + (1 + T^2)S^2$.

$$F_{dA_d-A_s}(0,-1,0) = \frac{S}{2}\left[\frac{1 + V^2 + S^2}{\sqrt{(1 + V^2 + S^2)^2 - 4V^2}} - 1\right], \qquad \text{G.5}$$

where $S = Z/Y$ and $V = R/Y$.

It has already been established that the absolute value signs on the direction cosines of equation G.1 can be removed for the geometry of this example. After making the necessary substitutions in equation G.1, the configuration factor between the differential area and the finite source area can be written as

$$F_{dA_d-A_s} = \cos\eta\left\{\frac{S}{2}\left[\frac{1+V^2+S^2}{\sqrt{(1+V^2+S^2)^2-4V^2}} - 1\right]\right\} + \sin\eta\left\{\frac{1}{2}\left[1 - \frac{U-2S^2T^2}{\sqrt{U^2-4S^2T^2}}\right]\right\}. \qquad \text{G.6}$$

In keeping with the situation analyzed in the Monte Carlo portion of this work, the exchange will be considered to be between two black surfaces. The medium suspending the droplet is the atmosphere which absorbs 60% of the radiation passing through it due to the presence of water vapor and carbon dioxide. With these assumptions, the rate of heat exchange, in Btu per hour, can be written as

$$H = E\sigma A_d F_{dA_d-A_s}(T_S^4 - T_d^4), \qquad \text{G.7}$$

where A_d = cross sectional area of droplet,

$F_{dA_d-A_s}$ = configuration factor,

T_s = source temperature,

T_d = droplet temperature,

and E = fraction of energy not absorbed by atmosphere.

In order to make the rate of exchange more realistic, the area of the droplet was taken as one half the initial cross sectional area in order to account for its diminishing size with evaporation. Other assumptions in this regard could have been made. This size is somewhat smaller than would arise from assuming an average cross section based on an average droplet volume equal to one half the original volume.

After establishing the net rate of heat exchange, it is possible to estimate the time required to evaporate the droplet in any specified location.

Configuration factors were computed, using equal G.6, for locations representing the centroids of the sixty subspaces of the accounting envelope for the circular source case. Next, the net rate of heat exchange was computed, using equation G.7, based on the average droplet cross section, a source temperature of $600^{\circ}R$, and a droplet temperature of $500^{\circ}R$.

The results of this calculation, transformed into the time required to evaporate the droplet, have been plotted on Figure G-2 for the subspaces along ray number 4. In addition to the curve based on the configuration factor approach to heat transfer, three curves obtained by the Monte Carlo method for similar droplet size, but at three different optical densities, have been added to this illustration for comparison. The Monte Carlo solutions were based on a strong forward scattering function, (F) and an absorption coefficient to extinction coefficient ratio of 0.4. This illustration is typical of the numerical agreement along the other ray lines. Data for an optical density of 10 km^{-1} has not been displayed on the illustration; however, it did produce excellent agreement with the configuration factor approach, being a little low for locations near the source and a little high for locations more remote from the source.

The comparison of results is suprisingly good considering the number of simplifying assumptions required. The agreement becomes quite good for the optically thin cases. This is probably due to the smaller number of droplets for these cases, which precludes a droplet nearer the source from shading a droplet at a greater distance.

While this study is of interest to the related work of this research, the results reported are not sufficient to draw significant quantitative conclusions.

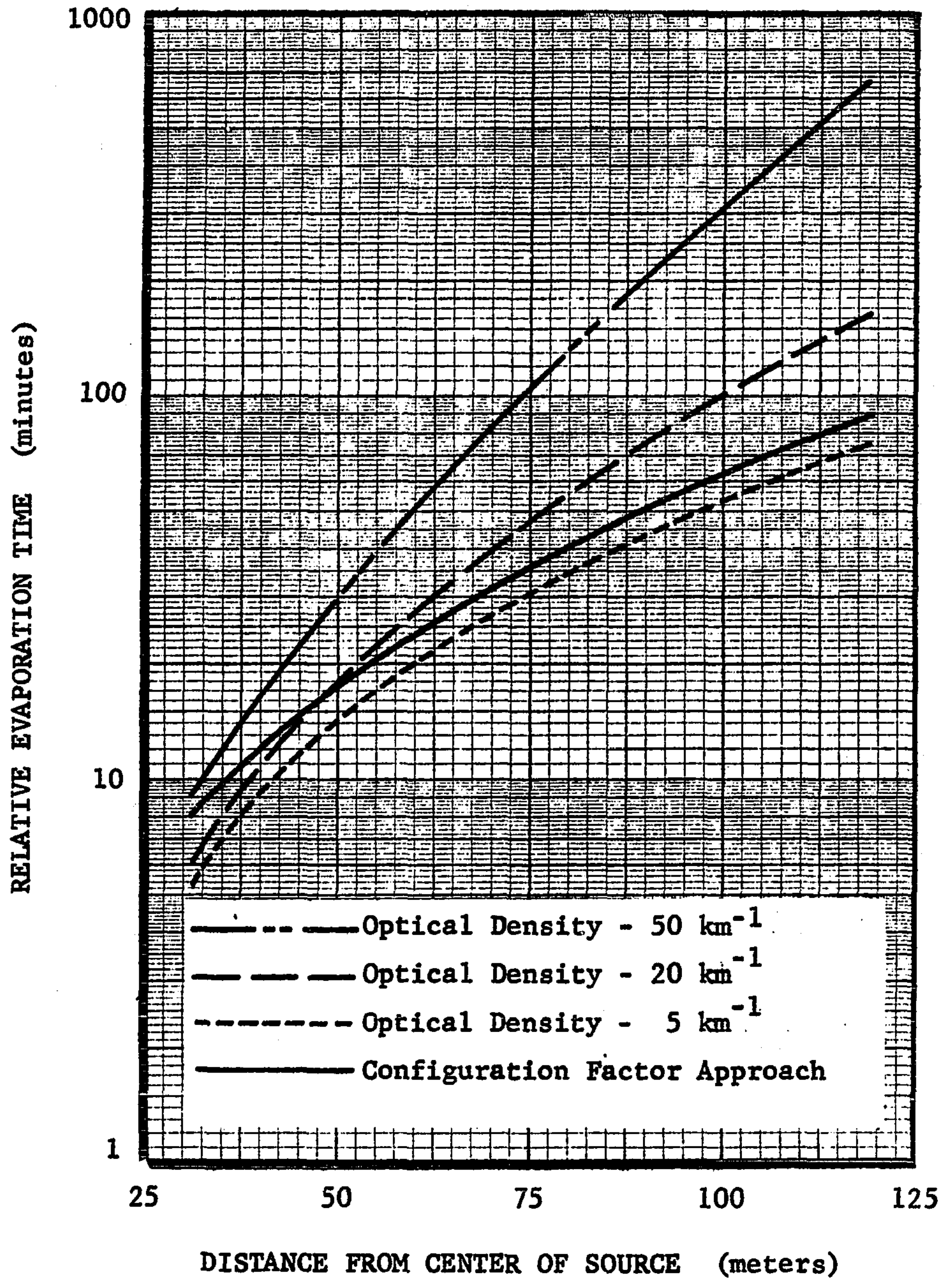

FIGURE G-2 COMPARATIVE RELATIVE EVAPORATION TIME CURVES

APPENDIX H

COMPUTER PROGRAMS

Legend for Use with Computer Programs

The following definitions are provided in order to clarify the coding used in the computer programs. In addition to these definitions, a number of comment cards have been incorporated in the programs in order to provide a subdivision of the program into related calculations

Code Symbol	Meaning
INABS	The total number of absorptions for which spatial distribution is to be collected prior to print out.
IX	Starting number for random number generating subroutine
R	Radius of circular source, meters
W	Half-width of rectangular source, meters
RMAX	Radius of hemispherical accounting shell, meters
WMAX	Radius of cylindrical accounting shell, meters
SCAT	Switching device for scattering; negative gives anisotropic, positive gives isotropic
DOPT	Optical density, km^{-1}; also volume extinction coefficient
WIN	Fraction of total emitted source energy which lies in the wavelength interval between 7.5 and 13.5 microns
AB	Ratio of absorption to extinction coefficients
EQ	Switching device for radiative equilibrium; positive is radiative equilibrium, negative is non-equilibrium (only non-equilibrium used in this study)

Code Symbol	Meaning
RDROP	Droplet radius, microns
DROPS	Droplet number density, drops per cubic centimeter
DELH	Latent heat of vaporization for water, Btu/lb
TS	Temperature of source, ^{o}R
ELMAX	Length to end of rectangular source from centered reference axis system
MABS(J,K)	Number of photons absorbed in the designated subspace
N	Number of original emissions from source
IY	A number generated by the random number subroutine to be used as the starting number for the next use of the subroutine
YFL	The pseudo-random number generated by the subroutine
NSCAT	Number of photon scatterings
NABS	Number of photon absorptions
NESC	Number of photon escapes in circular source case
NESCE	Number of photon escapes through end of accounting shell for rectangular source
NESCS	Number of photon escapes through sides and base of accounting shell for rectangular source
V(J,K)	Volume of designated subspace, cubic meters
VHEM	Volume of accounting hemisphere for circular source
WDROP	Weight of droplet, lb
WTOT	Liquid water content of aerosol, lb/cubic meter
QVAP	Heat required per unit volume to evaporate droplets, Btu/cubic meter
W1	Location of point of emission along Y axis for rectangular source
X	Rectangular coordinate in reference coordinate system, meters
Y	See above explanation for X
Z	See above explanation for X

Code Symbol	Meaning
COETA1	Cosine of the polar angle of emission in translated coordinate system
SIETA1	Sine of the polar angle of emission in translated coordinate system
PSI1	Azimuthal angle of emission in translated coordinate system
PHI1	Azimuthal angle to point of emission in circular case
R1	Radius to point of emission in circular case
ELPROB	Probable photon path length, meters
D1	Conversion for spherical coordinates to x coordinate in translated system
D2	Same as D1 but for y coordinate
D3	Same as D1 for for z coordinate
R2	Radius vector in reference axis system folded into Y-Z plane to determine whether photon has escaped
ETAS	Polar scattering angle in scattering coordinate system
PSIS	Azimuthal scattering angle in scattering coordinate system
D1S	Conversion for spherical coordinates in scattering to xs coordinate in rectangular scattering axis system
D2S	Same as D1S but for ys coordinate
D3S	Same as D1S but for zs coordinate
XS	Rectangular coordinate in scattering coordinate system
YS	See above explanation for XS
ZS	See above explanation for XS
ETA	Polar angle to point of interaction in reference coordinate system
THETA	Indexing search polar angle for accounting subspaces
RREF	Indexing search radius increment for accounting subspaces
P(J,K)	Fraction of original emissions absorbed in each designated subspace

Code Symbol	Meaning
Q(J,K)	Heat required to evaporate droplets contained in designated subspace, Btu
QTOTL	Heat flux emitted from source into aerosol Btu/hr
PQ(J,K)	Time in minutes to evaporate water droplets in each subspace

MONTE CARLO PROGRAM FOR RADIATION FROM A LONG RECTANGULAR SOURCE

```
C     RADIATION FROM A LONG RECTANGULAR SOURCE
C     SET GENERAL INITIAL CONDITIONS
      DIMENSION MABS(10,10),V(10,10),P(10,10),Q(10,10),PQ(10,10)
  100 READ(1,89)INABS,IX,W,WMAX,SCAT,DOPT,WIN
   89 FORMAT(2I10,5F10.4)
      IF(INABS)999,87,87
   87 READ(1,88)AB,EQ,RDROP,DROPS,DELH,TS,ELMAX
   88 FORMAT(7F10.4)
      PI=3.14159265
C     SET VARIOUS COUNTERS TO ZERO
      DO55 J=1,6
      DO55 K=1,10
   55 MABS(J,K)=0
      N=0
      IY=0
      YFL=0.0
      NSCAT=0
      NABS=0
      NESCE=0
      NESCS=0
C     VOLUMES OF SIXTY SUBSPACES (SQ.METERS)
      DO66 J=1,6
      DO66 K=1,10
   66 V(J,K)=(W*W*K*K-W*W*(K-1)*(K-1))*(PI/24.)
C     SET SPECIFIC CONDITIONS FOR THIS PROBLEM
      WRITE(3,91)SCAT,DOPT,AB,RDROP,DROPS,TS
   91 FORMAT('1',1X,'SCAT=',F4.1,2X,'DOPT=',F4.1,2X,'AB=',F4.1,2X,'RDROP
     1=',F4.1,2X,'DROPS=',F5.1,2X,'TS=',F5.1//)
      TS=TS/100.
      DOPT=DOPT/1000.
```

```
      RDROP=RDROP*.0001*.03281
      DROPS=DROPS*28320.
      WDROP=(4./3.)*PI*RDROP*RDROP*RDROP*62.5
      WTOT=WDROP*DROPS*35.31
      QVAP=DELH*WTOT
C     SELECT POINT OF EMISSION FROM RECTANGULAR SOURCE
    1 N=N+1
    3 CALL RANDU(IX,IY,YFL)
      IX=IY
      W1=W*YFL
      X=0.0
      Y=W1
      Z=0.0
C     SELECT POLAR AND AZIMUTHAL ANGLES OF EMISSION
      CALL RANDU(IX,IY,YFL)
      IX=IY
      COETA1=SQRT(YFL)
      SIETA1=SQRT(1.-COETA1*COETA1)
    2 CALL RANDU(IX,IY,YFL)
      IX=IY
      PSI1=2.*PI*YFL
C     DETERMINE PROBABLE PATH LENGTH
      CALL RANDU(IX,IY,YFL)
      IX=IY
      ELPROB=(-1./DOPT)*ALOG(YFL)
C     DETERMINE DIRECTION NUMBERS
      D1=SIETA1*COS(PSI1)
      D2=SIETA1*SIN(PSI1)
      D3=COETA1
C     DETERMINE COORDINATES AT END OF PROBABLE PATH
      X=X+ELPROB*D1
      Y=Y+ELPROB*D2
```

```
      Z=Z+ELPROB*D3
C     DETERMINE WHETHER PHOTON ESCAPES
   40 IF(Z)4,4,7
    4 NESCS=NESCS+1
      GO TO 1
    7 R2=SQRT(Y*Y+Z*Z)
      IF(WMAX-R2)8,8,70
    8 NESCS=NESCS+1
      GO TO 1
   70 IF(ELMAX-ABS(X))71,71,9
   71 NESCE=NESCE+1
      GO TO 1
C     DETERMINE WHETHER ABSORBED OR SCATTERED
    9 CALL RANDU(IX,IY,YFL)
      IX=IY
      IF(AB-YFL)18,18,19
   18 NSCAT=NSCAT+1
      IF(SCAT)17,17,20
C     PROBABLE PATH FOR ANISOTROPIC SCATTERING
   17 CALL RANDU(IX,IY,YFL)
      IX=IY
      ELPROB=(-1./DOPT)*ALOG(YFL)
C     DETERMINE SCATTERING POLAR ANGLE
      CALL RANDU(IX,IY,YFL)
      IX=IY
      ETAS=(-PI/13.5)*ALOG(YFL)
C     DETERMINE SCATTERING AZIMUTHAL ANGLE
      CALL RANDU(IX,IY,YFL)
      IX=IY
      PSIS=2.*PI*YFL
C     DETERMINE DIRECTION NUMBERS IN SCATTERING COORDINATES
      D1S=SIN(ETAS)*COS(PSIS)
```

```
      D2S=SIN(ETAS)*SIN(PSIS)
      D3S=COS(ETAS)
      XS=ELPROB*D1S
      YS=ELPROB*D2S
      ZS=ELPROB*D3S
C     TRANSFORM SCATTERING COMPONENTS
      X=X+XS*SIN(PSI1)+YS*COETA1*COS(PSI1)+ZS*SIETA1*COS(PSI1)
      Y=Y-XS*COS(PSI1)+YS*COETA1*SIN(PSI1)+ZS*SIETA1*SIN(PSI1)
      Z=Z-YS*SIETA1+ZS*COETA1
      GO TO 40
C     FIND SUBSPACE OF ABSORPTION
   19 NABS=NABS+1
      YY=ABS(Y)
      SL=Z/YY
      ETA=ATAN(SL)
      ETA=ETA*(180./PI)
C     SEARCH FOR SUBSPACE BY ETA
      THETA=75.0
      J=6
   79 IF(THETA-ETA)80,81,81
   80 GO TO 60
   81 THETA=THETA-15.0
      J=J-1
      GO TO 79
   60 RREF=112.5
      K=10
   61 IF(RREF-R2)62,62,63
   62 GO TO 50
   63 RREF=RREF-12.5
      K=K-1
      GO TO 61
   50 MABS(J,K)=MABS(J,K)+1
```

```
      IF(NABS-INABS)12,1000,1000
      IF(EQ)14,14,20
   14 GO TO 1
C     ISOTROPIC SCATTERING OR REEMISSION
   20 CALL RANDU(IX,IY,YFL)
      IX=IY
      COETA1=1.-2.*YFL
      GO TO 2
C     OUTPUT
 1000 WRITE(3,99)
   99 FORMAT(5X,'HISTORIES',2X,'END ESCAPES',2X,'SIDE ESCAPES',2X,'ABSOR
     1BED',2X,'SCATTERED'/)
      WRITE(3,98)N,NESCE,NESCS,NABS,NSCAT
   98 FORMAT(7X,I6,6X,I6,7X,I6,6X,I6,5X,I6//)
C     FIND ABSORPTION IN EACH SUBSPACE COMPARED TO ORIGINAL EMISSIONS
      WRITE(3,97)
   97 FORMAT(10X,'FRACTION OF ORIGINAL EMISSIONS ABSORBED IN EACH SUBSPA
     1CE'/)
      ITOTL=N
      ZTOTL=ITOTL
      DO11 J=1,6
      DO11 K=1,10
      P(J,K)=MABS(J,K)
   11 P(J,K)=P(J,K)/ZTOTL
      CONTINUE
      DO93 K=1,10
   93 WRITE(3,94)(P(J,K),J=1,6)
   94 FORMAT(6F12.6/)
C     EVAPORATIVE HEAT REQUIRED IN EACH SUBSPACE
      DO15 J=1,6
      DO15 K=1,10
   15 Q(J,K)=QVAP*V(J,K)
```

```
      LONG RECTANGULAR SOURCE PROGRAM      PAGE 6

      QTOTL=.1714*25.*3.281*3.281*TS*TS*TS*TS
      QTOTL=QTOTL*WIN
      WRITE(3,92)
   92 FORMAT('0',2X,'RELATIVE TIME IN MINUTES TO EVAPORATE WATER DROPLET
     1S IN EACH SUBSPACE'/)
      DO16 J=1,6
      DO16 K=1,10
   16 PQ(J,K)=(Q(J,K)/(QTOTL*P(J,K)))*60.
      DO95 K=1,10
   95 WRITE(3,96)(PQ(J,K),J=1,6)
   96 FORMAT(6F12.6/)
      GO TO 100
  999 CALL EXIT
      END
```

MONTE CARLO PROGRAM FOR RADIATION FROM A CIRCULAR SOURCE

```
C     RADIATION FROM FINITE CIRCULAR SOURCE
C     SET GENERAL INITIAL CINDITIONS
      DIMENSION MABS(10,10),V(10,10),P(10,10),Q(10,10),PQ(10,10)
C     SET SPECIFIC CONDITIONS FOR THIS PROBLEM
  100 READ(1,89)INABS,IX,R,RMAX,SCAT,DOPT,WIN
   89 FORMAT(2I10,5F10.4)
      IF(INABS)999,87,87
   87 READ(1,88)AB,EQ,RDROP,DROPS,DELH,TS
   88 FORMAT(6F10.4)
      PI=3.14159265
      WRITE(3,91)SCAT,DOPT,AB,RDROP,DROPS,TS
   91 FORMAT('1',2X,'SCAT=',F4.1,2X,'DOPT=',F4.1,2X,'AB=',F4.1,2X,'RDROP
     1=',F4.1,2X,'DROPS=',F5.1,2X,'TS=',F5.1//)
      TS=TS/100.
      DOPT=DOPT/1000.
      RDROP=RDROP*.0001*.03281
      DROPS=DROPS*28320.
      WDROP=(4./3.)*PI*RDROP*RDROP*RDROP*62.5
      WTOT=WDROP*DROPS*35.31
      QVAP=DELH*WTOT
      QTOTL=.1714*25.*25.*PI*3.281*3.281*TS*TS*TS*TS
      QTOTL=QTOTL*WIN
C     SET COUNTERS TO ZERO
      DO55 J=1,6
      DO55 K=1,10
   55 MABS(J,K)=0
      N=0
      NSCAT=0
      NABS=0
      NESC=0
```

```
      IY=0
      YFL=0.0
C     FIND VOLUMES OF SUB SPACES
      VHEM=(2./3.)*PI*RMAX*RMAX*RMAX
      DO66 J=1,6
      DO66 K=1,10
   66 V(J,K)=.001*(COS((6-J)*PI/12.)-COS((7-J)*PI/12.))*(K**3-(K-1)**3)*
     1VHEM
C     SELECT POINT OF EMISSION FROM CIRCULAR SOURCE
    1 N=N+1
    3 CALL RANDU(IX,IY,YFL)
      IX=IY
      R1=R*SQRT(YFL)
      CALL RANDU(IX,IY,YFL)
      IX=IY
      PHI1=2.*PI*YFL
      X=R1*COS(PHI1)
      Y=R1*SIN(PHI1)
      Z=0.0
C     SELECT POLAR AND AZIMUTHAL ANGLES OF EMISSION
      CALL RANDU(IX,IY,YFL)
      IX=IY
      COETA1=SQRT(YFL)
    2 CALL RANDU(IX,IY,YFL)
      IX=IY
      PSI1=2.*PI*YFL
      SIETA1=SQRT(1.-COETA1*COETA1)
C     DETERMINE PROBABLE PATH LENGTH
      CALL RANDU(IX,IY,YFL)
      IX=IY
      ELPROB=(-1./DOPT)*ALOG(YFL)
C     DETERMINE DIRECTION NUMBERS
```

```
      D1=SIETA1*COS(PSI1)
      D2=SIETA1*SIN(PSI1)
      D3=COETA1
C     DETERMINE COORDINATES AT END OF PROBABLE PATH
      X=X+ELPROB*D1
      Y=Y+ELPROB*D2
      Z=Z+ELPROB*D3
C     DETERMINE WHETHER PHOTON ESCAPES
   40 IF(Z)4,4,7
    4 NESC=NESC+1
      GO TO 1
    7 R2=SQRT(X*X+Y*Y+Z*Z)
      IF(RMAX-R2)8,8,9
    8 NESC=NESC+1
      GO TO 1
C     DETERMINE WHETHER ABSORBED OR SCATTERED
    9 CALL RANDU(IX,IY,YFL)
      IX=IY
      IF(AB-YFL)18,18,19
   18 NSCAT=NSCAT+1
      IF(SCAT)17,17,20
C     ANISOTROPIC SCATTERING
C     DETERMINE PROBABLE PATH LENGTH
   17 CALL RANDU(IX,IY,YFL)
      IX=IY
      ELPROB=(-1./DOPT)*ALOG(YFL)
C     DETERMINE SCATTERING POLAR ANGLE
      CALL RANDU(IX,IY,YFL)
      IX=IY
      ETAS=(-PI/13.5)*ALOG(YFL)
C     DETERMINE SCATTERING AZIMUTHAL ANGLE
      CALL RANDU(IX,IY,YFL)
```

```
      IX=IY
      PSIS=2.*PI*YFL
C     DETERMINE DIRECTION NUMBERS IN SCATTERING COORDINATES
      D1S=SIN(ETAS)*COS(PSIS)
      D2S=SIN(ETAS)*SIN(PSIS)
      D3S=COS(ETAS)
      XS=ELPROB*D1S
      YS=ELPROB*D2S
      ZS=ELPROB*D3S
C     TRANSFORM SCATTERING COMPONENTS
      X=X+XS*SIN(PSI1)+YS*COETA1*COS(PSI1)+ZS*SIETA1*COS(PSI1)
      Y=Y-XS*COS(PSI1)+YS*COETA1*SIN(PSI1)+ZS*SIETA1*SIN(PSI1)
      Z=Z-YS*SIETA1+ZS*COETA1
      GO TO 40
C     FIND SUBSPACE OF ABSORPTION
   19 NABS=NABS+1
      XY=SQRT(X*X+Y*Y)
      SL=Z/XY
      ETA=ATAN(SL)
      ETA=ETA*(180./PI)
C     SEARCH FOR SUBSPACE BY ETA
      THETA=75.0
      J=6
   79 IF(THETA-ETA)80,81,81
   80 GO TO 60
   81 THETA=THETA-15.0
      J=J-1
      GO TO 79
   60 RREF=112.5
      K=10
   61 IF(RREF-R2)62,62,63
   62 GO TO 50
```

```
   63 RREF=RREF-12.5
      K=K-1
      GO TO 61
   50 MABS(J,K)=MABS(J,K)+1
      IF(NABS-INABS)12,1000,1000
   12 IF(EQ)14,14,20
   14 GO TO 1
C     DETERMINE SCATTER OR REEMISSION ANGLES
   20 CALL RANDU(IX,IY,YFL)
      IX=IY
      COETA1=1.-2.*YFL
      GO TO 2
C     OUTPUT
 1000 WRITE(3,99)
   99 FORMAT(10X,'HISTORIES',5X,'ESCAPES',5X,'SCATTERED',5X,'ABSORBED'/)
      WRITE(3,98)N,NESC,NSCAT,NABS
   98 FORMAT(12X,I6,7X,I6,7X,I6,7X,I6//)
C     FIND ABSORPTION IN EACH SUBSPACE COMPARED TO ORIGINAL EMISSIONS
      WRITE(3,97)
   97 FORMAT(10X,'FRACTION OF ORIGINAL EMISSIONS ABSORBED IN EACH SUBSPA
     1CE'/)
      ITOTL=N
      ZTOTL=ITOTL
      DO11 J=1,6
      DO11 K=1,10
      P(J,K)=MABS(J,K)
   11 P(J,K)=P(J,K)/ZTOTL
      CONTINUE
      DO93 K=1,10
   93 WRITE(3,94)(P(J,K),J=1,6)
   94 FORMAT(6F12.6/)
C     MASS OF LIQUID WATER IN EACH SUBSPACE
```

```
      DO15 J=1,6
      DO15 K=1,10
   15 Q(J,K)=QVAP*V(J,K)
      WRITE(3,92)
   92 FORMAT('0',2X,'RELATIVE TIME IN MINUTES TO EVAPORATE WATER DROPLET
     1S IN EACH SUBSPACE'/)
      DO16 J=1,6
      DO16 K=1,10
   16 PQ(J,K)=(Q(J,K)/(QTOTL*P(J,K)))*60.
      DO95 K=1,10
   95 WRITE(3,96)(PQ(J,K),J=1,6)
   96 FORMAT(6F12.6/)
      GO TO 100
  999 CALL EXIT
      END
```

RANDOM NUMBER SUBROUTINE FOR USE WITH MONTE CARLO PROGRAMS

```
  SUBROUTINE RANDU(IX,IY,YFL)
  IY=IX*65539
  IF(IY)5,6,6
5 IY=IY+2147483647+1
6 YFL=IY
  YFL=YFL*.4656613E-9
  RETURN
  END
```